NASA
Technical
Paper
1979

April 1982

Power Spectral Measurements of Clear-Air Turbulence to Long Wavelengths for Altitudes up to 14 000 Meters

Harold N. Murrow,
William E. McCain,
and Richard H. Rhyne

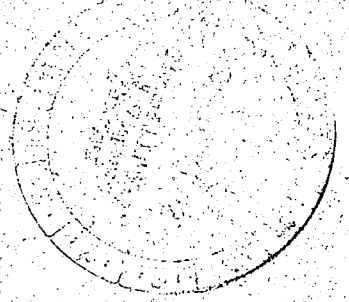

NASA

NASA Technical Paper 1979

1982

Power Spectral Measurements of Clear-Air Turbulence to Long Wavelengths for Altitudes up to 14 000 Meters

Harold N. Murrow,
William E. McCain,
and Richard H. Rhyne
Langley Research Center
Hampton, Virginia

National Aeronautics
and Space Administration

Scientific and Technical Information Branch

SUMMARY

Measurements of three components of clear-air atmospheric turbulence have been made with an airplane incorporating a special instrumentation system to provide accurate data resolution to wavelengths of approximately 12 500 m (40 000 ft). Flight samplings covered an altitude range from approximately 500 to 14 000 m (1500 to 46 000 ft) in various meteorological conditions. This report presents individual autocorrelation functions and power spectra for the three turbulence components from 43 data runs taken primarily from mountain-wave and jet-stream encounters. The flight location (Eastern or Western United States), date, time, run length, intensity level (standard deviation), and values of statistical degrees of freedom for each run are provided in tabular form.

The present data support previous data confirming that the Von Kármán model is a realistic representation of atmospheric turbulence at wavelengths shorter than about 1000 m (≈3000 ft). However, for wind-shear and mountain-wave situations, the spectral shape at long wavelengths (especially for horizontal components of gust velocity) does not conform to the Von Kármán expression. It, thus, appears that alternate models should be considered that take into account the fact that the overall spectra contain, in addition to a Von Kármán component, additional power at the longer wavelengths. The data presented in this report, along with detailed meteorological descriptions for each sampling flight presented in previously published reports, should provide adequate information for detailed meteorological correlations. Some time histories which contain predominant low-frequency wave motion are also presented.

INTRODUCTION

The required structural strength of portions of present-day transport airplanes is, in many cases, dictated by loads predicted to arise from atmospheric-turbulence encounters during the lifetime of the airplane. Presently favored turbulence design techniques (particularly in the United States) include the use of power spectral-density (PSD) methods (see, for example, ref. 1) which, in turn, require a mathematical model to describe atmospheric turbulence in power spectral form. The model presently used for this purpose, in most cases, is the so-called Von Kármán turbulence model which essentially describes the power spectral density or "power" of the turbulence as a function of wavelength or frequency. (See ref. 1.) A recognized shortcoming in the use of the Von Kármán model has been the lack of experimental verification of the power in the long-wavelength region. The advent of new, large, flexible high-speed airplanes such as supersonic transports has made the long-wavelength region more important. Accordingly, the National Aeronautics and Space Administration initiated a program aimed at providing accurate power spectral measurements of atmospheric turbulence to wavelengths of the order of 20 000 m (≈65 000 ft) in an attempt to describe better the power content of atmospheric turbulence. (See ref. 2.)

The variable in the Von Kármán model which determines the "knee frequency," or wavelength at which the PSD curve breaks over or flattens, is the integral scale value (or simply "scale") L, sometimes thought of as a maximum average eddy size. The value of L is the controlling factor of the model shape at long wavelength.

The value of L = 762 m (2500 ft), presently specified in military design requirements for altitudes above 762 m (2500 ft), has been considered to be conservative and not solidly based on experimental evidence. In contrast to the uncertainty surrounding the long-wavelength region, a considerable body of experimental evidence has confirmed the validity of the Von Kármán model in the shorter wavelength region. In this region, which encompasses the short period, Dutch roll, and structural mode responses of subsonic airplanes, the PSD drops off in proportion to the inverse wavelength $1/\lambda$ raised to the -5/3 power.

The three principal reasons why experimental data have not been available to date to validate the Von Kármán model at long wavelengths are given as follows:

First, rather long samples of continuous turbulence are required in order for the power spectral estimates to be statistically significant when data are processed to long wavelengths (i.e., low frequencies). Samples of sufficient duration are difficult to acquire. In addition, until recently it was believed that even relatively minor changes in the turbulence-intensity level during the data interval could not be tolerated. This concern has been alleviated by the work of reference 3.

Second, a great deal of difficulty has always been encountered in making sufficiently accurate motion measurements of the sampling airplane at very low frequency. Low-frequency motions, arising from the pilot's actions in controlling the airplane and/or from the changing horizontal wind field, as a function of distance or time which result in an apparent drift or trend in the motion time histories - if not correctly measured and accounted for - can result in large errors in experimental power spectral values in the long-wavelength region.

Third, the lack of adequate experimental PSD measurements at long wavelengths is due to the nonuniform (and perhaps, in some cases, improper) use of filtering techniques between different experimenters which affect the low-frequency part of the time histories and, thus, the long-wavelength end of the PSD. One type of filtering commonly employed, referred to as "prewhitening," flattens the spectrum (i.e., makes it similar to a white-noise spectrum) in order to minimize "spectral window" bias errors (ref. 1) during a stage of data reduction; and then at a later stage the resulting spectrum is corrected for the effect of the prewhitening filter. It was demonstrated in reference 4 that such a procedure distorts the power curve in the long-wavelength region of the PSD and, therefore, should not be used for processing the data to long wavelengths (or low frequency) where very narrow spectral windows are used. Various methods have also been proposed and used to filter or remove from the time histories the trends known to have been introduced either by gyro drift or by the accelerometer-integration process used to determine the linear airplane motions. Such detrending, without extreme care in application, can filter out real data as well as unwanted trend data in the long-wavelength range. Some early experimenters believed that the removal of such trends affected only the power spectral estimate at zero frequency. This belief was later shown to be incorrect, however, because of the finite width of the spectral window, or mathematical filter, used to obtain the PSD. (See ref. 5.)

The purpose of this report is to present power spectra of measured gust velocities for a variety of meteorological conditions, with emphasis on the long-wavelength region, and an assessment of the applicability of the Von Kármán model when this region is of importance. Several earlier reports are complementary to this report. References 4 and 5 address data-processing and measurement-system adequacy aspects. Two special publications (refs. 6 and 7) give some general and detailed analyses of data contained herein. References 8 and 9 describe the meteorological and opera-

tional aspects of the turbulence-sampling missions from which these data were obtained. Spectral characteristics related to meteorological conditions will be noted in this report; however, detailed statistical or meteorological analyses are not given. It is believed that with this report and references 8 and 9, significant meteorological correlations and analyses can be made according to specific requirements. Power spectra are presented from 43 data runs (together with their autocorrelation functions) obtained from atmospheric turbulence generated by 14 different specific meteorological conditions (flights). Some of the more unusual time histories are also presented (generally associated with a mountain wave or extremely large wind shear) in order to illustrate the nature and source of high power at the very long wavelengths.

SYMBOLS

Values are presented herein in the International System of Units (SI) and, where considered useful, also in U.S. Customary Units. Measurements and calculations were made in U.S. Customary Units.

f	frequency, Hz
L	integral scale value, m (ft)
R	autocorrelation function
R_N	normalized autocorrelation function, $R(r)/R(0)$
r	lag distance, or spatial lag, km (ft)
Δt	time-sampling interval, sec
u,v,w	longitudinal, lateral, and vertical components of gust velocity, respectively, m/sec (ft/sec)
V	true airspeed, m/sec (ft/sec)
$\overline{V}$	average true airspeed during run, m/sec (ft/sec)
α	angle of attack
β	angle of sideslip
λ	wavelength, m or km (ft)
σ	standard deviation (intensity level)
σ^2	variance
Φ	power spectral density
Ω	spatial frequency, $2\pi/\lambda$

Abbreviations:

ACF	autocorrelation function
CA	California
dof	degrees of freedom
GMT	Greenwich mean time
PSD	power spectral density
U.S.	United States
VA	Virginia

AIRPLANE, INSTRUMENTATION, AND MEASUREMENT ACCURACY

Figure 1 is a photograph of the sampling airplane. Selection of the airplane was based on its ruggedness, altitude- and operating-range capability, ease of instrumentation installation, and availability. Other details concerning the airplane are given in reference 8.

The instrumentation system and measurement accuracies are described in reference 10. Principal airflow measurements are α, β, and V; and incremental values measured from their mean are used. Other measurements, which defined the airplane motions, were applied to obtain the corrected airflow values. Estimated accuracies for measured quantities are given in reference 10. Data-reduction procedures are given in reference 5, which also contains results from an in-flight assessment of the effect of integrated system accuracies on gust-velocity time histories.

DATA ACQUISITION AND PROCESSING

A total of 46 flights with a total of 77 data runs were made over an 18-month period. The flights were conducted in two geographical areas, referred to as Eastern and Western United States (U.S.). A total of 30 flights were conducted in the Eastern U.S., and 16 flights were performed in the Western U.S. For the Eastern U.S. flights, the sampling airplane was based at Langley Air Force Base, Virginia; and for the Western U.S. flights, the airplane was operated from Edwards Air Force Base, California. The operating areas over which the data were acquired are shown in figures 2 and 3. Pertinent topographical features are also shown in figures 2 and 3. The flight numbers pertinent to data presented herein are encircled and located in the general area where the flight runs were made. Note in figure 2 that flight 27 data were obtained northeast of Washington, D.C. - in the New York City vicinity. After "quick-look" assessments with regard to turbulence intensity and continuity during a run, data were processed from a total of 43 runs from 14 flights. Meteorological aspects of the flights are described in references 8 and 9.

The longitudinal, lateral, and vertical components, respectively, of gust velocity are defined in reference 5, and measurements that are required for their determination are given. (As will be discussed later, an antialiasing filter was not required.) The autocorrelation functions and power spectra were determined from

time-history data digitized in 0.05-sec increments giving a Nyquist frequency $\frac{1}{2\ \Delta t}$ of 10 Hz. The values of PSD are presented as a function of inverse wavelength (given in cycles/m); the inverse wavelength was determined from the ratio of $f/\bar{V}$ $\left(\text{given in } \frac{\text{cycles/sec}}{\text{m/sec}}\right)$ where $\bar{V}$ is the average true airspeed during a run.

The autocorrelation functions (ACF) have been normalized to remove intensity effects by dividing the function by its variance or its value for which there is no time shift or lag distance. The power spectra, however, are not normalized; therefore, the area under the spectral curves is equivalent to the variance σ^2. Thus, the PSD plots shift vertically according to the intensity.

The PSD and ACF data were all processed by using 1024 time lags. The mechanics of the data processing thus provide an effective spectral-window width of 0.0195 Hz when the Blackman-Tukey algorithm and Hann window are used. (See ref. 4.) Since the Nyquist frequency is 10 Hz, power estimates are provided at frequency increments of 10/1024 = 0.009766 Hz. On the ACF plots, time lag has been changed to a spatial lag r by multiplying the time lag by the mean true airspeed for the run.

Before discussing the results in detail, a factor applicable to a number of the longitudinal PSD plots will be mentioned. For many of the longitudinal-component cases presented, it should be noted that the flattening of the power spectrum at the high-frequency or short-wavelength region is a result of the use of a restrictor provided for the pitot-static tube for high-altitude flights. The use of two different restrictors for flight operations above and below an altitude of 9100 m (30 000 ft) to provide the proper damping for the sensitive airspeed measurement is discussed in reference 10. In a number of instances, the high-altitude restrictor was installed because of a planned mission at high altitude. However, when the high-altitude turbulence was not found, in-flight diversions to a lower altitude resulted in unavoidable use of the wrong restrictor. Consequently, the slope is incorrect at frequencies higher than the point of deviation from the -5/3 slope in the PSD curves for the longitudinal component.

RESULTS AND DISCUSSION

Table I presents basic meteorological and geographical information about the flights. Further details about each flight are given in table IV of reference 8. The flight- and run-number designation is retained from the actual, sampling, flight designation in order to allow correlation with references 8 and 9. As shown in table I, 3 general classifications were selected, and 14 specific conditions were identified. It should be pointed out that even though a predominate meteorological condition prevails, other meteorological influences were present to some degree. (See refs. 8 and 9.) The general geographic location is identified in table I as either VA (Virginia) or CA (California).

Table II presents the test conditions and some of the measured statistical data for all the data runs identified in table I. Table II lists, similarly to table I, the flight numbers, dates, and data-run numbers from references 8 and 9 for ease in correlation. The figure numbers refer to the corresponding ACF and PSD plots presented herein. Specific data listed for each data run include mean altitude, run length in distance and time, statistical degrees of freedom (dof) for individual power estimates (according to the method of ref. 11), and the intensity or standard-deviation values for the vertical, lateral, and longitudinal turbulence components. A goal of the study was to acquire data that would provide at least 24 statistical

degrees of freedom; however, from table II it is seen that this goal was not achieved in a number of cases. Three cases which are not considered acceptable are presented to demonstrate the degree of scatter in individual turbulence power estimates resulting from having low statistical degrees of freedom (flight 30, run 4; flight 39, run 10; flight 41, run 8).

The autocorrelation and power spectra are presented in figures 4 to 46. The order of presentation follows the order of table II. The format is as follows: the normalized autocorrelation function is presented at the top of the figure, and the power spectrum is presented in the lower part of the figure. In each case, for reference, a curve is included for an analytical autocorrelation function and a power spectrum defined by the Von Kármán expression. (See ref. 1.) Thus, for the longitudinal component,

$$\Phi_u(\Omega) = \sigma_u^2 \frac{2L}{\pi} \frac{1}{[1 + (1.339L\Omega)^2]^{5/6}}$$

and for the transverse components,

$$\Phi_w(\Omega) = \Phi_v(\Omega) = \sigma^2 \frac{L}{\pi} \frac{1 + 8/3(1.339L\Omega)^2}{[1 + (1.339L\Omega)^2]^{11/6}}$$

where Ω is the spatial frequency $2\pi/\lambda$. An integral scale value L of 762 m (2500 ft), which is presently specified in the design specification MIL-A-008861A (see ref. 12) for continuous turbulence analysis at altitudes above 762 m (2500 ft), was arbitrarily selected for the reference. It is to be noted that L as used in the Von Kármán expressions is actually the L value associated with the longitudinal component and is twice the L value of the transverse components. (See ref. 1, p. 13.) In each case, the reference curve was translated vertically to cause the curve at short wavelengths to coincide with the measured data. Thus, the standard-deviation value of the reference is different for each individual spectrum. Each figure is in three parts to present in order the vertical, lateral, and longitudinal gust-velocity data for a given flight and run.

As stated previously, the principal purpose of this sampling program was to investigate the long-wavelength air motion and measure its magnitude or power relative to the shorter wavelength turbulence such as has been measured in several earlier sampling programs. Figures 4 to 26 present turbulence data categorized according to mountain-wave or orographic phenomena.

Figure 4 presents results for a 680-sec run made at an altitude of about 1924 m (6311 ft) over the Appalachian Mountains in Western Virginia. (See table II.) The number of statistical degrees of freedom is 27. In figure 4(a), it can be seen that at the higher frequency or shorter wavelengths the variation of power density with frequency exhibits the -5/3 slope characteristic of most previous measurements and corresponds to the prediction of the Von Kármán expression. Below an inverse wavelength of about 10^{-3} cycles/m, however, the data deviate significantly from the reference Von Kármán curve. In this region, the power is less than the reference curve by roughly a factor of 2 for an inverse-wavelength interval of about 10^{-1} cycles/m,

and then the slope or power increases and the curve crosses over the reference curve for the longer wavelengths measured. This increase in power at long wavelengths would be expected from observation of the normalized autocorrelation function which is presented at the top portion of the figure. The low point of this autocorrelation function, which extends well into the negative region and occurs between a lag distance r of 6 km (19 685 ft) to 7 km (22 966 ft), is typical of cases where atmospheric turbulence is superimposed upon a strong wave. The autocorrelation function for the longitudinal components shown in figure 4(c) has a similar appearance because the run was made perpendicular to the waves. The minimum occurs at one-half wavelength of the strong wave. This can be verified by examination of the time history which is presented in figure 47(a). (Some significant time histories are discussed in the appendix and are presented in figs. 47 to 49.) Here, it is seen that the average transverse time of 1 cycle of the mountain wave is about $1\frac{1}{2}$ min, which produces a one-half wavelength of approximately 6.3 km (20 669 ft) when the average true airspeed for the run of 139.6 m/sec (458 ft/sec) is taken into account. (An understanding of the appearance of autocorrelation functions associated with mountain waves can be related to the fact that the autocorrelation function of a pure sine wave is essentially a cosine function starting at 1 at $r = 0$ and going to -1 at $r = \lambda/2$, and then back to 1 at $r = \lambda$.)

The reference curve on the ACF plot (fig. 4(c)) is for the Von Kármán model with $L = 762$ m (2500 ft). As can be seen, the experimental ACF is unlike that for the Von Kármán model because of the predominance of the wave effect. It is to be noted that the one-half wavelength of 6.3 km (≈20 600 ft) indicated by the ACF should translate to a strong peak in the power spectrum at about 8×10^{-5} cycles/m. However, such a long wavelength is essentially below the resolution capability of the present spectral analysis.

Several of the autocorrelation functions (those with very low statistical degrees of freedom) exhibit discontinuities. For example, figure 15(b) has a discontinuity at $r = 9$ km (≈29 500 ft). For runs processed with a large number of lags in comparison to the run length (thus producing low statistical degrees of freedom), such discontinuities are observable at a value of r equivalent to one-half the run length and result from "noise" introduced by the mechanics of the data-reduction procedure.

Evidence of strong periodic content is discernable for all of the mountain-wave flights (figs. 4 to 26) from examination of the ACF in a manner similar to that previously discussed in the example of figures 4(a) and 4(c). The strength of the wave, and the velocity component upon which it appears, is highly correlated with the relative angle between the flight track and the orientation of the ridge tops. The vertical and longitudinal gust-velocity components exhibit strong-wave content for tracks perpendicular to the ridge tops. Little evidence of waves is present for tracks parallel to the ridge for any component, since waves were not being intercepted by the airplane.

In general, the PSD of figures 4 to 26 shows that mountain-wave turbulence produces greater long-wavelength power than the Von Kármán model. This is particularly true for the vertical and longitudinal components when the flight path is perpendicular to the ridge line or wave orientation. In fact, with the possible exception of the vertical component shown in figure 17(a), none of the mountain-wave data come very close to fitting the Von Kármán model at low frequencies with a value of reference L of 762 m (2500 ft). Even for this run, the knee of the PSD does not fit very well. Since no strong wave is discernable on any component of this run, the turbulence could have been generated by rough terrain only (rather than by a mountain

range or ridge line) and, therefore, possibly should not be classed as "mountain-wave turbulence." Although the PSD of the longitudinal component for flight 34, run 5, fits the reference model quite well (fig. 19(c)), the ACF indicates a wave effect at $\lambda/2$ of about 7 km (≈23 000 ft) which would result in power higher than the reference at an inverse wavelength somewhat lower than the lowest point of the PSD.

At the higher inverse wavelengths, all of the data seem to have the -5/3 power drop-off of the Von Kármán model, with the possible exception of the vertical component of flight 39 (runs 3, 5, and 7) shown in figures 22(a), 23(a), and 24(a), respectively. The power drop-off for these runs seems to be slightly less steep; the cause for this is not known.

Another general observation is that for data which include wavelengths such as those presented herein, the standard deviation for the horizontal components is nearly always greater than that for the vertical components. This is easily observed from inspection of table II. Since long-scale variations are a part of the nature of the overall wind field which, of course, is horizontal in direction, the horizontal components will exhibit more overall power. This suggests that although the turbulence is isotropic at short wavelengths, as has been traditionally assumed, isotropy does not hold for turbulence in the atmosphere at long wavelengths.

Figures 27 to 35 present the spectral data for wind shear including the cases where the jet stream is directly involved. From inspection of table II(b), it is seen that the variability in standard deviation was small. The intensity of the vertical component was always lower than that for the horizontal components and did not exceed 0.9 m/sec (2.9 ft/sec), whereas the intensity of the horizontal components was somewhat more variable from sample to sample.

In contrast to the mountain-wave turbulence, a number of the vertical-component cases contain less power in the long-wavelength region than the reference curve for the Von Kármán model. (For example, see fig. 28(a).) In every case, however, the horizontal components contain much greater power in the long-wavelength region than the reference curve. Examination of the ACF for the cases of wind shear and/or jet-stream effects indicates that the time histories are dominated by low-frequency drift or trendlike effects, which would show up in the PSD at frequencies near zero. This is evidenced in the ACF by a curve with low slope. The spectra all appear to follow the -5/3 slope of the Von Kármán model in the shorter wavelength region.

After studying the ACF of flight 38 (figs. 31(a) and 32(a)), it is apparent that a strong wave is present on the vertical component. The indication is, therefore, that the turbulence for this flight was predominately "mountain wave" in nature, rather than the "short-wave-trough movement" suggested in reference 9.

Figures 36 to 46 present data that are considered to represent special meteorological conditions that cannot be considered representative of the other categories. On flight 8 (fig. 36), turbulence associated with convection was sampled at an altitude of ≈460 m (1500 ft). This case was presented previously in reference 6 and is shown to fit the Von Kármán model remarkably well when a value of L of 305 m (1000 ft) is used for the vertical component. Somewhat larger values of L are required to fit the horizontal components: about 600 m (≈2000 ft) for the lateral component and 1200 m (≈4000 ft) for the longitudinal component. Sample time histories are shown for this low-altitude convective turbulence in reference 6. Although the time histories for all three components are very similar in appearance, the ACF and PSD indicate that even low-altitude convective turbulence is not isotropic in the long-wavelength region. The rapid drop in the power spectra at the

shortest wavelength end (i.e., below the -5/3 reference curve) for figure 36 is a result of an experiment employing a digital antialiasing filter. It was determined that aliasing was not a problem, and use of the filter was, therefore, discontinued for all other data.

Flight 32, run 4, was originally presented as a high-altitude wind-shear case in reference 6. (See fig. 39.) The meteorological and other aspects of this flight have also been reported in detail in reference 7. The meteorological analyses indicated that the turbulence encountered on this flight was triggered by wind shear; however, some of the runs appeared to contain orographic effects, and the intensity was generally greater for those than for the remaining cases for wind shear and/or jet-stream effects. For that reason, flight 32 was grouped with the "special cases" in the present paper. The time history of run 4, which is shown in reference 6 (also see the appendix of the present paper), is believed to be typical of high-altitude wind shear and shows no orographic or wave effects. The horizontal components are illustrative of the cause of the high power near zero frequency on the PSD curves, which is typical of wind-shear turbulence. As previously shown in reference 6, the vertical component for run 4 (fig. 39(a)) fits the Von Kármán model quite well, indicating an L value of about 305 m (1000 ft). The horizontal components have considerable more power at the long wavelengths and do not conform to the Von Kármán model, as is evident from the ACF curves.

Another special case which appears to conform to the Von Kármán model quite well, as far as the vertical component is concerned, is flight 42, run 6. (See fig. 44(a).) Flight 42 was conducted in mixed conditions associated with low-altitude thermal convective action and sea-breeze convergence. (See ref. 9.) Run 6 was a low-altitude run exhibiting moderate and greater turbulence intensity. The horizontal components for these data also contain much more power at the long wavelengths than the reference curve, with the ACF curves indicating that the power is at a very low frequency.

Data presented herein indicate that the Von Kármán model is good at short wavelengths, but significant differences can be present at long wavelengths depending on the atmospheric situation. Some recent studies related to alternate modeling of atmospheric turbulence are reported in references 13 to 17. In general, the alternate models take into account the fact that, for power spectral representation to long wavelengths such as the measurements described herein, "turbulence" by the conventional definition may be described by a curve composed of a Von Kármán component which is adequate at short wavelengths; but an additional term must be included to account for the additional power at the longer wavelengths because of the special long-wave content.

The time histories presented for figures 47 to 49 are discussed in the appendix for cases of wave motion to point out significant characteristics that cannot be easily observed from power spectra.

CONCLUDING REMARKS

Measurements of three components of clear-air atmospheric turbulence have been made with an airplane incorporating a special instrumentation system to provide accurate data resolution to wavelengths of approximately 12 500 m (40 000 ft). Flight samplings covered an altitude range from 500 to 14 000 m (1500 to 46 500 ft) in various meteorological conditions. Individual autocorrelation functions and power spectra have been presented for the three turbulence components from 43 data runs.

The majority of the data are from mountain-wave and jet-stream encounters. The use of power spectral-density design techniques for the response of airplanes to atmospheric turbulence requires a mathematical model describing atmospheric turbulence in power spectral form.

The present data support previous data confirming that the Von Kármán model is a realistic representation of atmospheric turbulence at wavelengths shorter than about 1000 m (3281 ft), and it is thus usable for designing subsonic airplanes whose primary response modes fall below this wavelength. (Past successful airplane design, of course, bears this out.) It should be noted that experimental limitations in this measurement program (primarily those of record or sample length) prevent the reliable resolution of integral scale values L greater than about 1800 m (≈6000 ft) since location of the "knee" of the Von Kármán model for such high L values is at a longer wavelength than data can be reliably processed. The present data, however, show that although the design value of L of 762 m (2500 ft) specified in MIL-A-008861A, when tied to the appropriate intensity level σ, results in proper subsonic design loads, it does not realistically represent what takes place in the atmosphere at wavelengths greater than 1000 m (≈3000 ft).

The limitations of the Von Kármán turbulence model at wavelengths greater than 1000 m (≈3000 ft) are of particular significance for many situations involving windshear and mountain-wave conditions. The difficulty in specifying an appropriate value of L makes its use difficult for other types of turbulence as well.

Models which appear to be capable of realistically describing atmospheric turbulence behavior throughout the total range of wavelengths are described in NASA CR-145247 and CR-2913. It appears that an analytical model consisting of the sum of a "slow component" as a function of time, plus an amplitude-modulating function of time multiplied by a so-called "Von Kármán component," would be required to describe many of the power spectra presented in this report. However, the determination of statistical parameters to insert into such a model to represent adequately an overall airplane turbulence experience would seem to be a formidable task.

A practical approach, and possibly just as accurate, for overall design-loads prediction in a wavelength region greater than about 1000 m (≈3000 ft) would be to use the Von Kármán equation with a fixed and conservatively larger value of L. The model used in this fashion would be recognized as being approximate only, and it would also require additional research to determine appropriate combinations of L and σ.

Langley Research Center
National Aeronautics and Space Administration
Hampton, VA 23665
March 3, 1982

APPENDIX

SELECTED TIME HISTORIES

Examples of wave phenomena can be seen in the time histories of figure 47. In figure 47(a), the three components of gust velocity are shown for a 14-min data run of a track diagonal to the ridges at an altitude of 1924 m (6311 ft) in what was classified in reference 13 as an Appalachian mountain-wave situation. The low-frequency oscillations prominent on the vertical and longitudinal time histories are characteristic of mountain waves. It would appear that the predominant wavelength is about 13 km (≈8 miles, 1.5 min). The turbulence intensity is quite variable, but it is interesting to note that the intensity is always high for all components on the positive slope of the wave. Figure 47(b) is a 9-min portion of a run on the same flight parallel to the ridges. Again, a significant wave pattern is obvious on the vertical and longitudinal components. Gust-velocity time histories from other runs of the same flight are shown in figures 47(c), 47(d), and 47(e).

Time histories for a 5-min run in a mountain-wave situation at about 14 000 m (≈46 000 ft) near the Sierras is presented in figure 48. In this case, the turbulence intensity is low, but wave motion is very predominant with a peak-to-peak longitudinal gust velocity of about 19 m/sec (62 ft/sec) over a 1-min interval. Oscillations in the vertical gust velocity were of lower amplitude and at a higher frequency, about 1.5 cycles/min.

Some other interesting wave phenomena are shown in figure 49 for a flight at an altitude of about 10 700 m (≈35 000 ft) that was categorized in reference 9 as being predominantly influenced by jet-stream effects, but in the presence of mountain waves. The time histories clearly show the very long wavelength (low-frequency) effects of shear on the horizontal components (especially noticeable in fig. 49(d)) with the shorter waves present on all components. The turbulence intensity ranged from light to very light.

REFERENCES

1. Houbolt, John C.; Steiner, Roy; and Pratt, Kermit G.: Dynamic Response of Airplanes to Atmospheric Turbulence Including Flight Data on Input and Response. NASA TR R-199, 1964.

2. Murrow, Harold N.; and Rhyne, Richard H.: The MAT Project - Atmospheric Turbulence Measurements With Emphasis on Long Wavelengths. Proceedings of the Sixth Conference on Aerospace and Aeronautical Meteorology of the American Meteorological Society, Nov. 1974, pp. 313-316.

3. Mark, William D.; and Fischer, Raymond W.: Investigation of the Effects of Nonhomogeneous (or Nonstationary) Behavior on the Spectra of Atmospheric Turbulence. NASA CR-2745, 1976.

4. Keisler, Samuel R.; and Rhyne, Richard H.: An Assessment of Prewhitening in Estimating Power Spectra of Atmospheric Turbulence at Long Wavelengths. NASA TN D-8288, 1976.

5. Rhyne, Richard H.: Flight Assessment of an Atmospheric Turbulence Measurement System with Emphasis on Long Wavelengths. NASA TN D-8315, 1976.

6. Rhyne, Richard H.; Murrow, Harold N.; and Sidwell, Kenneth: Atmospheric Turbulence Power Spectral Measurements to Long Wavelengths for Several Meteorological Conditions. Aircraft Safety and Operating Problems, NASA SP-416, 1976, pp. 271-286.

7. Waco, David E.: Mesoscale Wind and Temperature Fields Related to an Occurrence of Moderate Turbulence Measured in the Stratosphere Above Death Valley. Mon. Weather Rev., vol. 106, no. 6, June 1978, pp. 850-858.

8. Davis, Richard E.; Champine, Robert A.; and Ehernberger, L. J.: Meteorological and Operation Aspects of 46 Clear Air Turbulence Sampling Missions With an Instrumented B-57B Aircraft, Volume I - Program Summary. NASA TM-80044, 1979.

9. Waco, David E.: Meteorological and Operational Aspects of 46 Clear Air Turbulence Sampling Missions With an Instrumented B-57B Aircraft, Volume II (Appendix C) - Turbulence Missions. NASA TM-80045, 1979.

10. Meissner, Charles W., Jr.: A Flight Instrumentation System for Acquisition of Atmospheric Turbulence Data. NASA TN D-8314, 1976.

11. Otnes, Robert K.; and Enochson, Loren: Digital Time Series Analysis. John Wiley & Sons, Inc., c.1972.

12. Airplane Strength and Rigidity - Flight Loads. Mil. Specif. MIL-A-008861A (USAF), Mar. 31, 1971.

13. Sidwell, Kenneth: A Mathematical Study of a Random Process Proposed as an Atmospheric Turbulence Model. NASA CR-145200, 1977.

14. Sidwell, Kenneth: A Qualitative Assessment of a Random Process Proposed as an Atmospheric Turbulence Model. NASA CR-145247, 1977.

15. Mark, William D.: Characterization of Nongaussian Atmospheric Turbulence for Prediction of Aircraft Response Statistics. NASA CR-2913, 1977.

16. Mark, William D.; and Fischer, Raymond W.: Statistics of Some Atmospheric Turbulence Records Relevant to Aircraft Response Calculations. NASA CR-3464, 1981.

17. Mark, William D.: Characterization, Parameter Estimation, and Aircraft Response Statistics of Atmospheric Turbulence. NASA CR-3463, 1981.

TABLE I.- PREDOMINANT METEOROLOGICAL CONDITION AND GENERAL GEOGRAPHICAL LOCATION FOR FLIGHT DATA RUNS PRESENTED

Flight	Number of data runs presented	Predominant meteorological condition (a)	Flight location (a)
Mountain-wave and/or orographic effects			
20	5	Appalachian Mountain wave	VA
28	3	Low-altitude wind shear and orographic effects	CA
29	3	Mountain-wave and low-level orographic effects; rotor zone	CA
30	2	Mountain wave	CA
33	1	Low-level orographic effects	CA
34	3	Low-level mountain wave	CA
39	6	Mountain wave and intense upper front	CA
Wind-shear and/or jet-stream effects			
24	3	Strong vertical and horizontal wind shears below jet stream	VA
27	1	Low-level jet stream with vertical wind shear below	VA
38	3	Short-wave-trough movement	CA
41	2	Fast-moving wave trough with vertical and horizontal wind shears	CA
Special cases			
8	1	Low-altitude convection	VA
32	4	Complex orographic effects; vertical wind shear; jet stream (Death Valley flight)	CA
42	6	Low-altitude convection and sea-breeze convergence	CA

[a]Information for this column is taken from reference 8.

TABLE II.- TEST CONDITIONS AND MEASURED STATISTICAL DATA

(a) Turbulence data according to mountain-wave and/or orographic effects

Figure	Data run	Mean altitude	Data-run length		Statistical dof for power spectra	σ_w	σ_v	σ_u
		m (ft)	Distance, km (ft)	Time, sec	(a)	m/sec (ft/sec)	m/sec (ft/sec)	m/sec (ft/sec)
Flight 20 on December 3, 1974; 16:46 to 18:59 GMT								
4	1	1 924 (6 311)	94.9 (311 352)	680.00	27	2.22 (7.28)	1.98 (6.48)	3.79 (12.42)
5	2	1 891 (6 205)	74.6 (244 751)	549.95	21	1.44 (4.74)	1.44 (4.73)	2.45 (8.05)
6	3	1 882 (6 173)	93.9 (308 071)	686.00	27	1.87 (6.13)	2.34 (7.68)	3.21 (10.53)
7	4	1 899 (6 231)	55.6 (182 415)	419.00	16	1.65 (5.42)	3.59 (11.77)	2.24 (7.35)
8	5	1 920 (6 298)	44.0 (144 357)	333.00	13	1.59 (5.22)	3.60 (11.80)	2.90 (9.50)
Flight 28 on February 14, 1975; 13:22 to 15:31 GMT								
9	4	1 537 (5 042)	88.0 (288 714)	646.00	25	1.50 (4.92)	3.07 (10.08)	2.04 (6.68)
10	6	1 897 (6 223)	68.6 (225 066)	496.00	19	1.41 (4.62)	2.61 (8.56)	2.19 (7.19)
11	8	1 157 (3 796)	124.8 (409 449)	912.00	36	1.92 (6.29)	4.17 (13.67)	3.94 (12.94)
Flight 29 on February 20, 1975; 19:07 to 21:38 GMT								
12	6	10 432 (34 225)	98.2 (322 178)	537.00	21	1.10 (3.61)	5.20 (17.07)	3.51 (11.50)
13	7	7 152 (23 464)	190.8 (625 984)	1018.00	40	1.07 (3.51)	1.92 (6.31)	2.08 (6.82)
14	8	1 151 (3 777)	106.3 (348 753)	796.00	31	1.73 (5.66)	6.43 (21.09)	3.15 (10.33)

[a]See reference 11.

TABLE II.- Continued

(a) Concluded

Figure	Data run	Mean altitude	Data-run length		Statistical dof for power spectra	σ_w	σ_v	σ_u
		m (ft)	Distance, km (ft)	Time, sec	(a)	m/sec (ft/sec)	m/sec (ft/sec)	m/sec (ft/sec)
Flight 30 on March 7, 1975; 21:42 to 00:47 GMT								
15	4	14 114 (46 306)	18.1 (59 383)	91.00	4	0.68 (2.23)	2.56 (8.40)	1.03 (3.38)
16	8	14 265 (46 800)	148.7 (487 861)	754.40	29	1.34 (4.41)	5.39 (17.69)	4.30 (14.11)
Flight 33 on March 28, 1975; 18:47 to 20:48 GMT								
17	2	2 638 (8 656)	89.00 (291 995)	592.00	23	1.27 (4.16)	3.45 (11.33)	3.90 (12.80)
Flight 34 on April 4, 1975; 18:50 to 21:30 GMT								
18	3	4 342 (14 245)	55.6 (182 415)	306.15	12	2.05 (6.71)	3.78 (12.39)	2.64 (8.66)
19	5	3 874 (12 709)	59.7 (195 866)	332.00	13	2.34 (7.68)	4.84 (15.87)	2.80 (9.19)
20	7	3 892 (12 770)	88.5 (290 354)	485.95	19	3.82 (12.52)	5.51 (18.09)	3.58 (11.73)
Flight 39 on May 20, 1975; 18:13 to 20:26 GMT								
21	2	3 210 (10 532)	60.6 (198 819)	338.50	13	1.06 (3.48)	2.38 (7.80)	4.81 (15.79)
22	3	4 127 (13 539)	45.4 (148 950)	248.00	10	0.96 (3.16)	2.48 (8.15)	4.70 (15.43)
23	5	4 135 (13 566)	86.0 (282 152)	456.00	18	1.08 (3.54)	4.04 (13.25)	4.16 (13.65)
24	7	4 180 (13 715)	77.7 (254 921)	406.95	16	1.12 (3.67)	3.19 (10.45)	6.65 (21.83)
25	9	4 208 (13 805)	108.9 (357 283)	561.00	22	1.42 (4.65)	7.01 (23.00)	3.02 (9.92)
26	10	4 157 (13 638)	19.2 (62 992)	100.05	4	2.08 (6.83)	4.63 (15.19)	3.65 (11.98)

[a]See reference 11.

TABLE II.- Continued

(b) Turbulence data according to wind-shear and/or jet-stream effects

Figure	Data run	Mean altitude	Data-run length		Statistical dof for power spectra	σ_w	σ_v	σ_u
		m (ft)	Distance, km (ft)	Time, sec	(a)	m/sec (ft/sec)	m/sec (ft/sec)	m/sec (ft/sec)
Flight 24 on December 17, 1974; 16:12 to 18:04 GMT								
27	6	5 903 (19 366)	83.3 (273 294)	457.00	18	0.46 (1.50)	2.31 (7.95)	2.35 (7.70)
28	7	5 891 (19 328)	98.7 (323 819)	535.00	21	0.48 (1.57)	3.04 (9.96)	3.96 (12.98)
29	9	5 904	[b]131.9 (432 743)	[b]715.00	[b]28	0.71 (2.32)	3.23 (10.59)	3.01 (9.89)
		(19 369)	[c]65.1 (213 583)	[c]353.00	[c]14			
Flight 27 on January 30, 1975; 15:48 to 18:07 GMT								
30	13	10 605 (34 793)	51.8 (169 948)	280.00	11	0.58 (1.90)	1.03 (3.39)	2.23 (7.30)
Flight 38 on April 24, 1975; 22:10 to 00:54 GMT								
31	5	10 637 (34 898)	63.58 (208 596)	337.00	13	0.75 (2.47)	2.83 (9.27)	2.41 (7.92)
32	6	10 705 (35 120)	132.4 (434 383)	694.00	27	0.67 (2.20)	3.10 (10.18)	1.70 (5.58)
33	7	10 649 (34 938)	145.7 (478 018)	780.95	31	0.89 (2.92)	5.18 (17.00)	4.78 (15.68)
Flight 41 on May 21, 1975; 21:50 to 00:34 GMT								
34	8	7 368 (24 172)	34.8 (114 173)	184.00	7	0.72 (2.37)	1.49 (4.89)	1.55 (5.09)
35	10	7 411 (24 314)	46.8 (153 543)	247.05	10	0.79 (2.60)	2.16 (7.09)	2.32 (7.61)

[a]See reference 11.
[b]Values for w data only.
[c]Values for v and u data.

TABLE II.- Concluded

(c) Special meteorological cases

Figure	Data run	Mean altitude	Data-run length		Statistical dof for power spectra	σ_w	σ_v	σ_u
		m (ft)	Distance, km (ft)	Time, sec	(a)	m/sec (ft/sec)	m/sec (ft/sec)	m/sec (ft/sec)
Flight 8 on June 19, 1974; 18:09 to 19:32 GMT								
36	2	460 (1 509)	147.6 (484 252)	1146.35	45	1.15 (3.78)	1.18 (3.86)	1.34 (4.41)
Flight 32 on March 26, 1975; 19:46 to 22:19 GMT								
37	2	12 989 (42 615)	115.8 (379 921)	634.00	25	2.24 (7.34)	8.41 (27.60)	3.33 (10.92)
38	3	13 056 (42 835)	65.1 (213 583)	367.00	14	2.04 (6.68)	4.72 (15.50)	3.17 (10.40)
39	4	12 984 (42 600)	136.8 (448 819)	728.80	28	2.45 (8.05)	7.32 (24.02)	4.47 (14.67)
40	7	13 070 (42 879)	130.6 (428 478)	699.00	27	1.52 (4.99)	8.75 (28.72)	5.70 (18.69)
Flight 42 on June 13, 1975; 18:11 to 20:17 GMT								
41	2	4 420 (14 500)	84.8 (278 215)	423.95	17	1.91 (6.28)	2.21 (7.25)	2.80 (9.20)
42	3	4 420 (14 500)	102.6 (336 614)	512.95	20	1.79 (5.86)	2.27 (7.46)	2.07 (6.80)
43	4	4 420 (14 500)	57.7 (189 304)	290.85	11	1.41 (4.63)	2.90 (9.53)	2.25 (7.39)
44	6	1 676 (5 500)	79.0 (259 186)	544.80	21	2.05 (6.74)	2.69 (8.81)	4.26 (13.99)
45	8	3 200 (10 500)	54.0 (177 165)	272.00	11	1.76 (5.76)	2.84 (9.33)	1.56 (5.12)
46	9	3 200 (10 500)	66.5 (218 176)	334.85	13	2.39 (7.83)	3.15 (10.34)	2.14 (7.01)

[a]See reference 11.

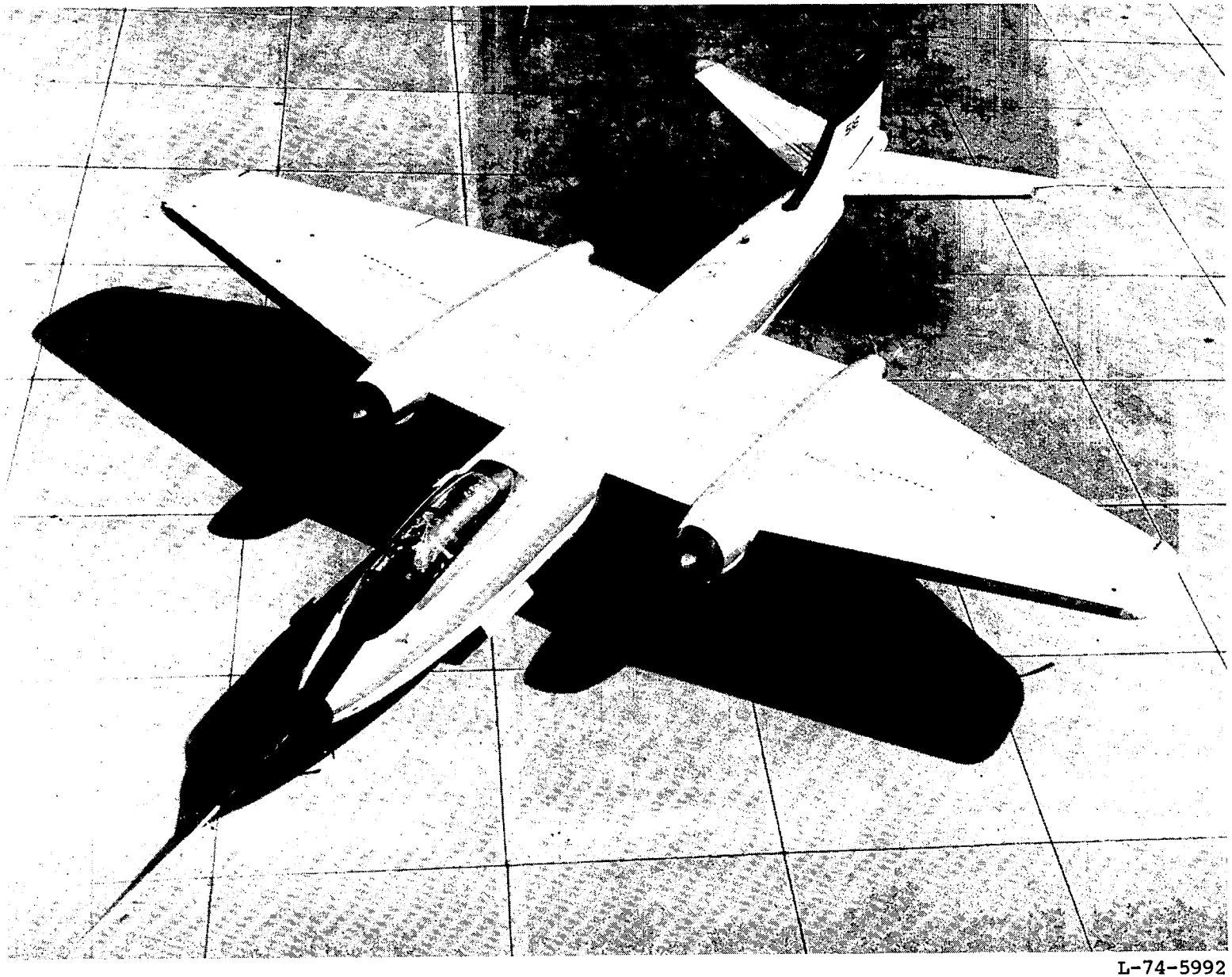

L-74-5992

Figure 1.- Photograph of the sampling airplane.

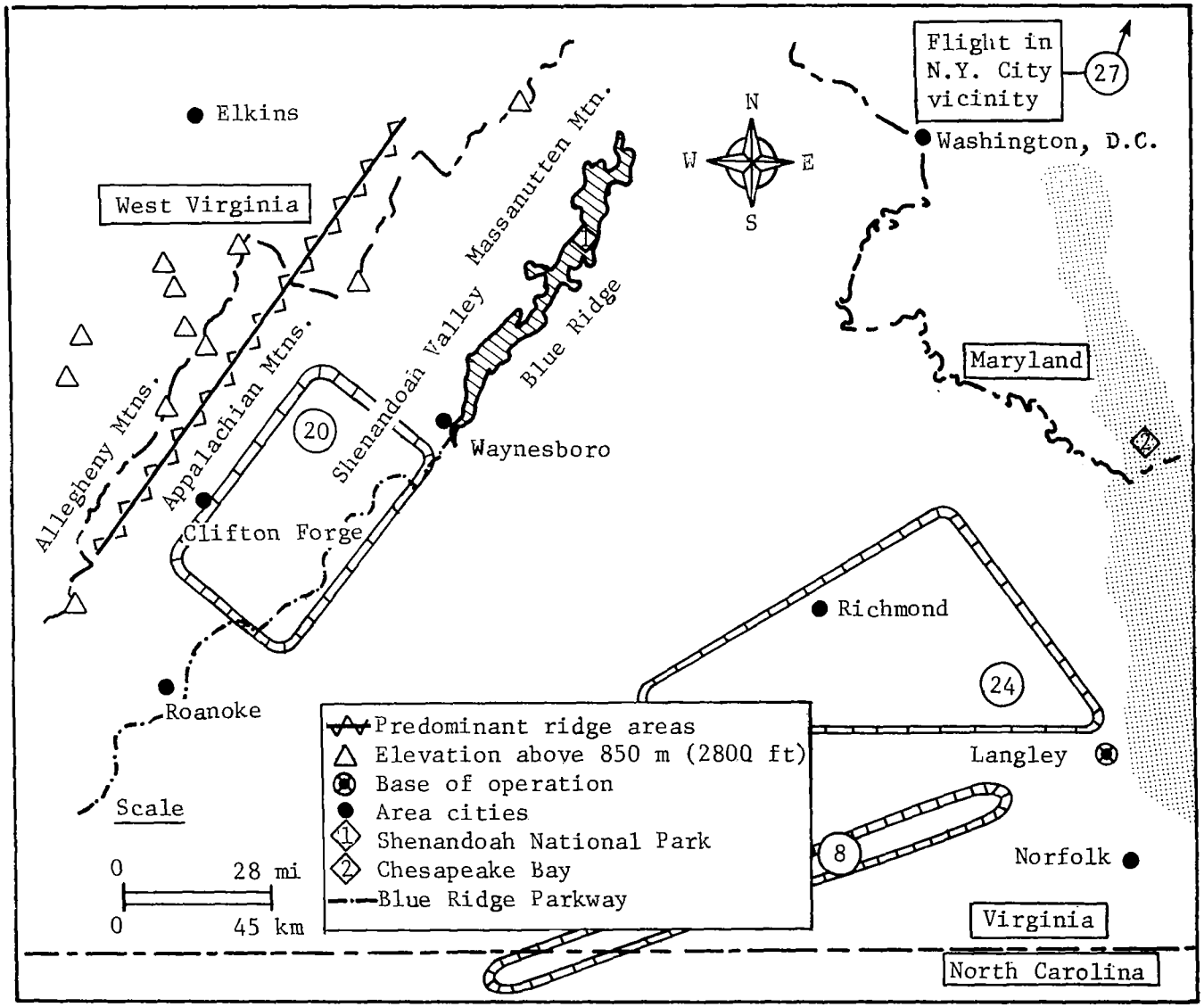

Figure 2.- Location of flight tracks for flights in the Eastern United States.

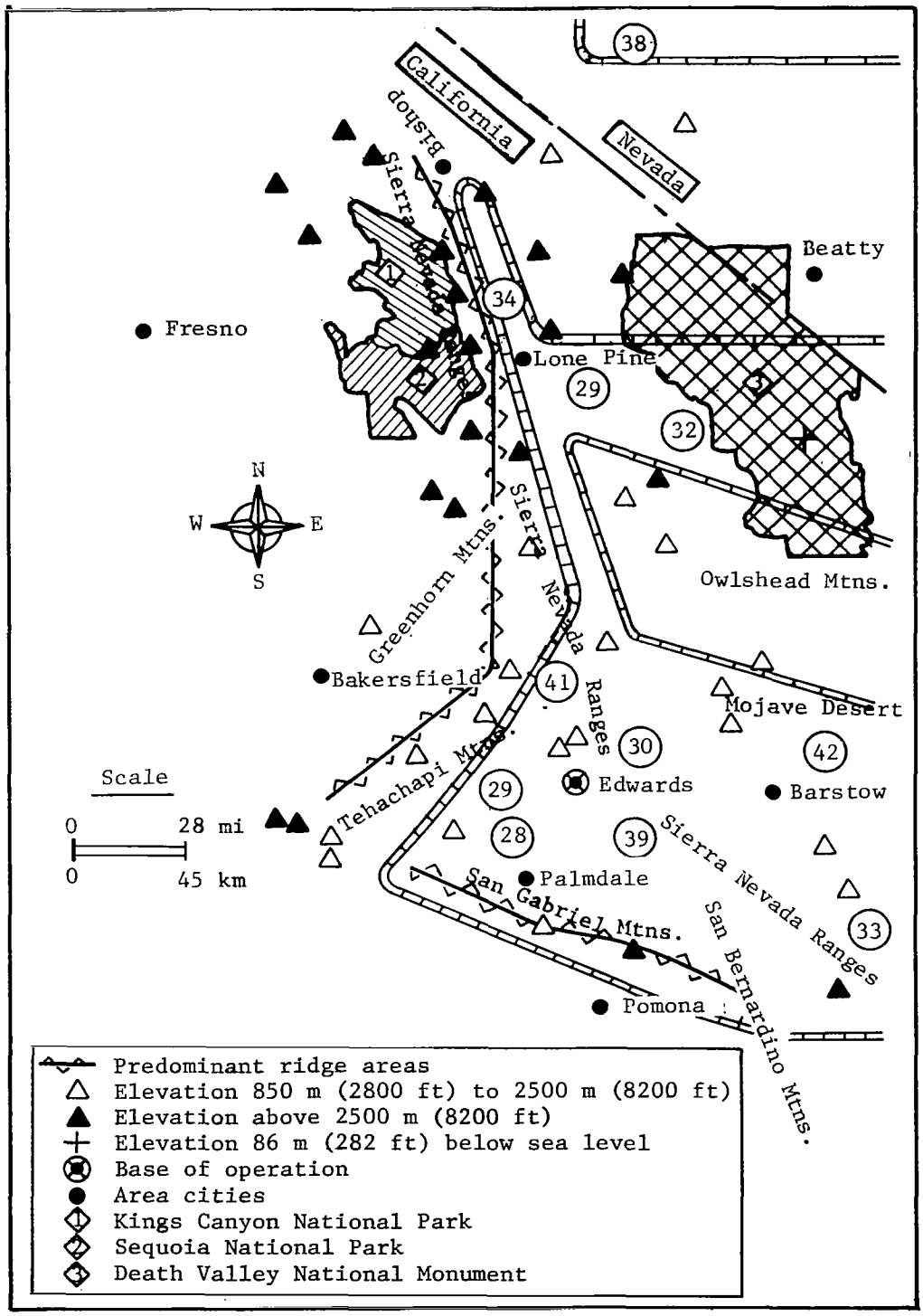

Figure 3.- Location of flight tracks for flights in the Western United States.

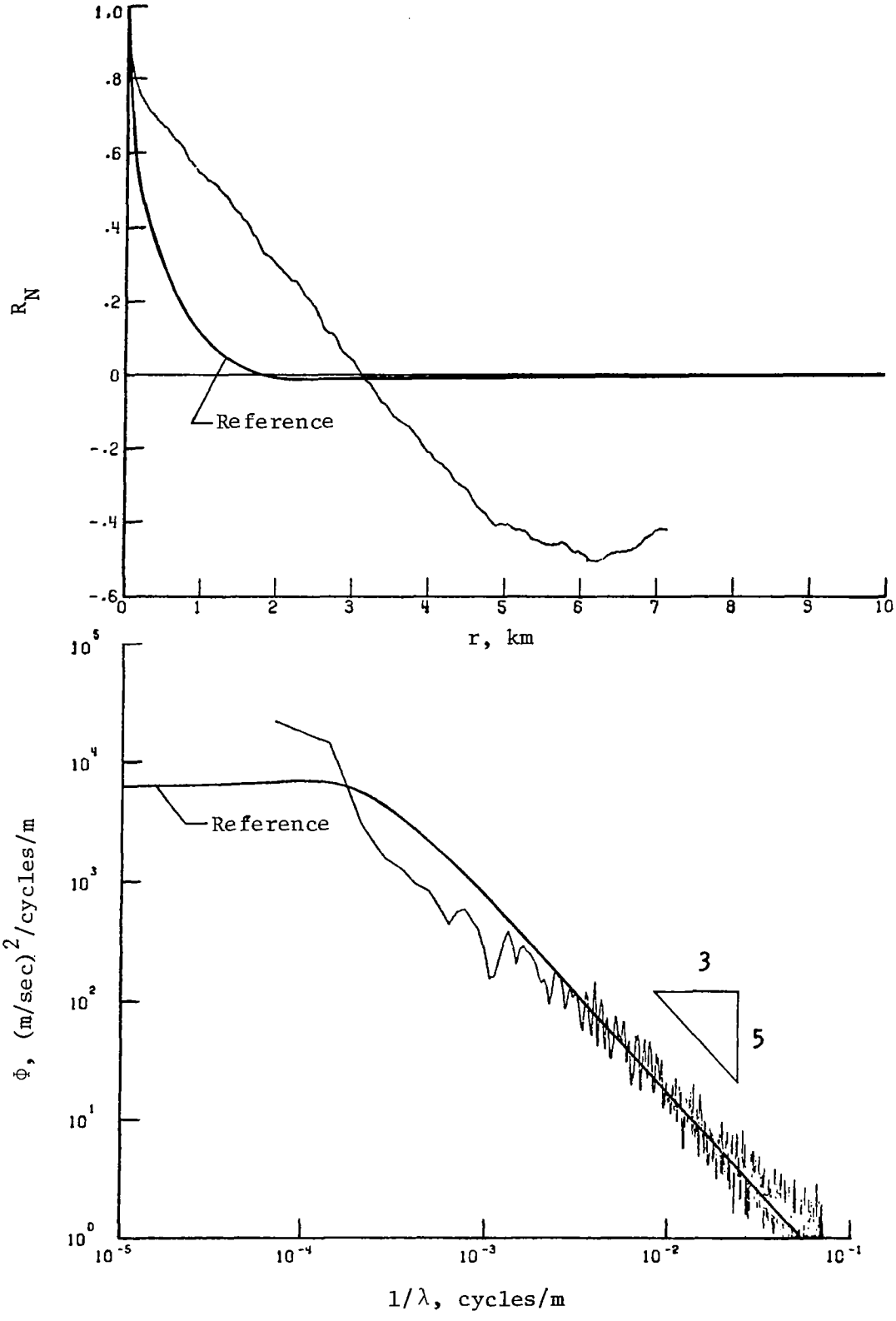

(a) Vertical component of gust velocity.

Figure 4.- Power spectra and autocorrelation functions for flight 20, run 1.

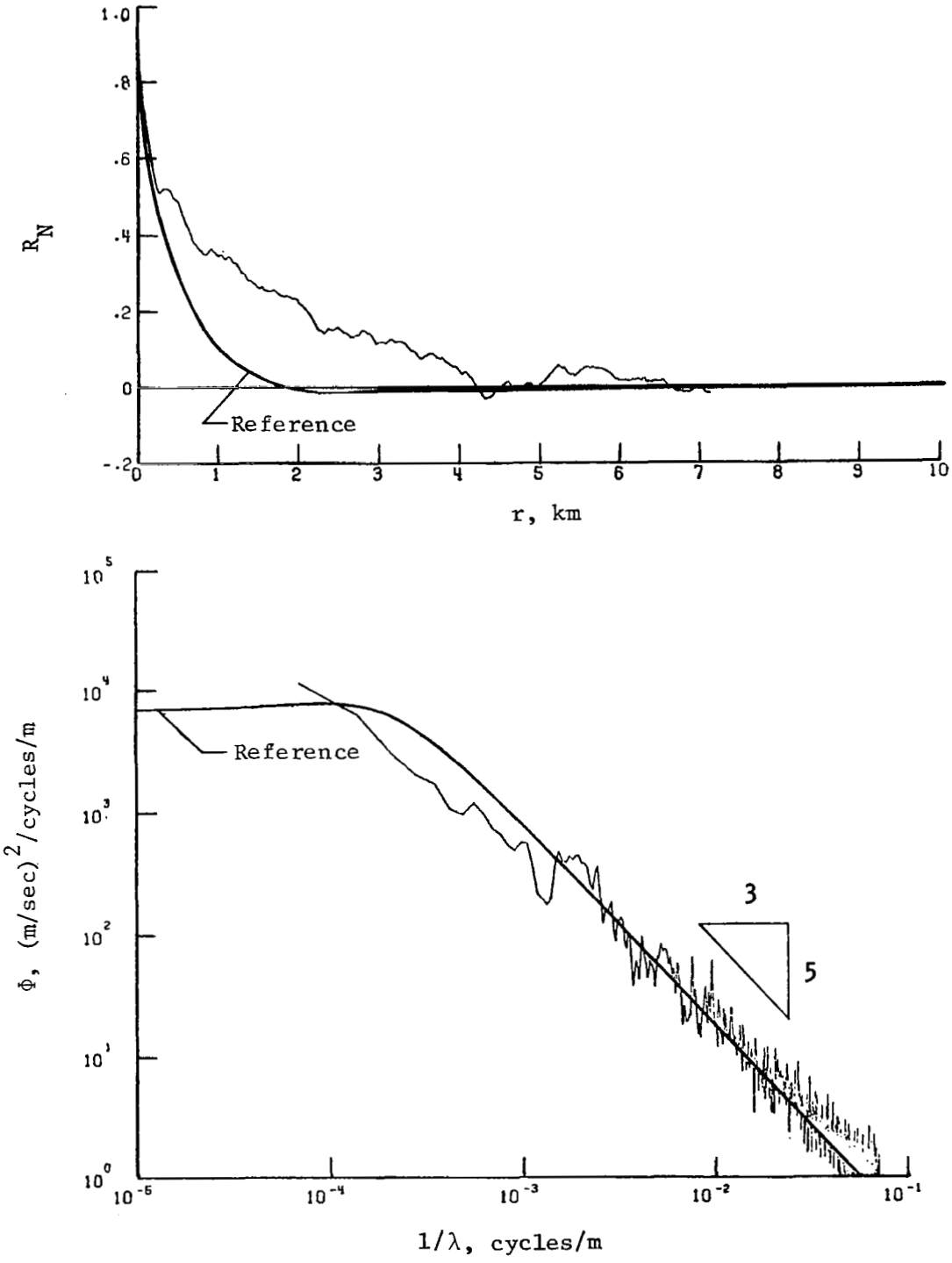

(b) Lateral component of gust velocity.

Figure 4.- Continued.

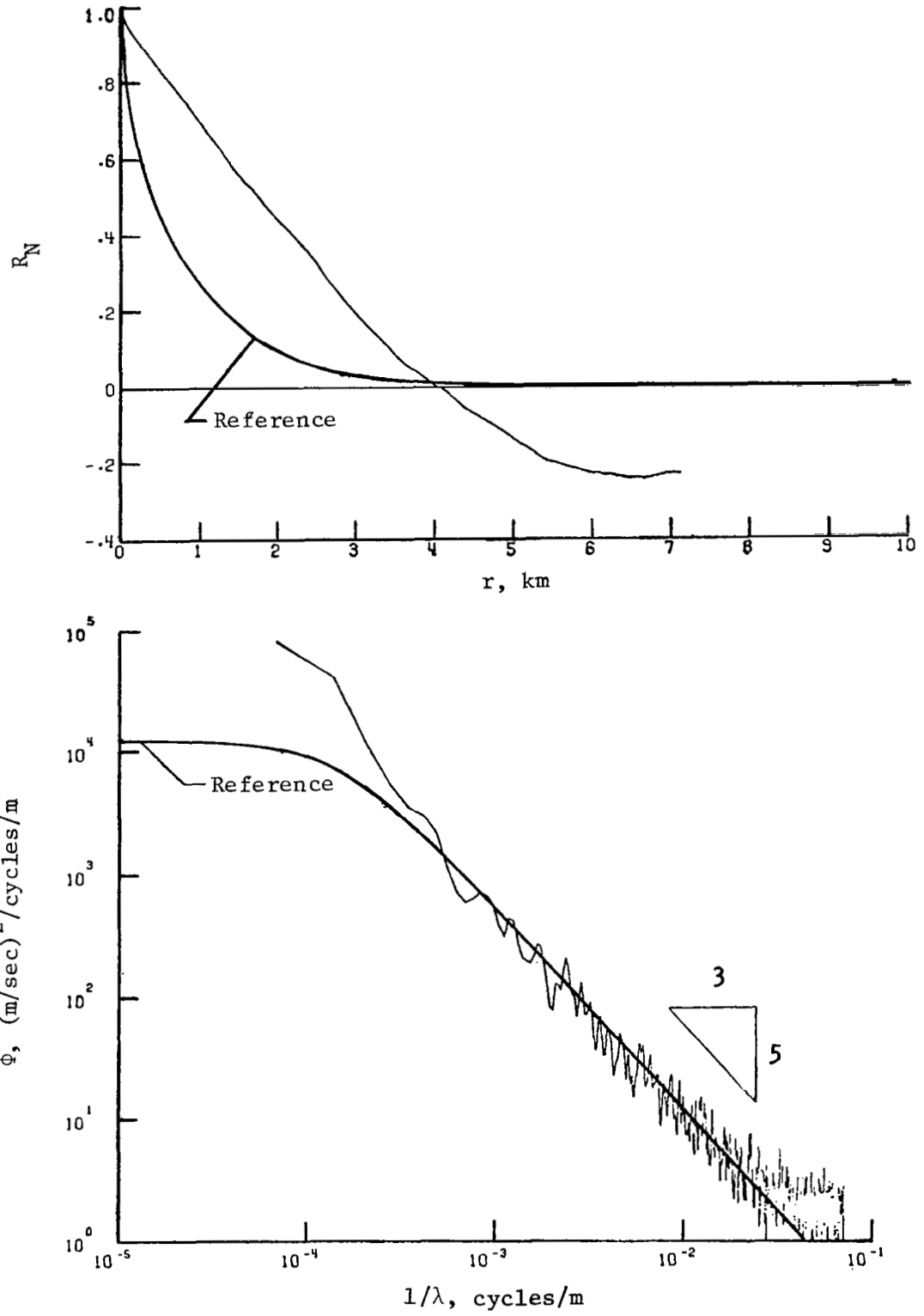

(c) Longitudinal component of gust velocity.

Figure 4.- Concluded.

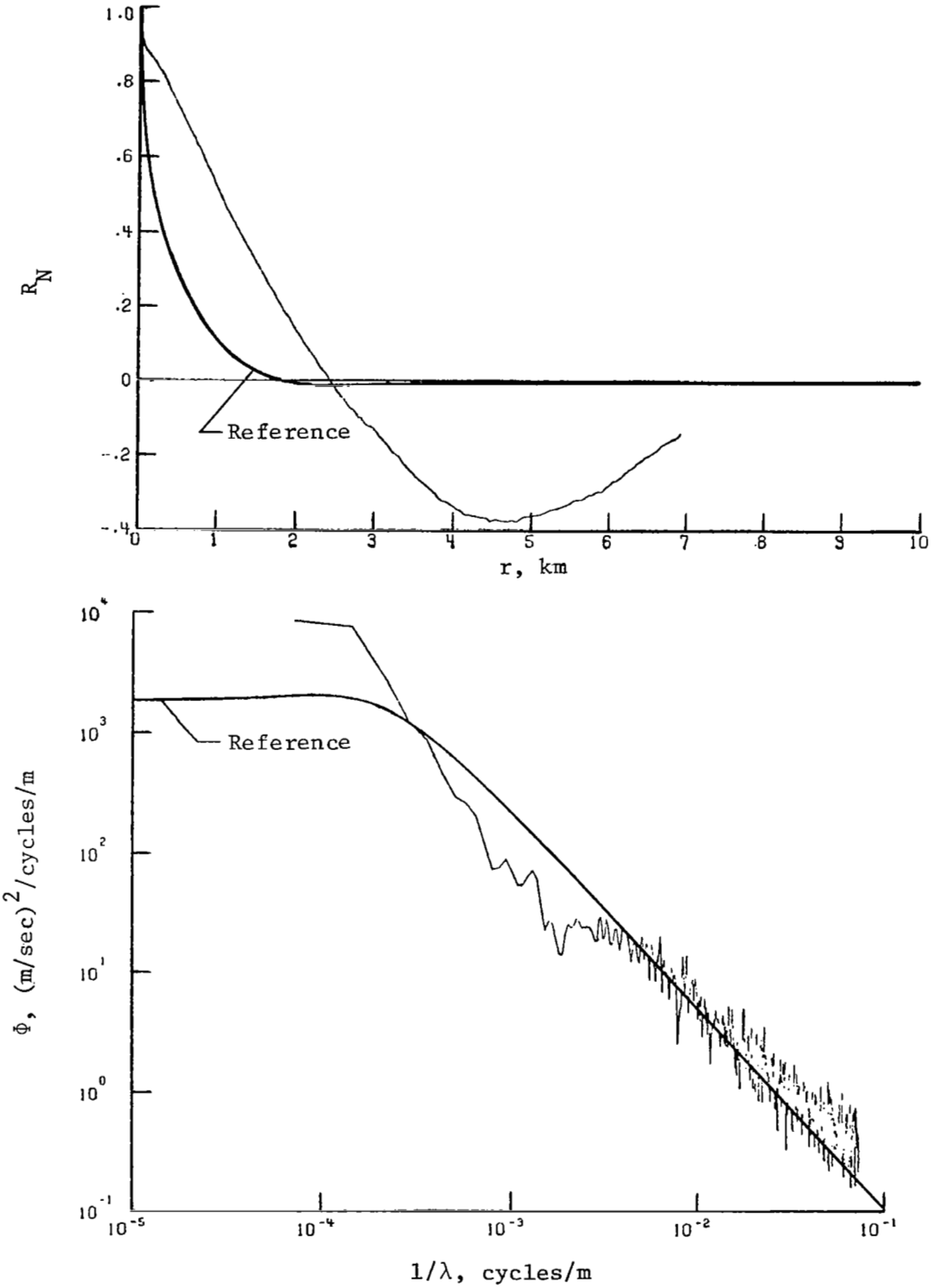

(a) Vertical component of gust velocity.

Figure 5.- Power spectra and autocorrelation functions for flight 20, run 2.

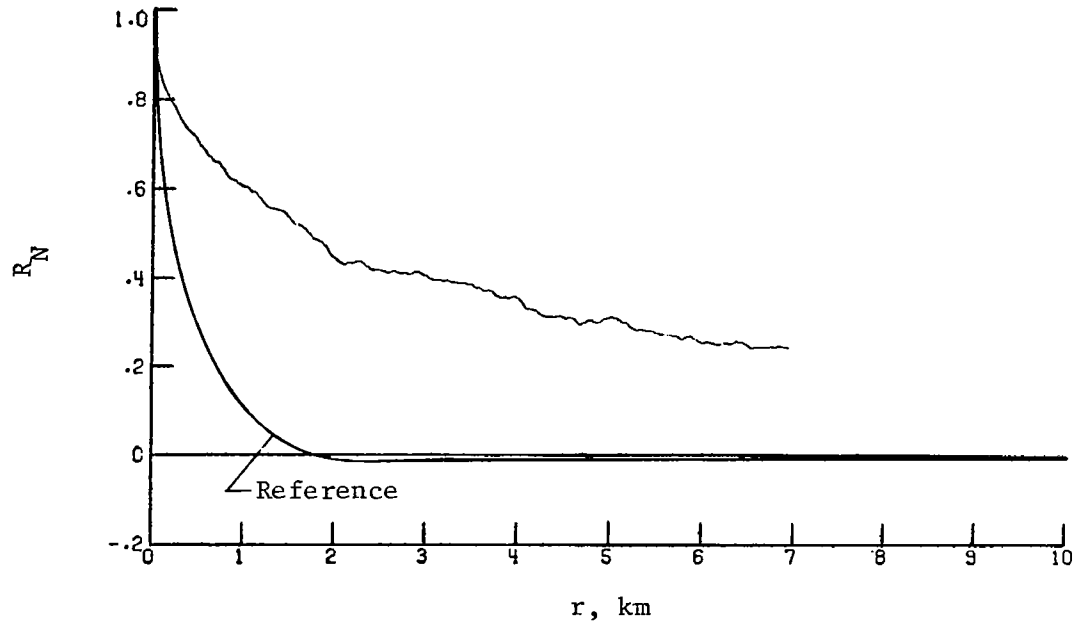

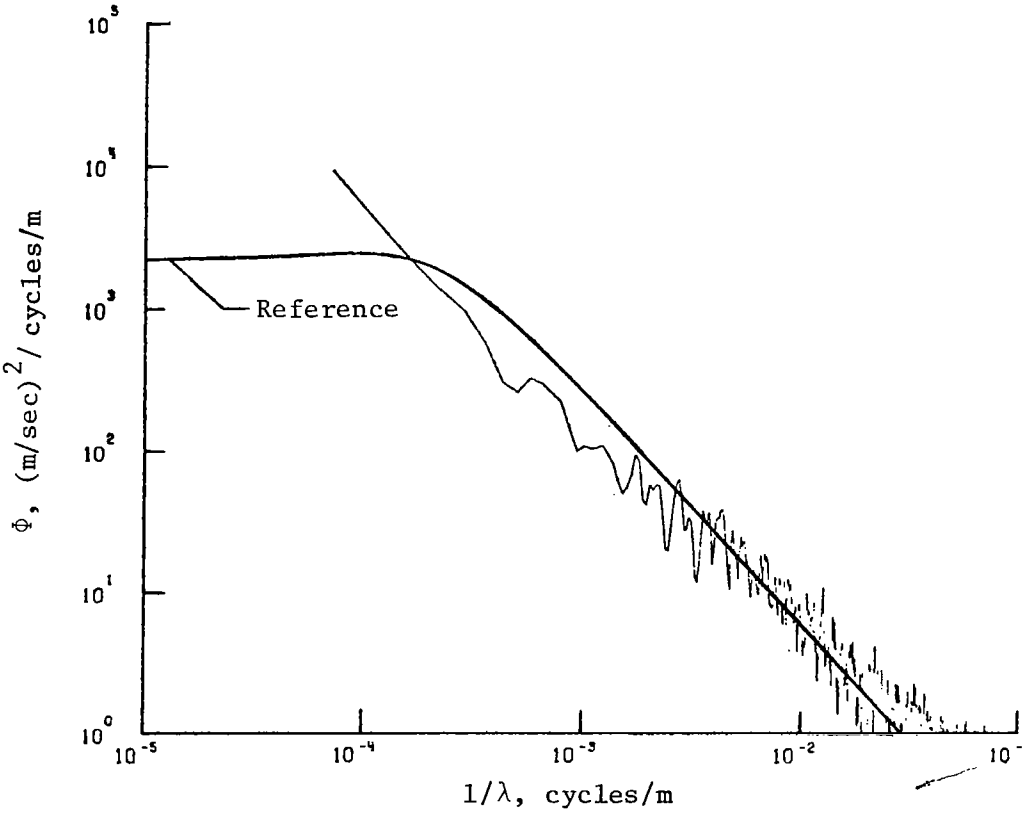

(b) Lateral component of gust velocity.

Figure 5.- Continued.

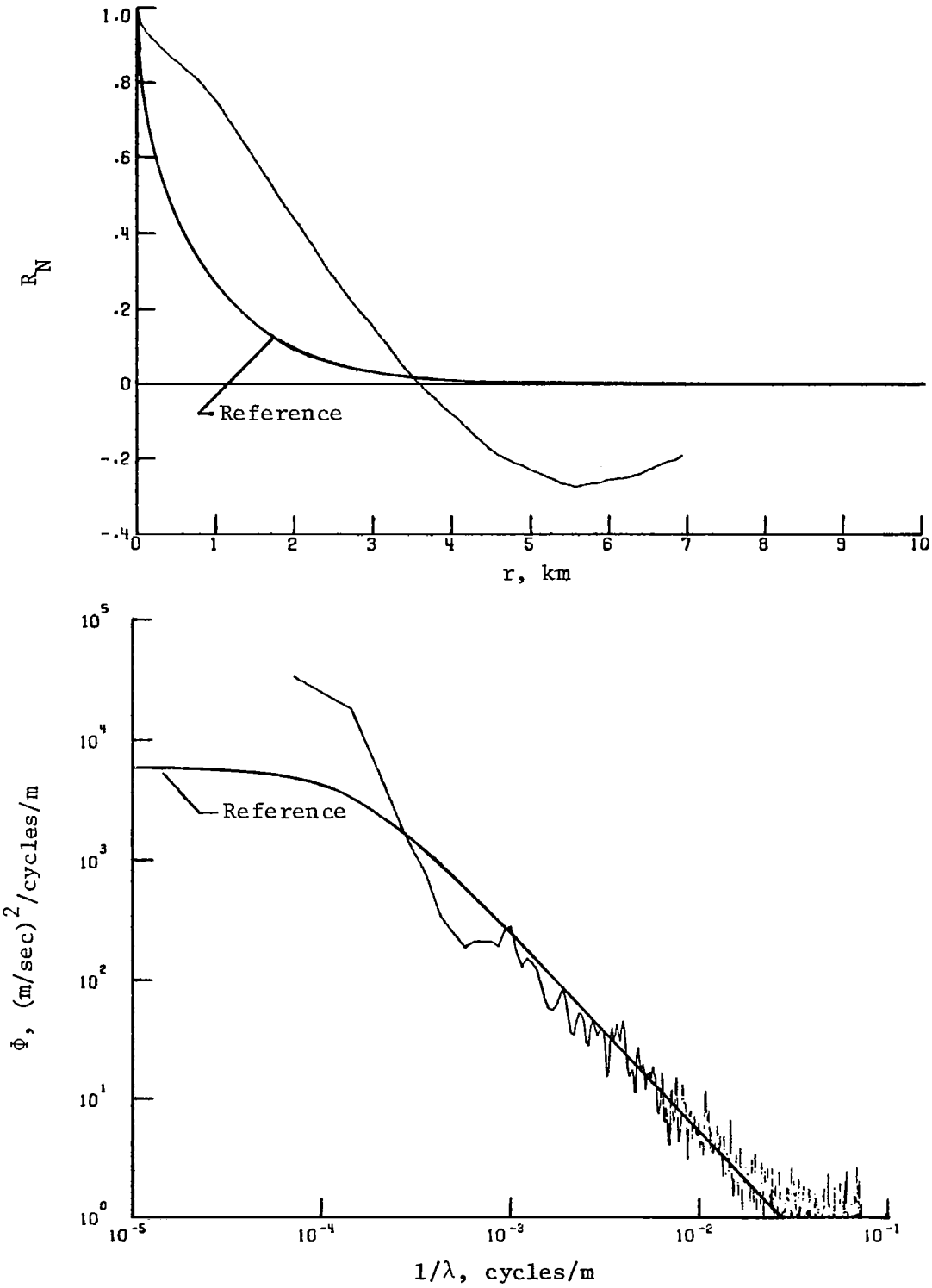

(c) Longitudinal component of gust velocity.

Figure 5.- Concluded.

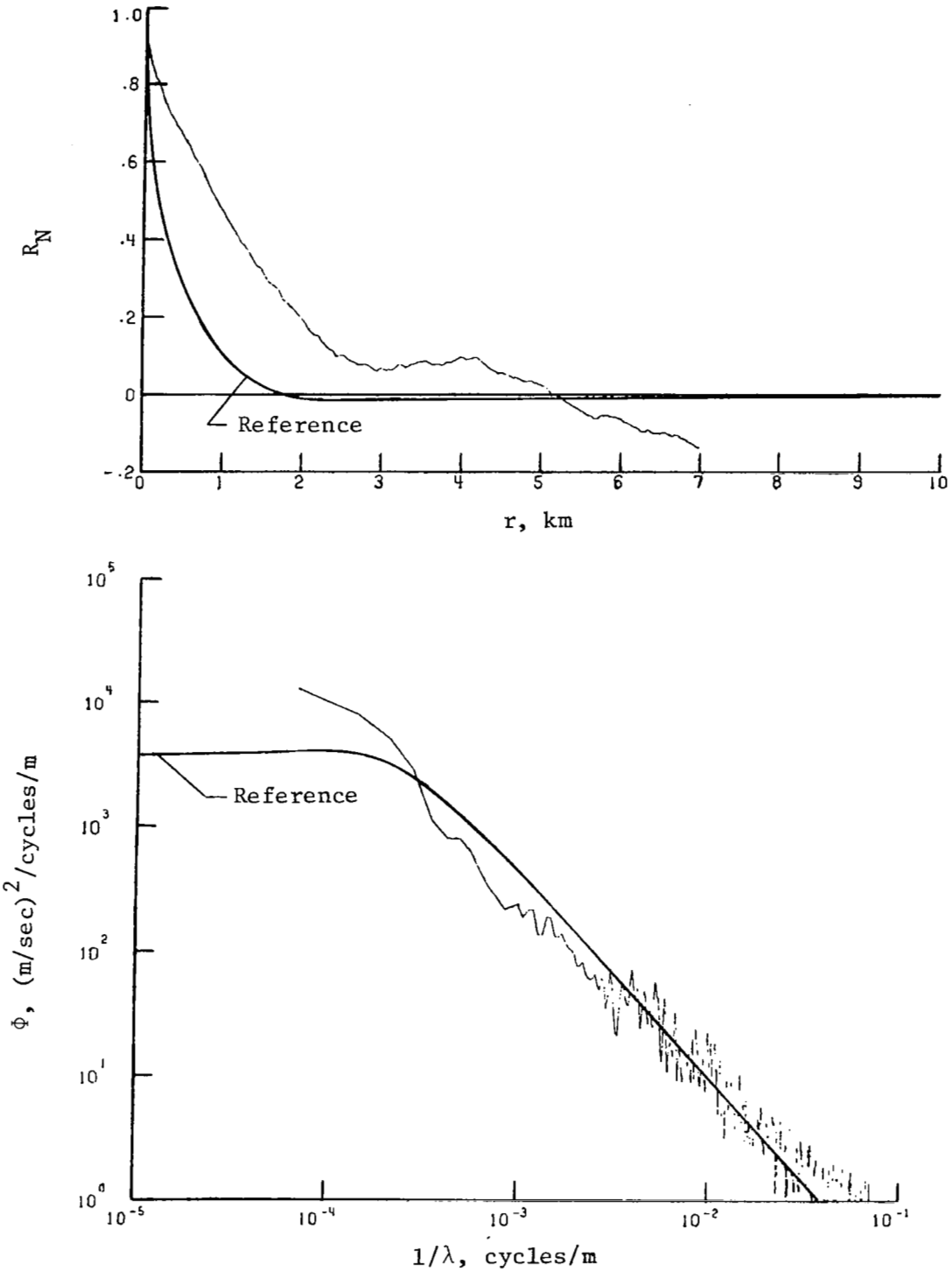

(a) Vertical component of gust velocity.

Figure 6.- Power spectra and autocorrelation functions for flight 20, run 3.

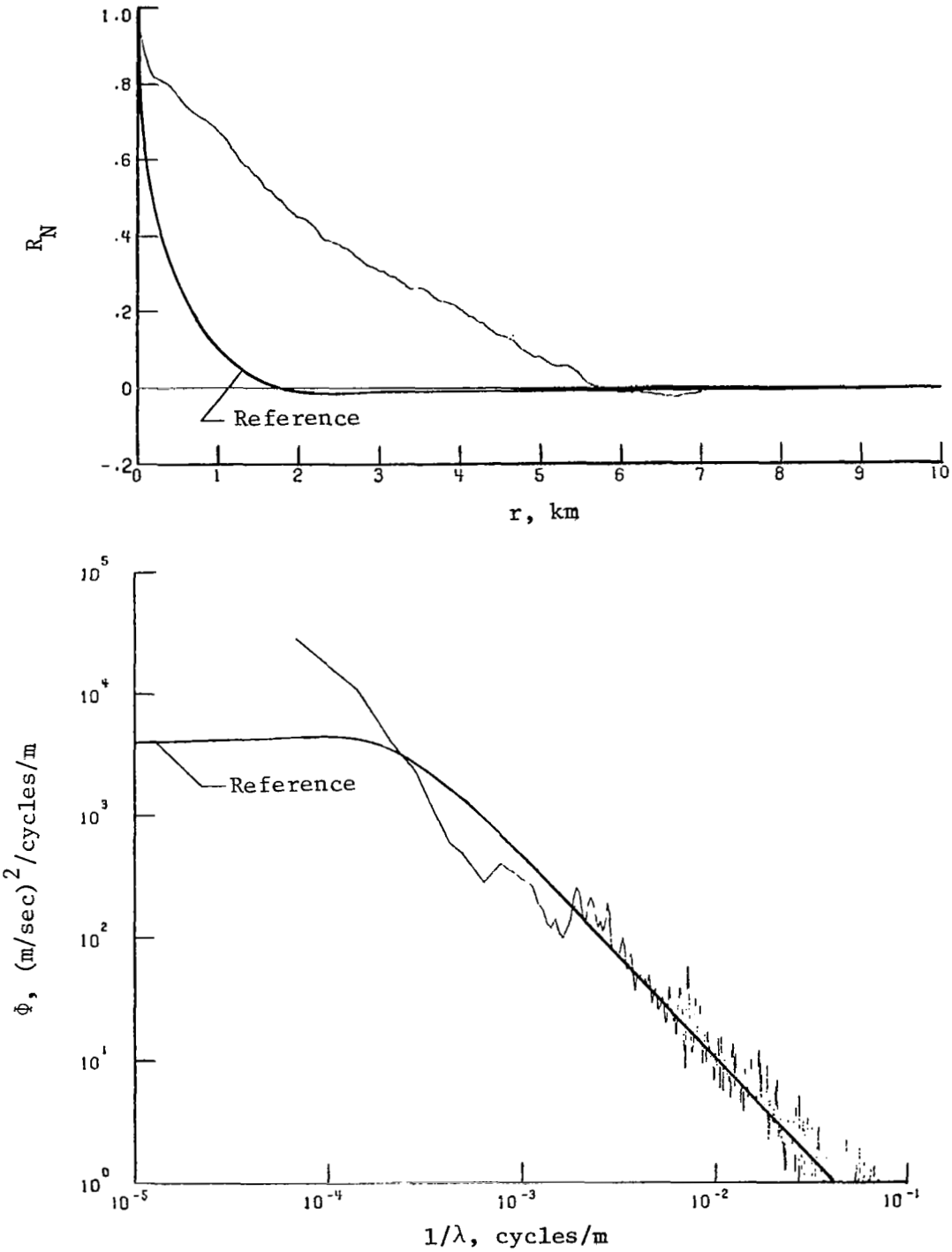

(b) Lateral component of gust velocity.

Figure 6.- Continued.

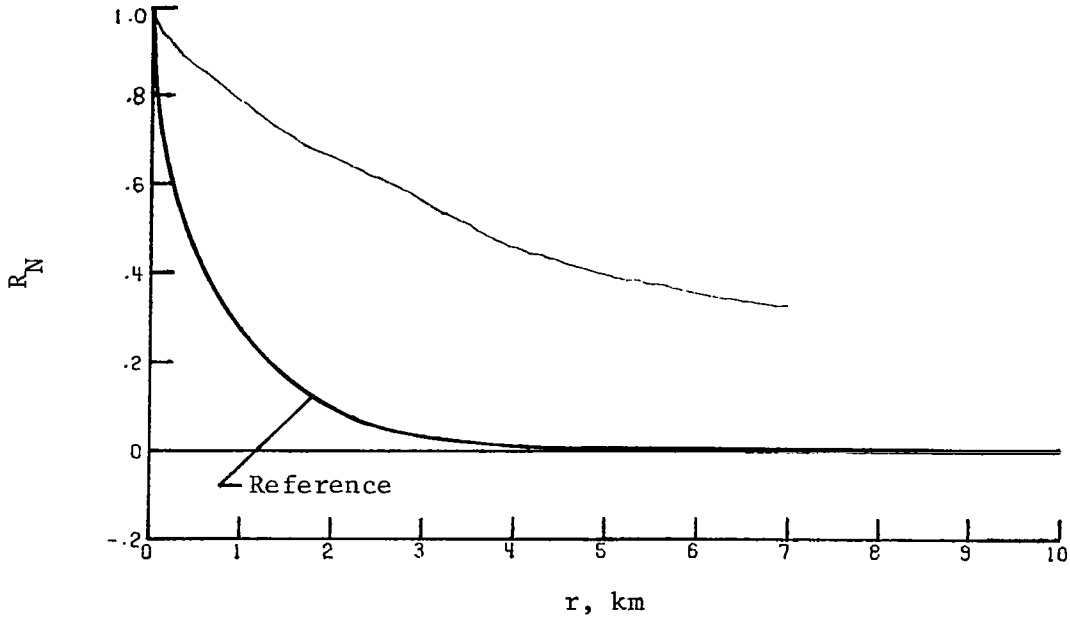

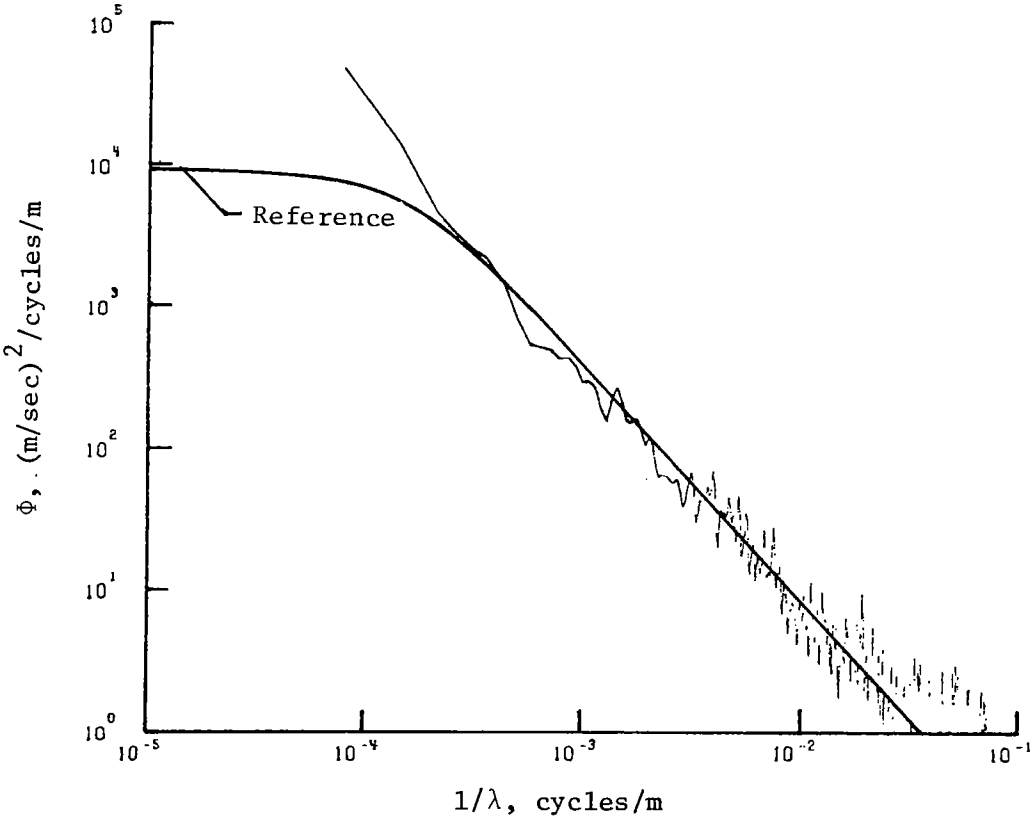

(c) Longitudinal component of gust velocity.

Figure 6.- Concluded.

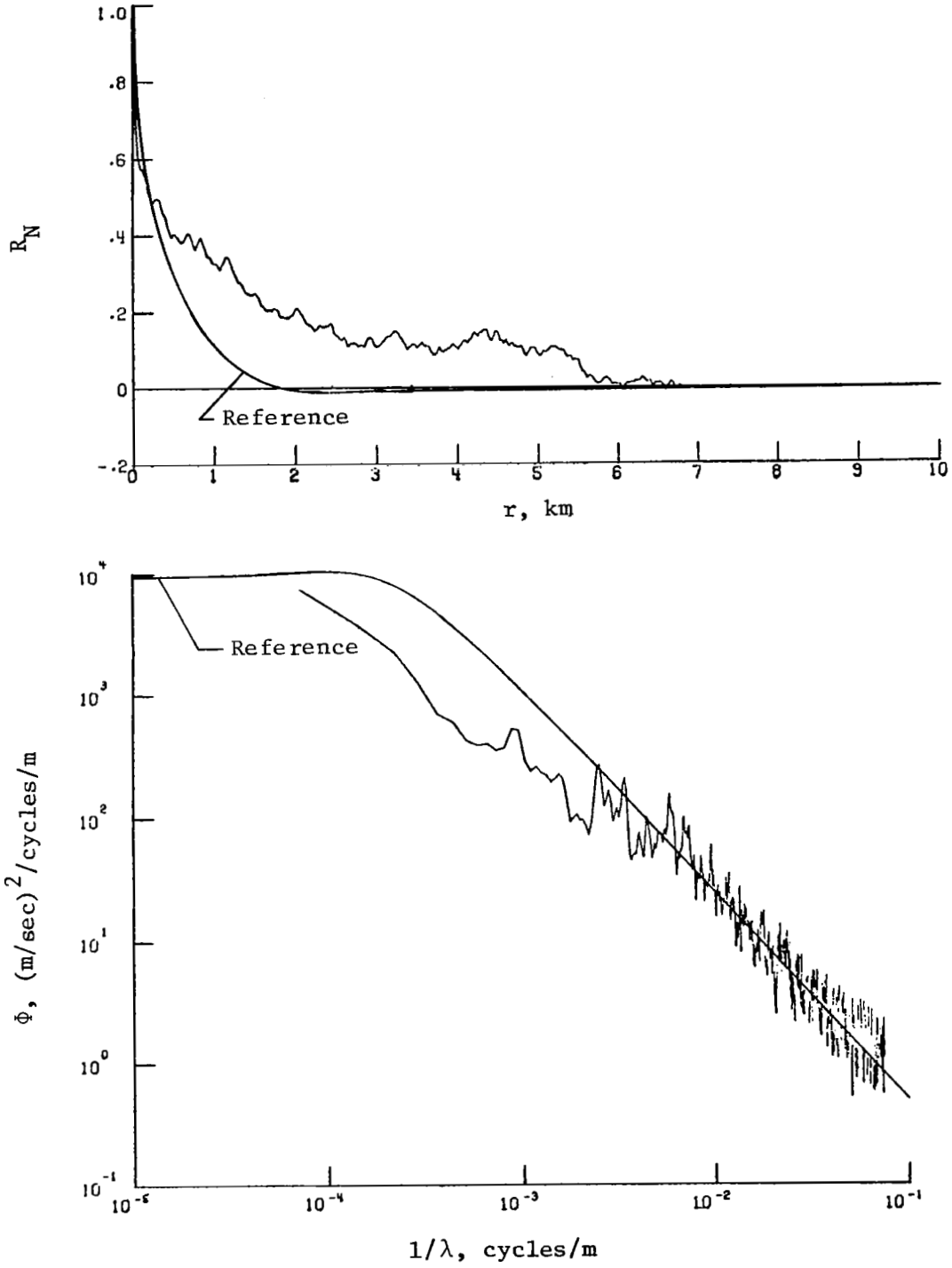

(a) Vertical component of gust velocity.

Figure 7.- Power spectra and autocorrelation functions for flight 20, run 4.

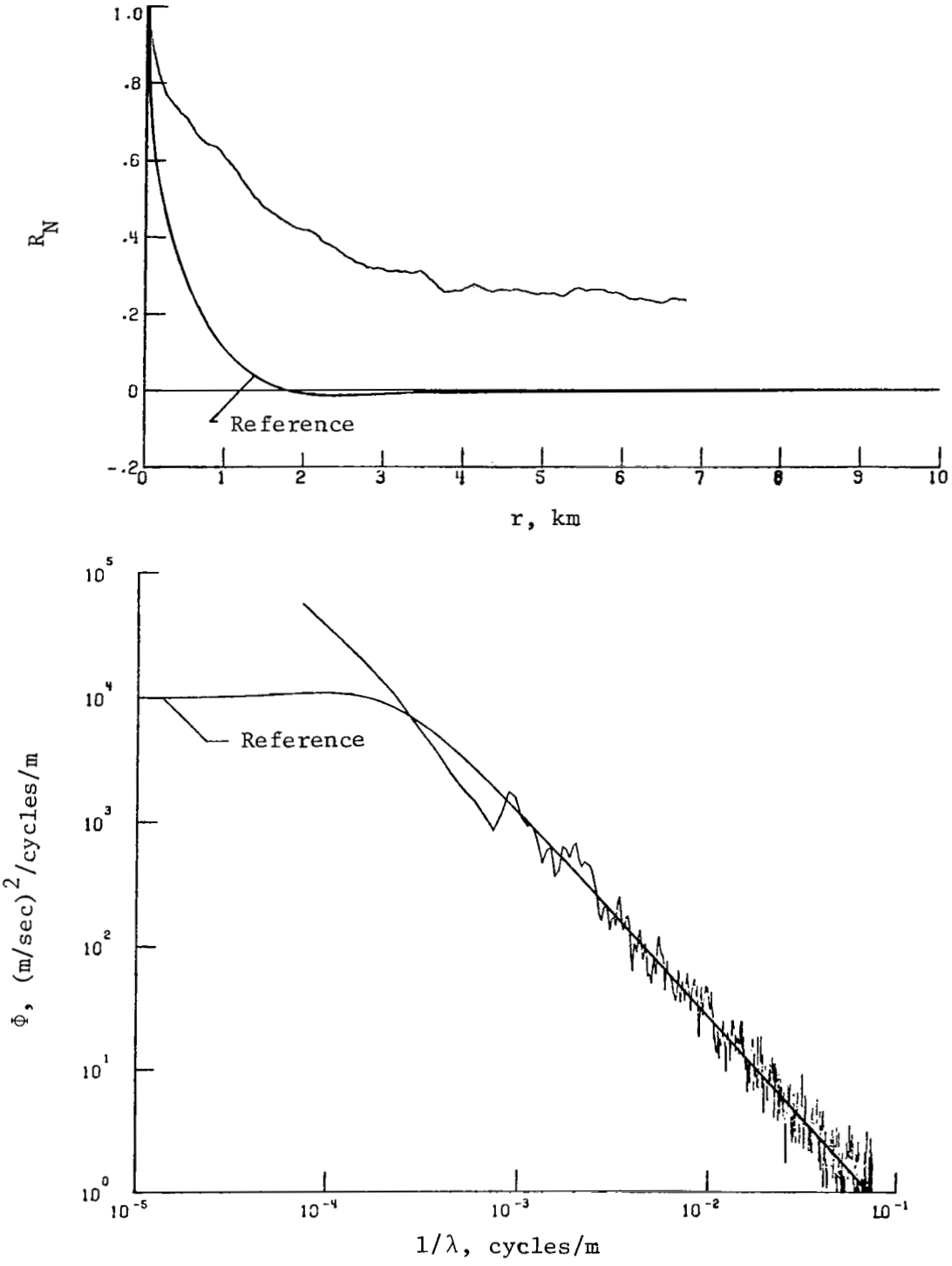

(b) Lateral component of gust velocity.

Figure 7.- Continued.

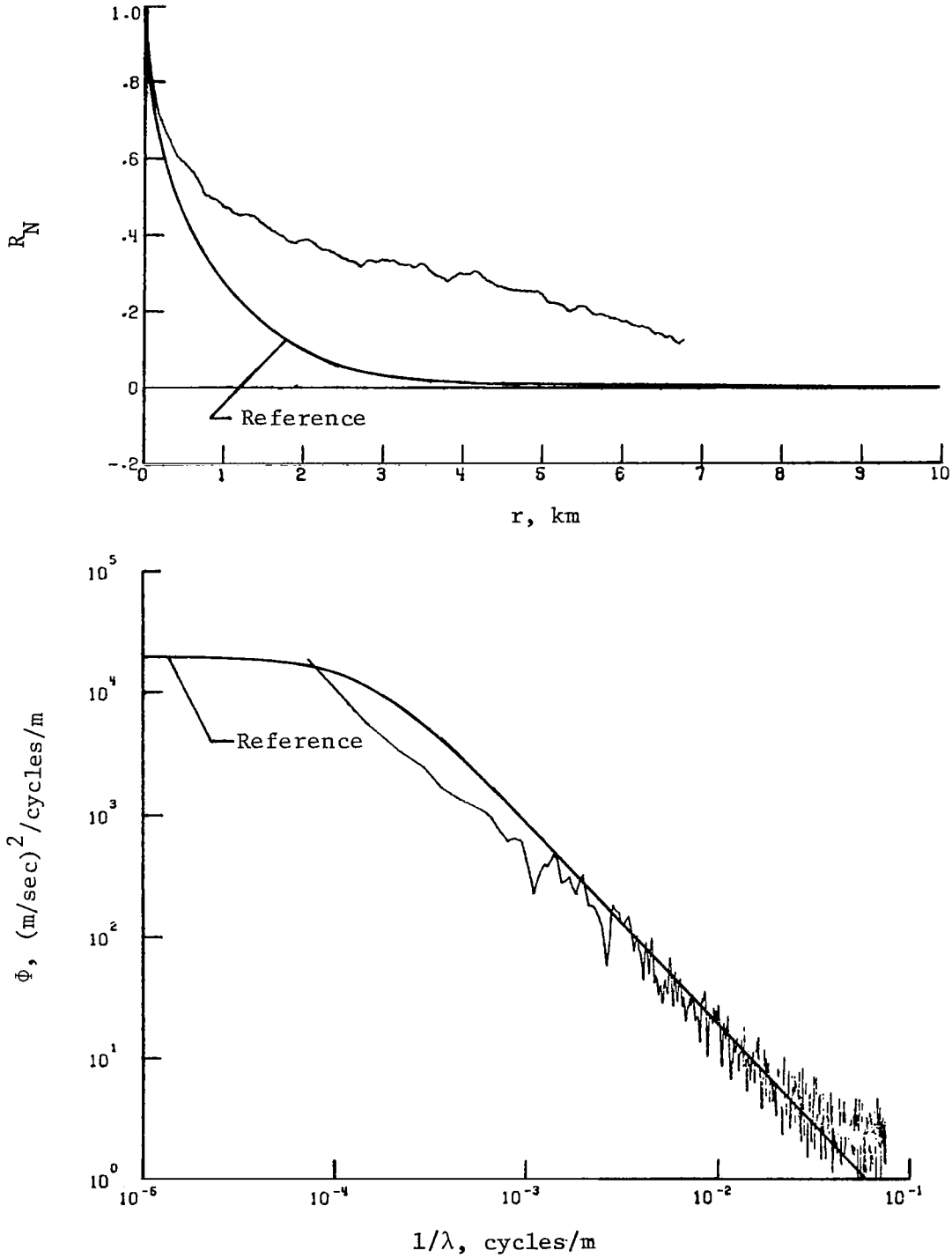

(c) Longitudinal component of gust velocity.

Figure 7.- Concluded.

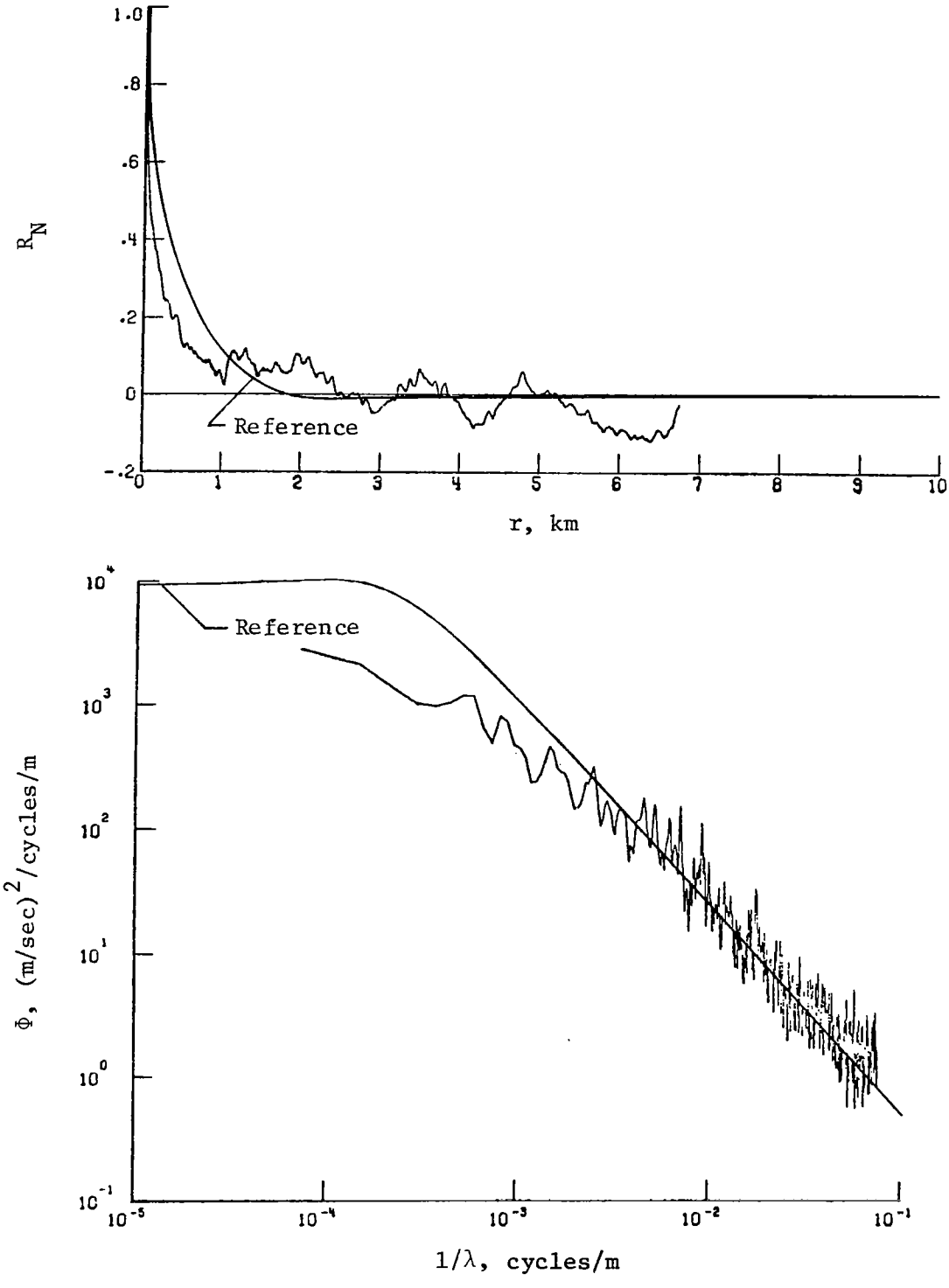

(a) Vertical component of gust velocity.

Figure 8.- Power spectra and autocorrelation functions for flight 20, run 8.

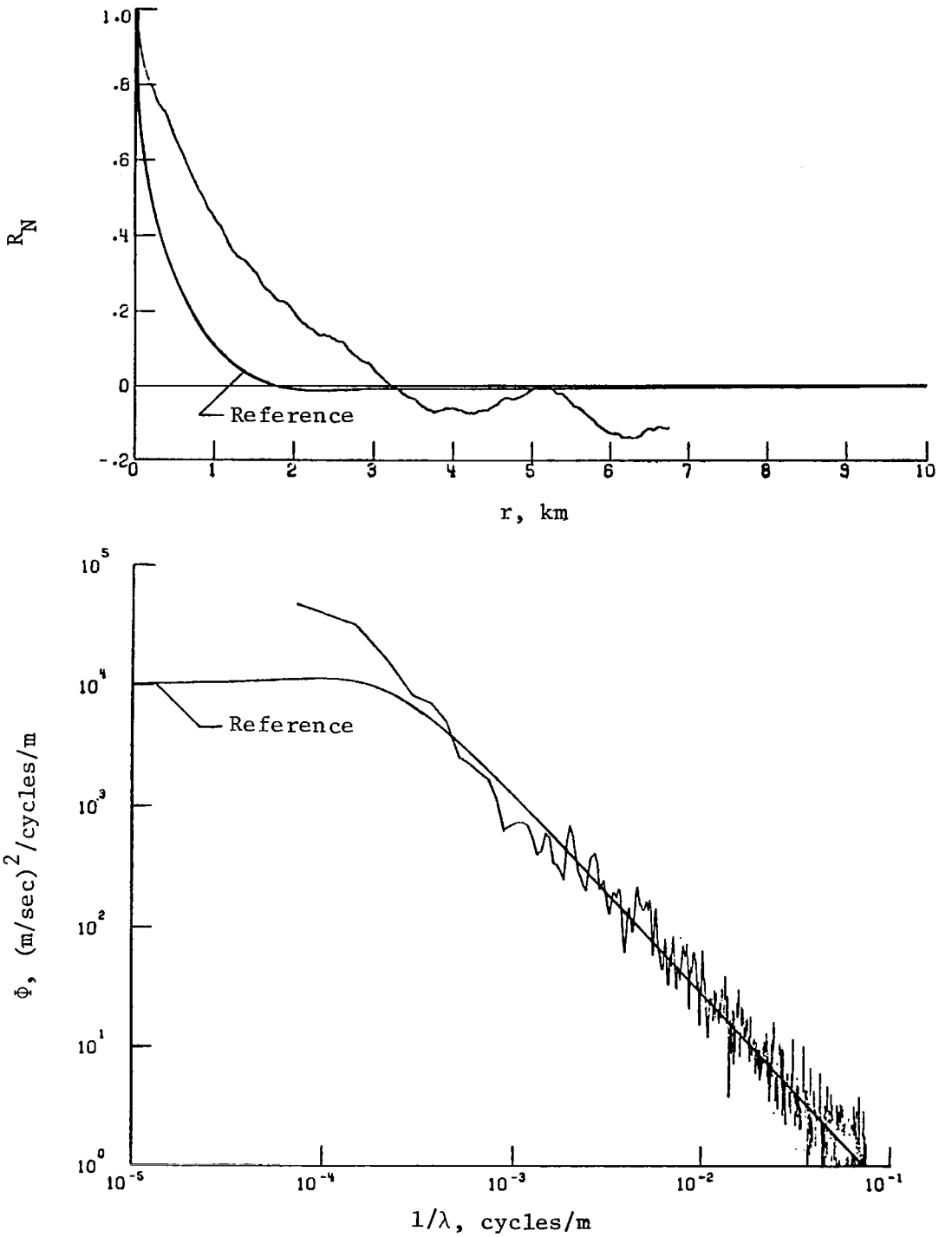

(b) Lateral component of gust velocity.

Figure 8.- Continued.

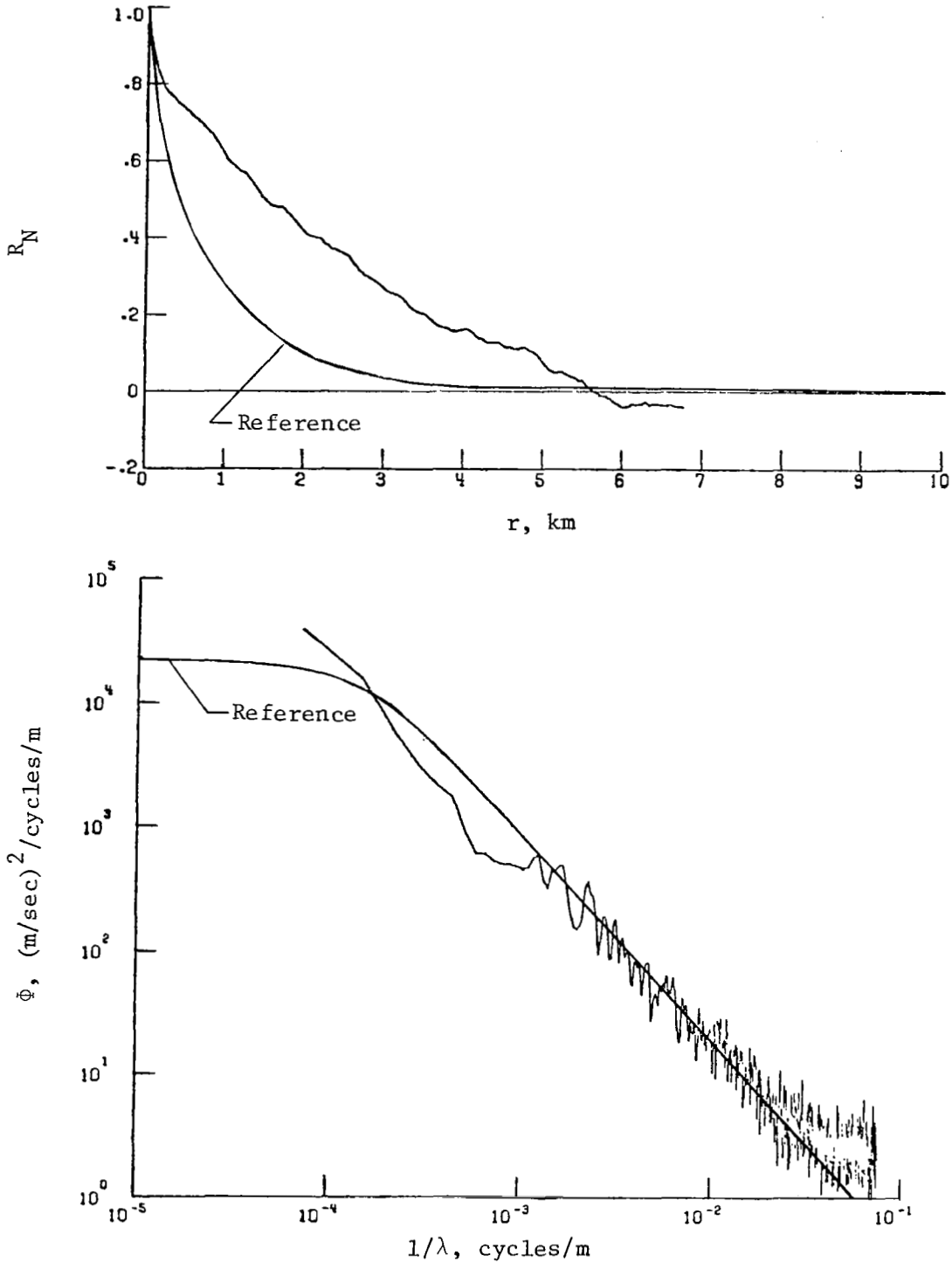

(c) Longitudinal component of gust velocity.

Figure 8.- Concluded.

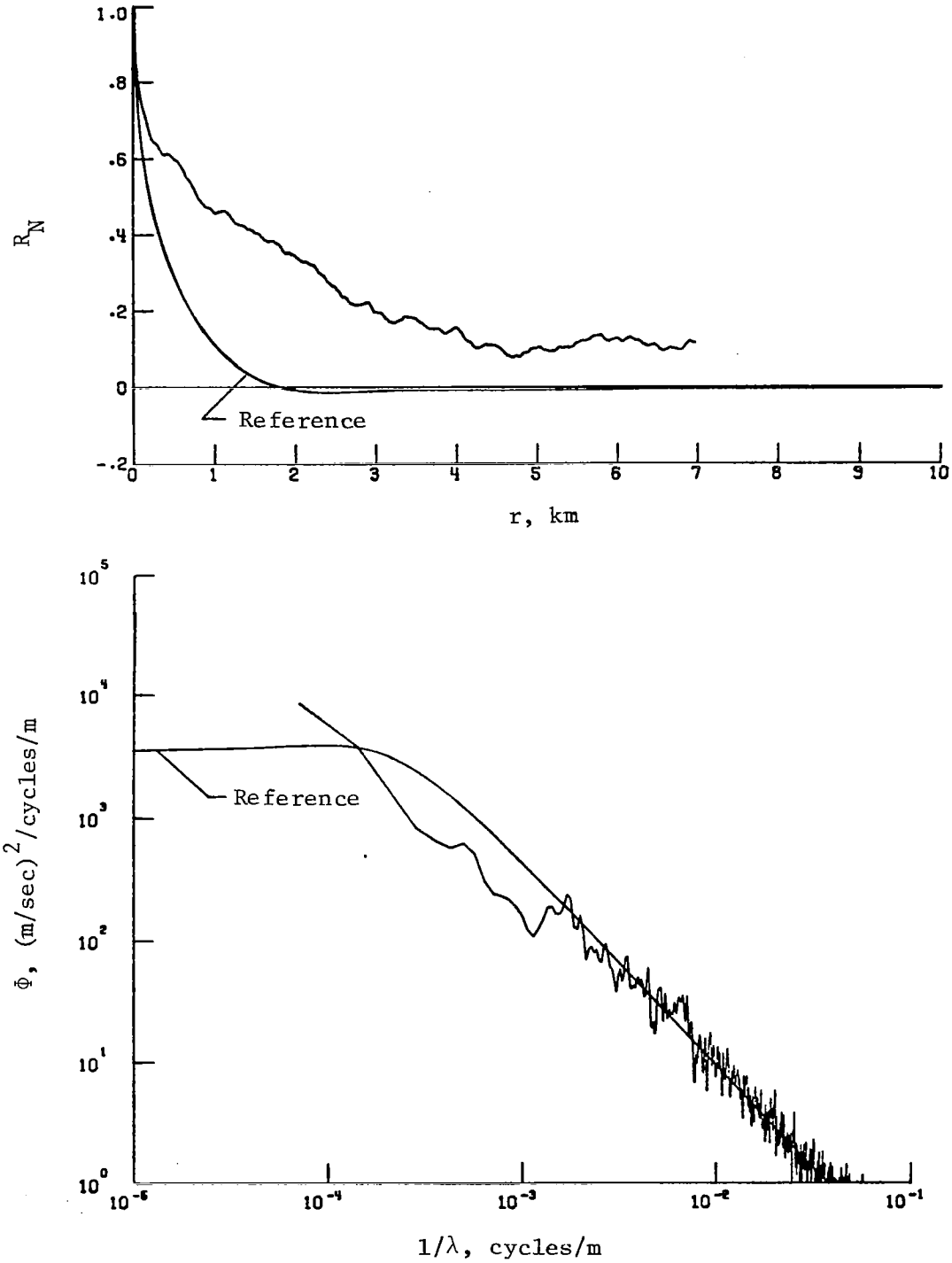

(a) Vertical component of gust velocity.

Figure 9.- Power spectra and autocorrelation functions for flight 28, run 4.

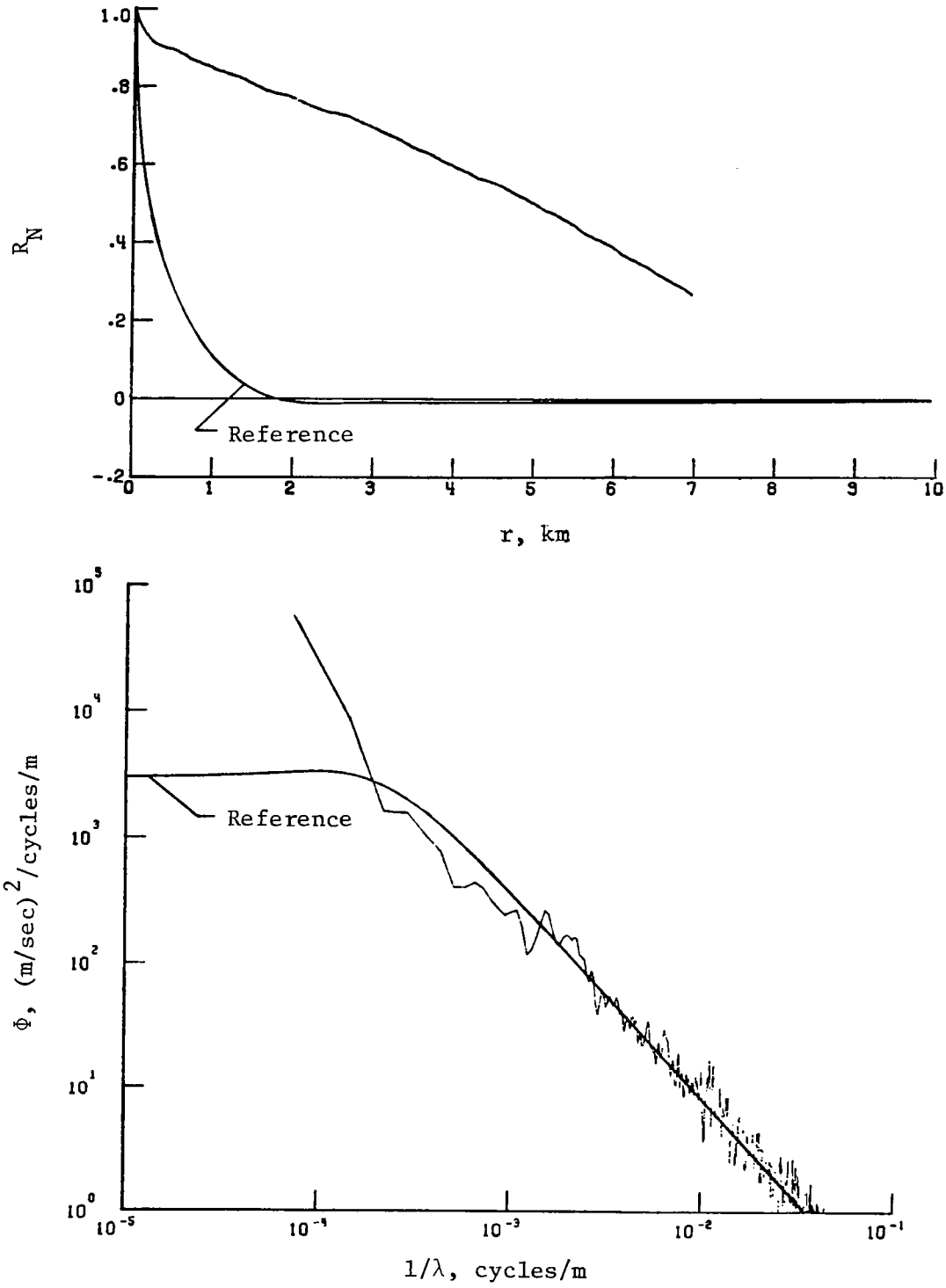

(b) Lateral component of gust velocity.

Figure 9.- Continued.

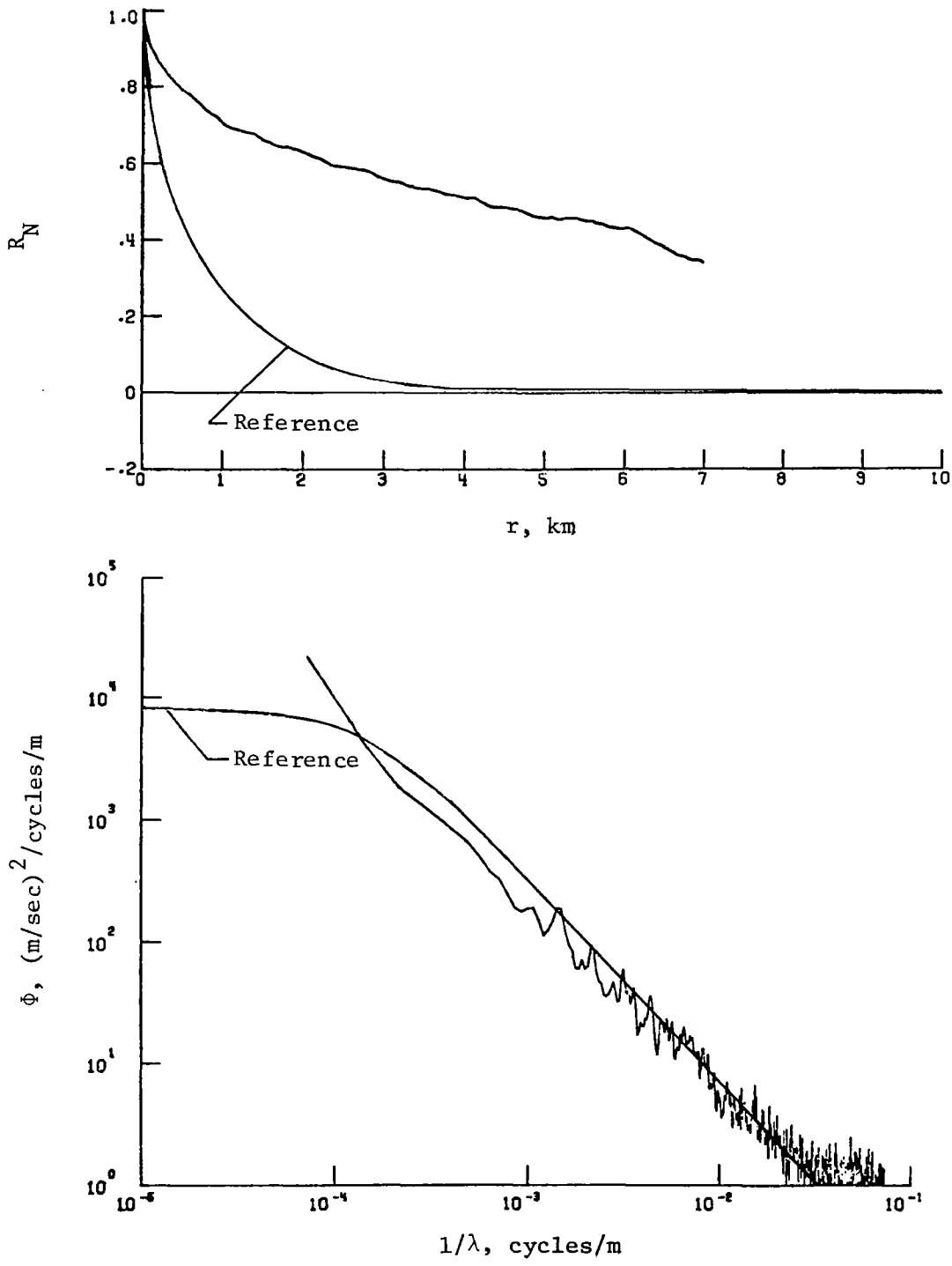

(c) Longitudinal component of gust velocity.

Figure 9.- Concluded.

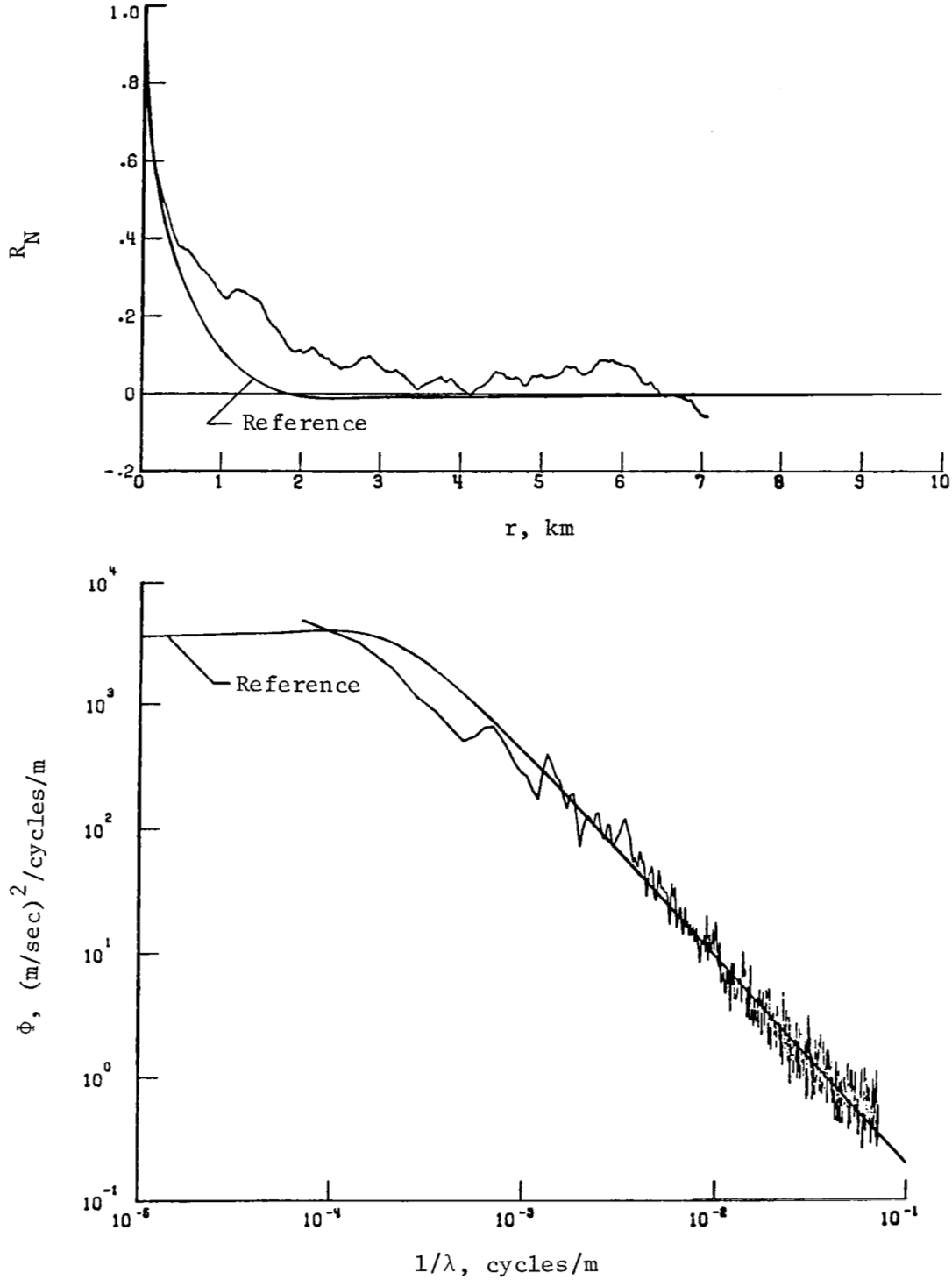

(a) Vertical component of gust velocity.

Figure 10.- Power spectra and autocorrelation functions for flight 28, run 6.

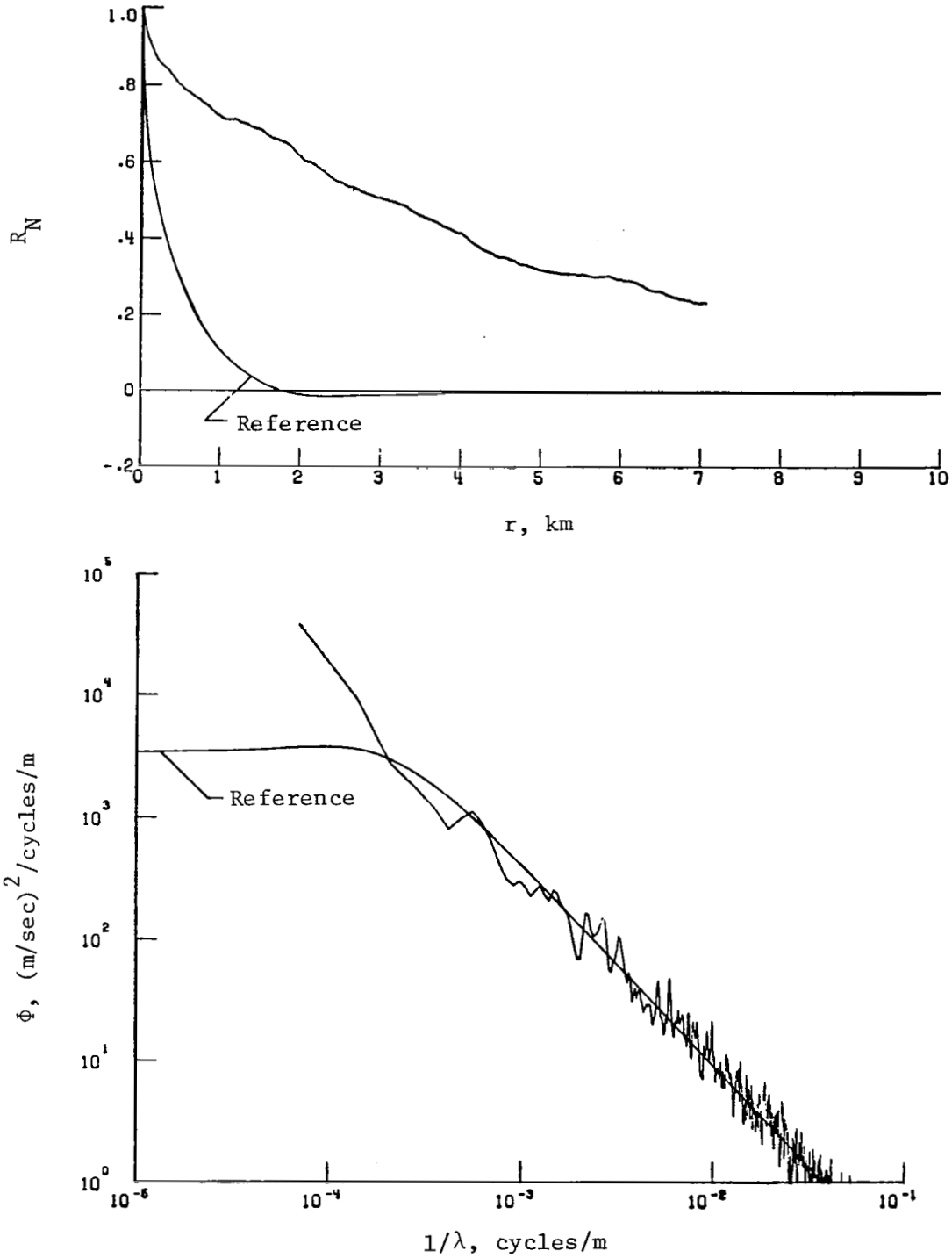

(b) Lateral component of gust velocity.

Figure 10.- Continued.

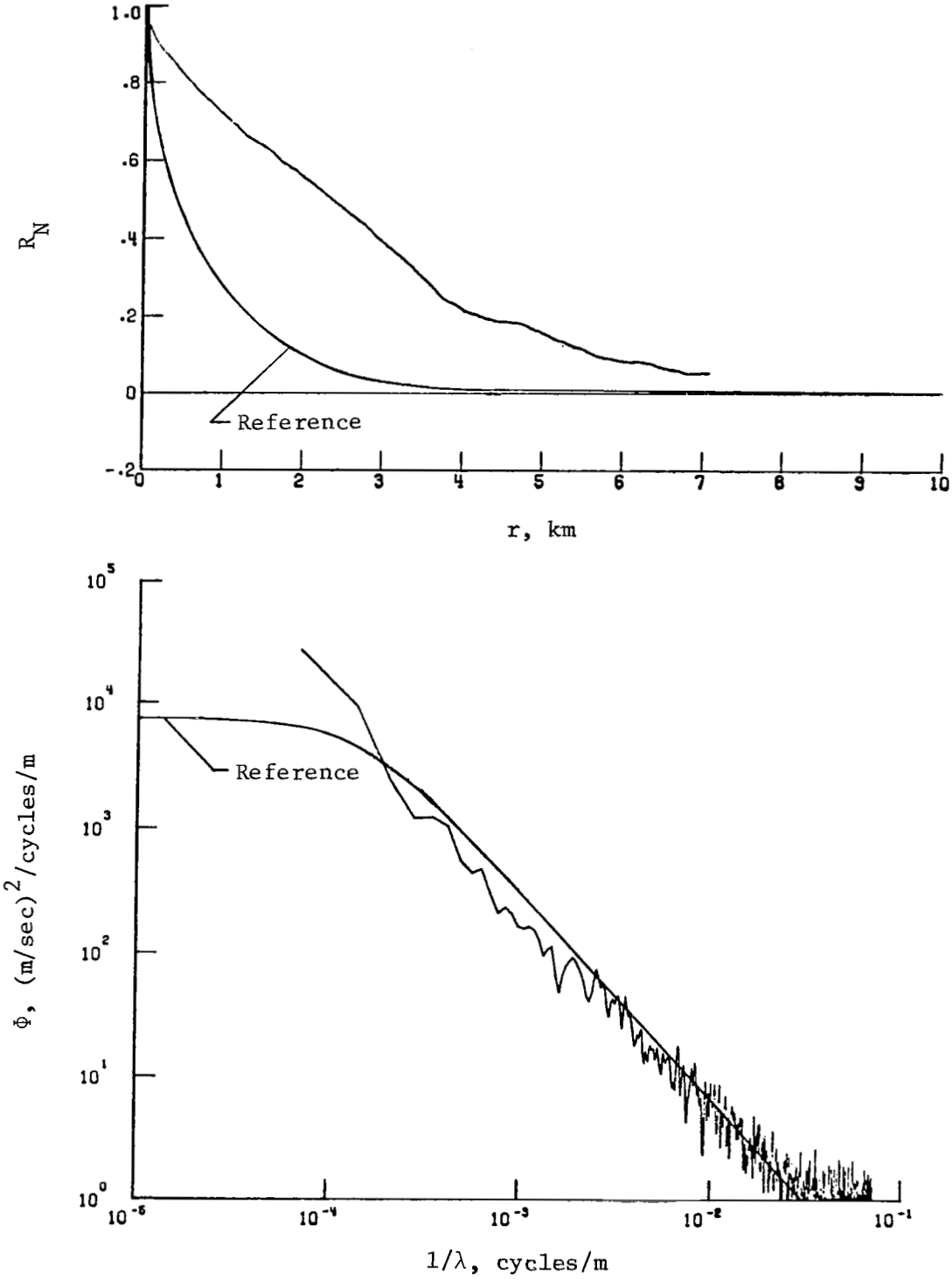

(c) Longitudinal component of gust velocity.

Figure 10.- Concluded.

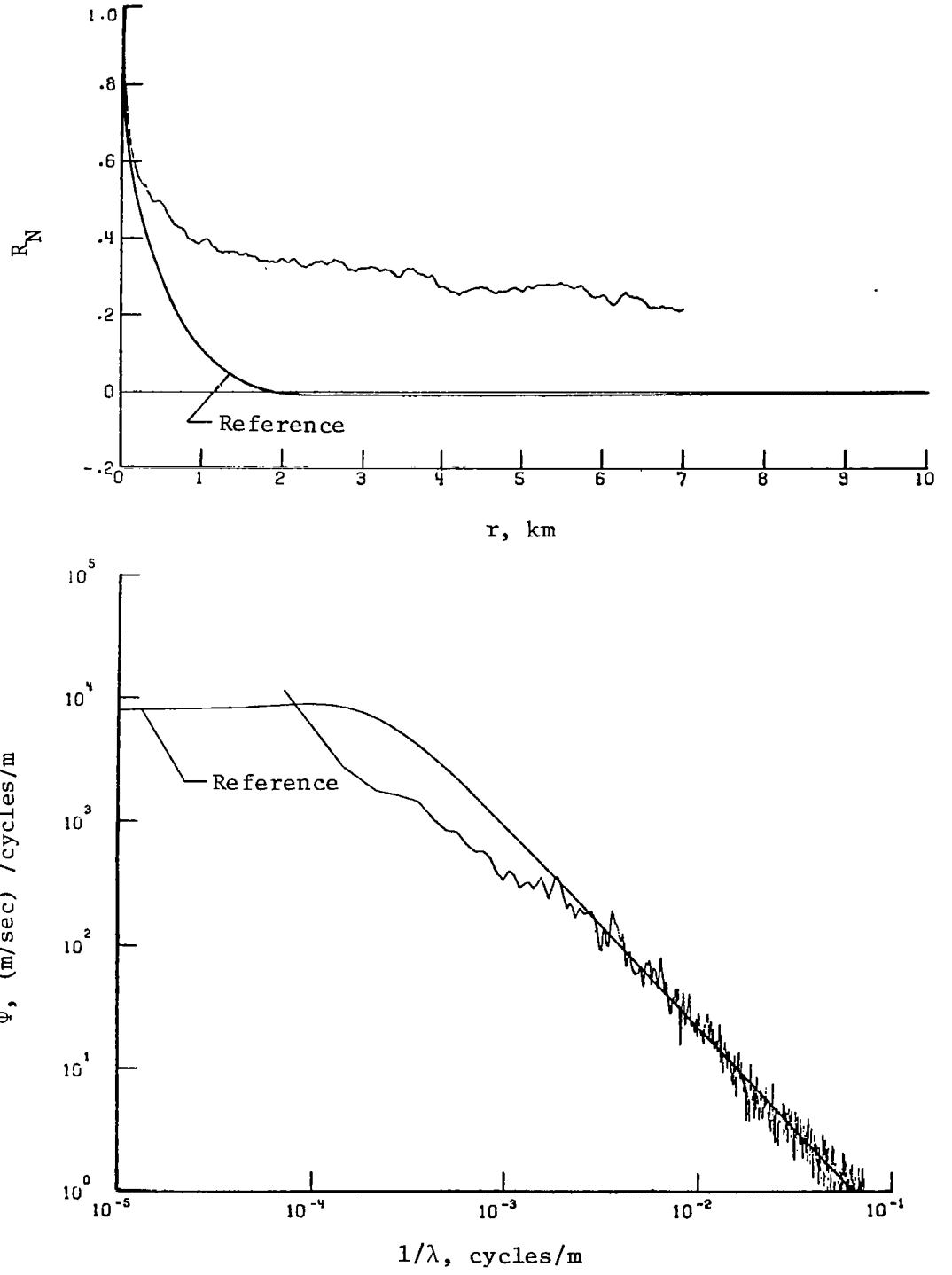

(a) Vertical component of gust velocity.

Figure 11.- Power spectra and autocorrelation functions for flight 28, run 8.

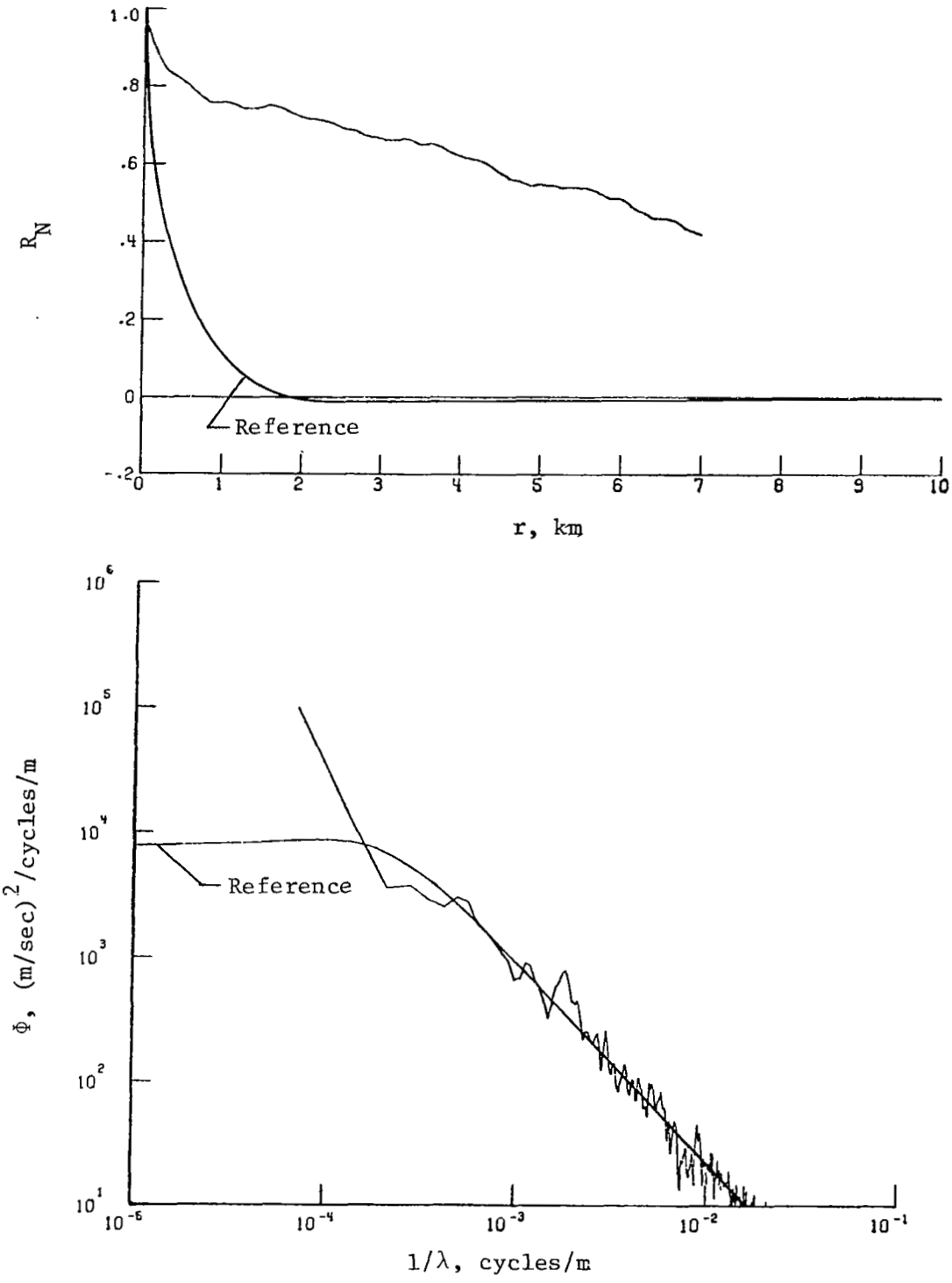

(b) Lateral component of gust velocity.

Figure 11.- Continued.

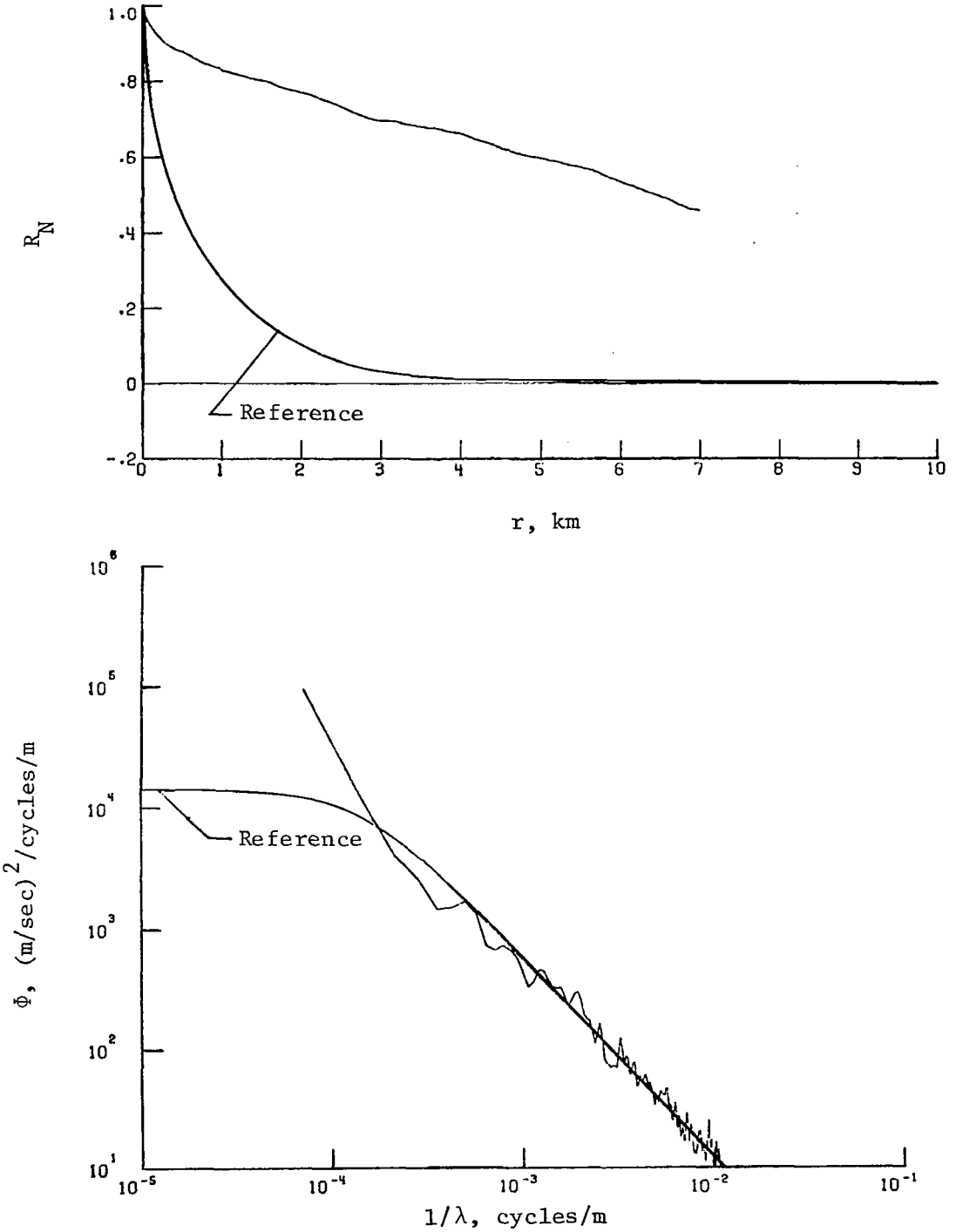

(c) Longitudinal component of gust velocity.

Figure 11.- Concluded.

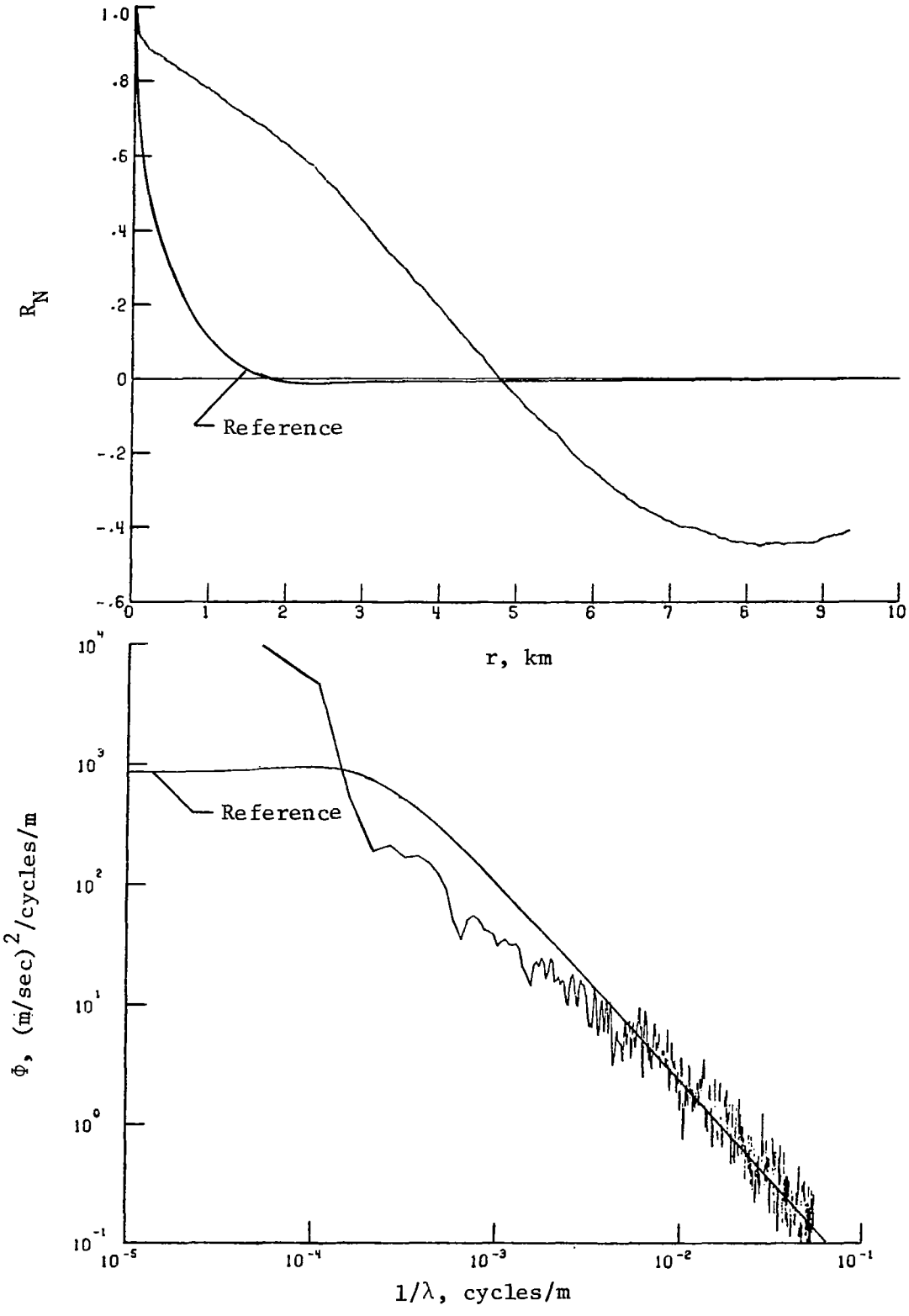

(a) Vertical component of gust velocity.

Figure 12.- Power spectra and autocorrelation functions for flight 29, run 6.

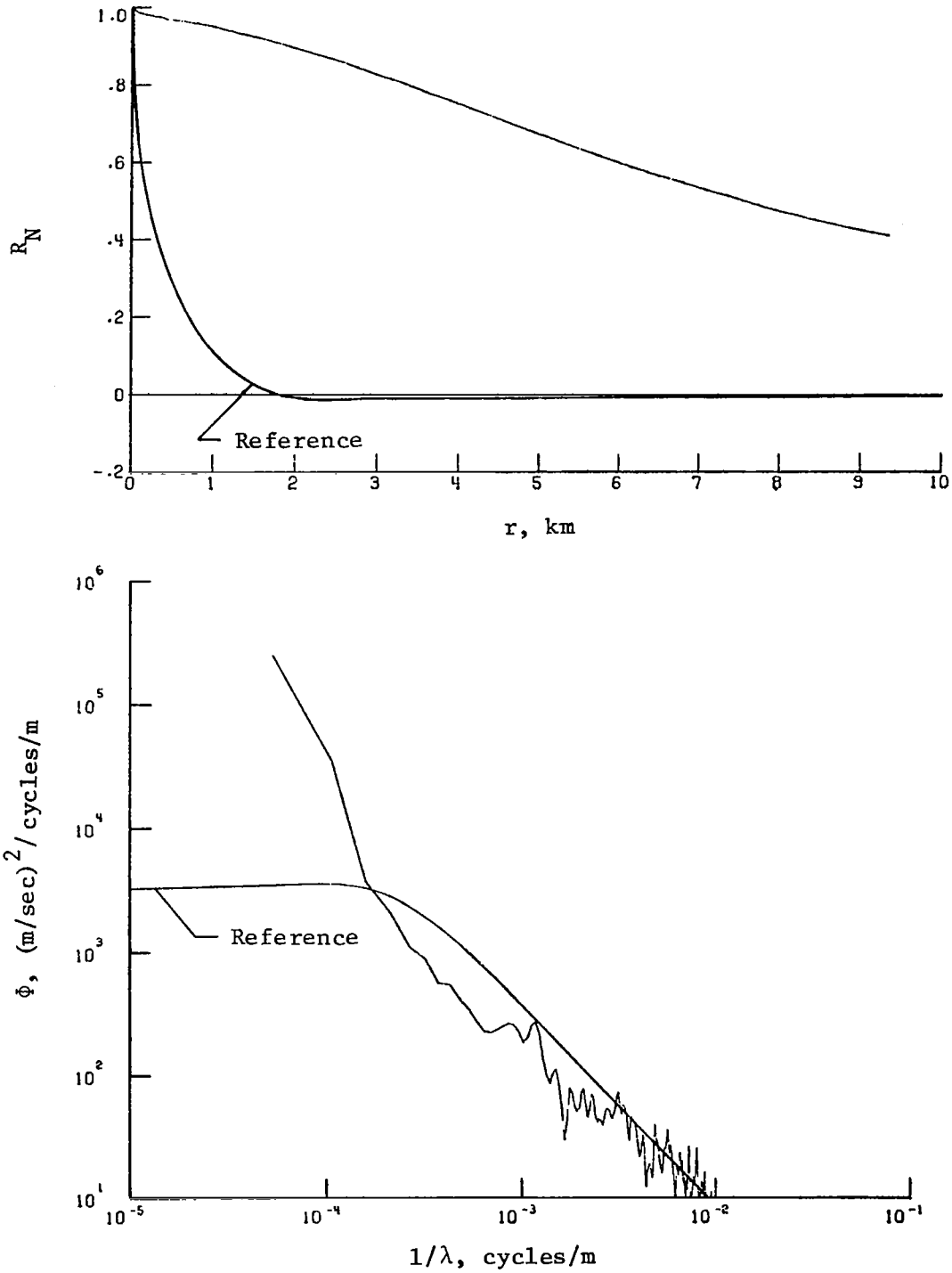

(b) Lateral component of gust velocity.

Figure 12.- Continued.

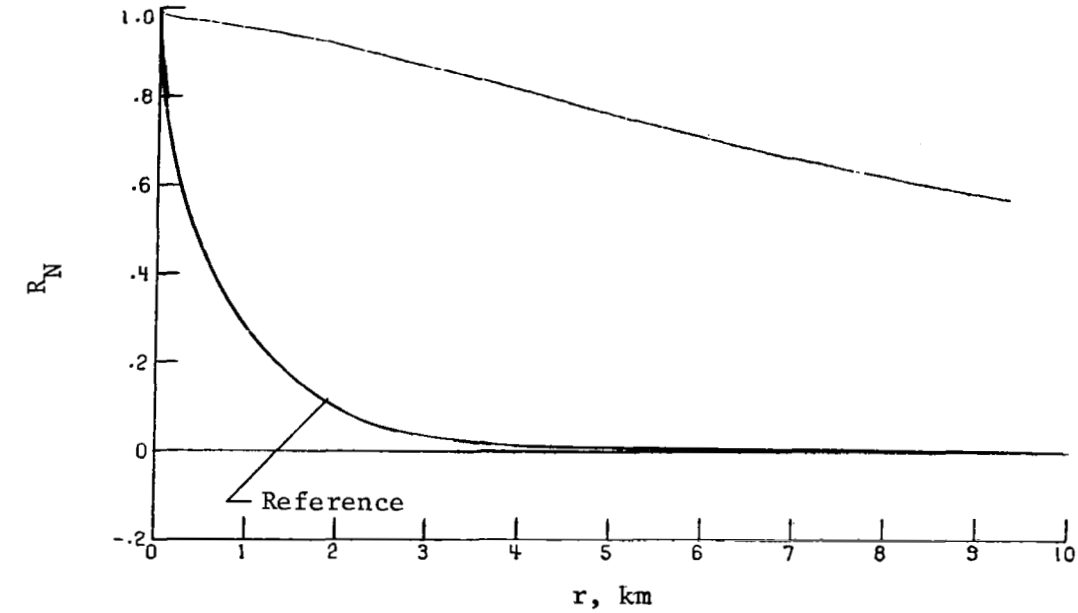

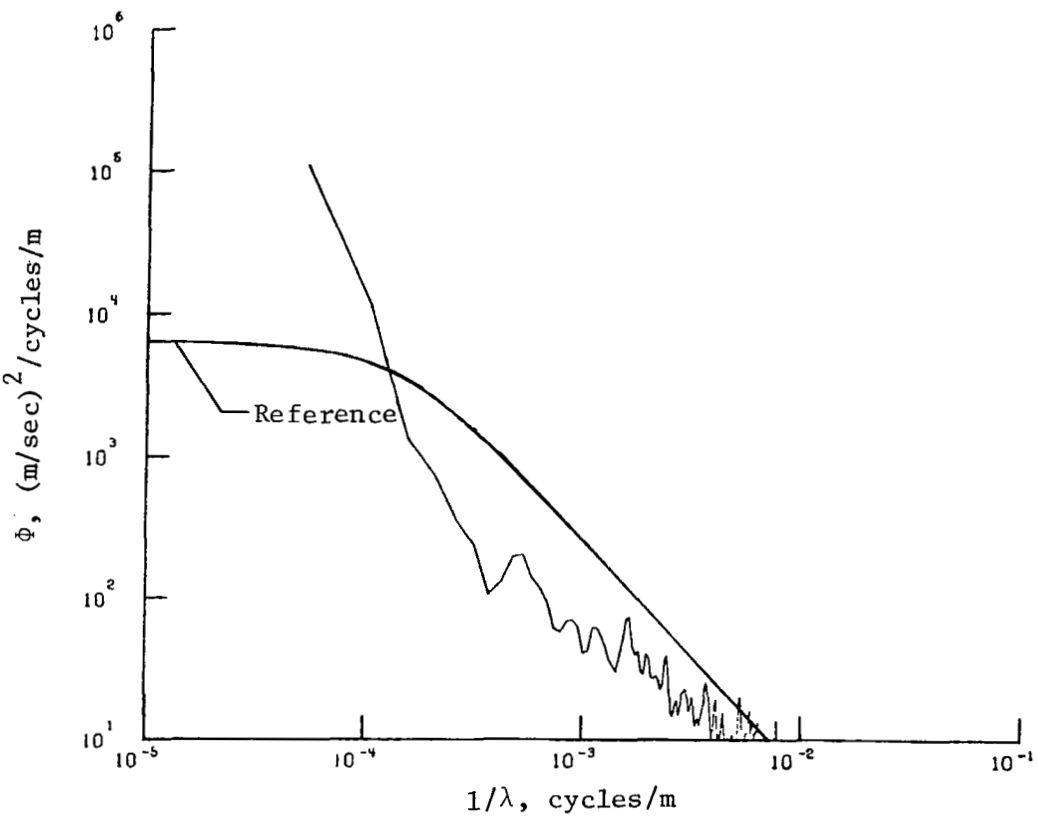

(c) Longitudinal component of gust velocity.

Figure 12.- Concluded.

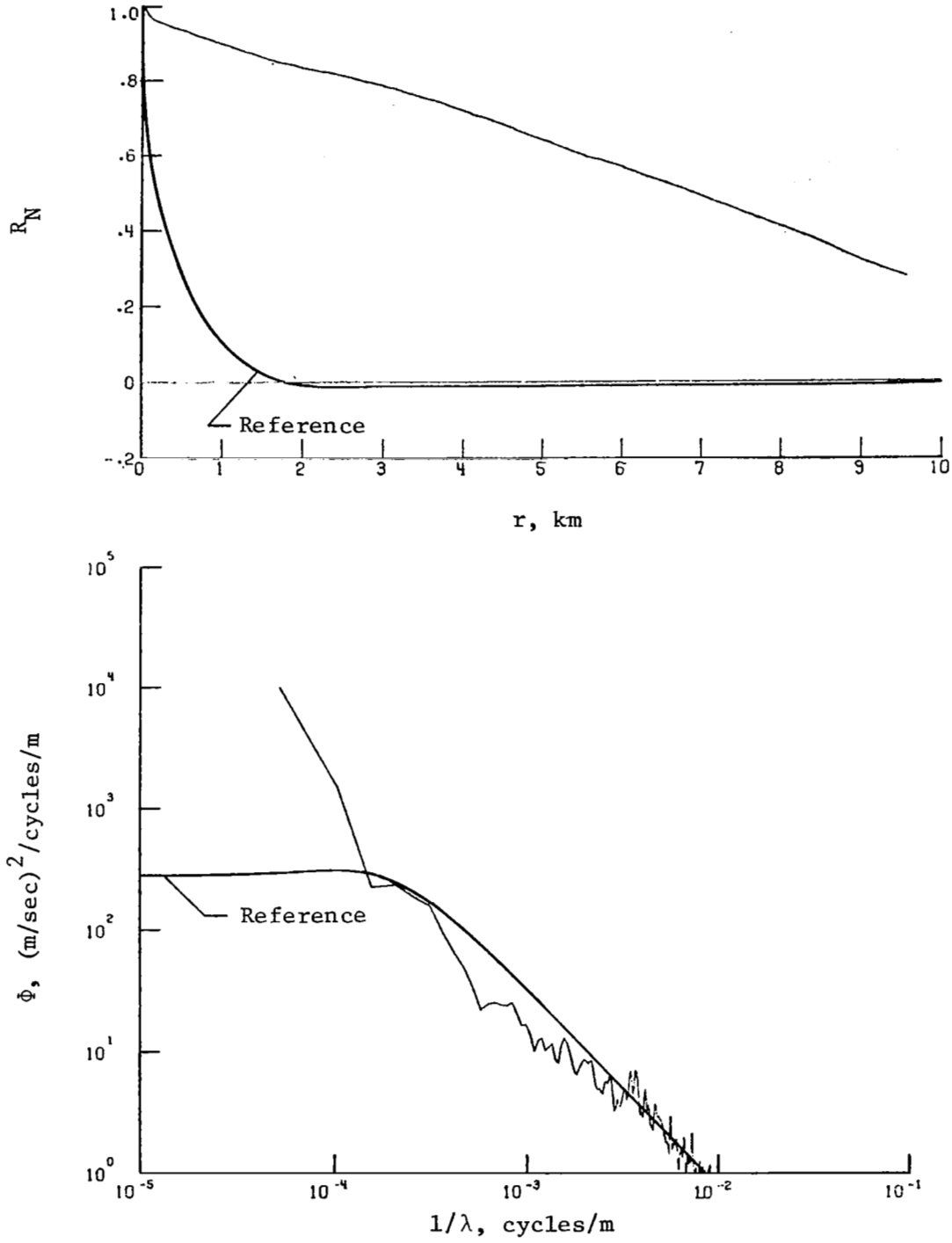

(a) Vertical component of gust velocity.

Figure 13.- Power spectra and autocorrelation functions for flight 29, run 7.

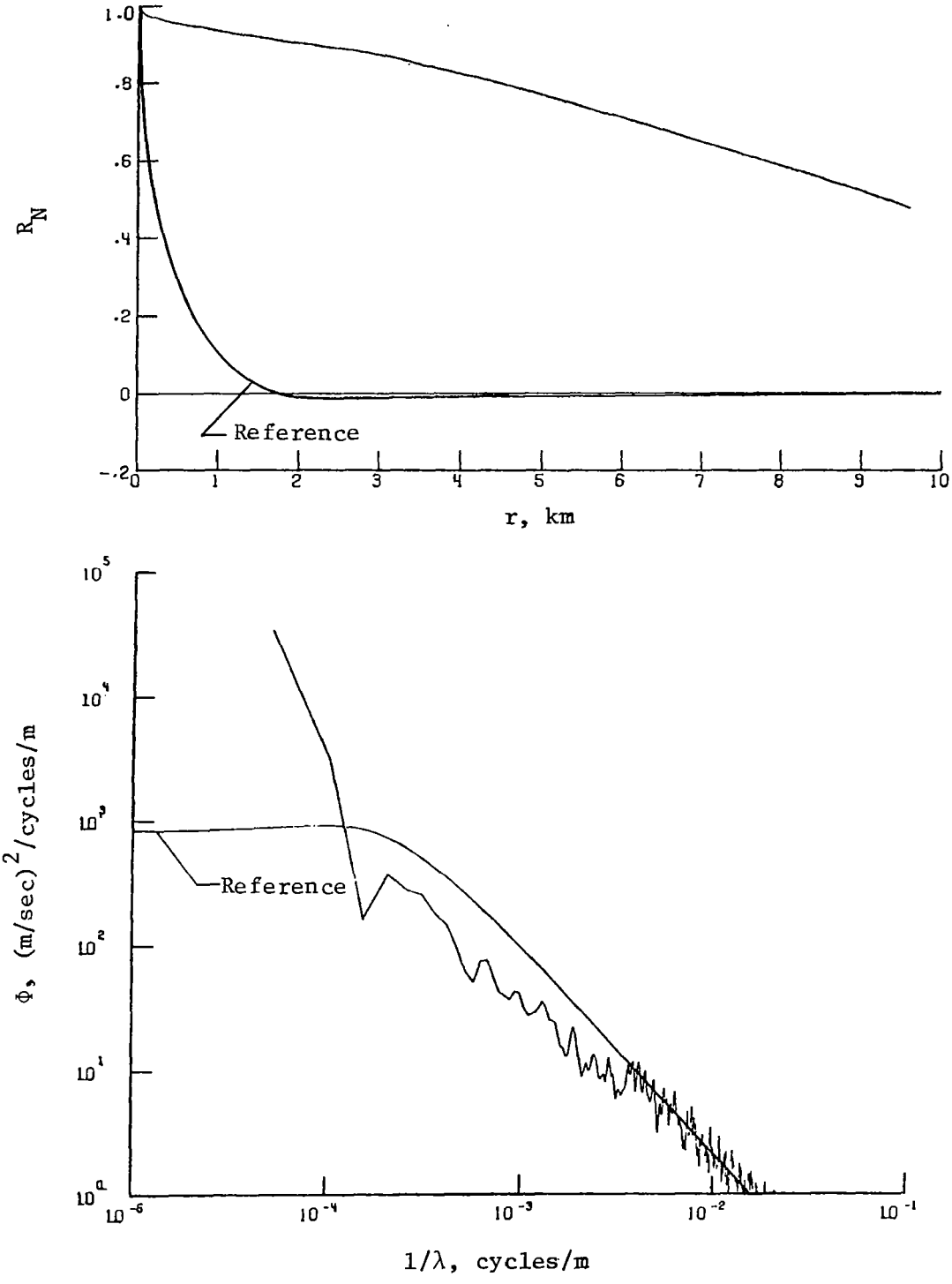

(b) Lateral component of gust velocity.

Figure 13.- Continued.

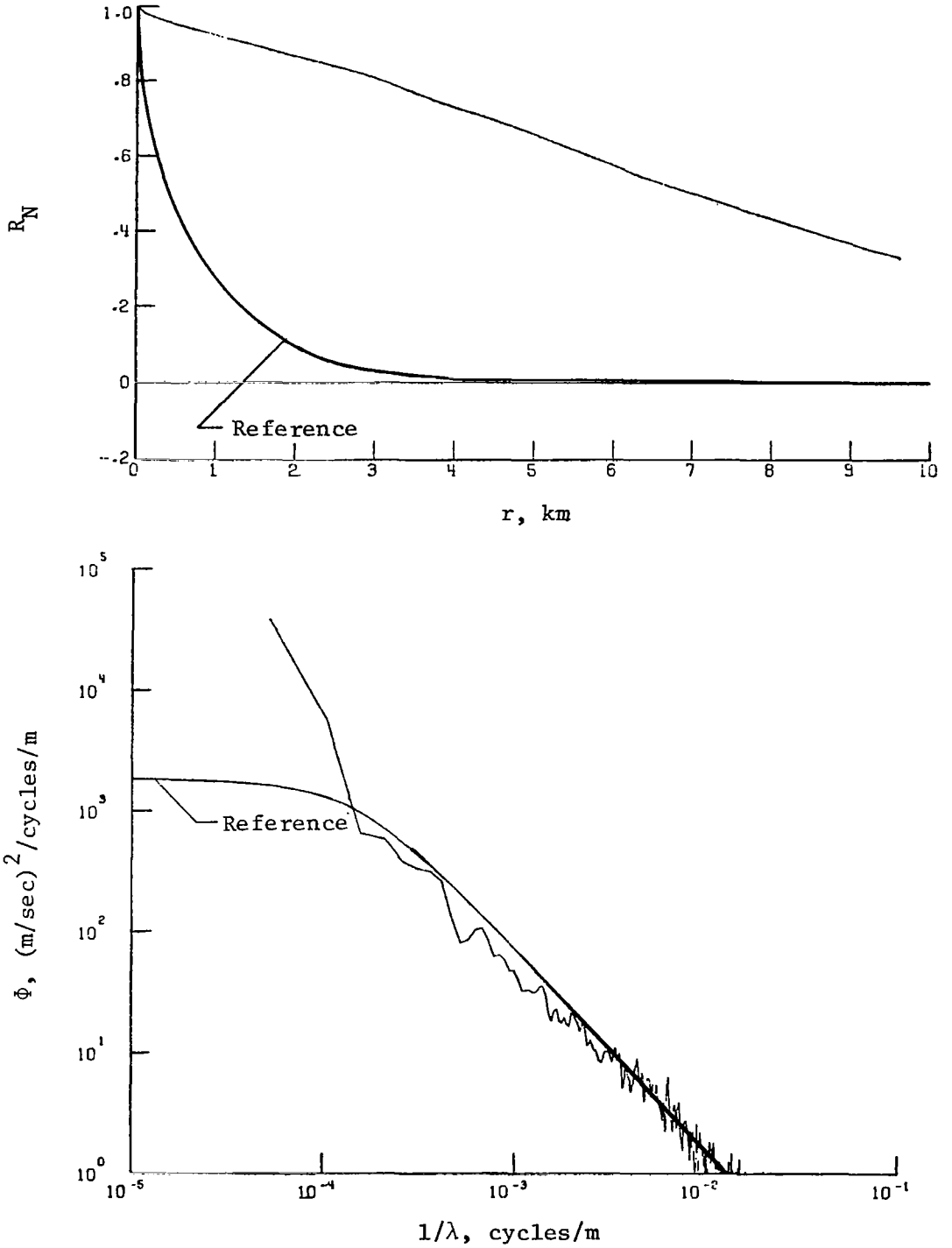

(c) Longitudinal component of gust velocity.

Figure 13.- Concluded.

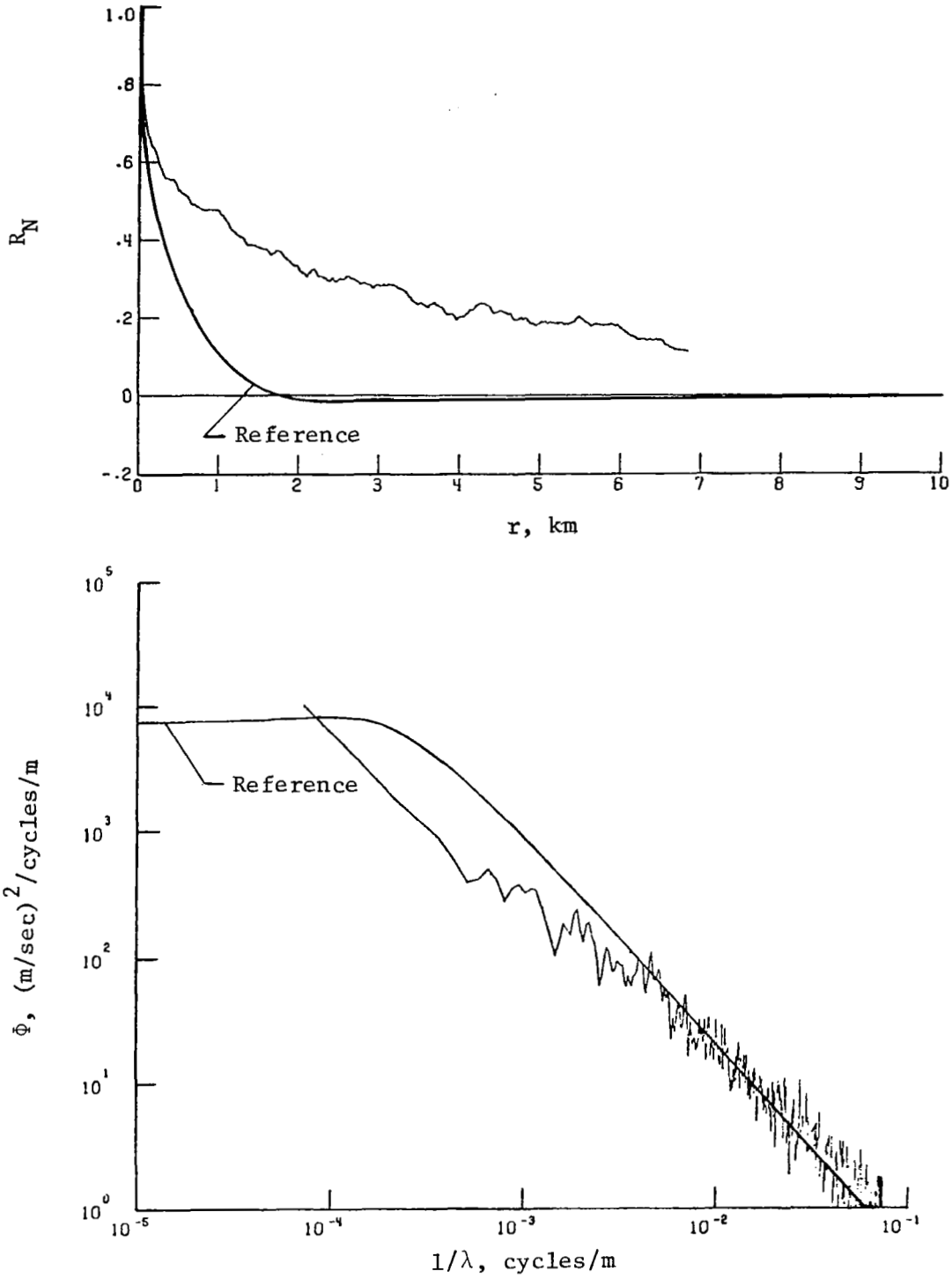

(a) Vertical component of gust velocity.

Figure 14.- Power spectra and autocorrelation functions for flight 29, run 8.

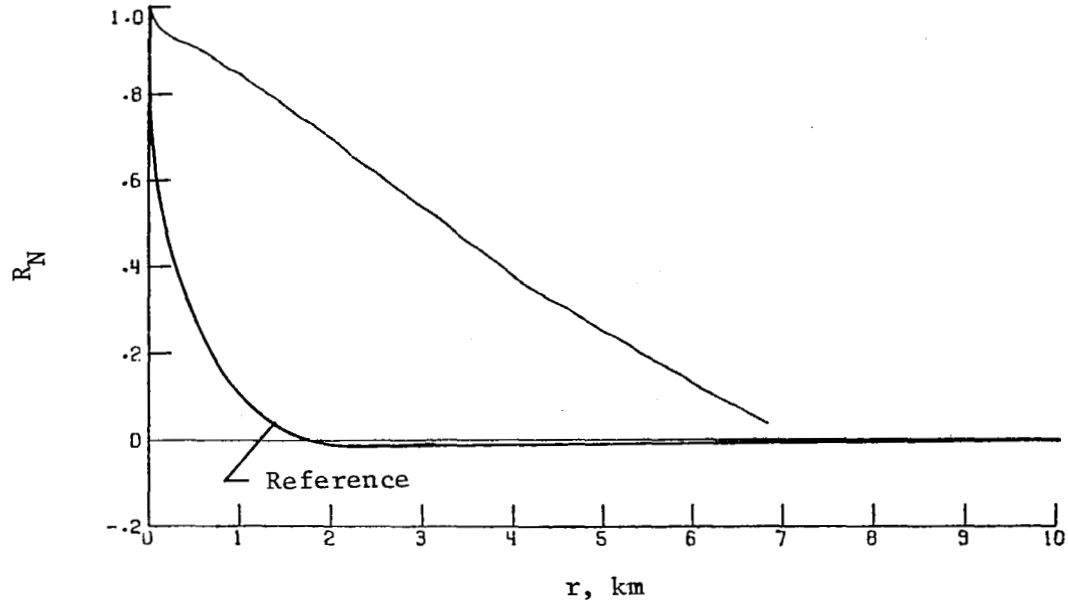

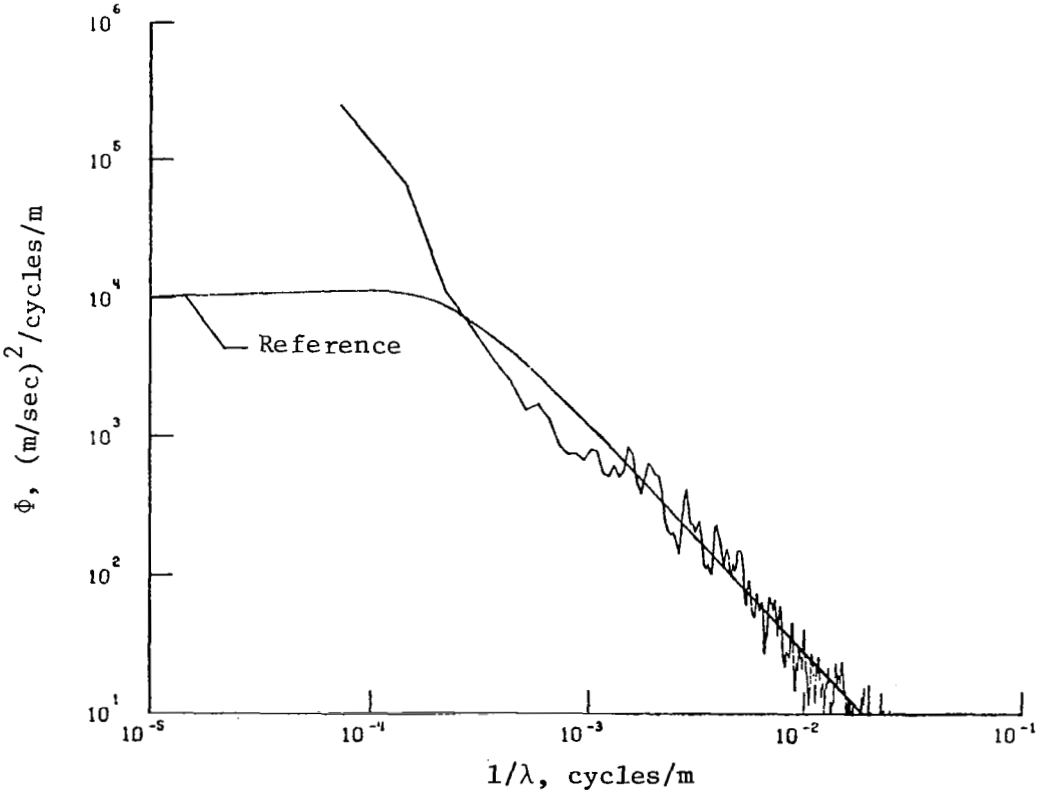

(b) Lateral component of gust velocity.

Figure 14.- Continued.

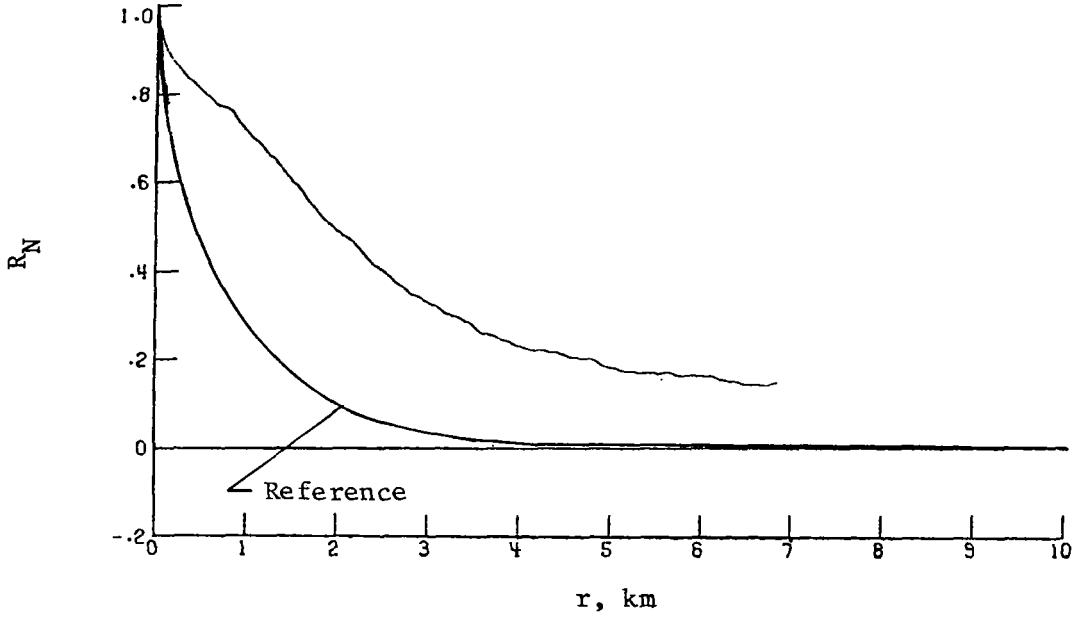

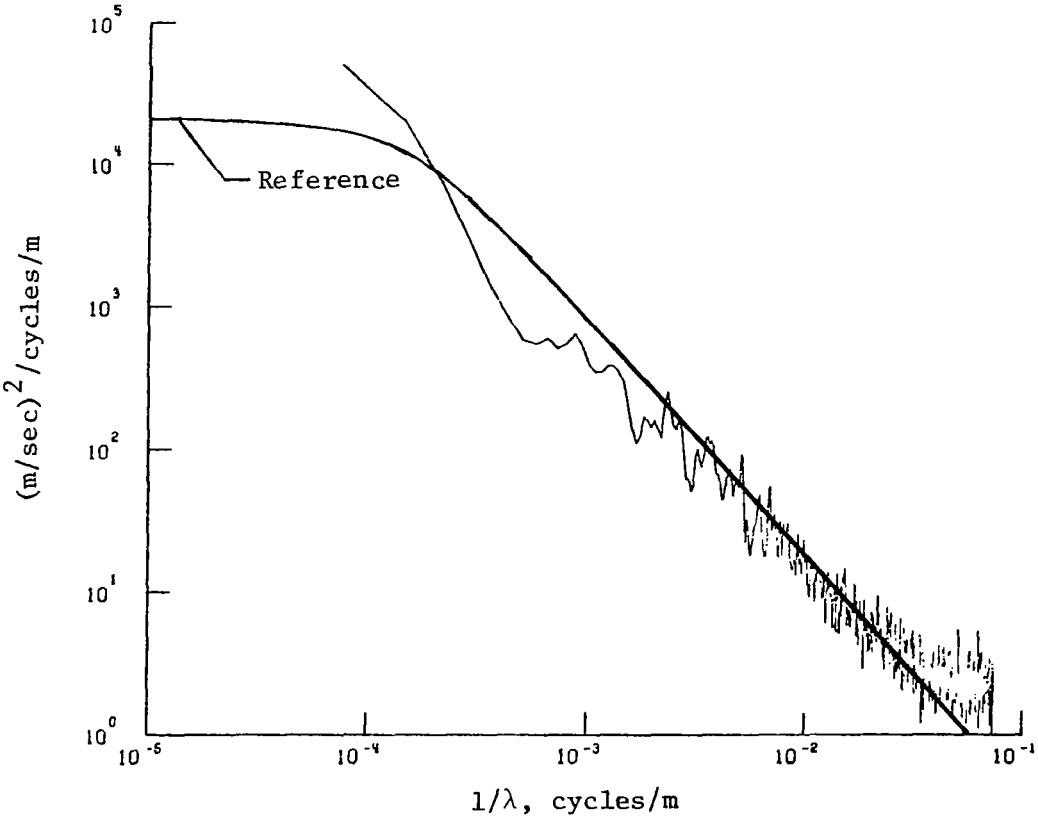

(c) Longitudinal component of gust velocity.

Figure 14.- Concluded.

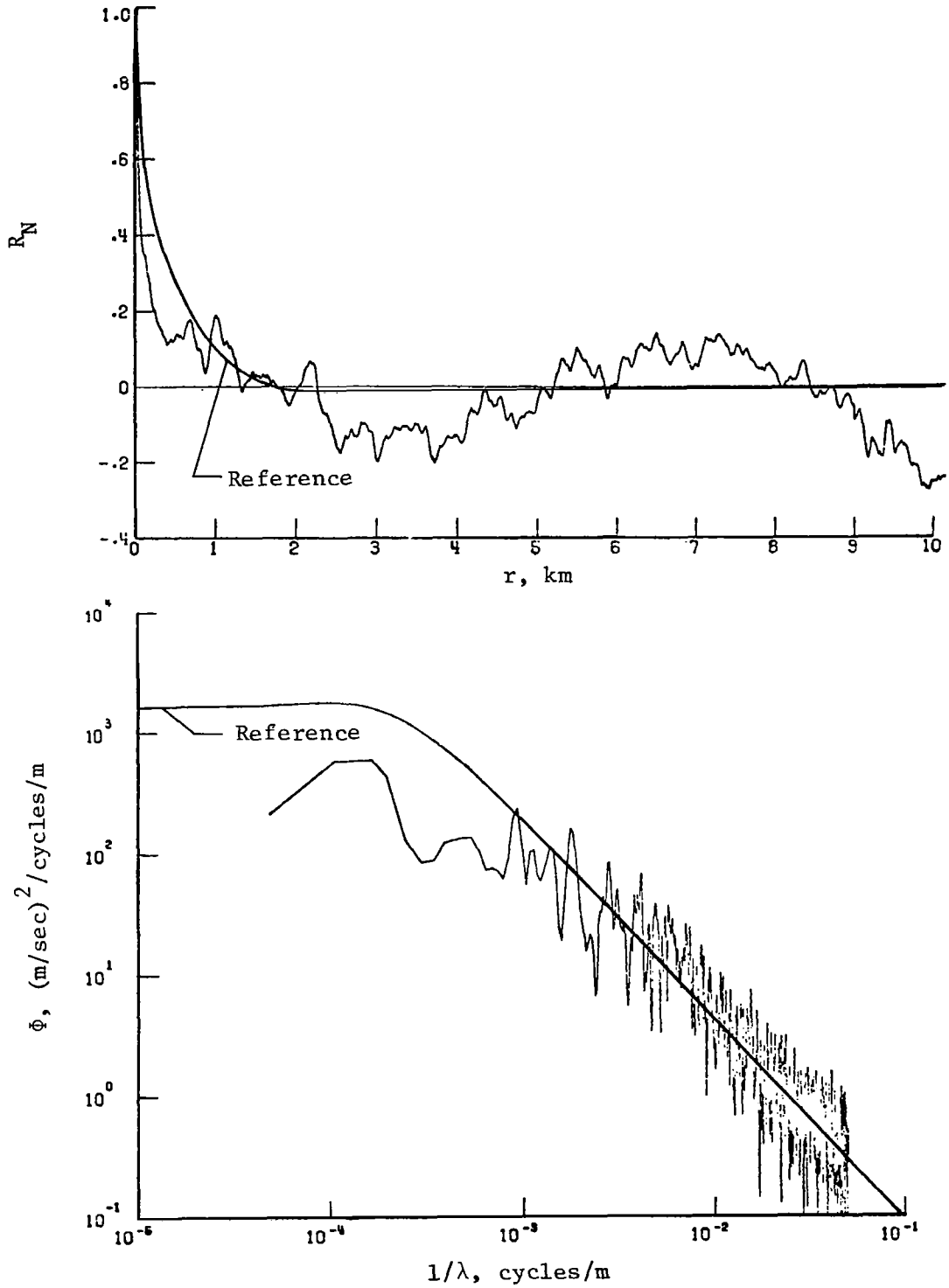

(a) Vertical component of gust velocity.

Figure 15.- Power spectra and autocorrelation functions for flight 30, run 4.

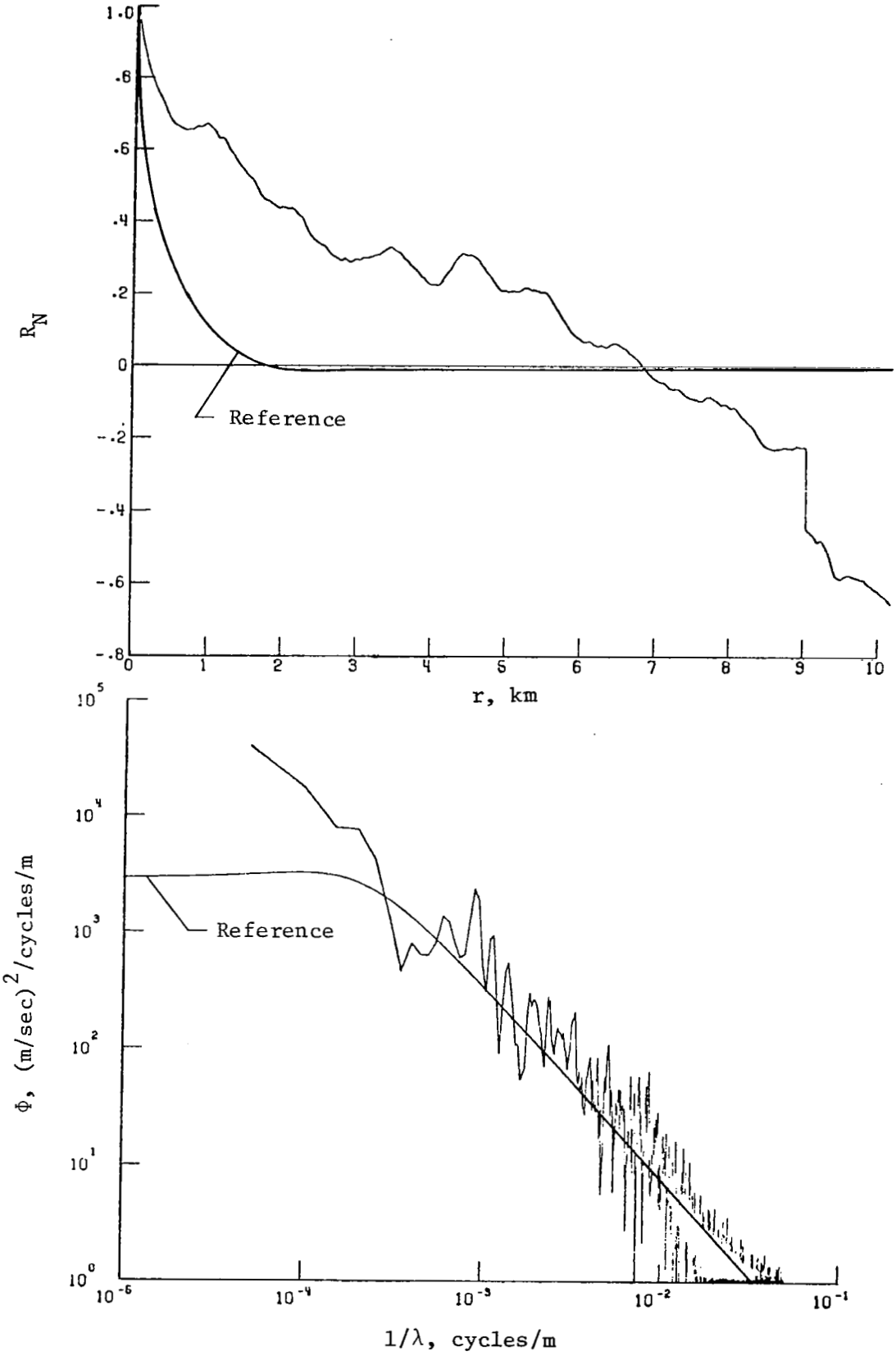

(b) Lateral component of gust velocity.

Figure 15.- Continued.

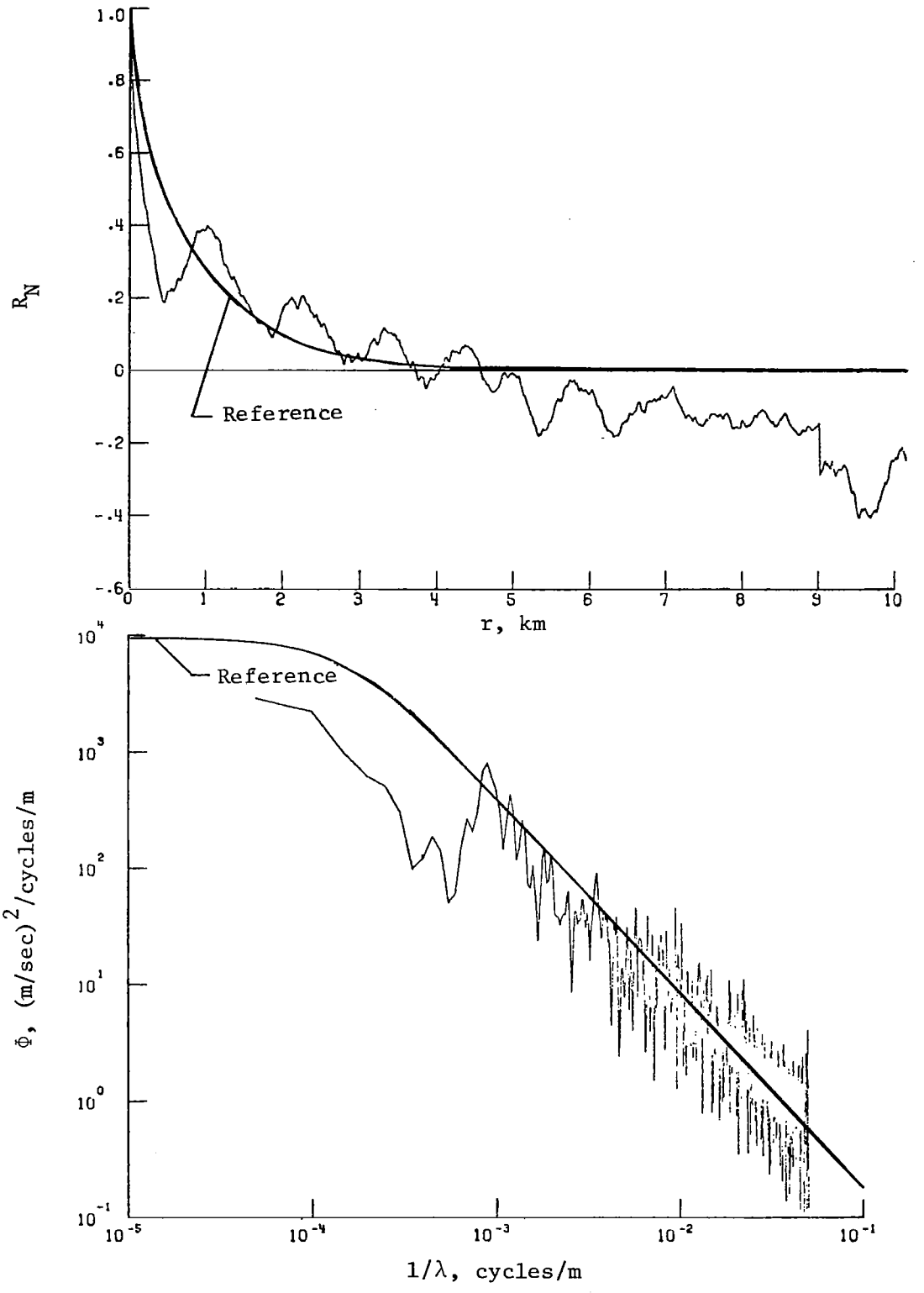

(c) Longitudinal component of gust velocity.

Figure 15.- Concluded.

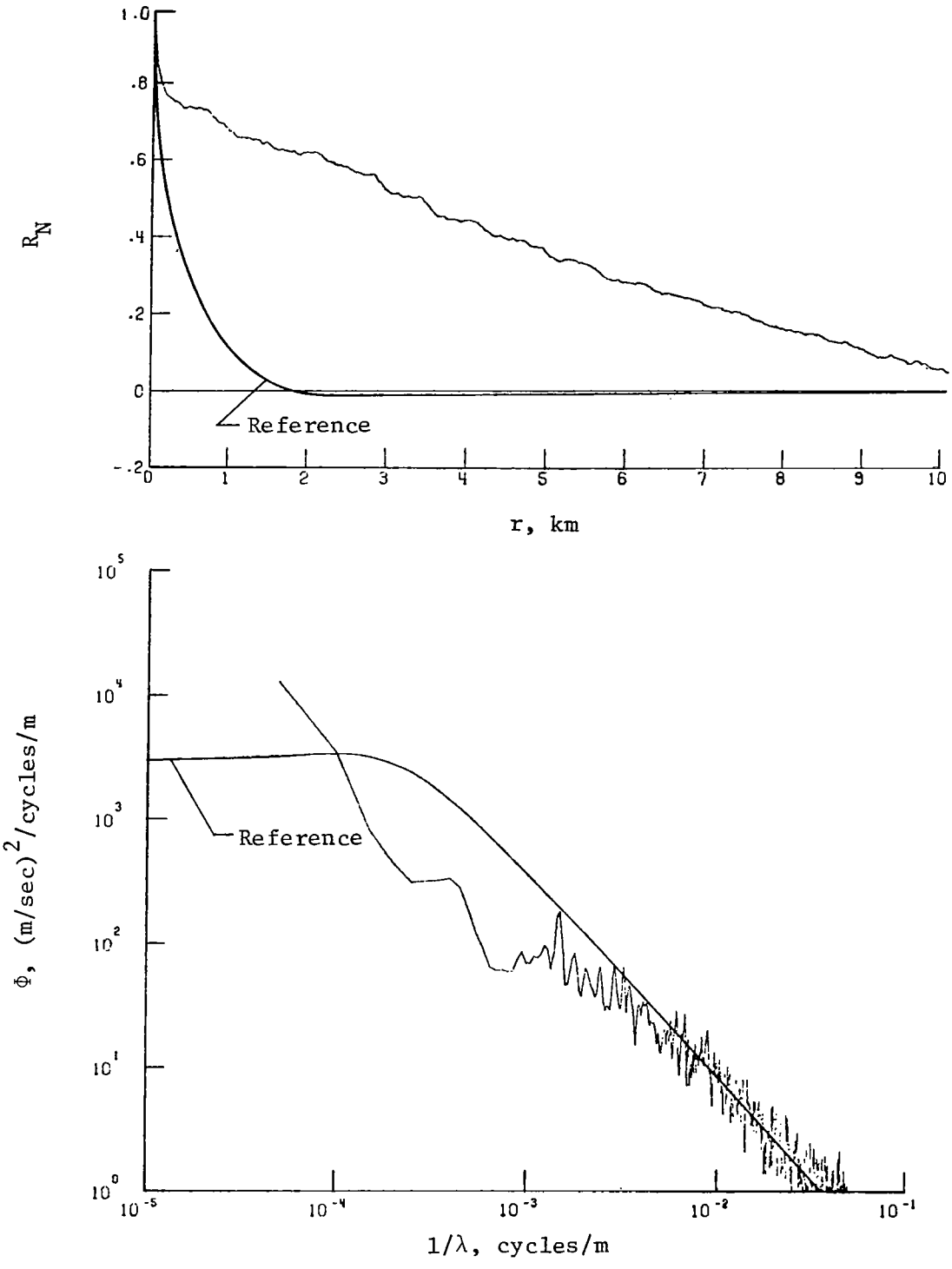

(a) Vertical component of gust velocity.

Figure 16.- Power spectra and autocorrelation functions for flight 30, run 8.

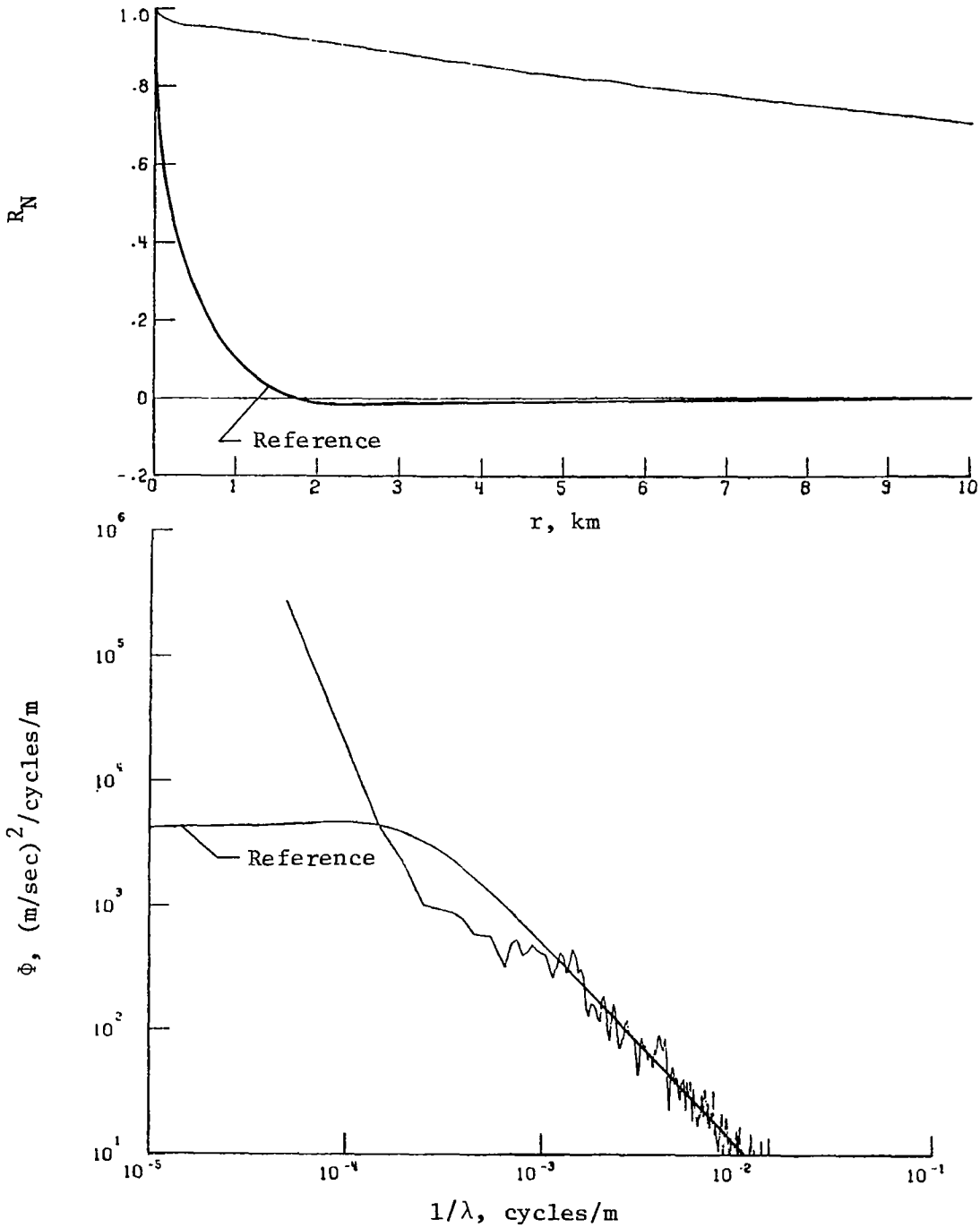

(b) Lateral component of gust velocity.

Figure 16.- Continued.

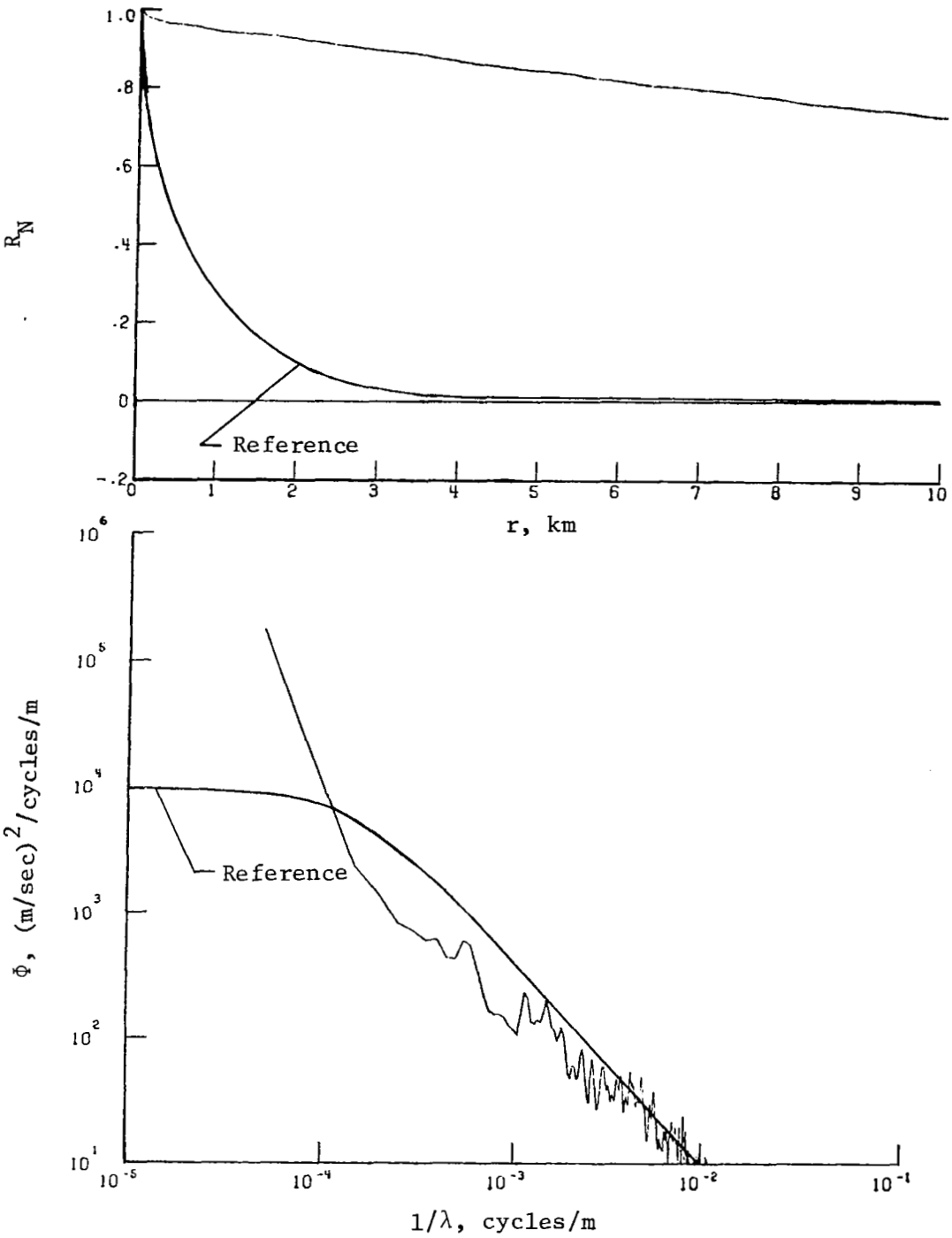

(c) Longitudinal component of gust velocity.

Figure 16.- Concluded.

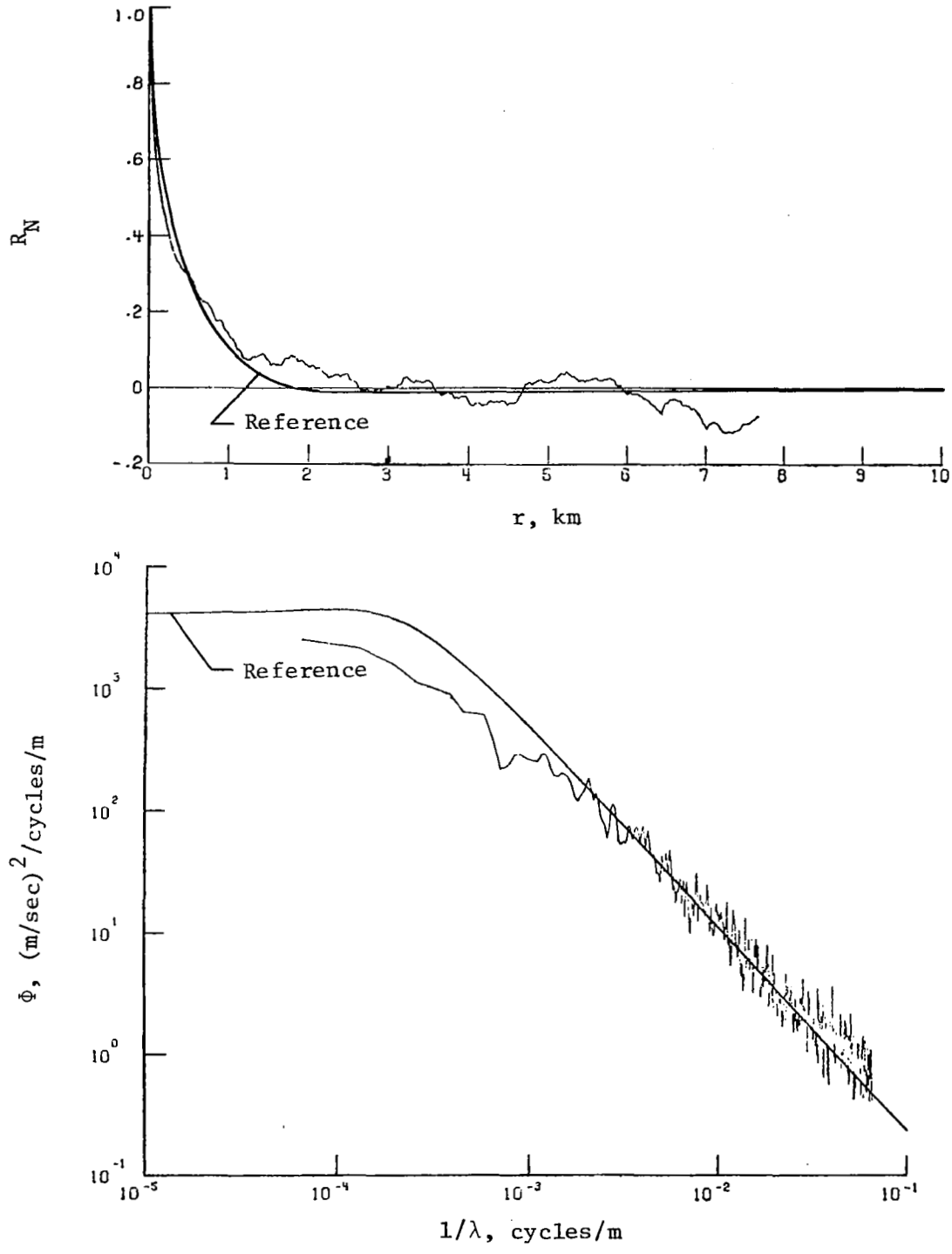

(a) Vertical component of gust velocity.

Figure 17.- Power spectra and autocorrelation functions for flight 33, run 2.

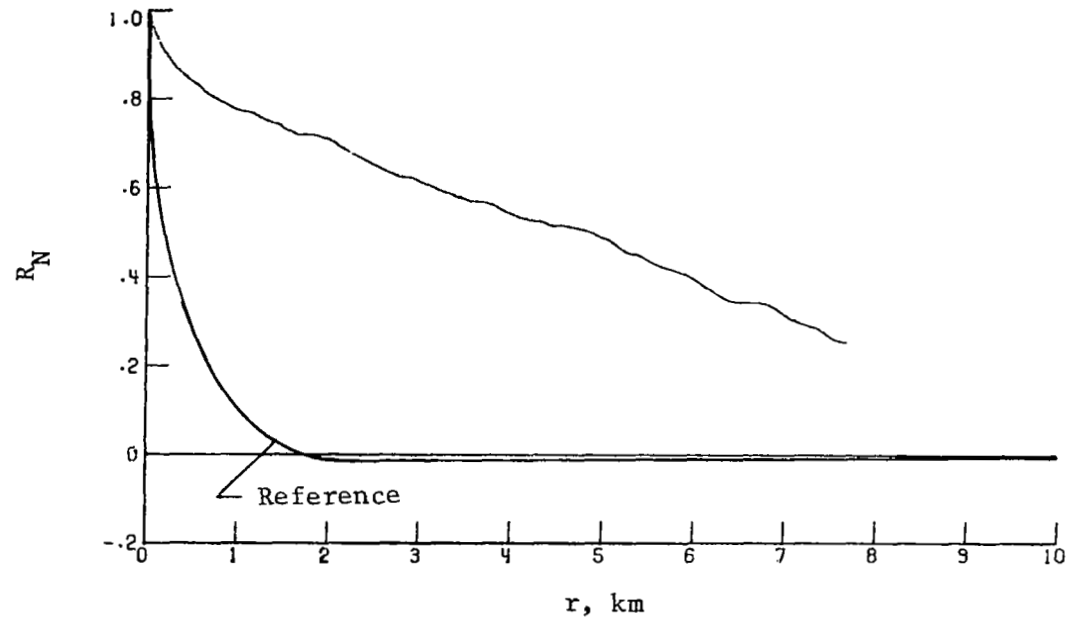

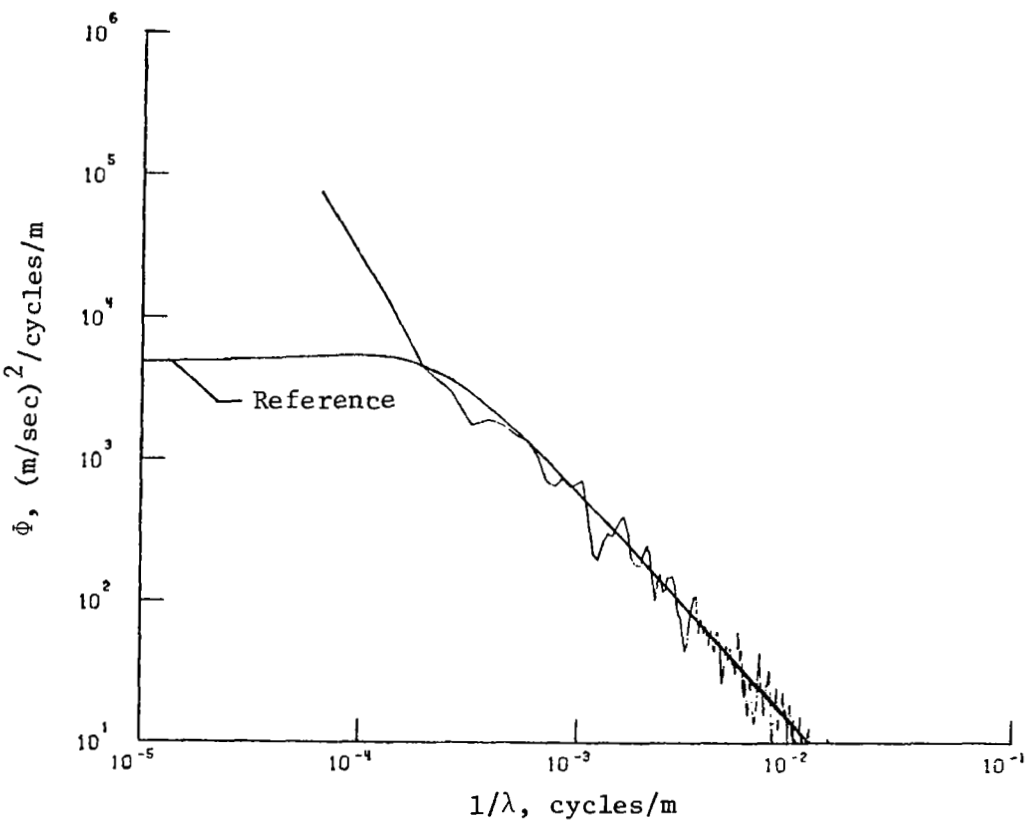

(b) Lateral component of gust velocity.

Figure 17.- Continued.

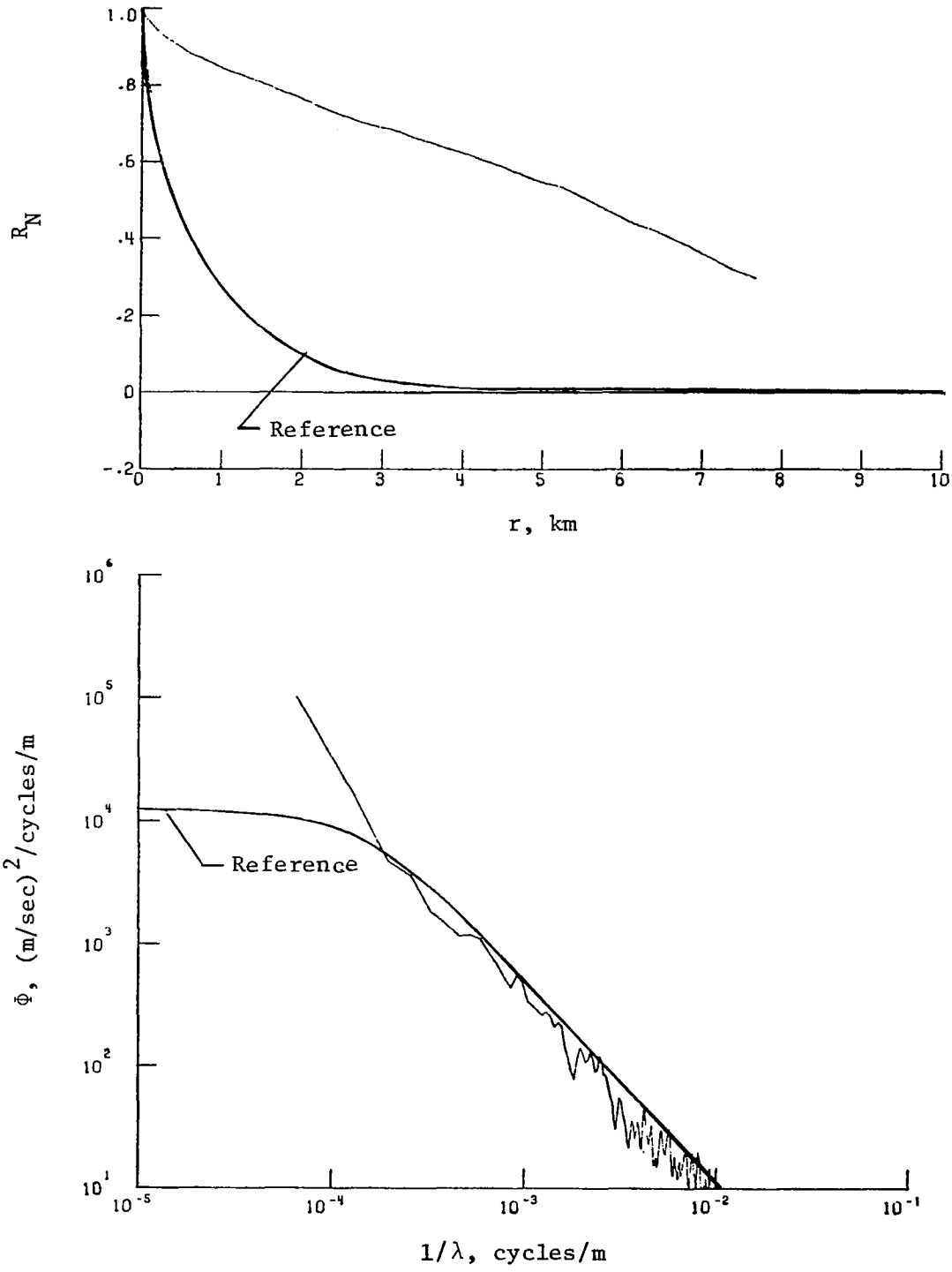

(c) Longitudinal component of gust velocity.

Figure 17.- Concluded.

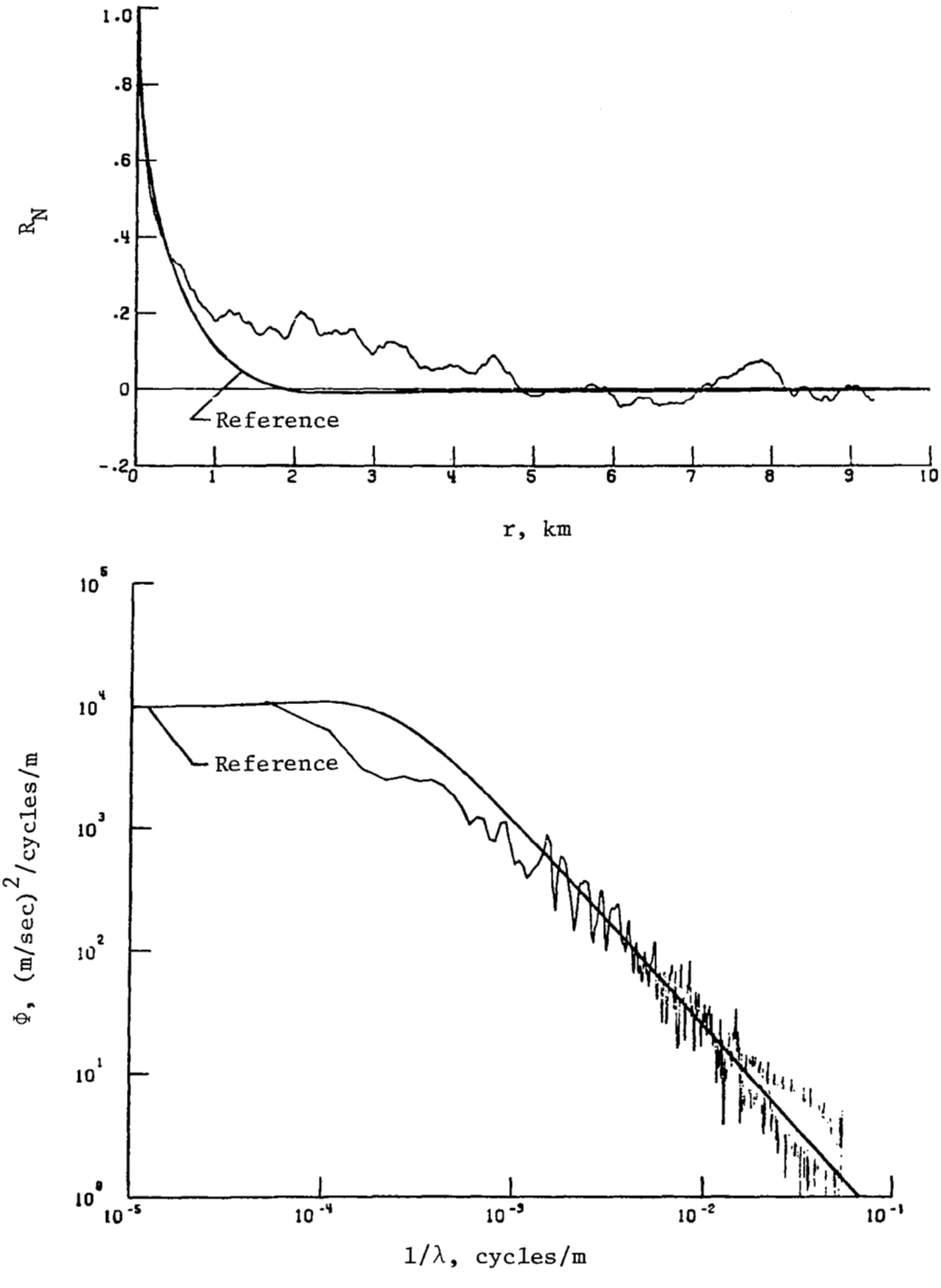

(a) Vertical component of gust velocity.

Figure 18.- Power spectra and autocorrelation functions for flight 34, run 3.

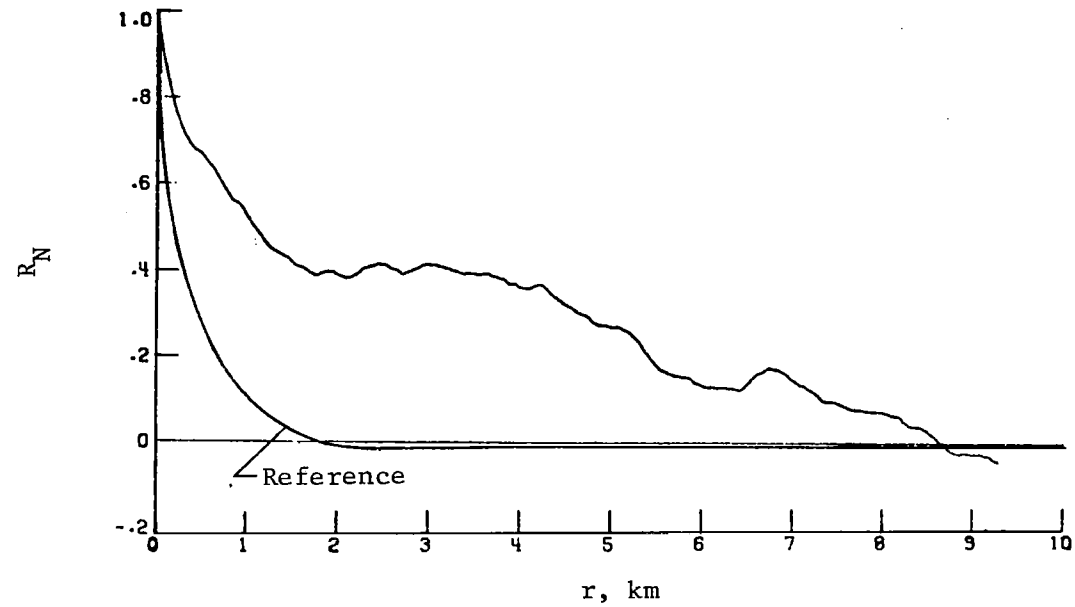

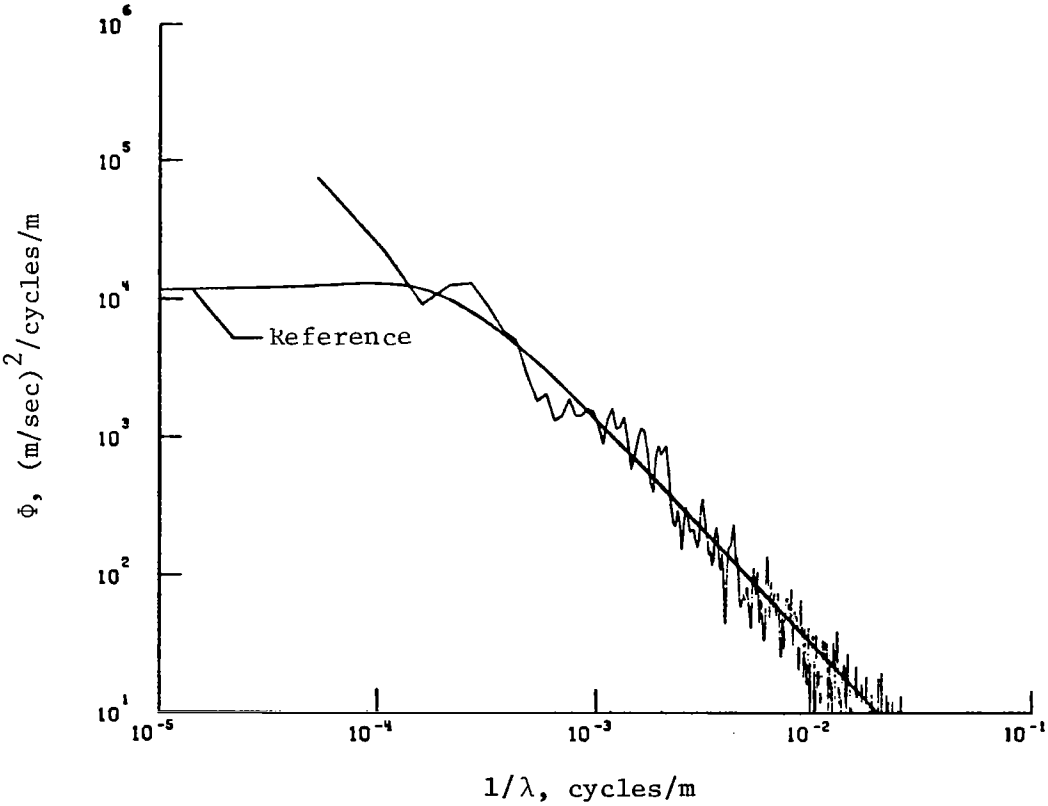

(b) Lateral component of gust velocity.

Figure 18.- Continued.

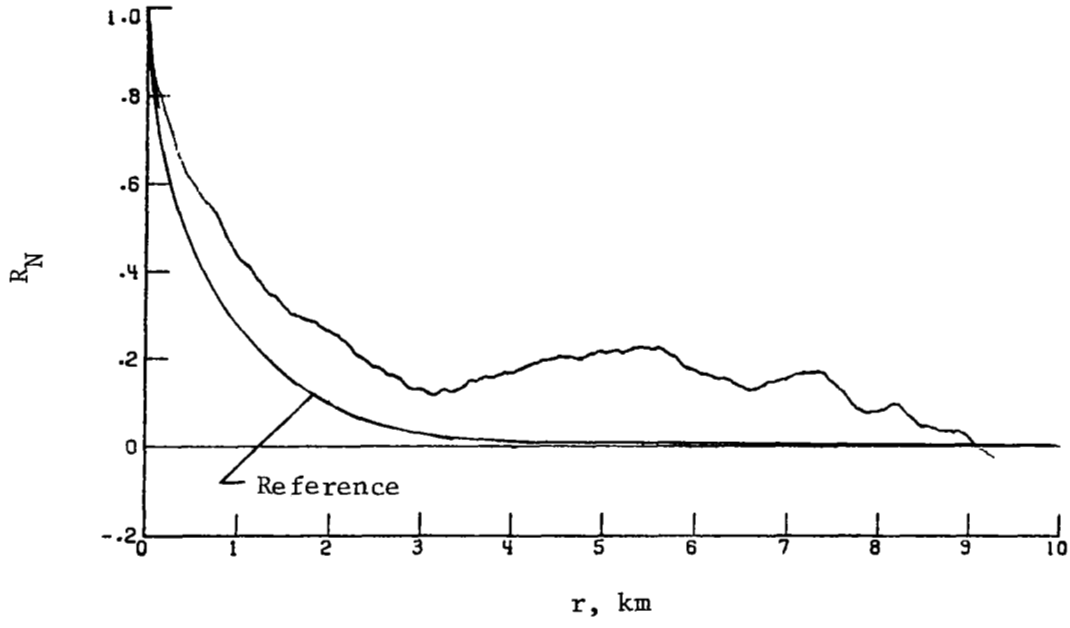

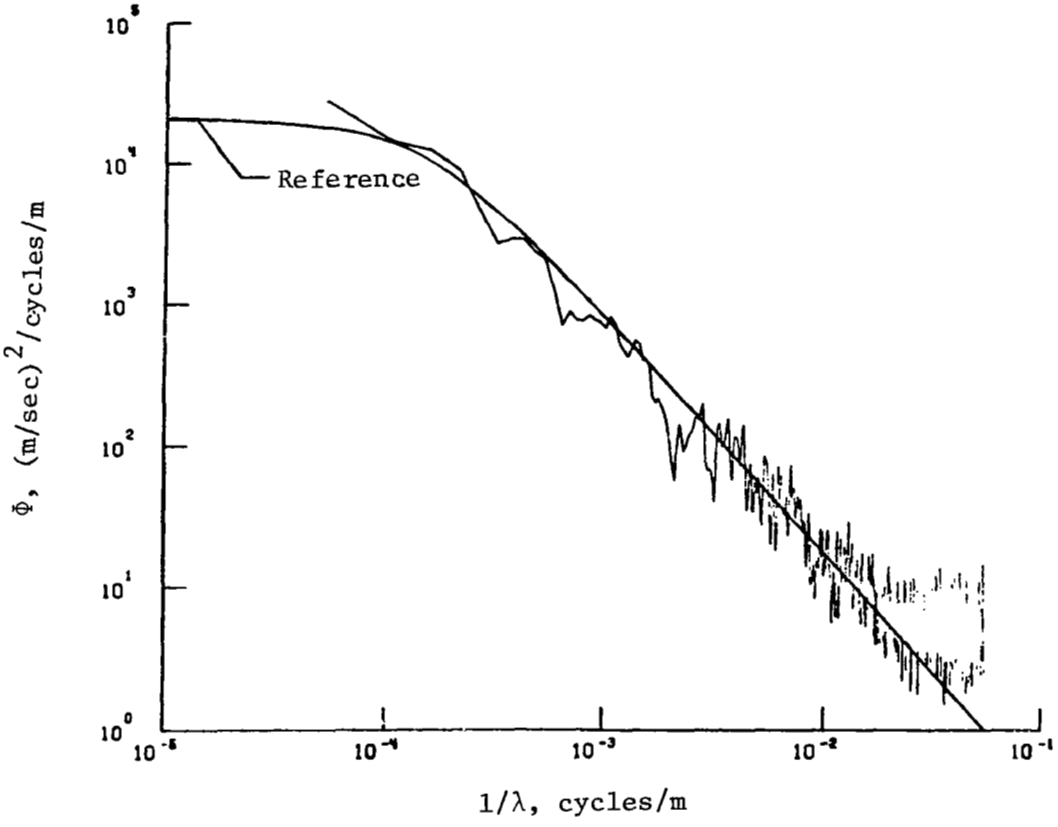

(c) Longitudinal component of gust velocity.

Figure 18.- Concluded.

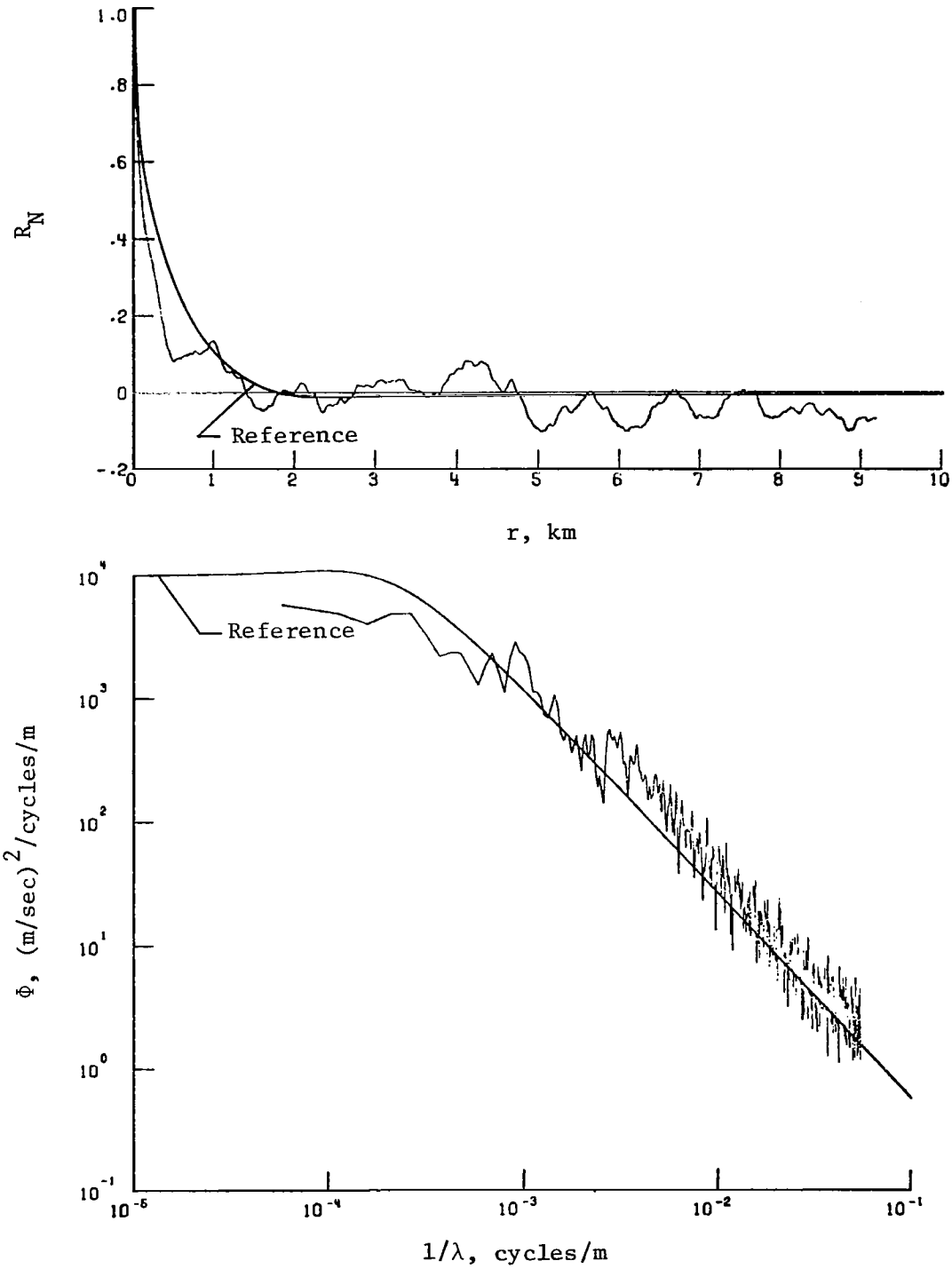

(a) Vertical component of gust velocity.

Figure 19.- Power spectra and autocorrelation functions for flight 34, run 5.

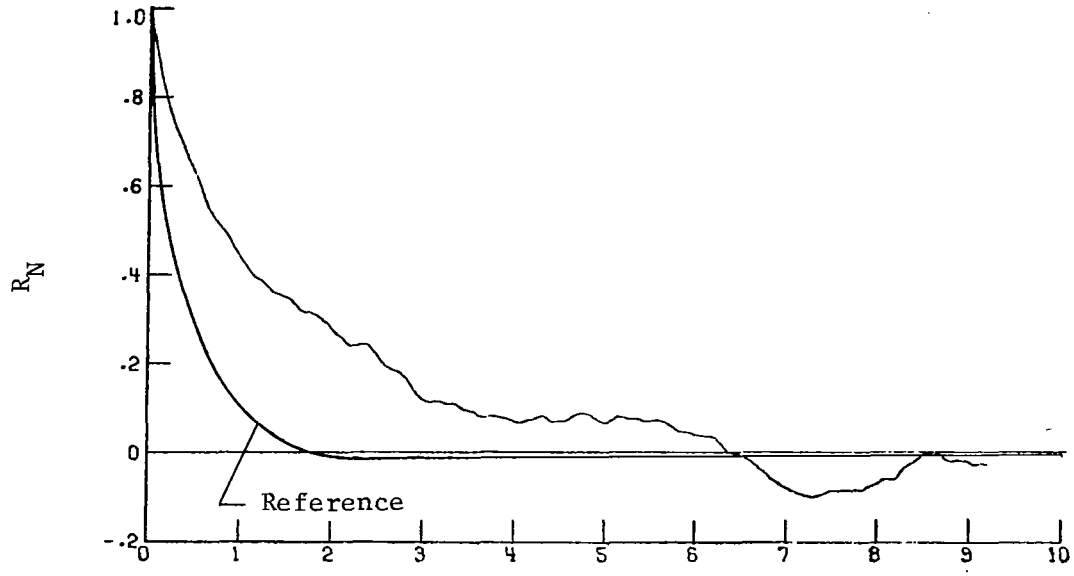

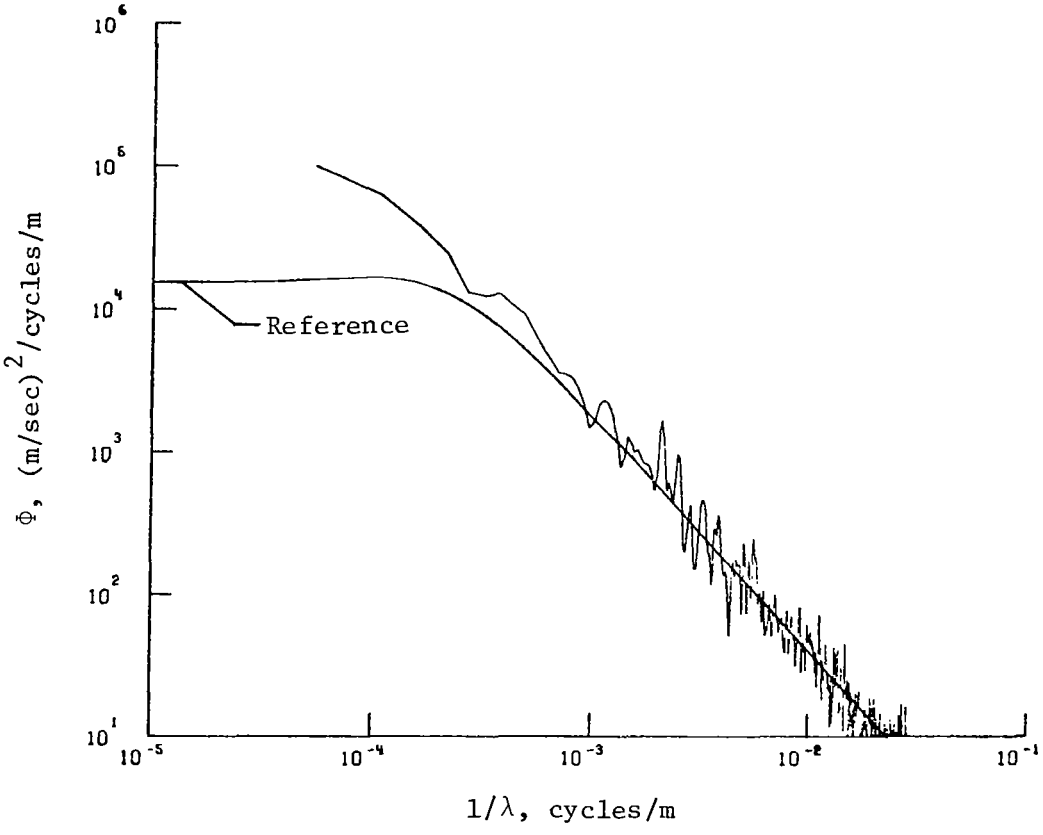

(b) Lateral component of gust velocity.

Figure 19.- Continued.

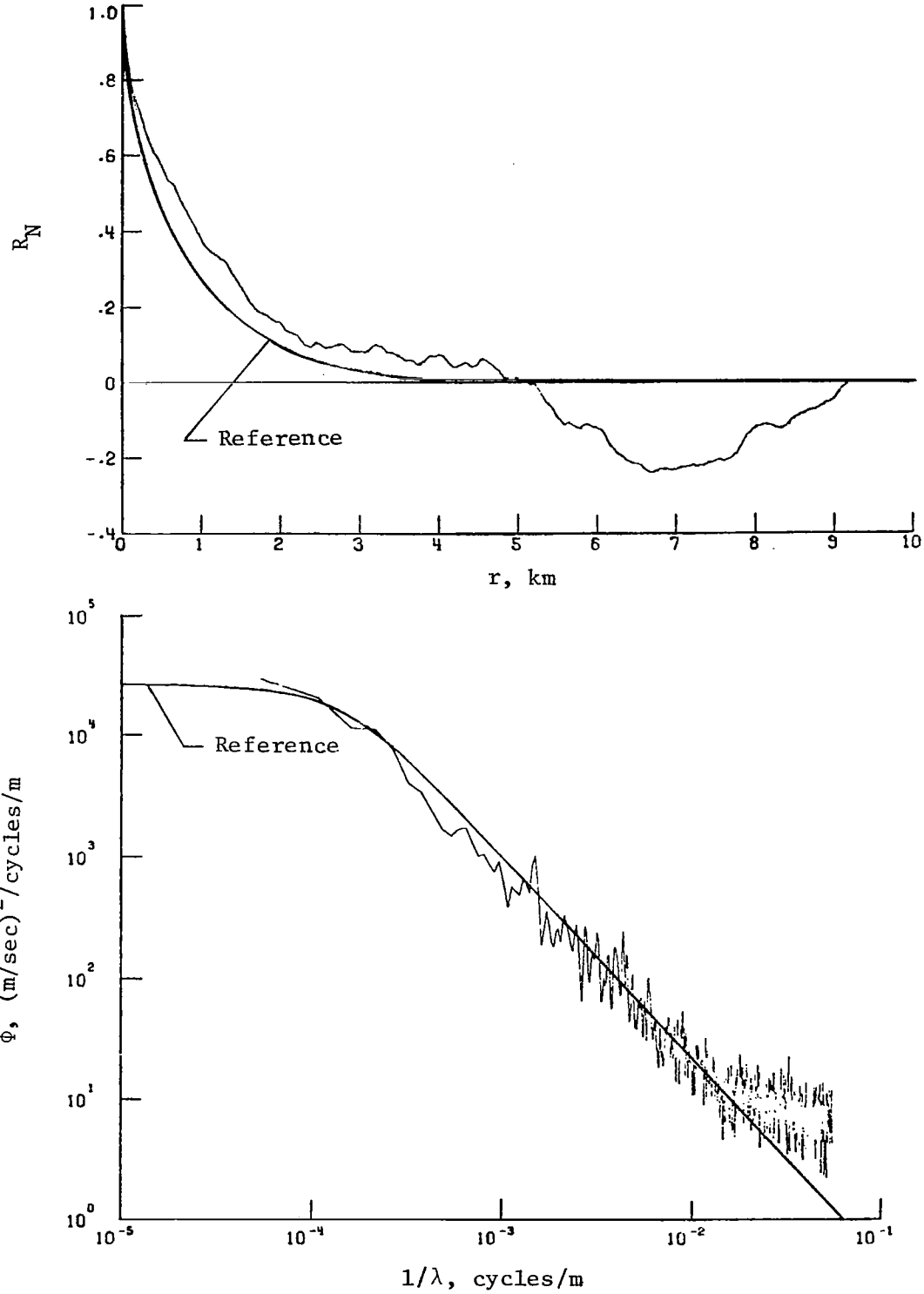

(c) Longitudinal component of gust velocity.

Figure 19.- Concluded.

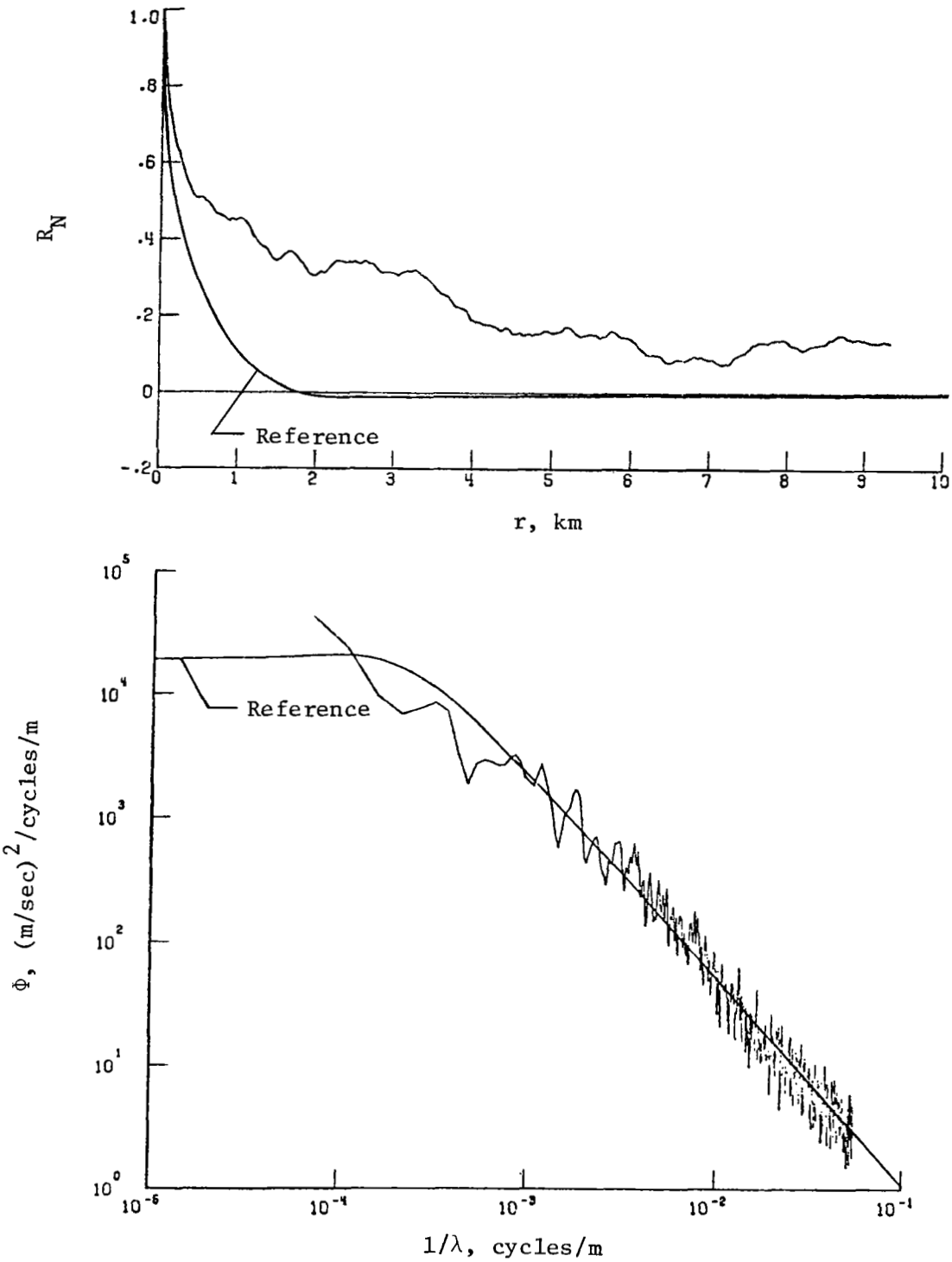

(a) Vertical component of gust velocity.

Figure 20.- Power spectra and autocorrelation functions for flight 34, run 7.

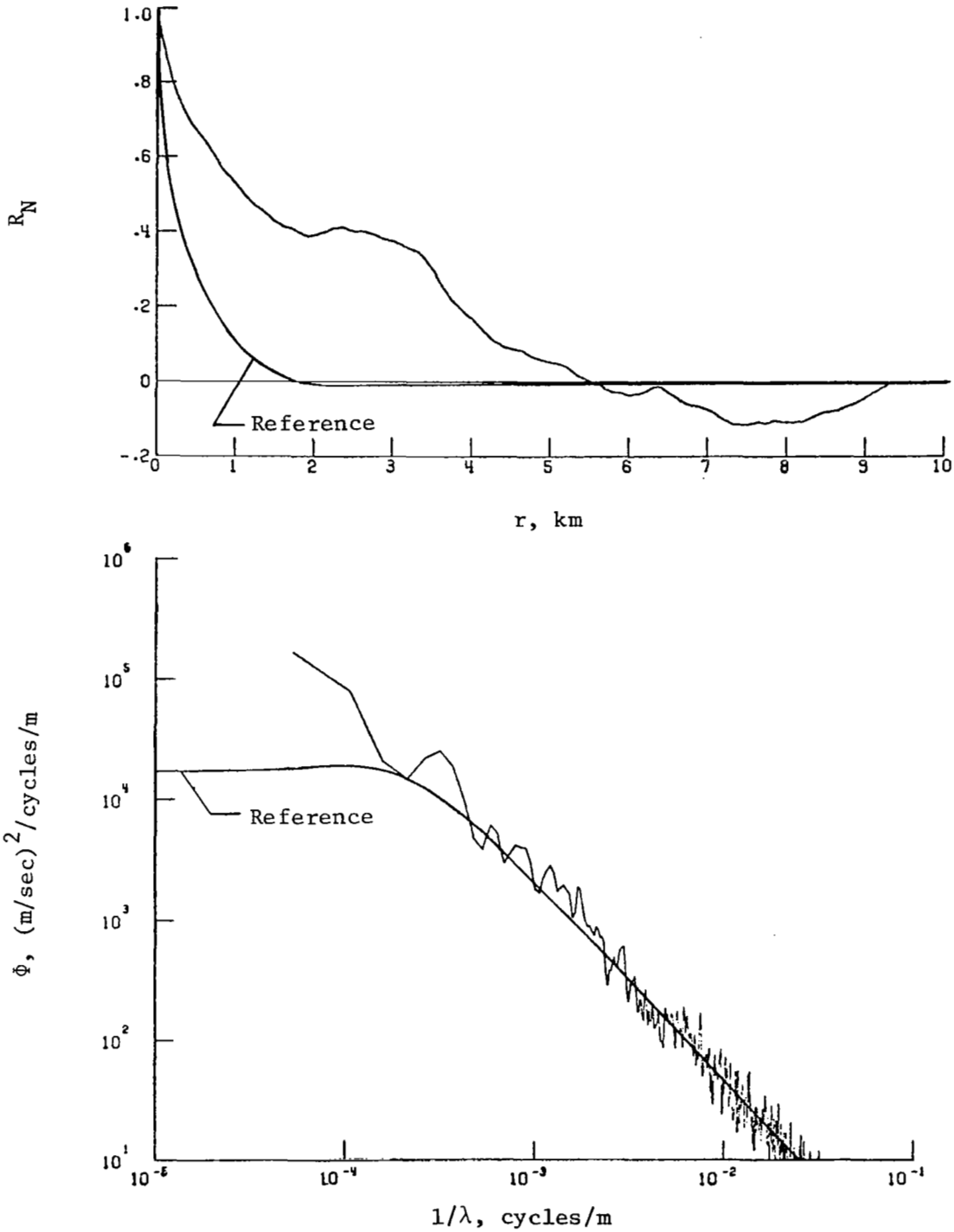

(b) Lateral component of gust velocity.

Figure 20.- Continued.

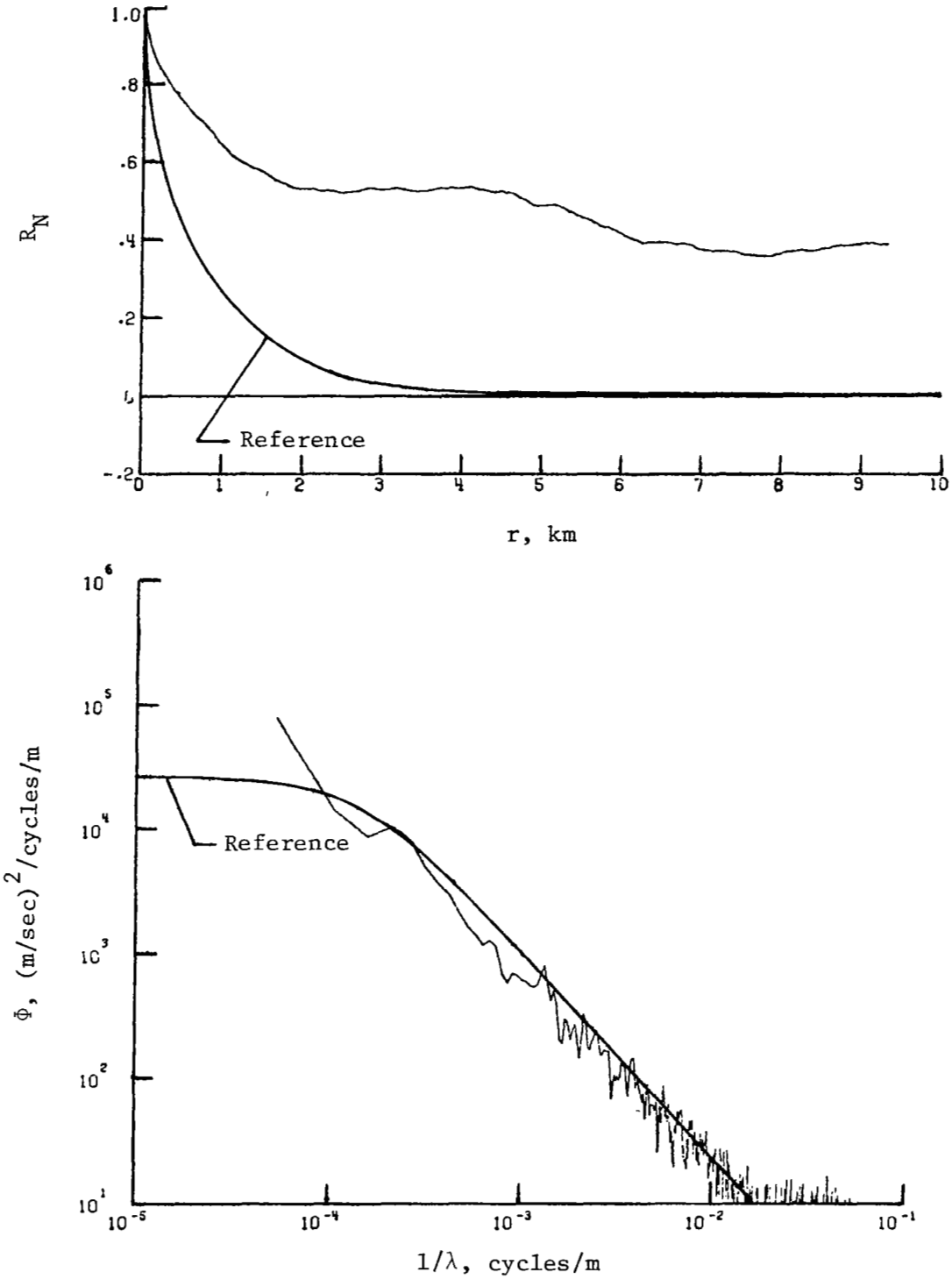

(c) Longitudinal component of gust velocity.

Figure 20.- Concluded.

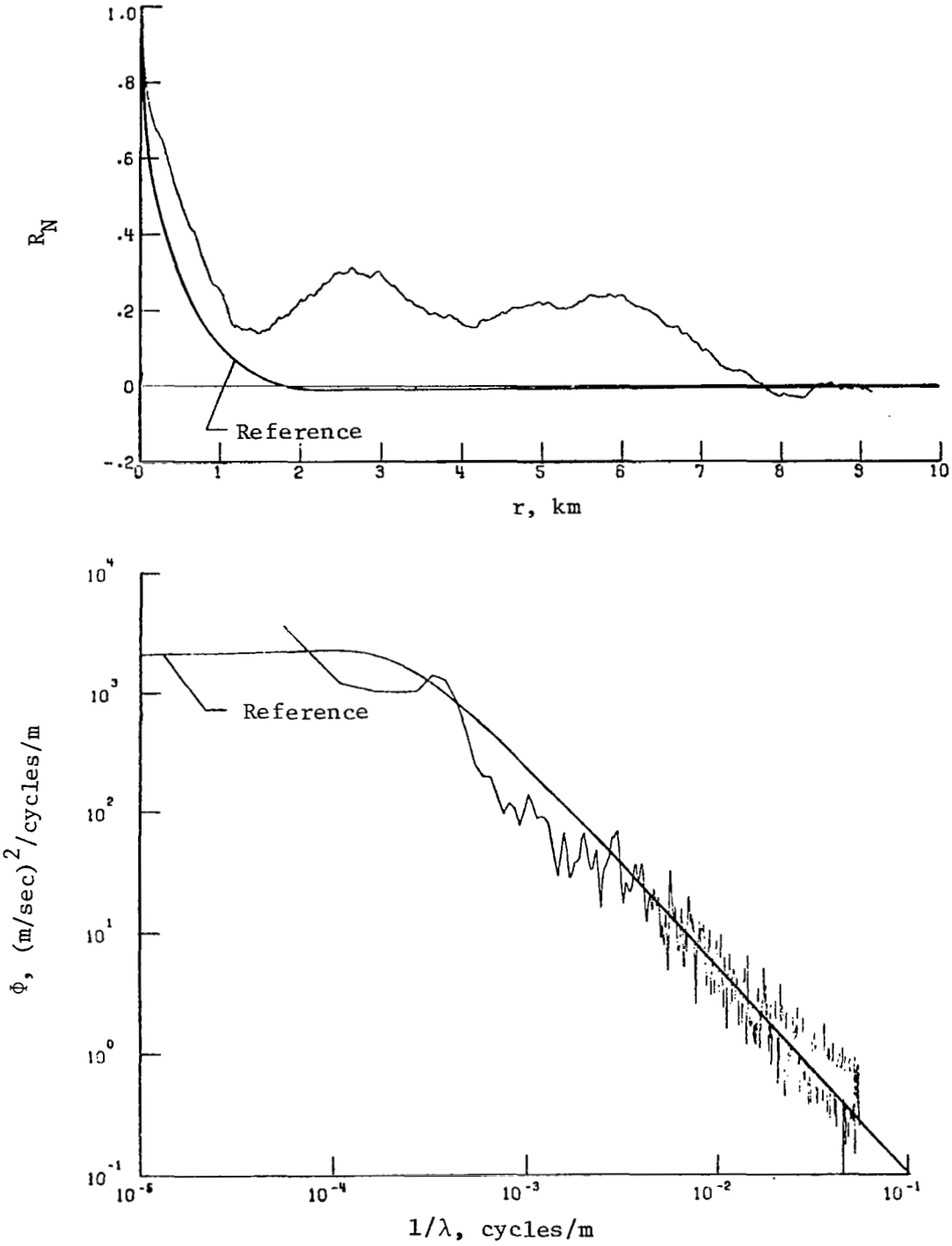

(a) Vertical component of gust velocity.

Figure 21.- Power spectra and autocorrelation functions for flight 39, run 2.

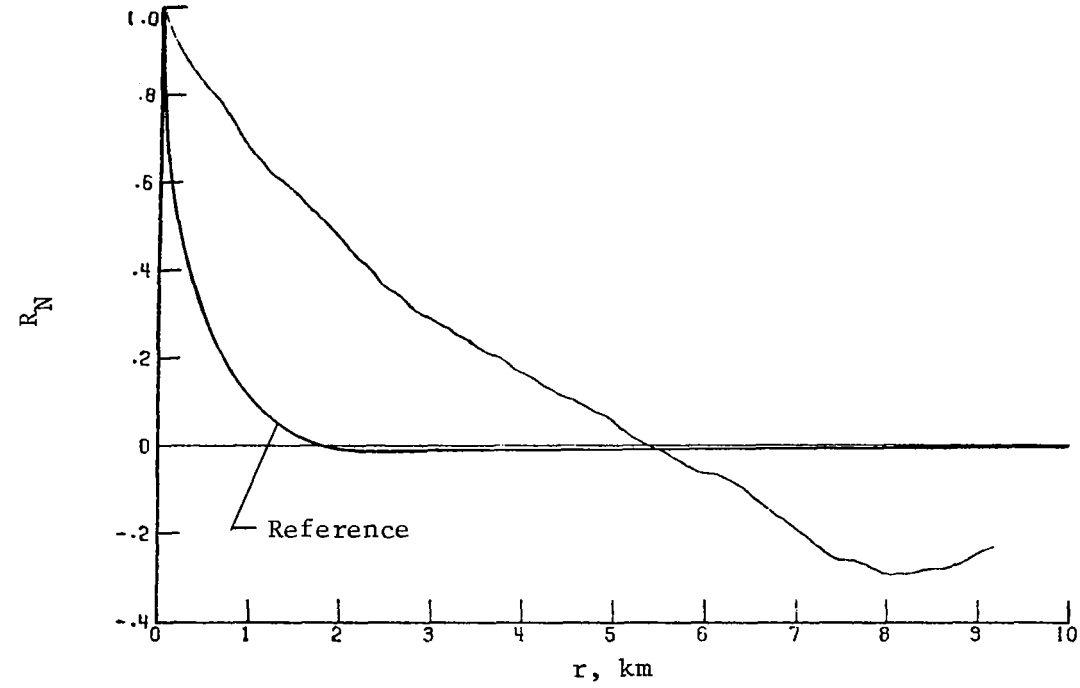

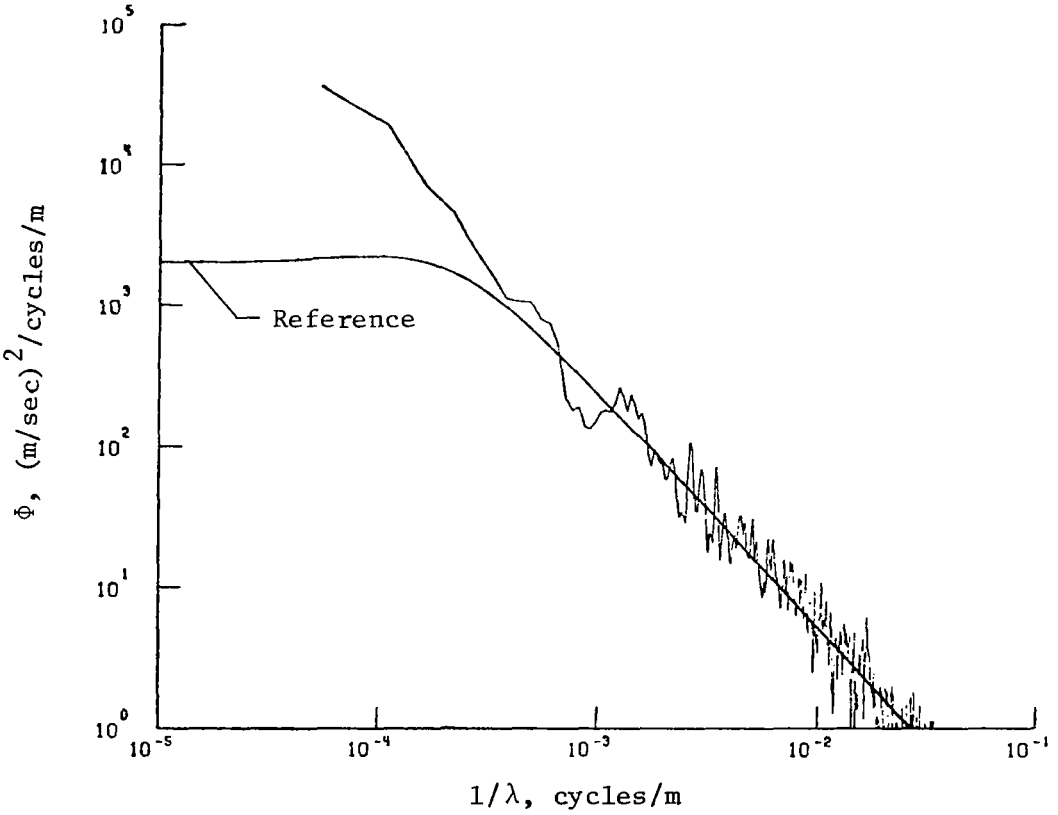

(b) Lateral component of gust velocity.

Figure 21.- Continued.

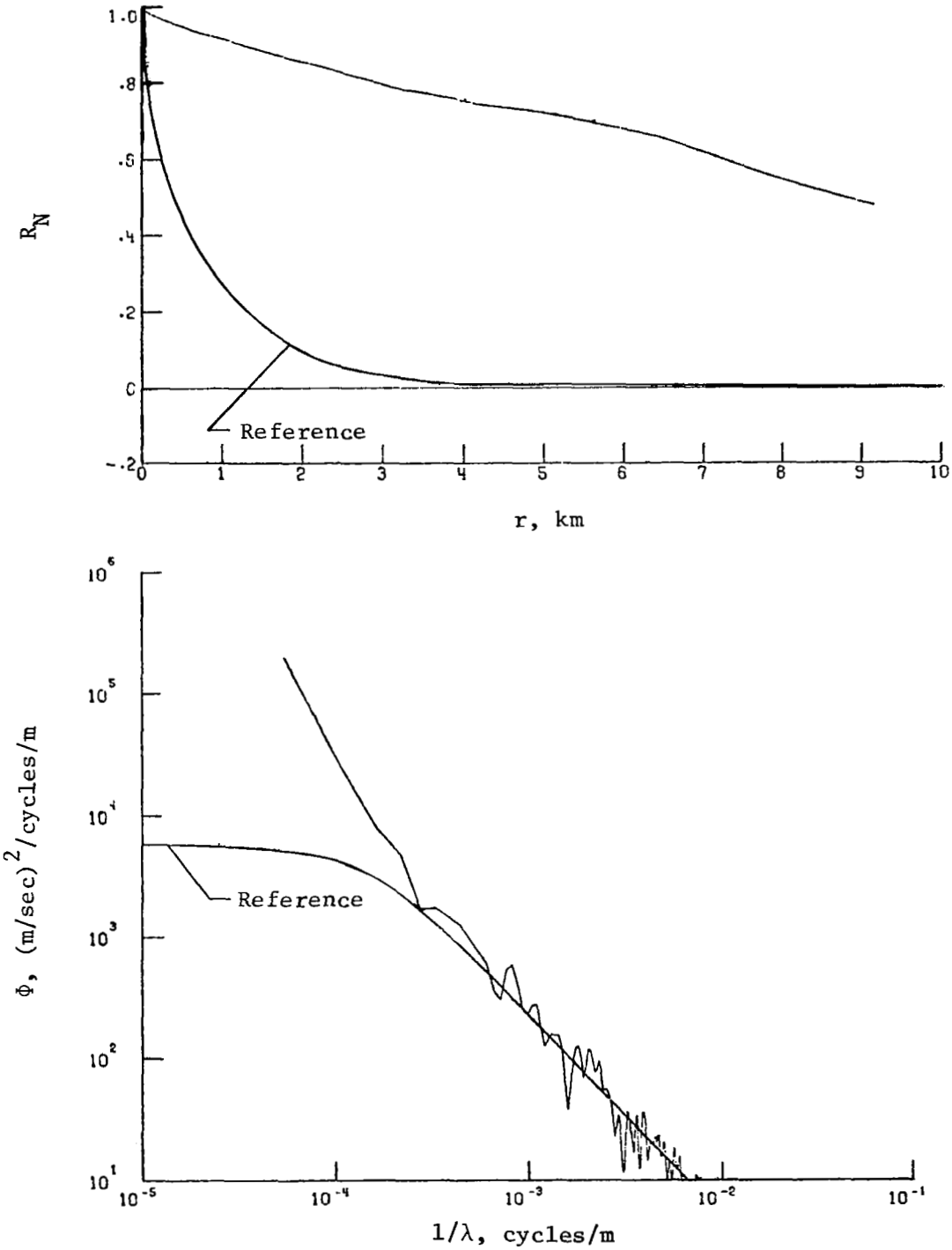

(c) Longitudinal component of gust velocity.

Figure 21.- Concluded.

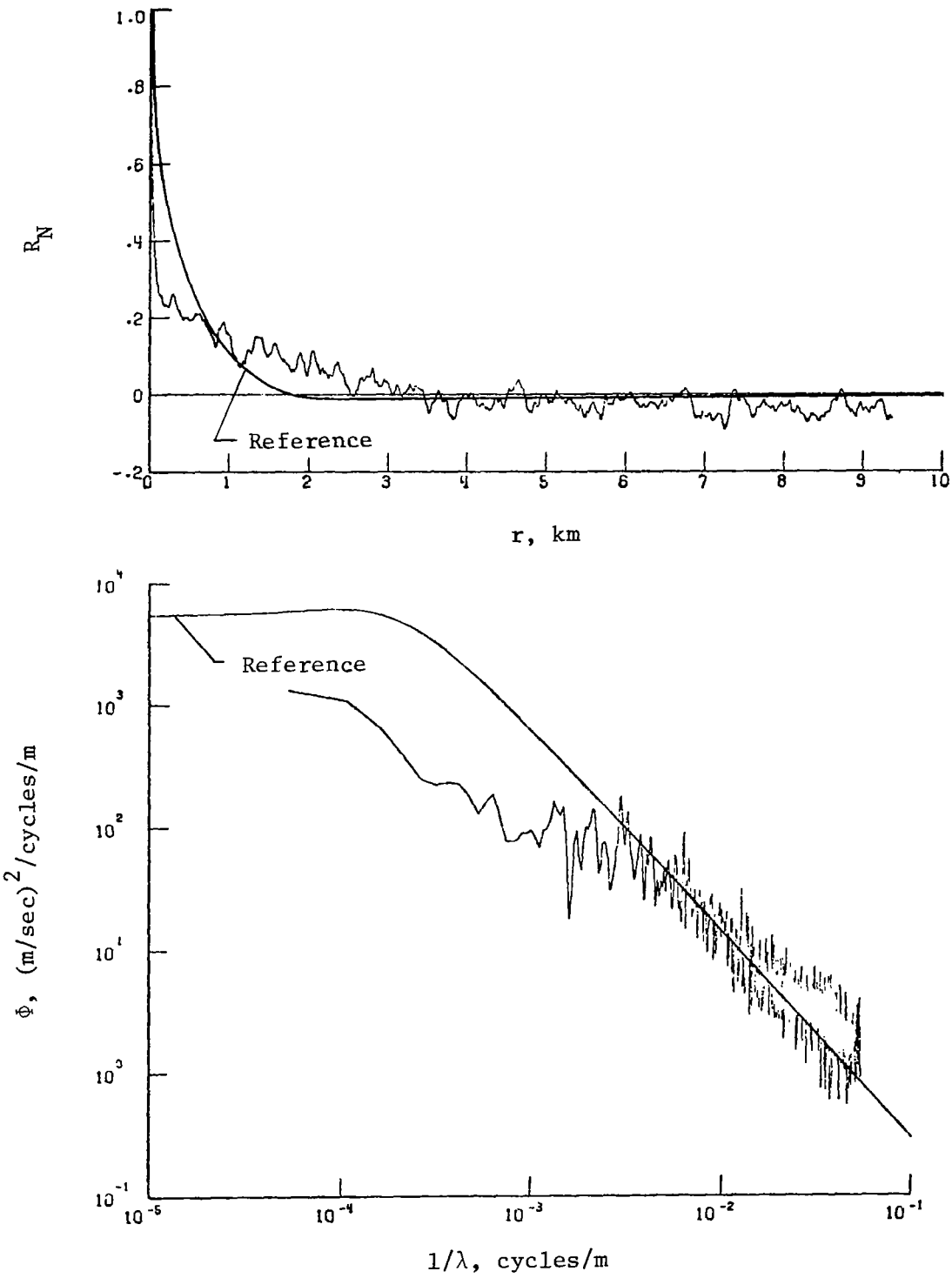

(a) Vertical component of gust velocity.

Figure 22.- Power spectra and autocorrelation functions for flight 39, run 3.

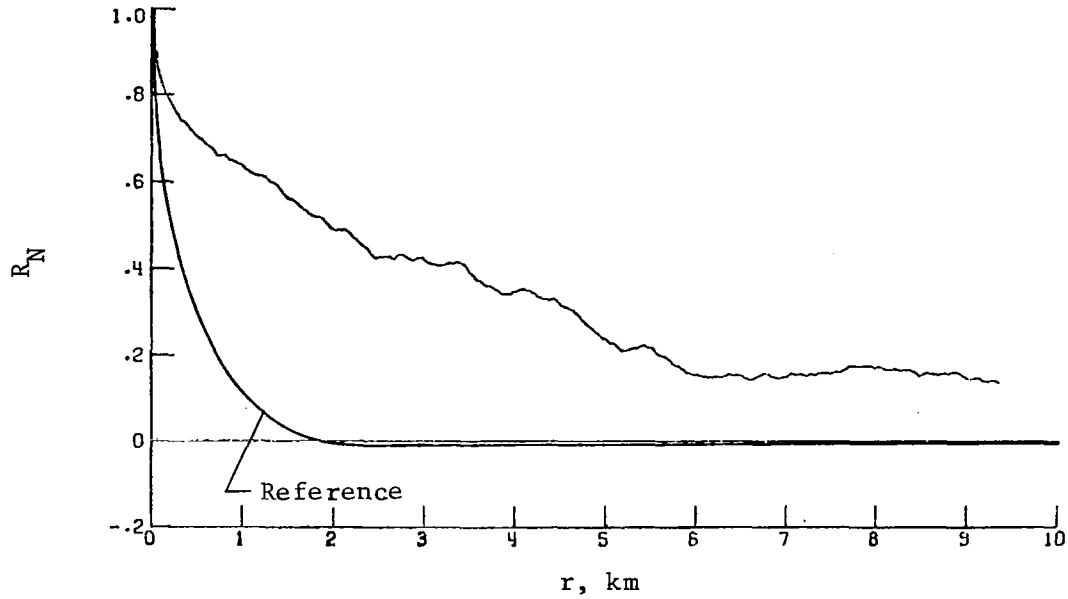

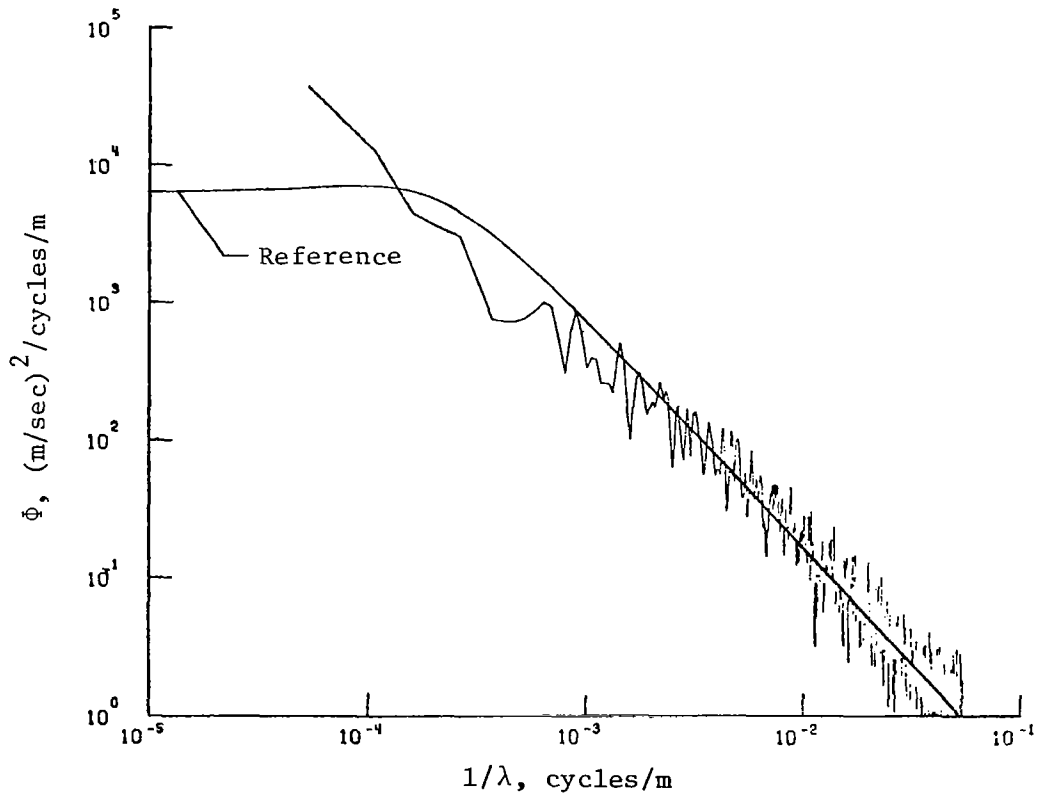

(b) Lateral component of gust velocity.

Figure 22.- Continued.

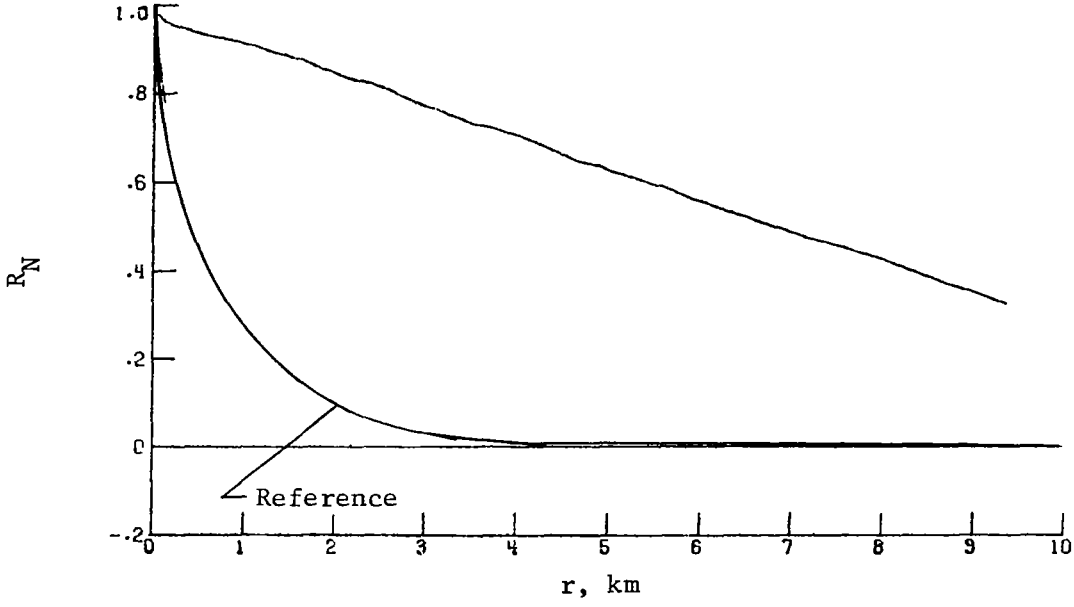

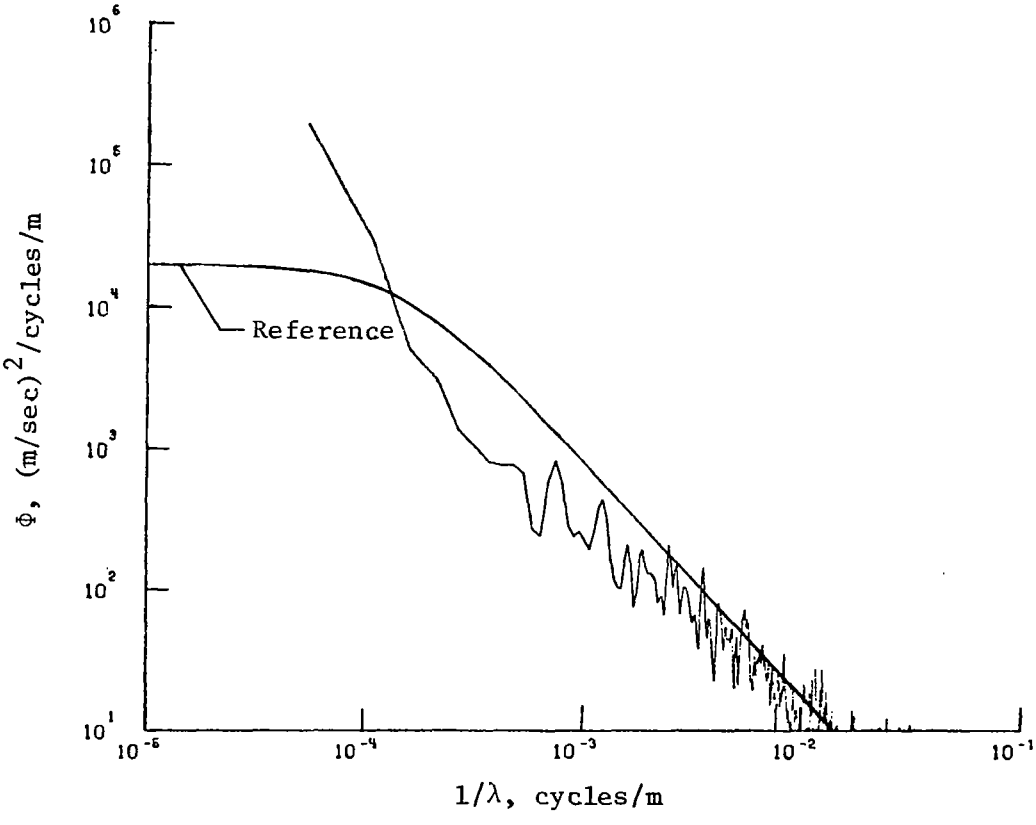

(c) Longitudinal component of gust velocity.

Figure 22.- Concluded.

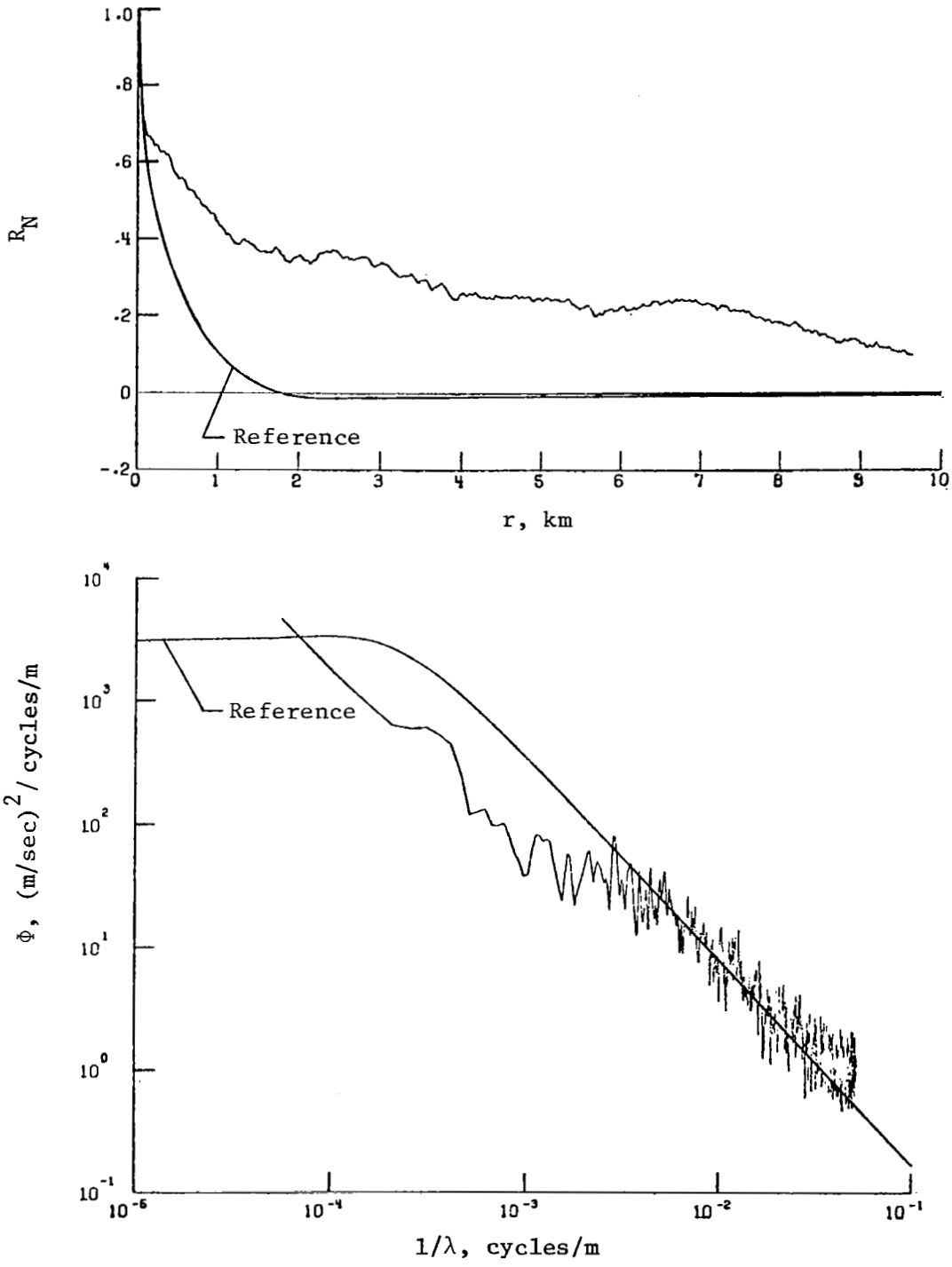

(a) Vertical component of gust velocity.

Figure 23.- Power spectra and autocorrelation functions for flight 39, run 5.

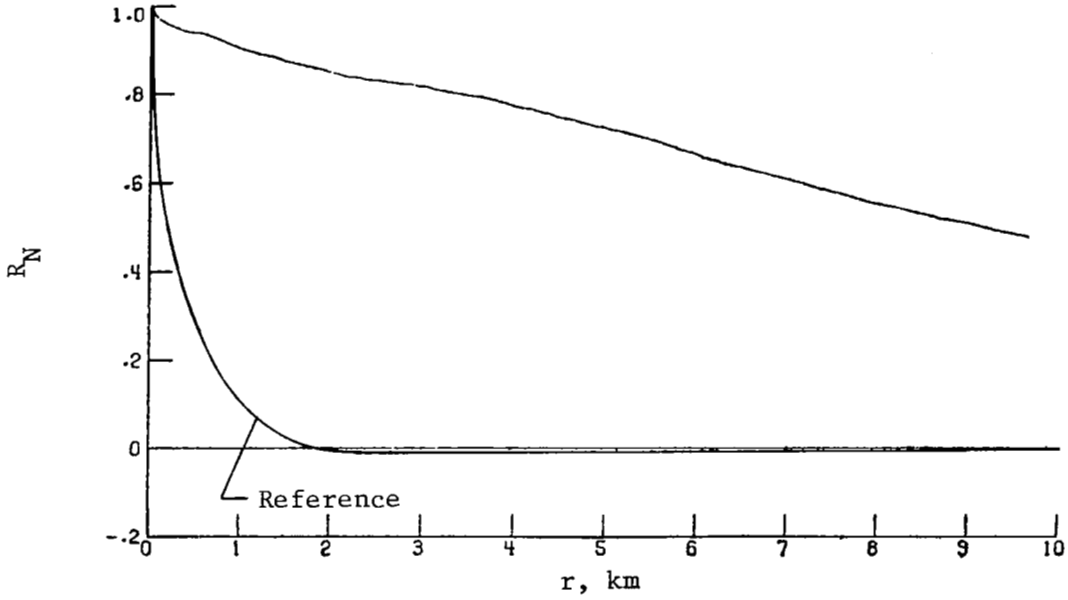

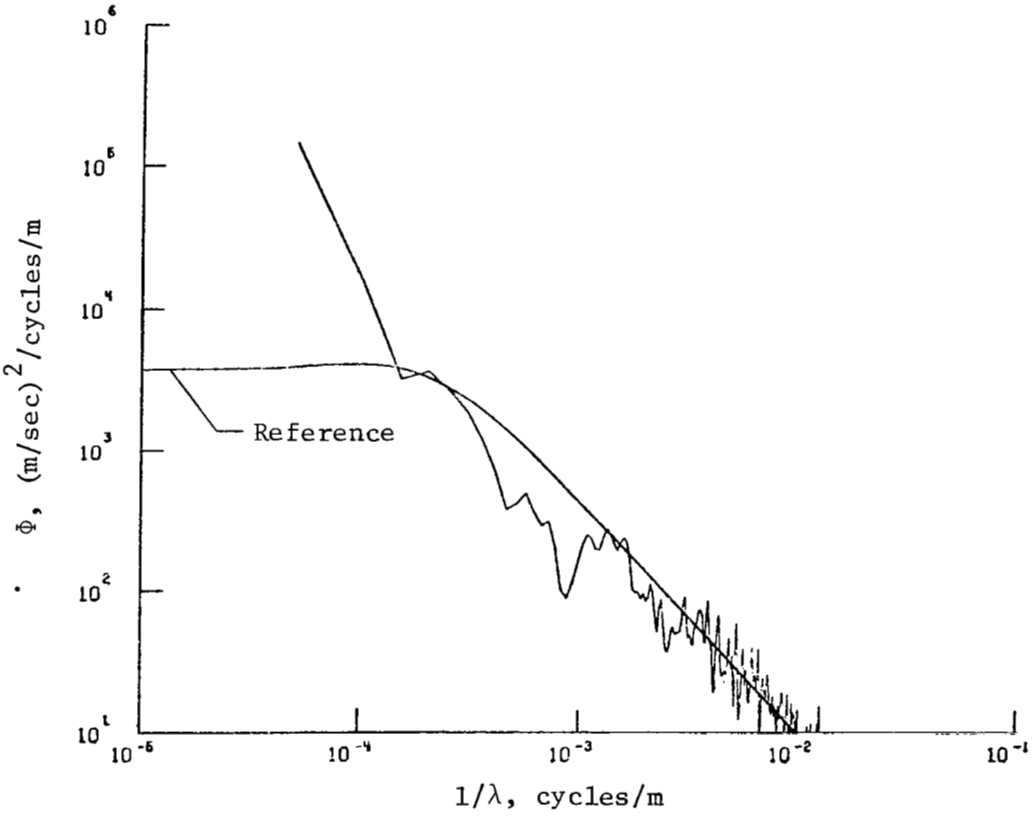

(b) Lateral component of gust velocity.

Figure 23.- Continued.

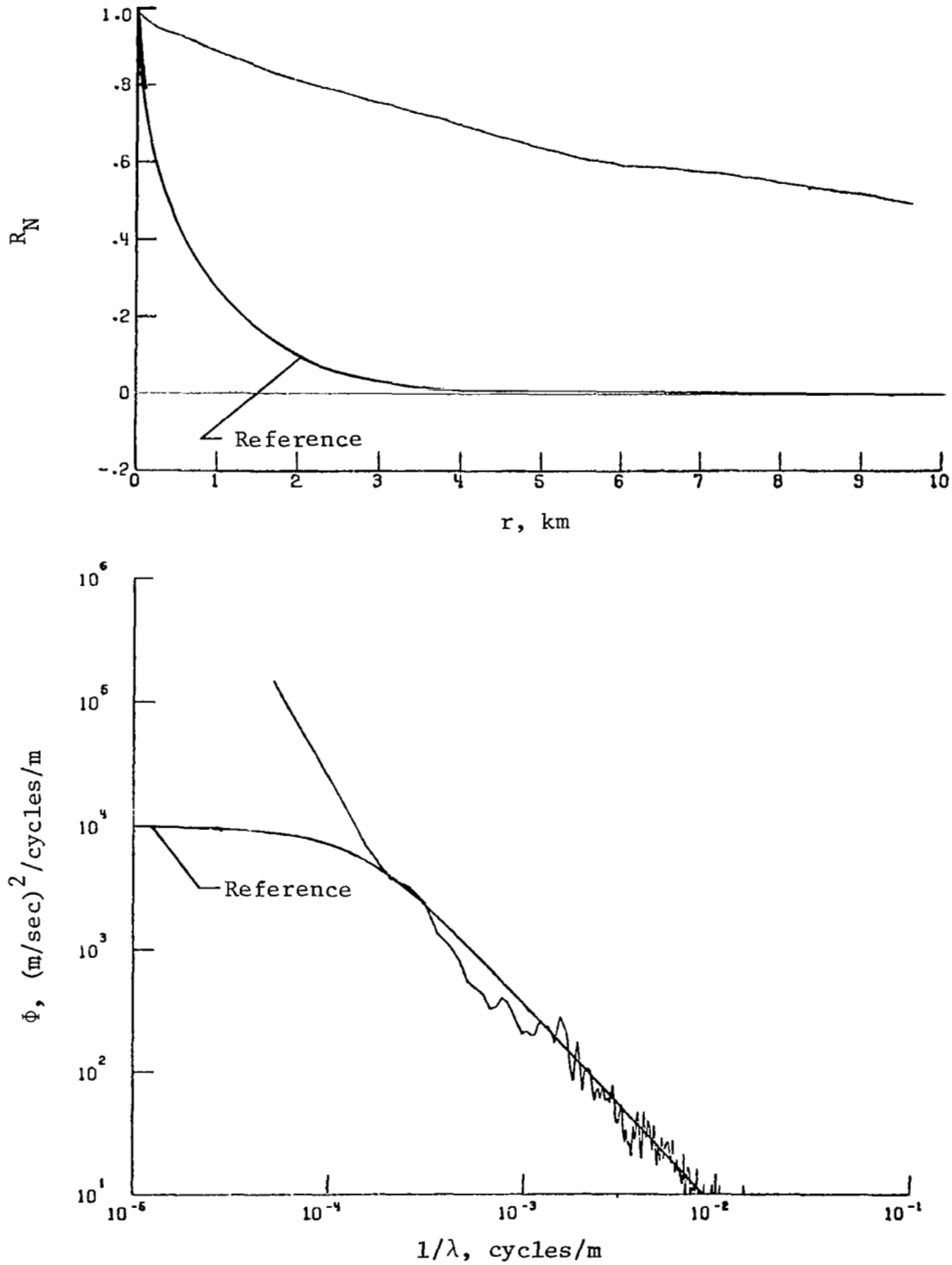

(c) Longitudinal component of gust velocity.

Figure 23.- Concluded.

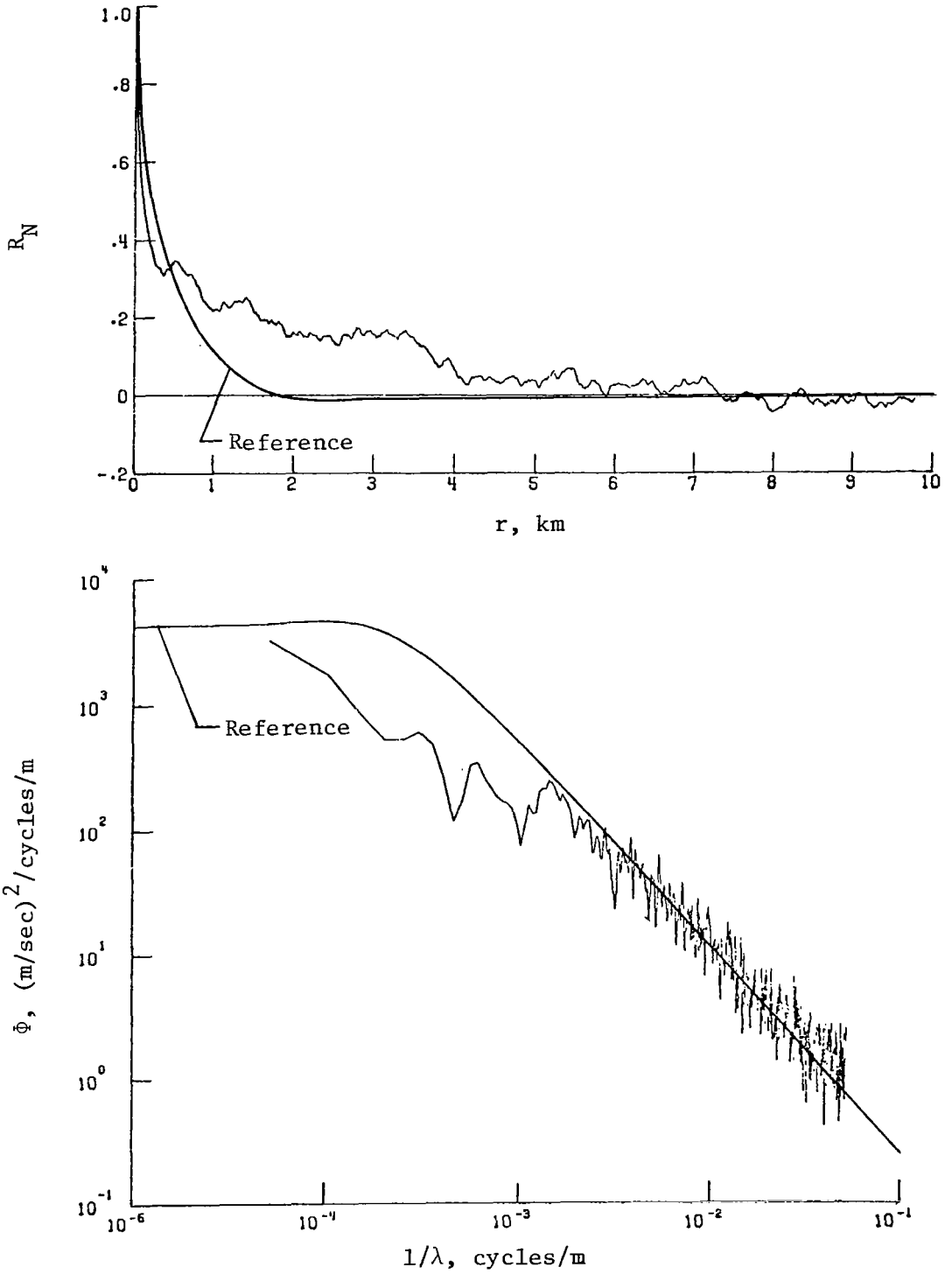

(a) Vertical component of gust velocity.

Figure 24.- Power spectra and autocorrelation functions for flight 39, run 7.

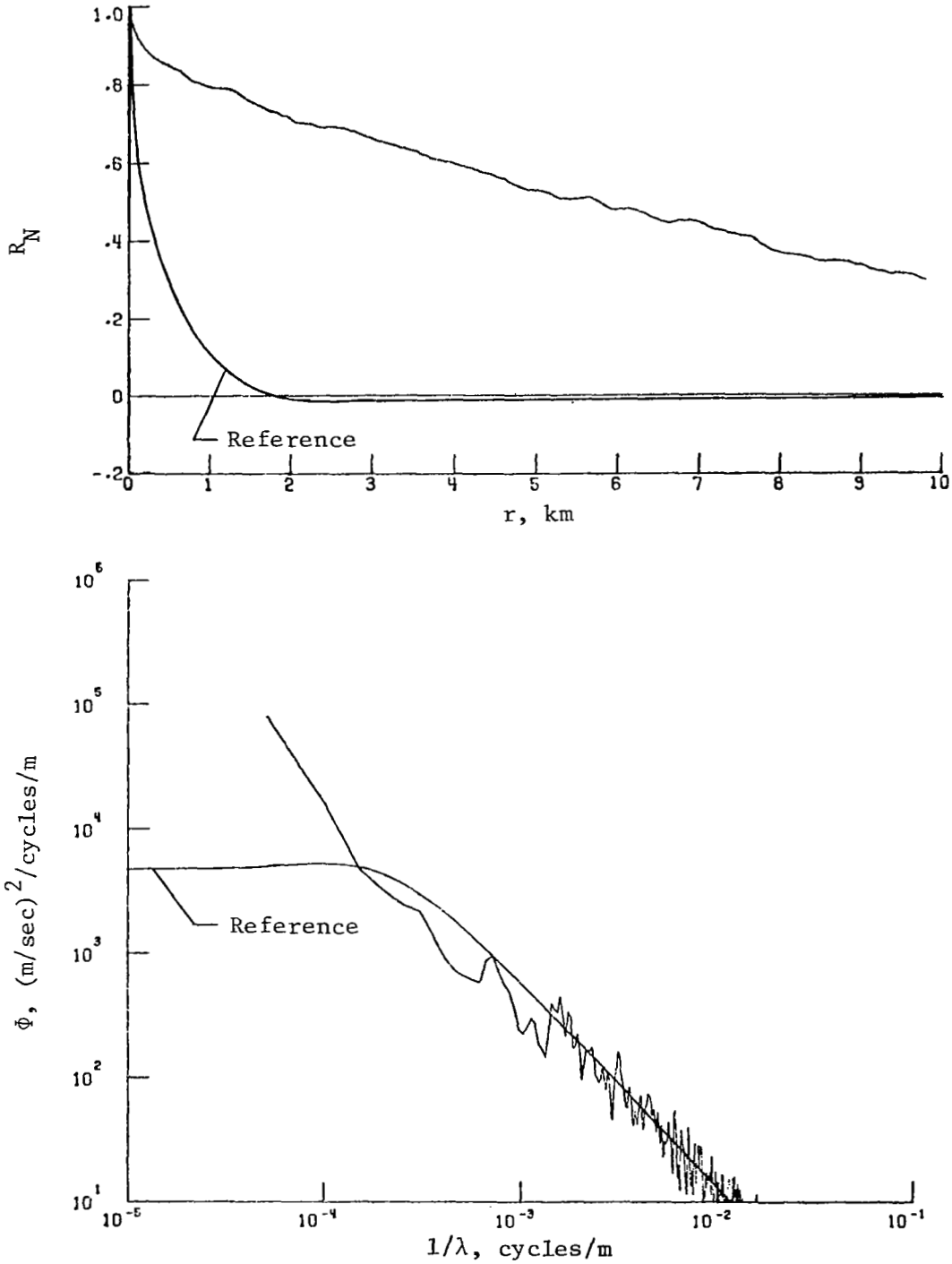

(b) Lateral component of gust velocity.

Figure 24.- Continued.

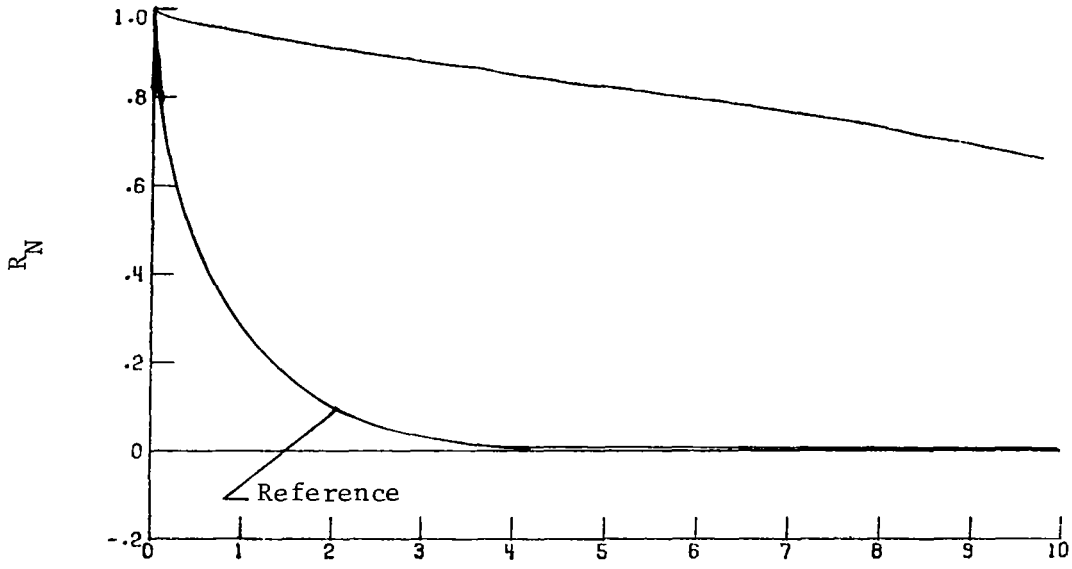

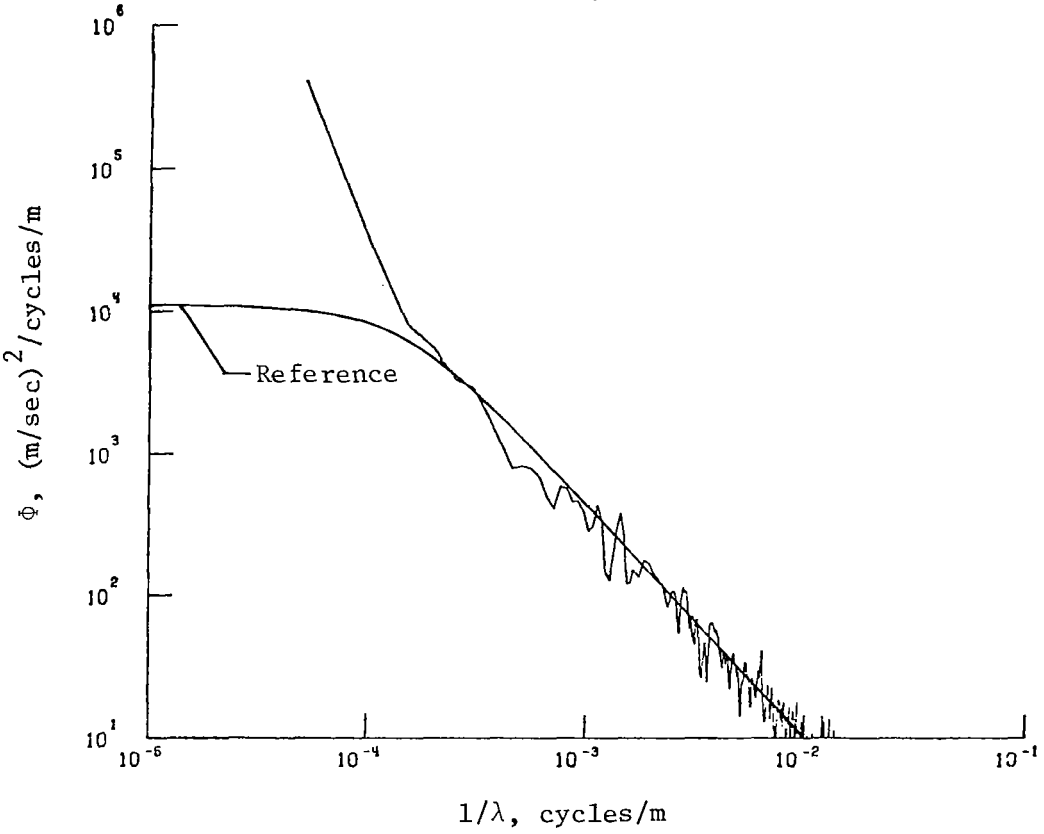

(c) Longitudinal component of gust velocity.

Figure 24.- Concluded.

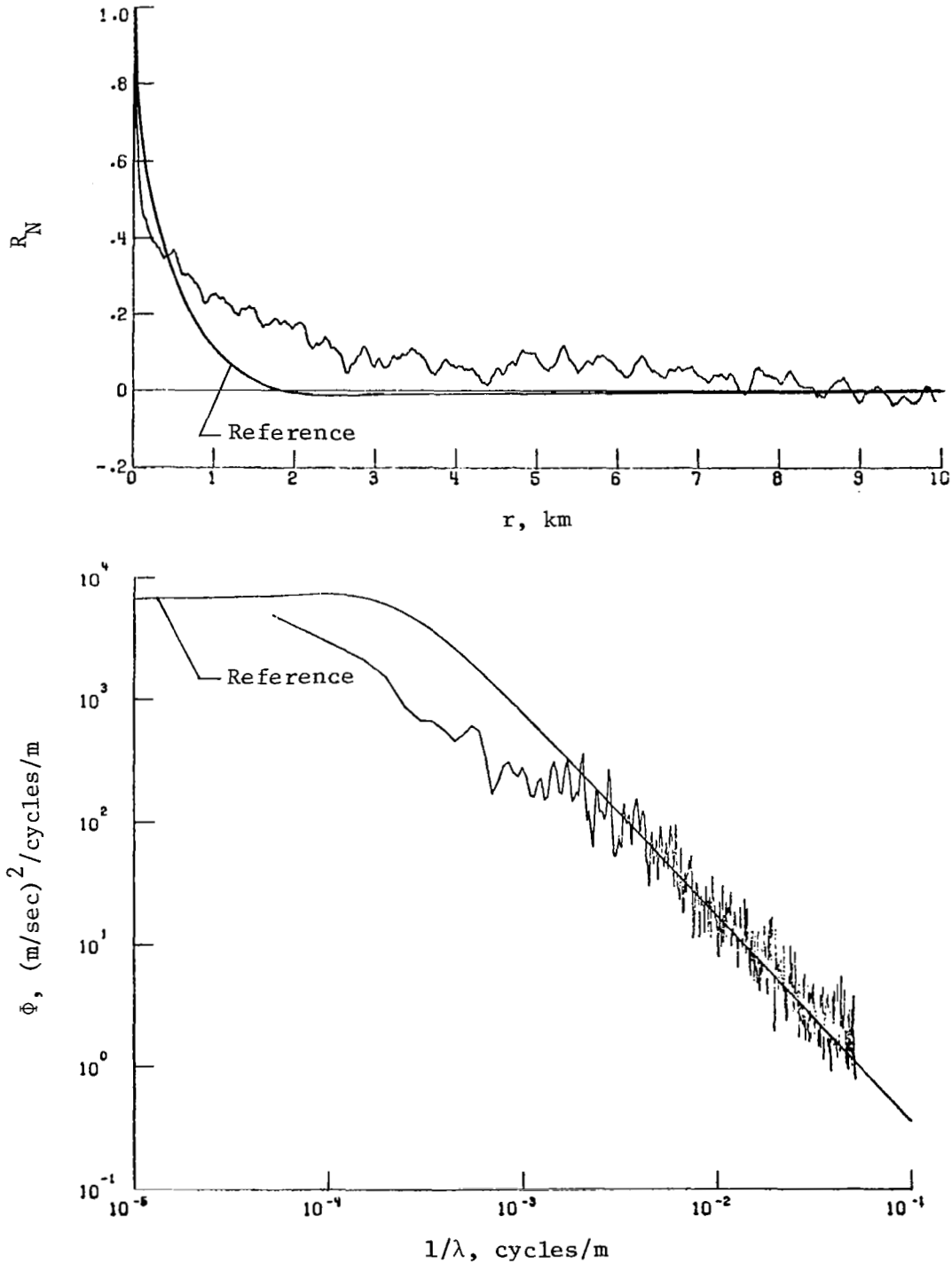

(a) Vertical component of gust velocity.

Figure 25.- Power spectra and autocorrelation functions for flight 39, run 9.

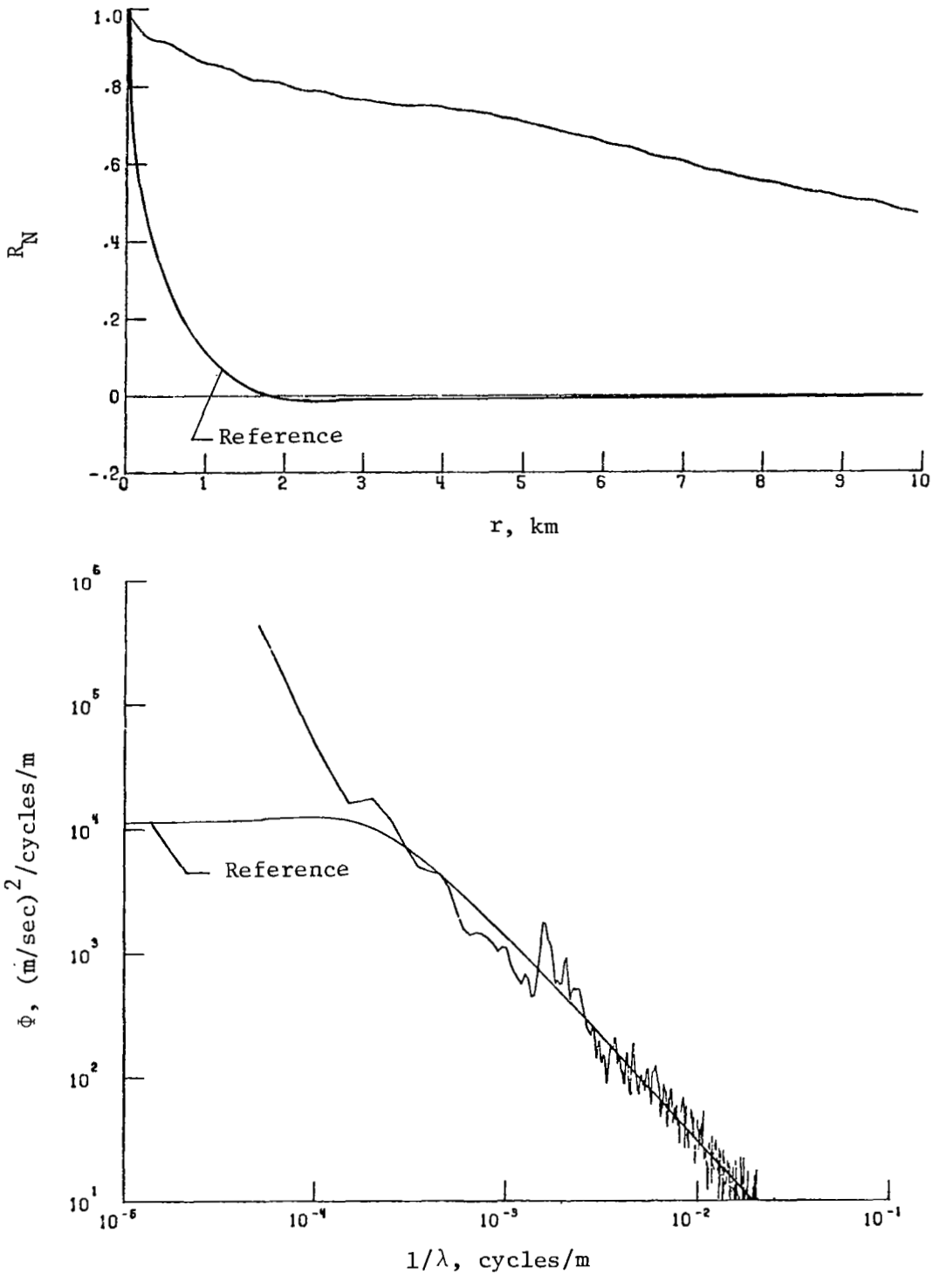

(b) Lateral component of gust velocity.

Figure 25.- Continued.

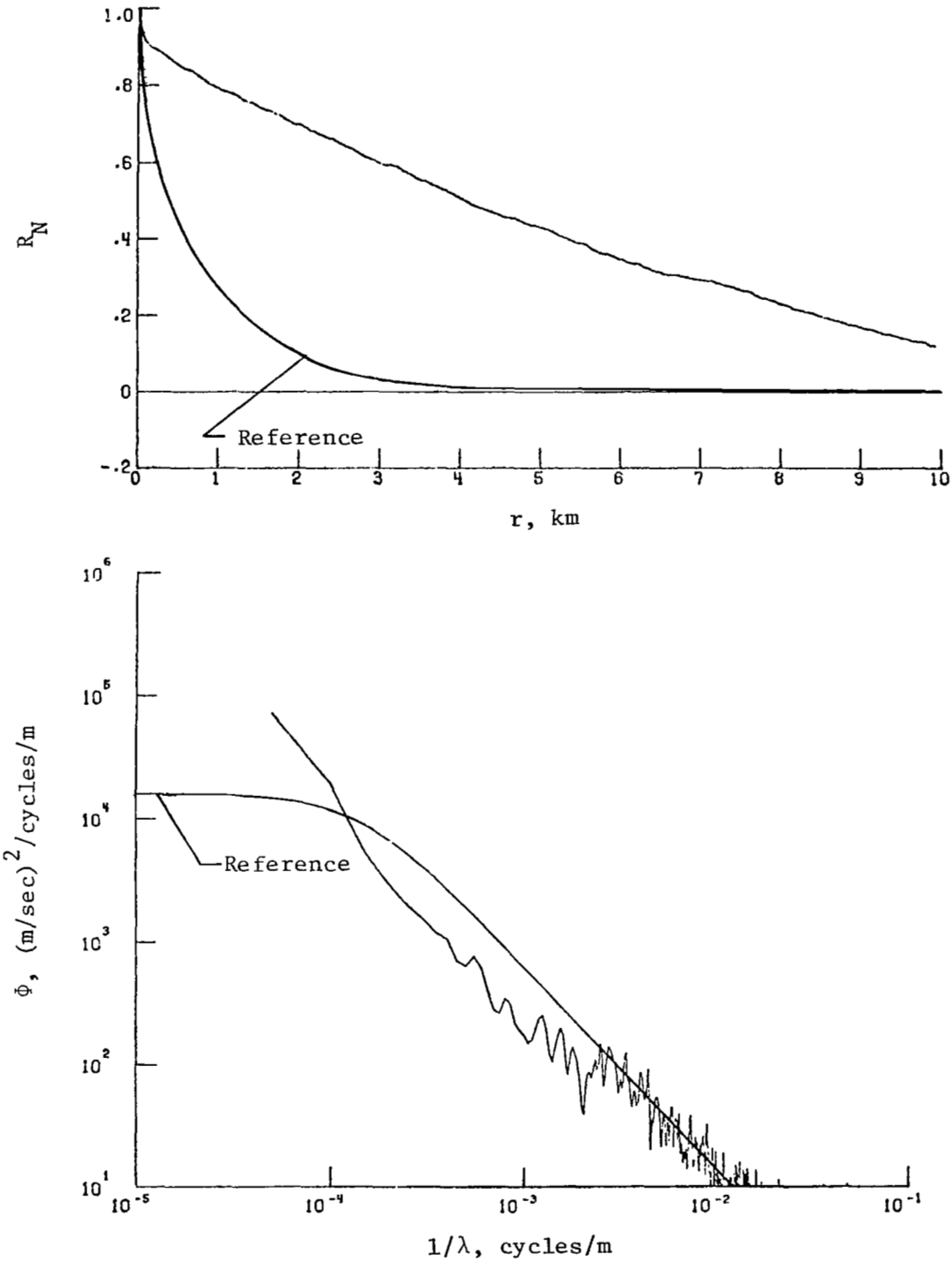

(c) Longitudinal component of gust velocity.

Figure 25.- Concluded.

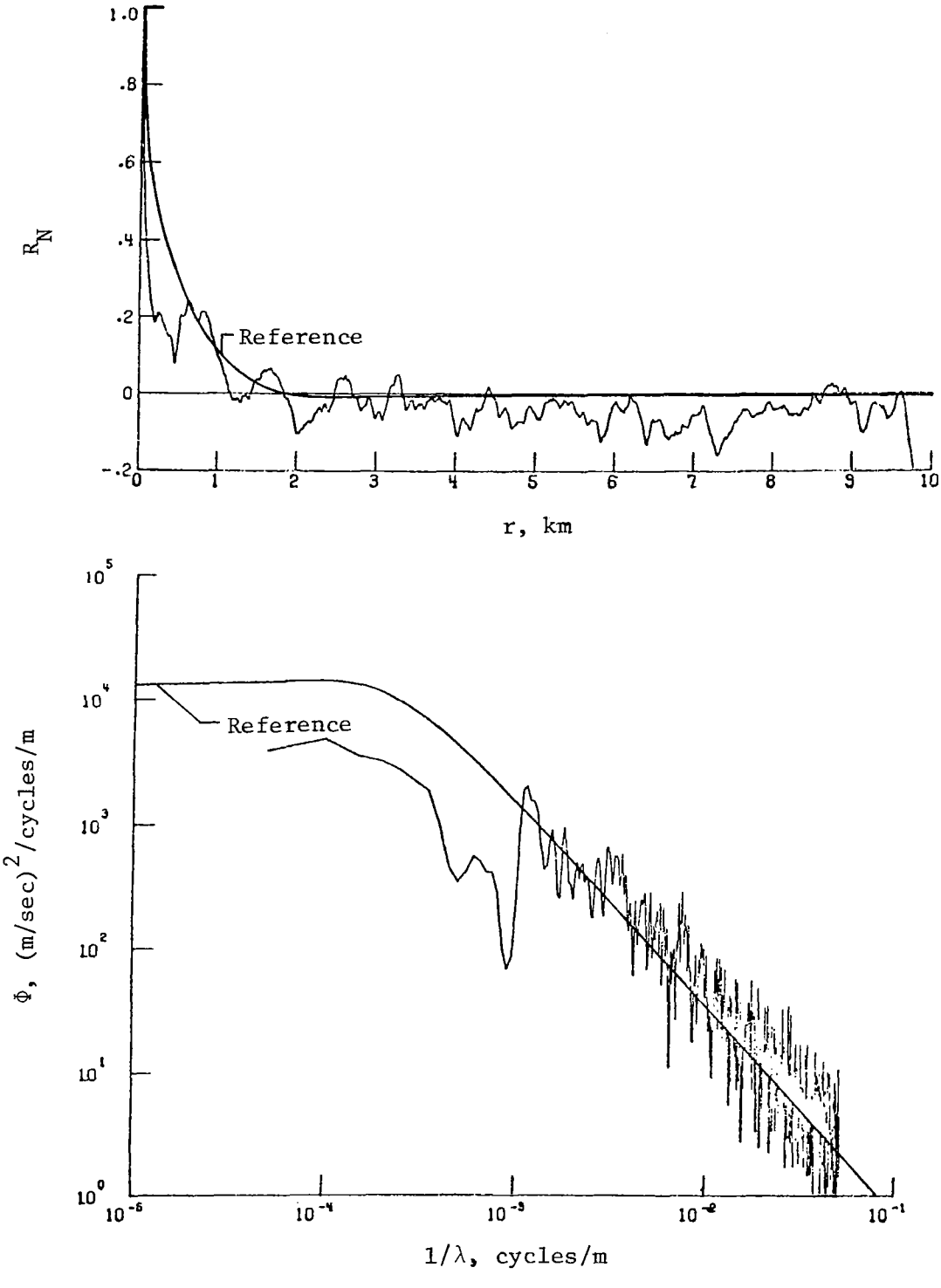

(a) Vertical component of gust velocity.

Figure 26.- Power spectra and autocorrelation functions for flight 39, run 10.

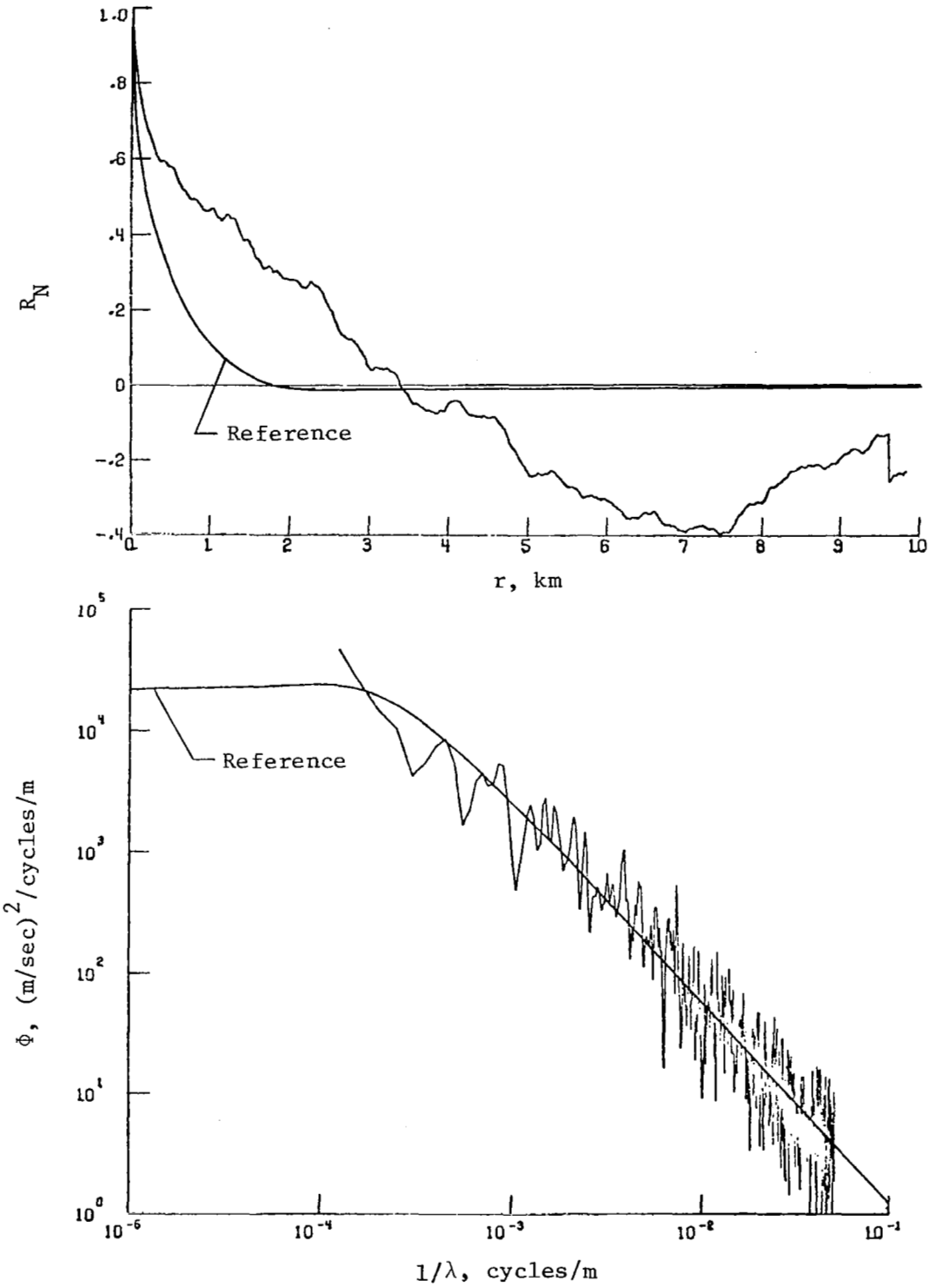

(b) Lateral component of gust velocity.

Figure 26.- Continued.

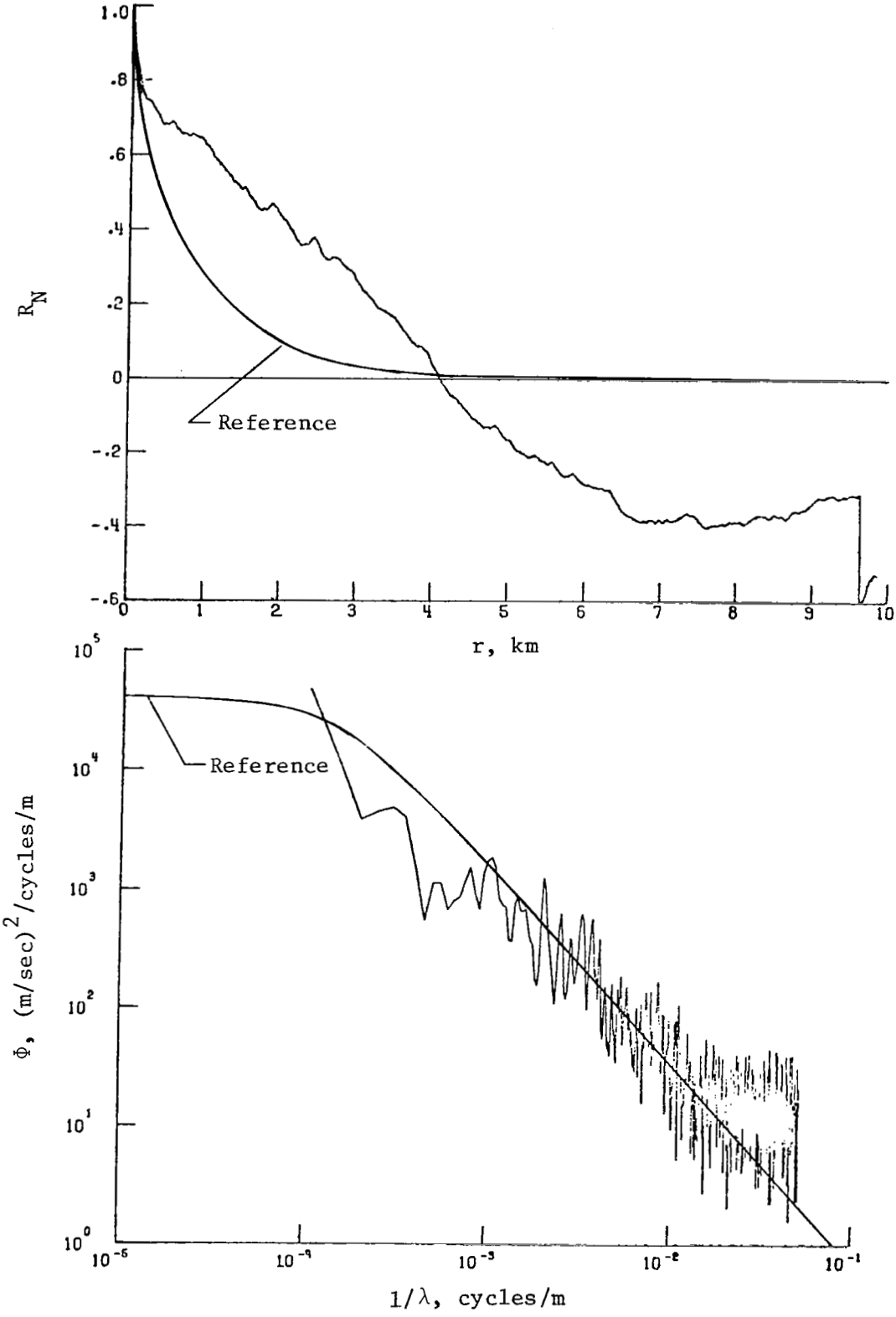

(c) Longitudinal component of gust velocity.

Figure 26.- Concluded.

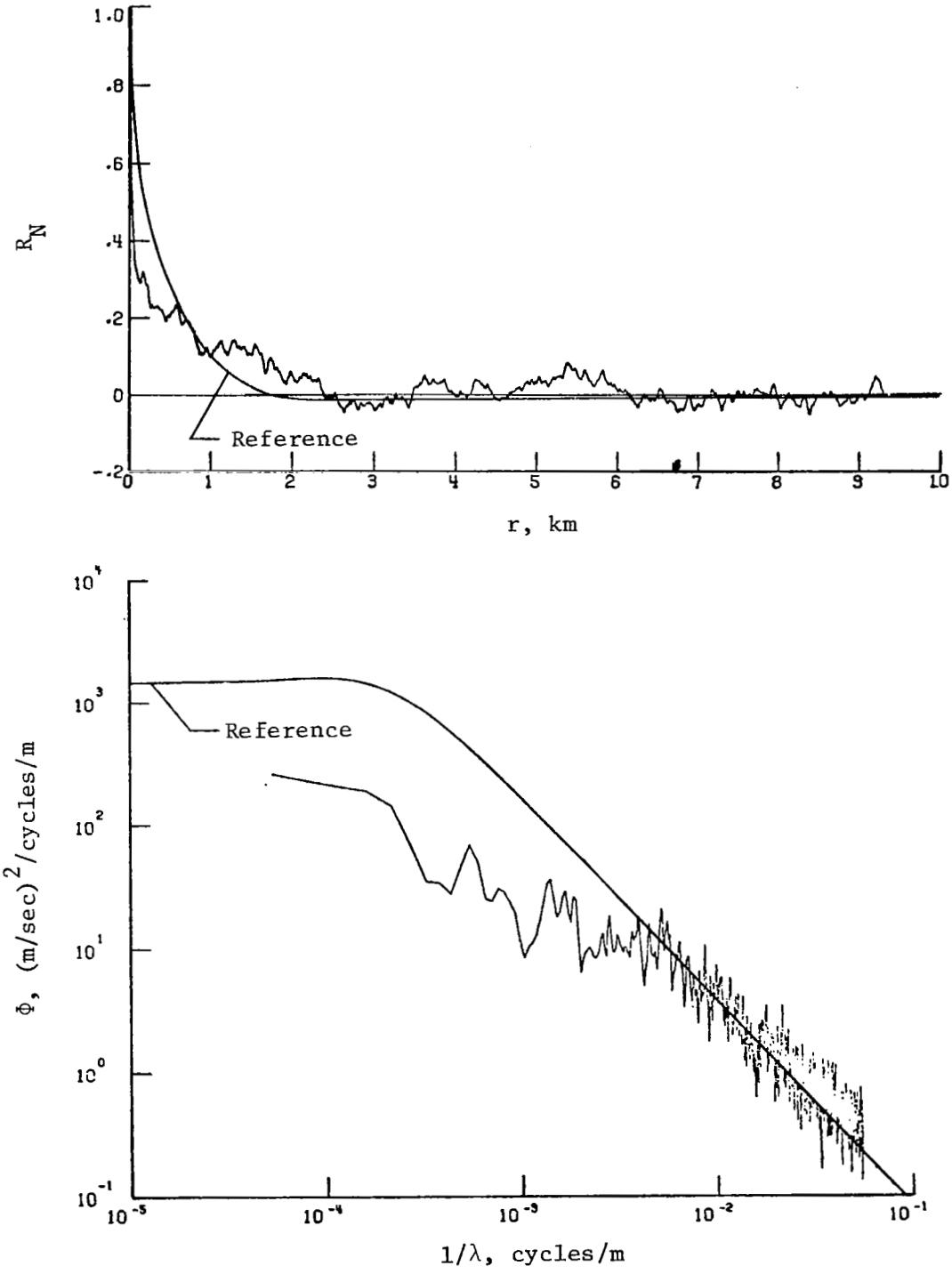

(a) Vertical component of gust velocity.

Figure 27.- Power spectra and autocorrelation functions for flight 24, run 6.

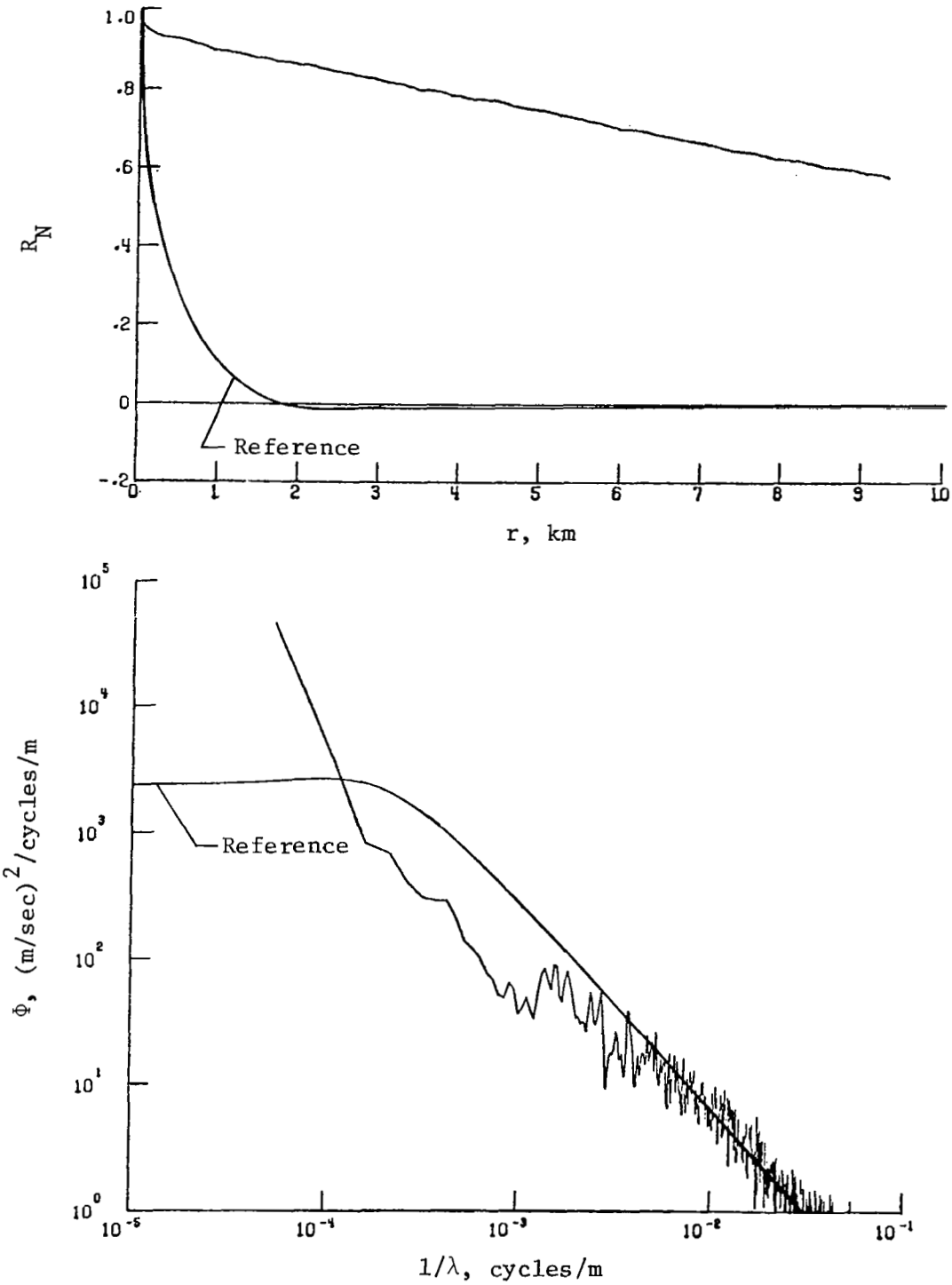

(b) Lateral component of gust velocity.

Figure 27.- Continued.

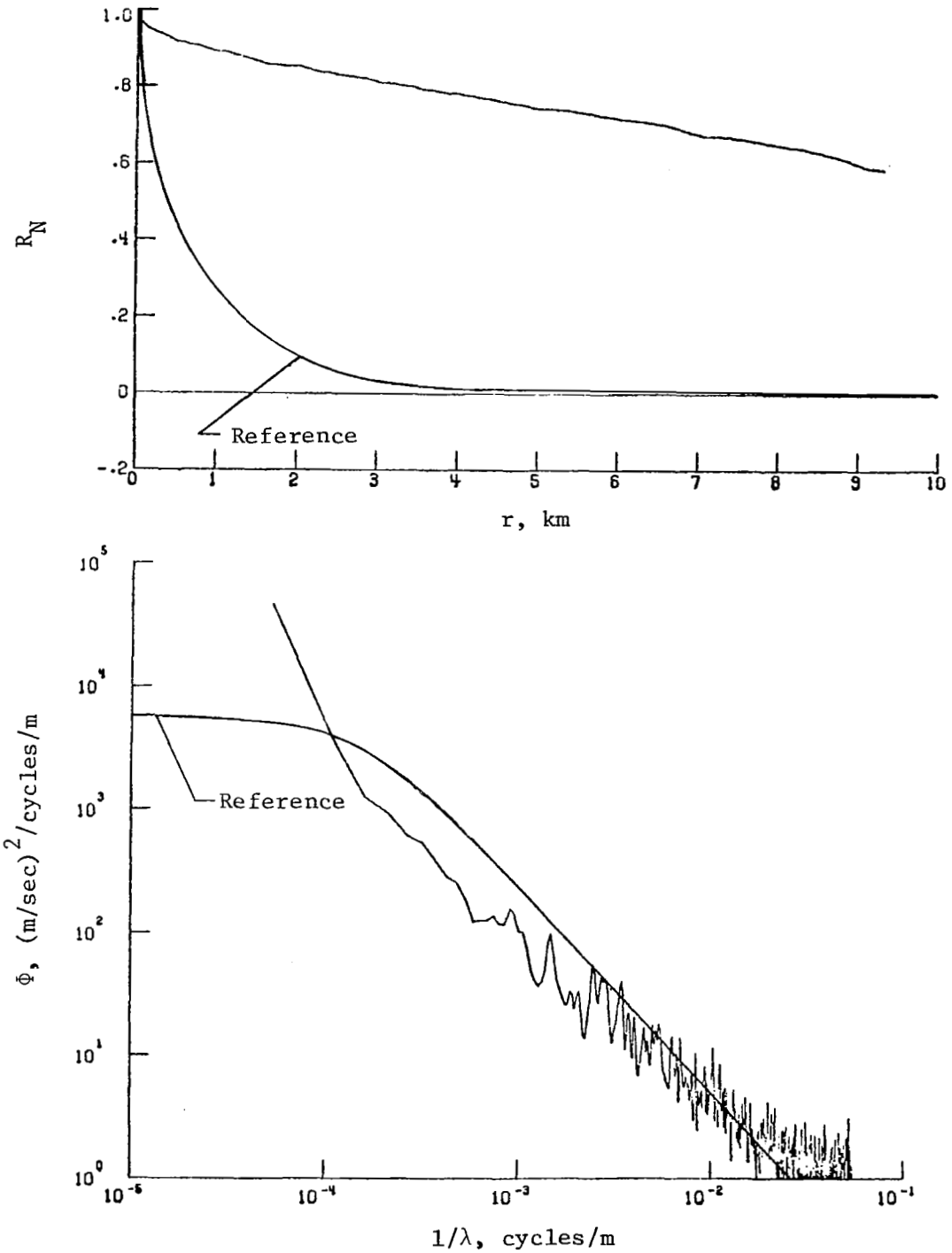

(c) Longitudinal component of gust velocity.

Figure 27.- Concluded.

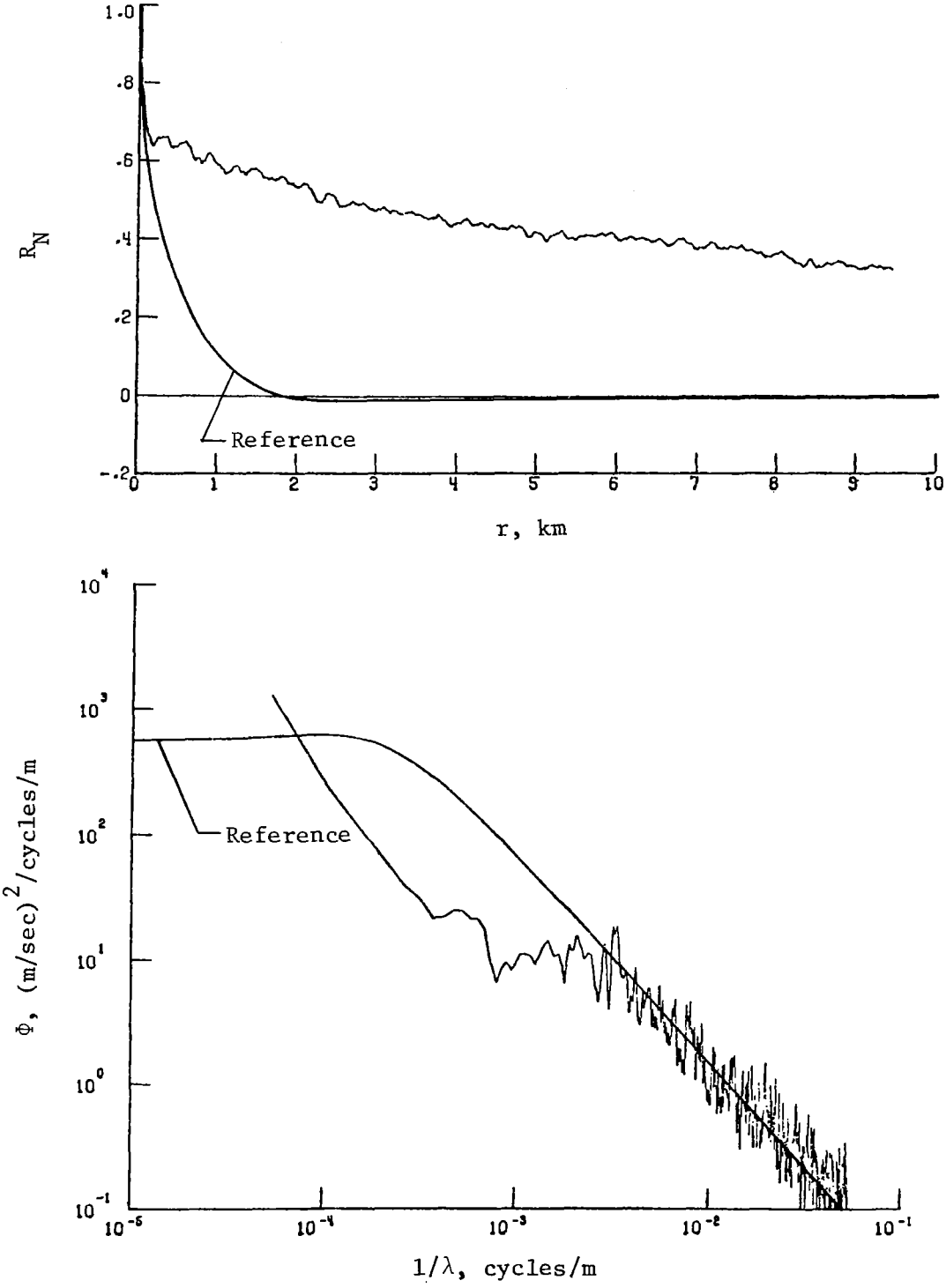

(a) Vertical component of gust velocity.

Figure 28.- Power spectra and autocorrelation functions for flight 24, run 7.

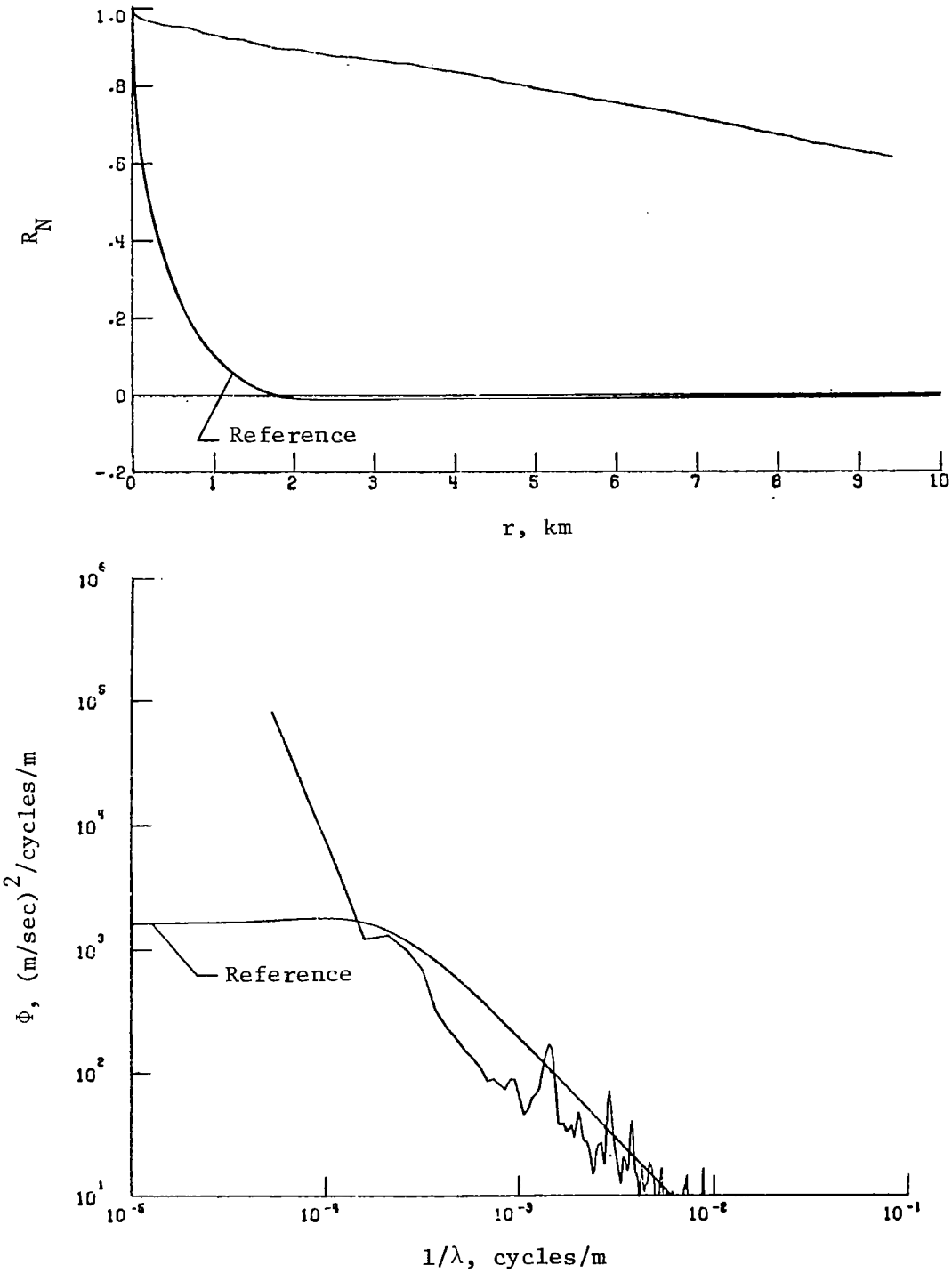

(b) Lateral component of gust velocity.

Figure 28.- Continued.

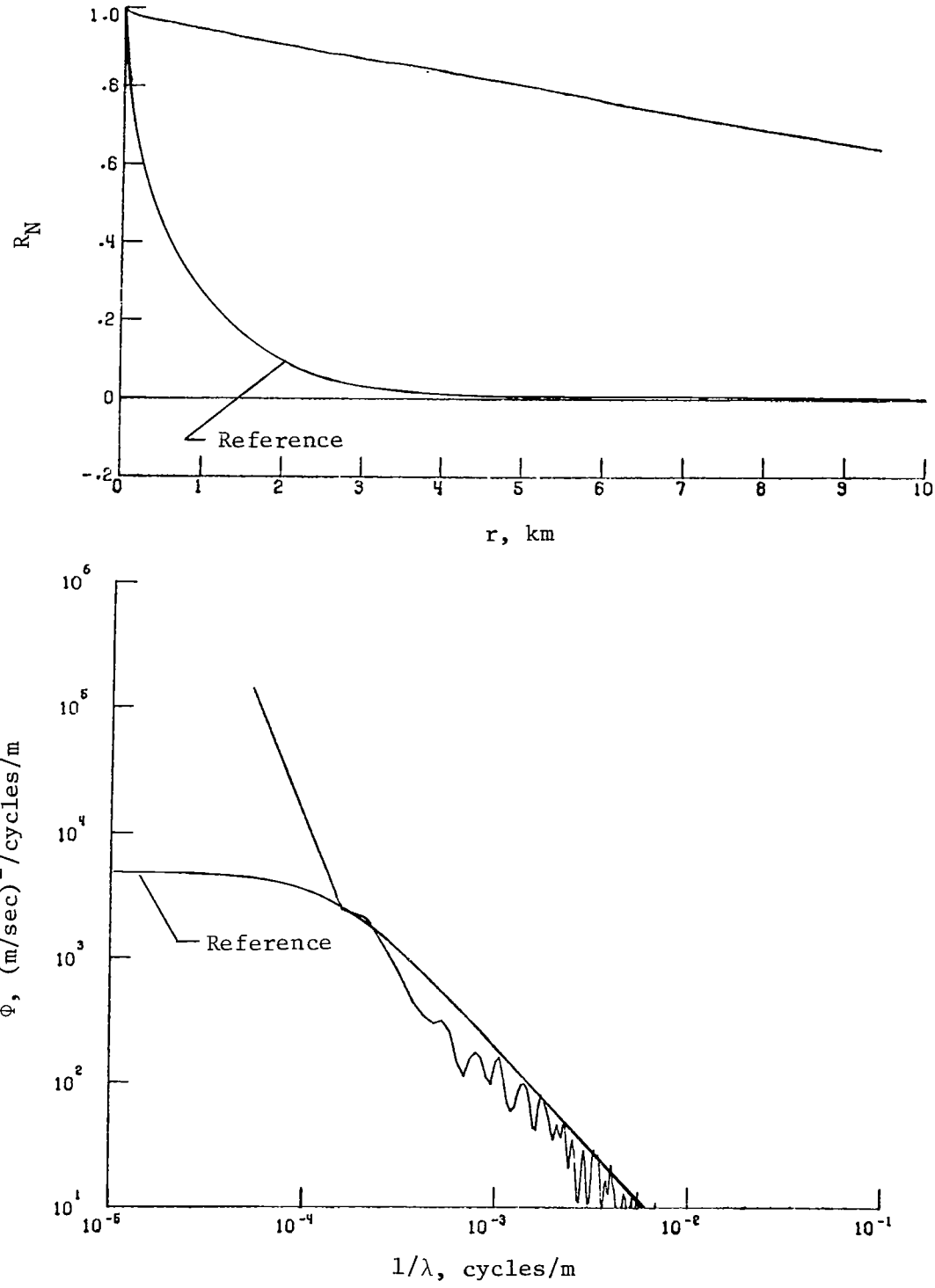

(c) Longitudinal component of gust velocity.

Figure 28.- Concluded.

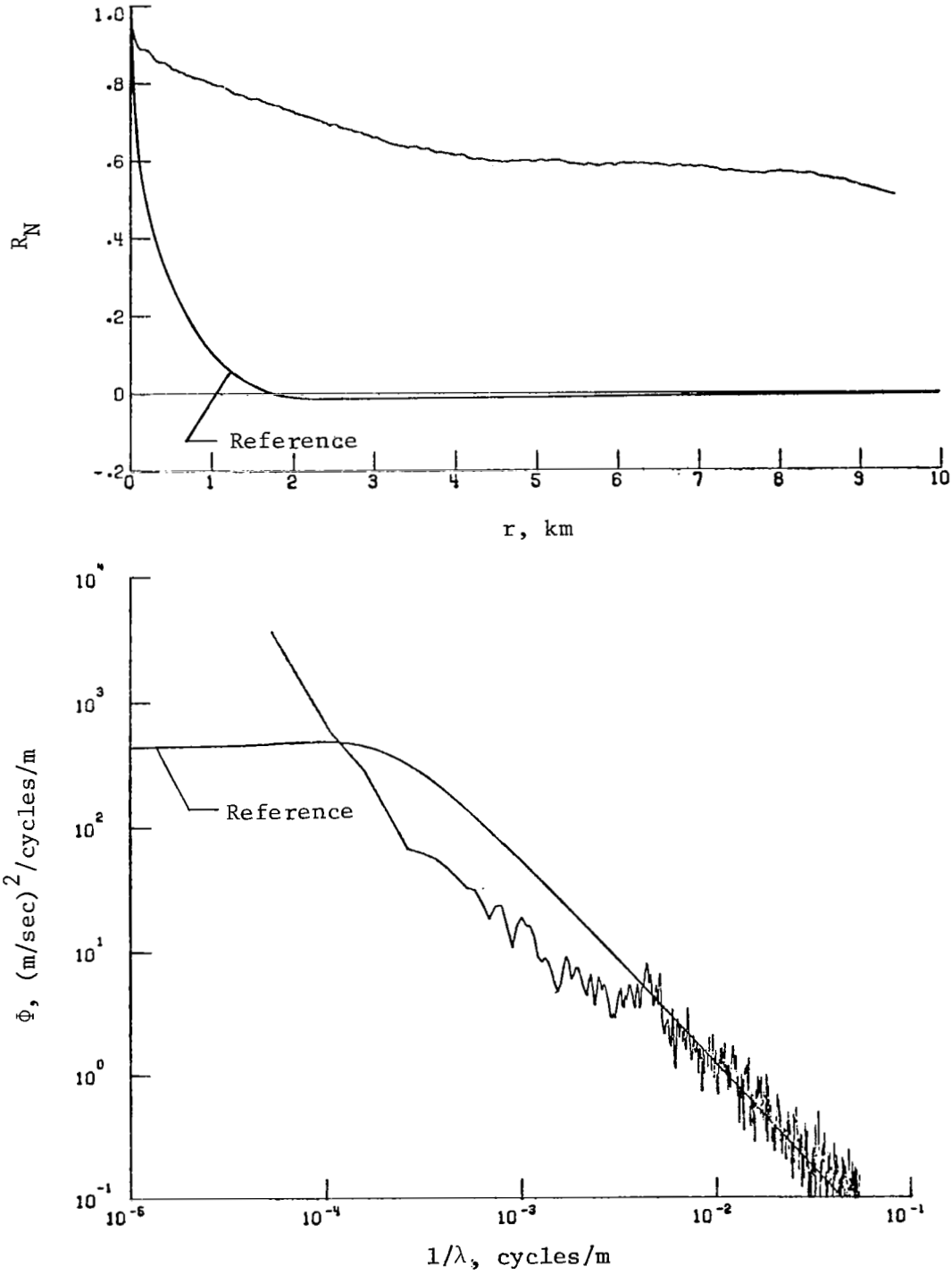

(a) Vertical component of gust velocity.

Figure 29.- Power spectra and autocorrelation functions for flight 24, run 9.

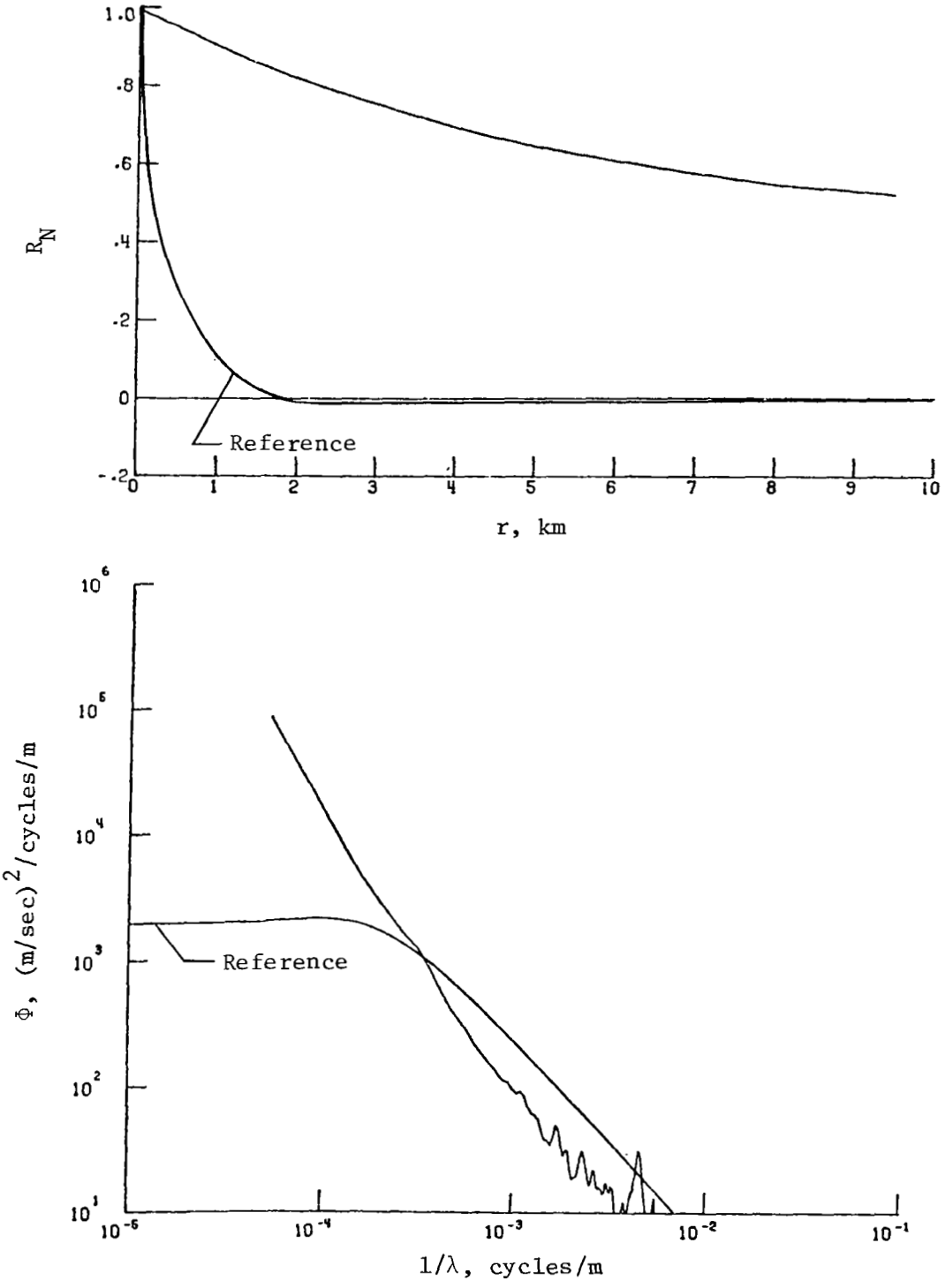

(b) Lateral component of gust velocity.

Figure 29.- Continued.

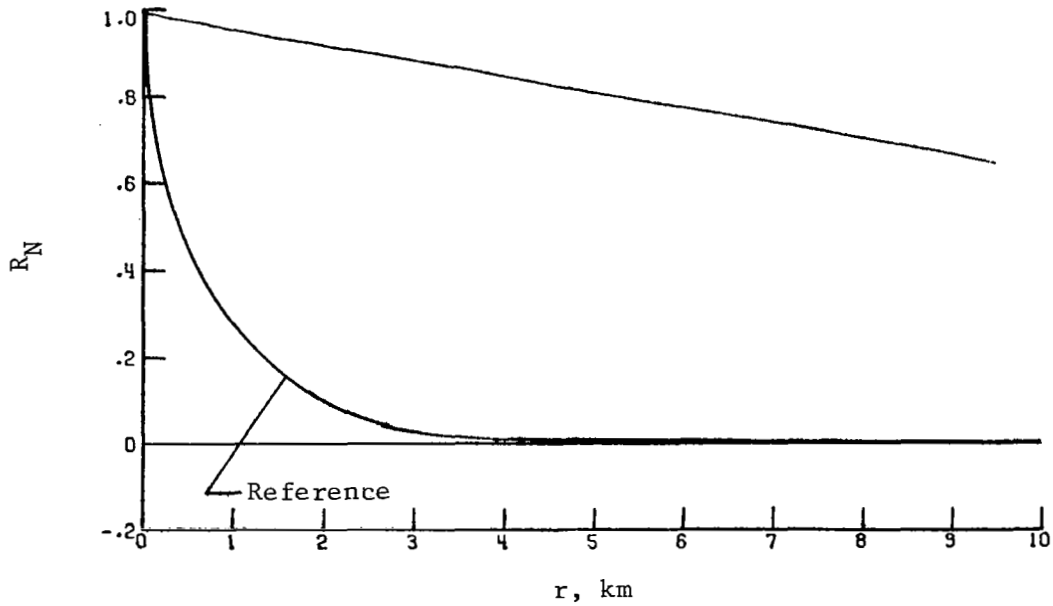

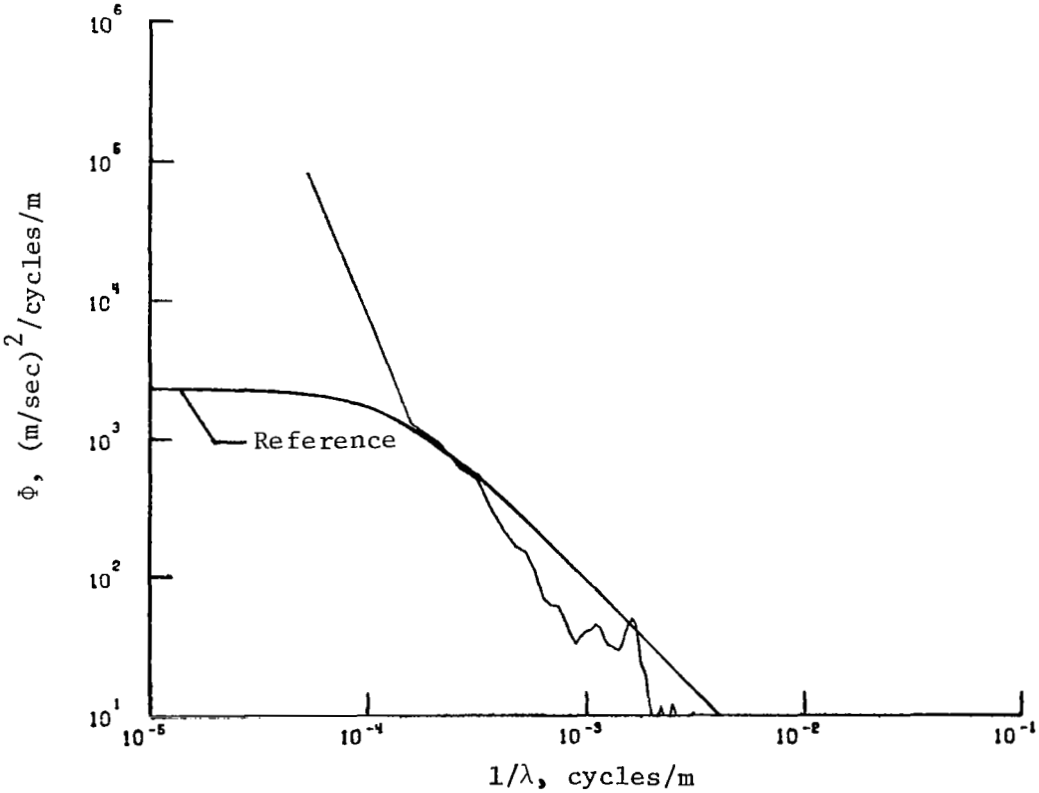

(c) Longitudinal component of gust velocity.

Figure 29.- Concluded.

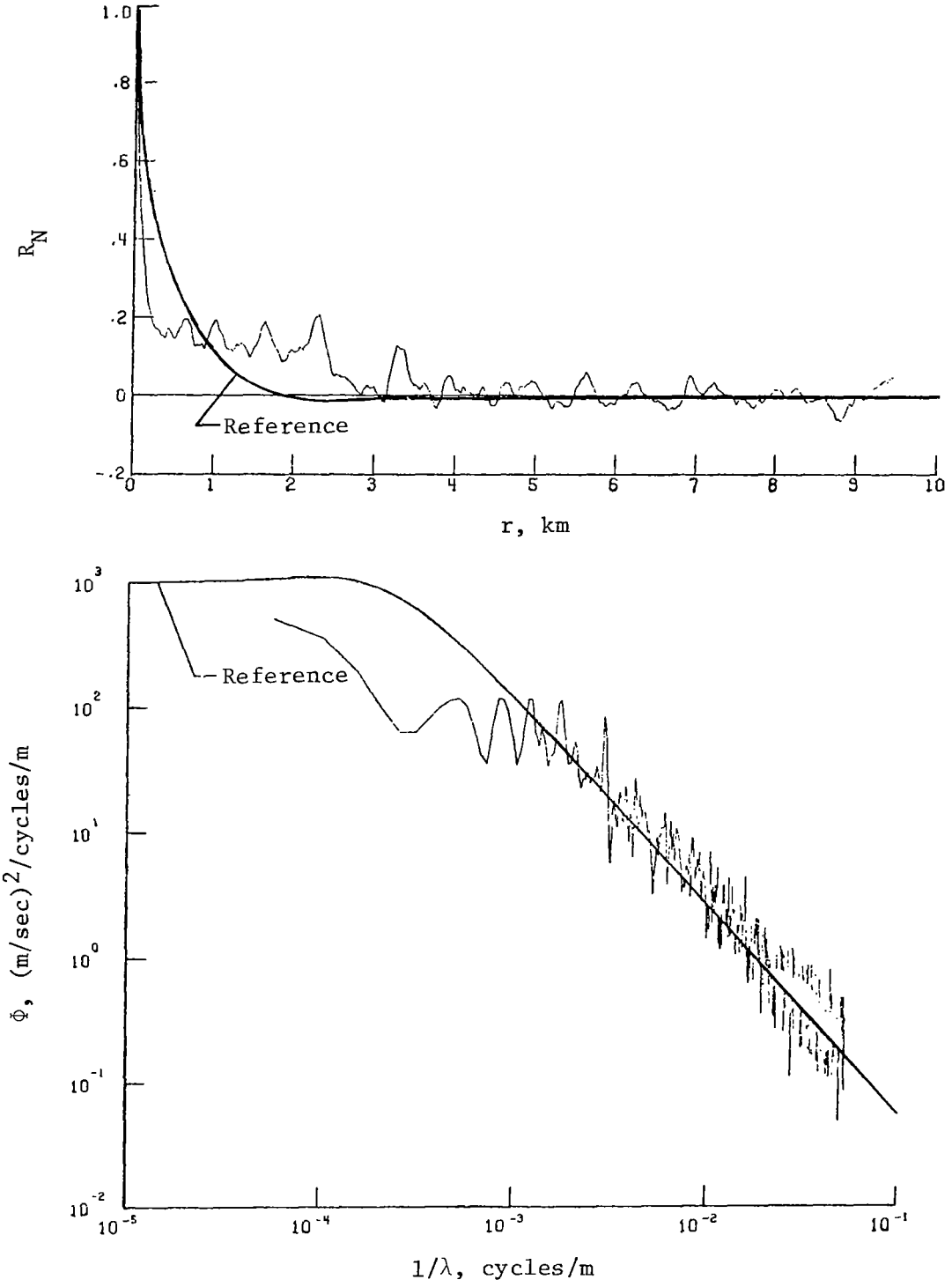

(a) Vertical component of gust velocity.

Figure 30.- Power spectra and autocorrelation functions for flight 27, run 13.

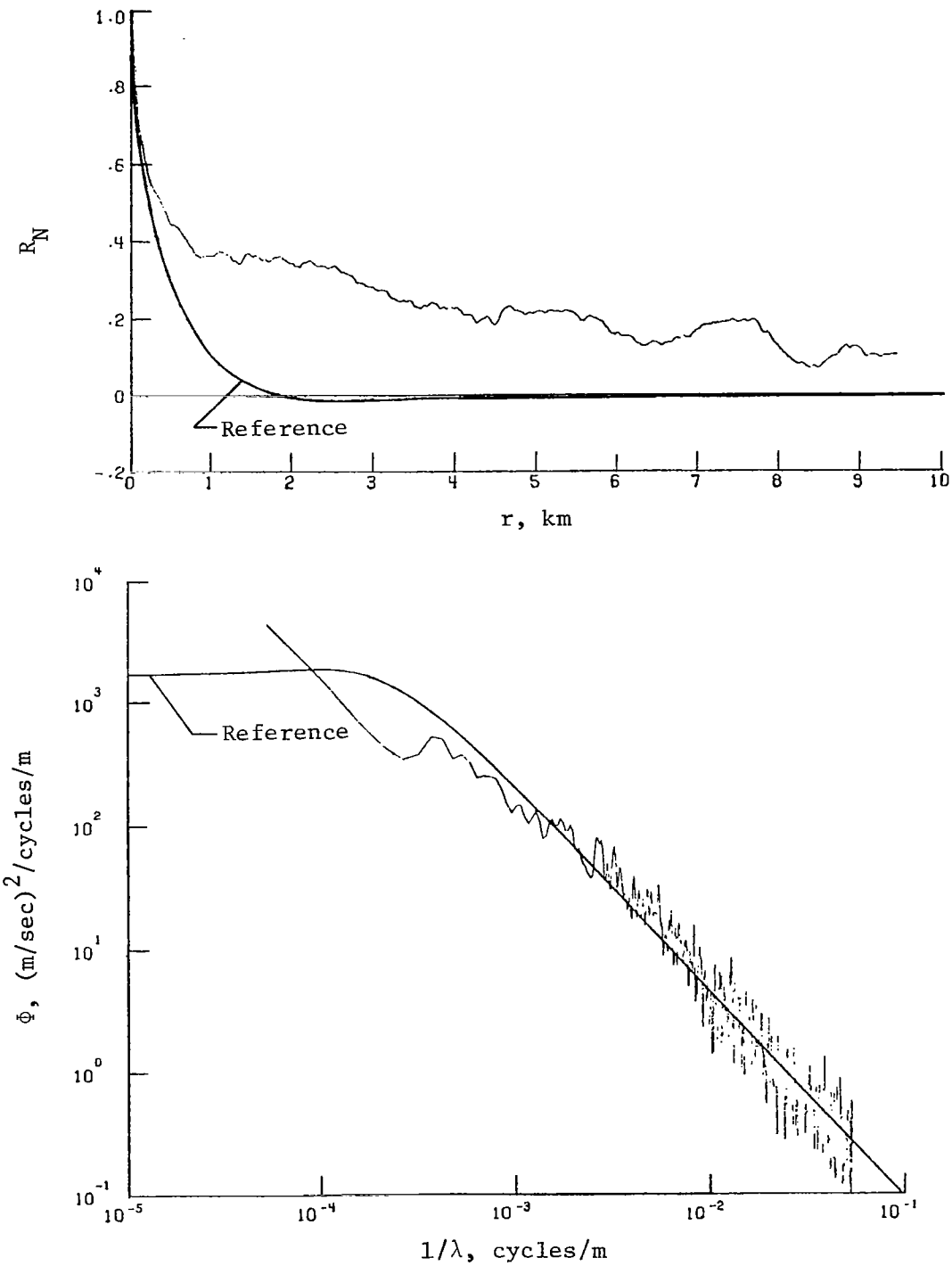

(b) Lateral component of gust velocity.

Figure 30.- Continued.

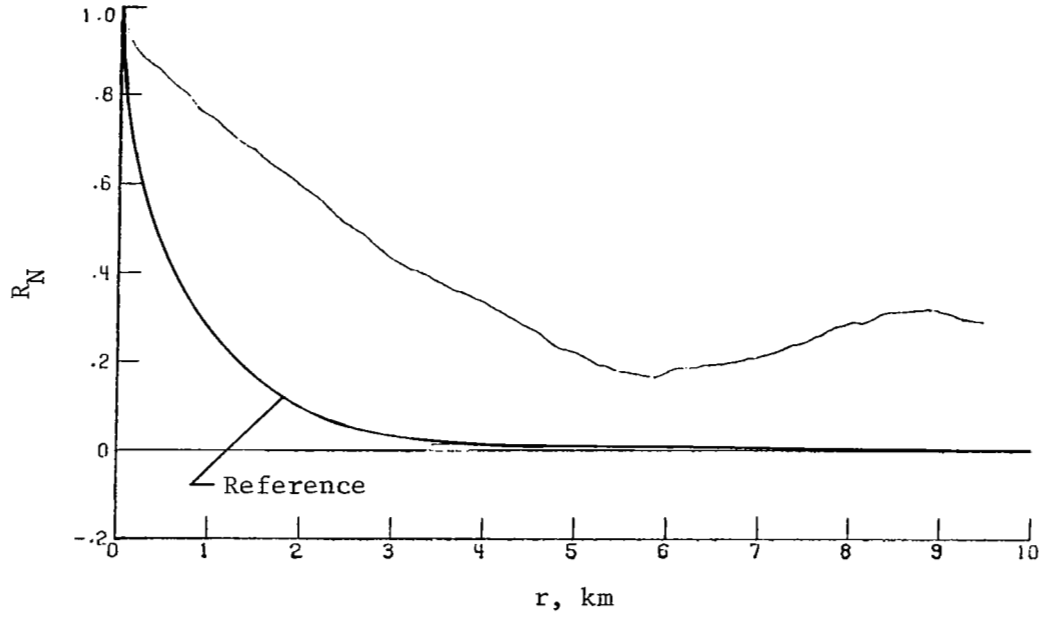

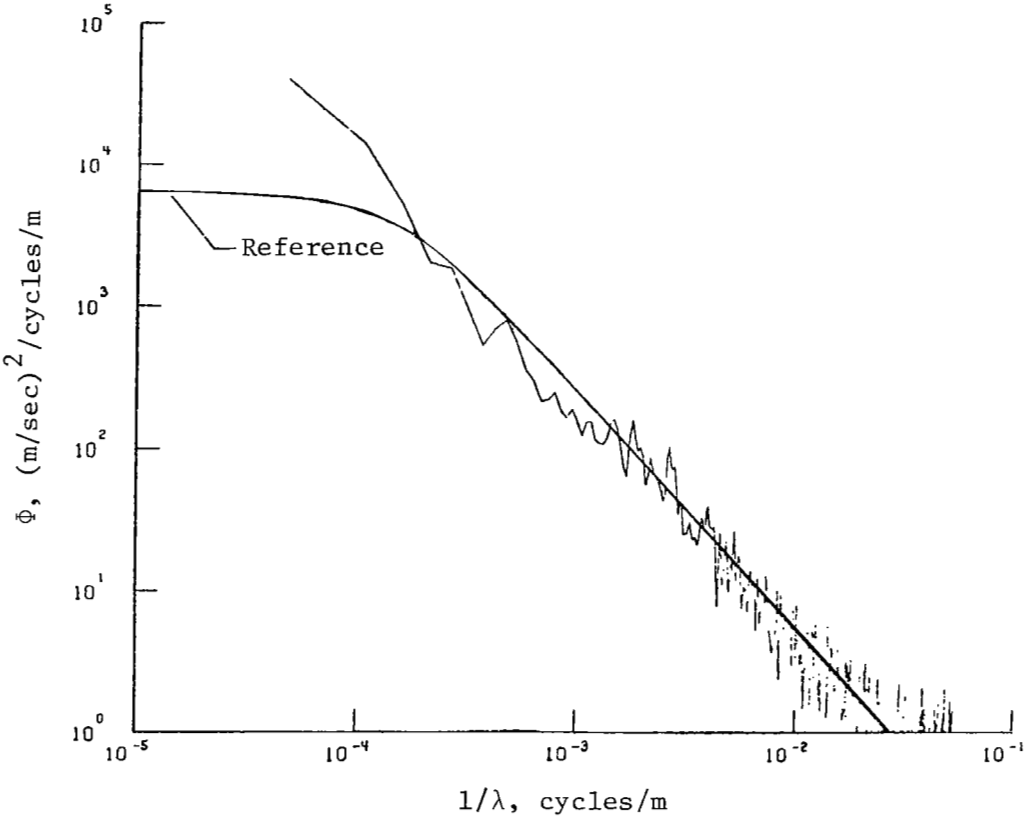

(c) Longitudinal component of gust velocity.

Figure 30.- Concluded.

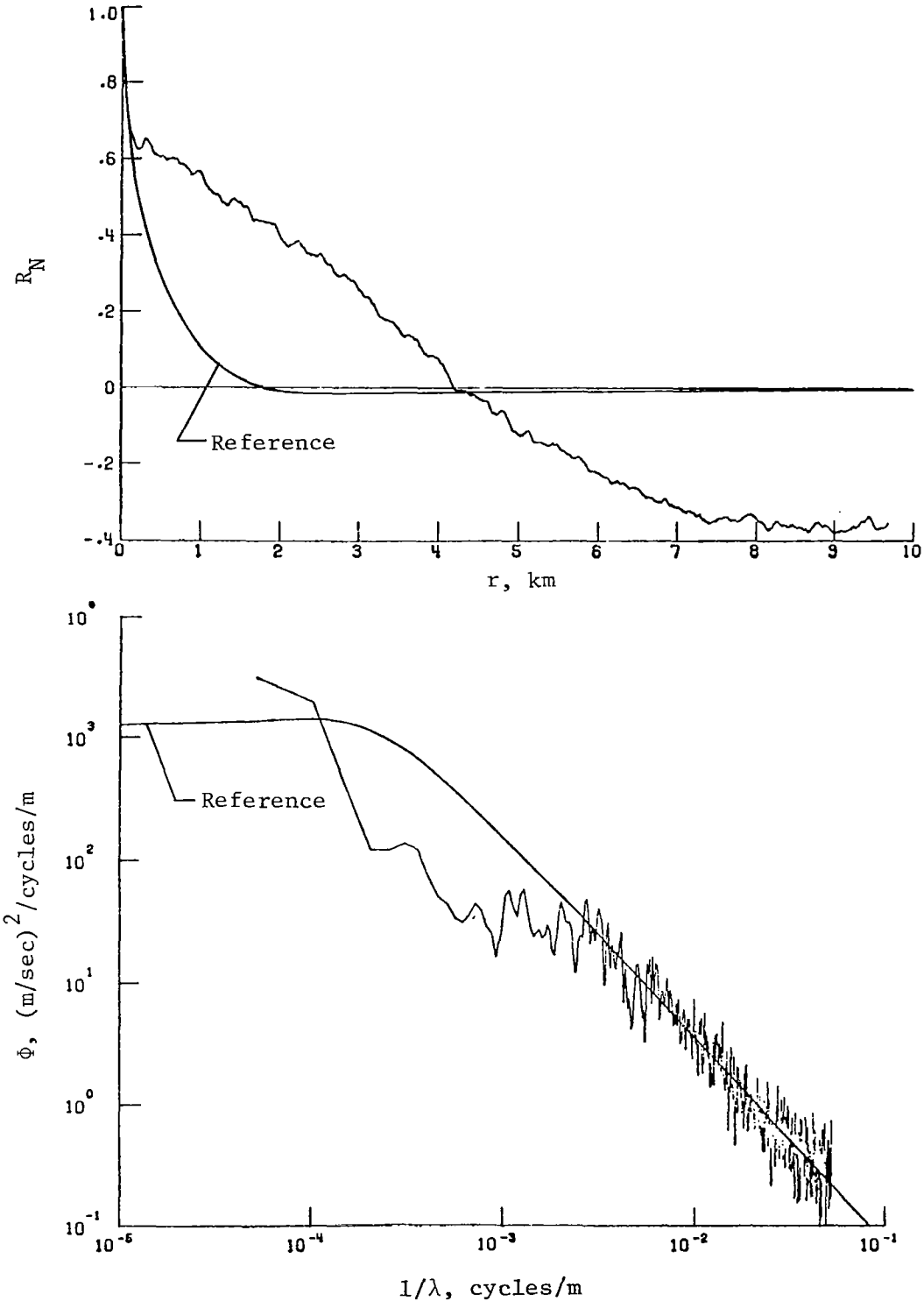

(a) Vertical component of gust velocity.

Figure 31.- Power spectra and autocorrelation functions for flight 38, run 5.

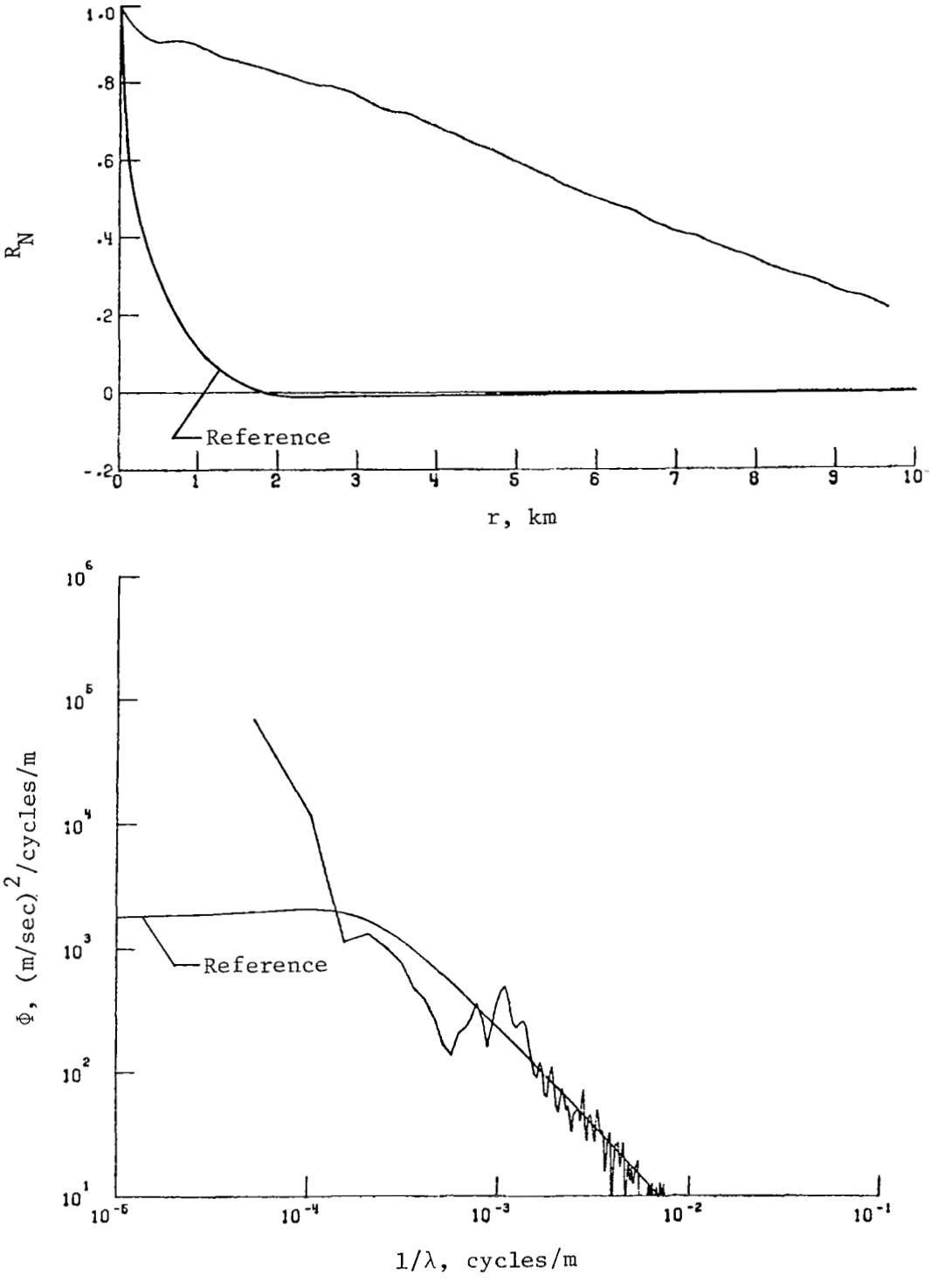

(b) Lateral component of gust velocity.

Figure 31.- Continued.

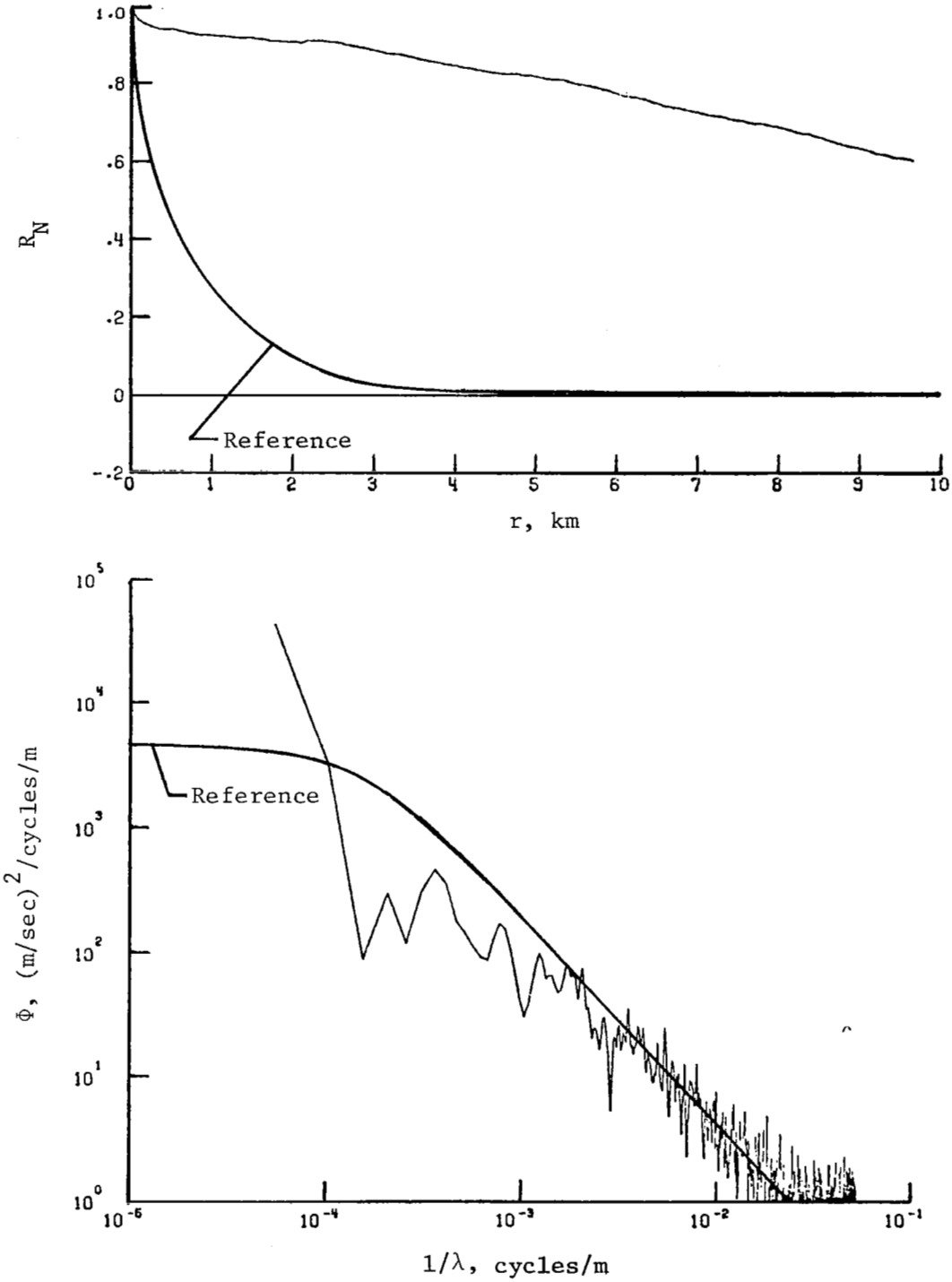

(c) Longitudinal component of gust velocity.

Figure 31.- Concluded.

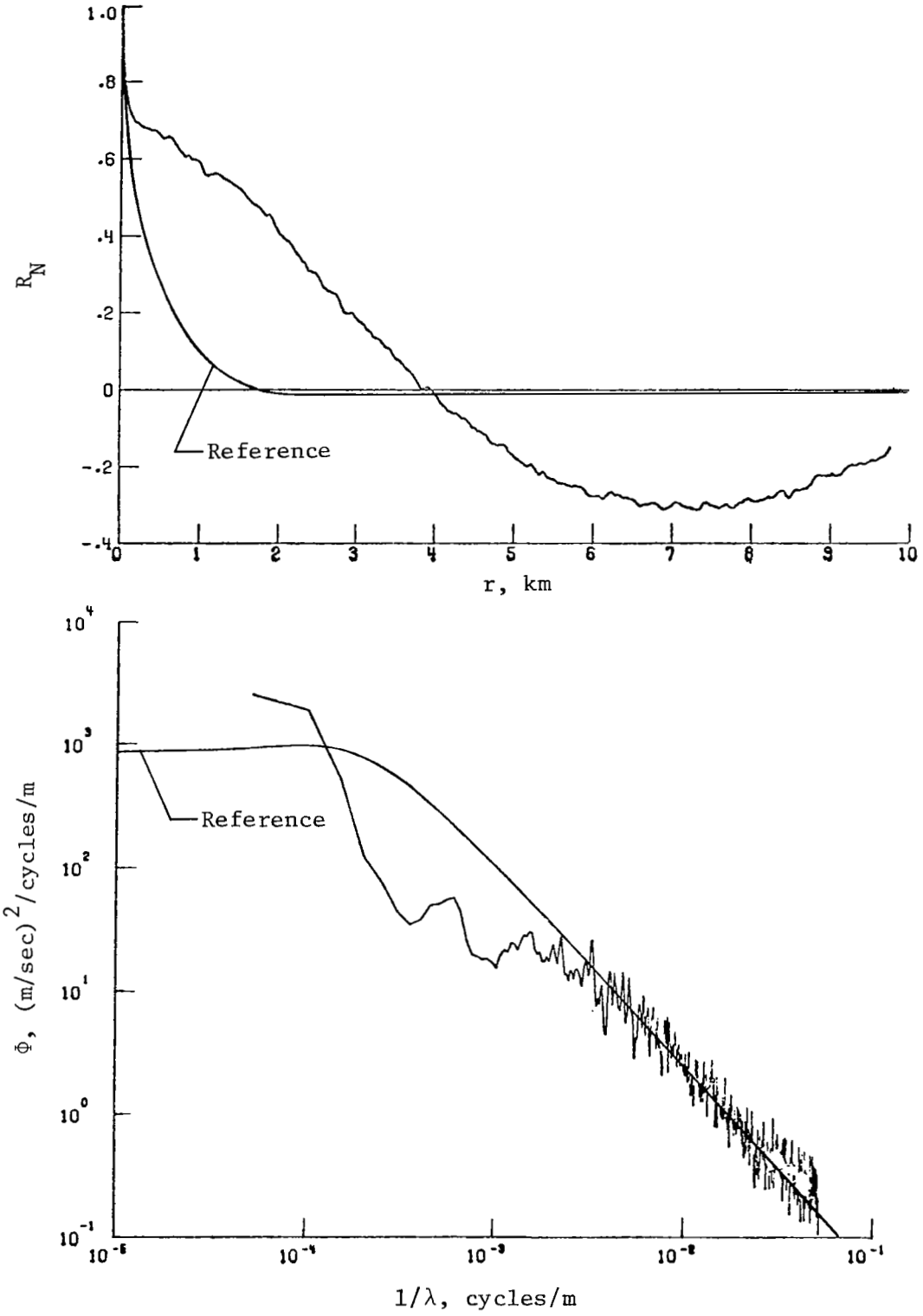

(a) Vertical component of gust velocity.

Figure 32.- Power spectra and autocorrelation functions for flight 38, run 6.

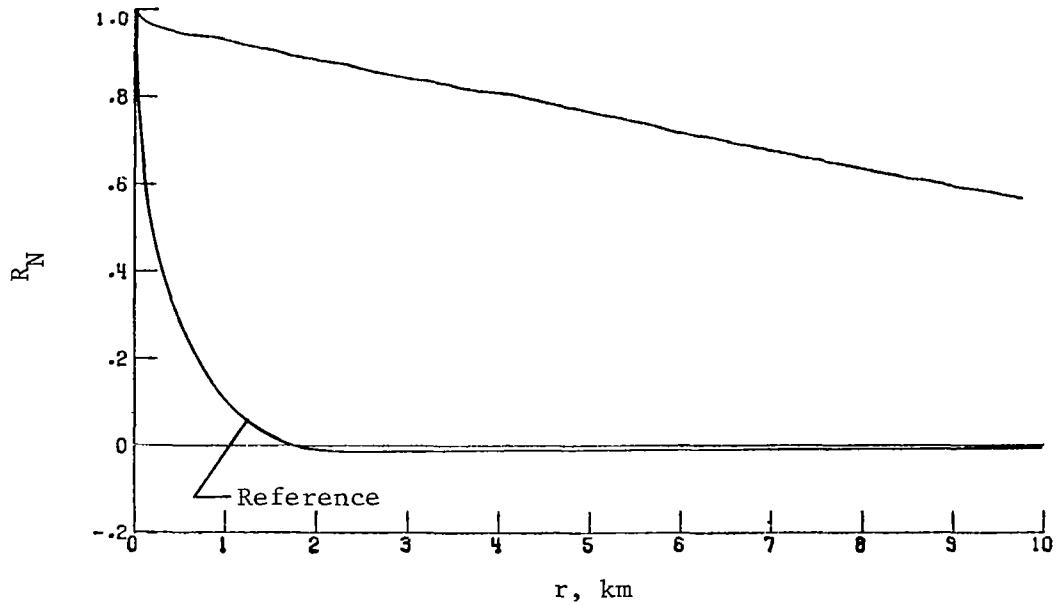

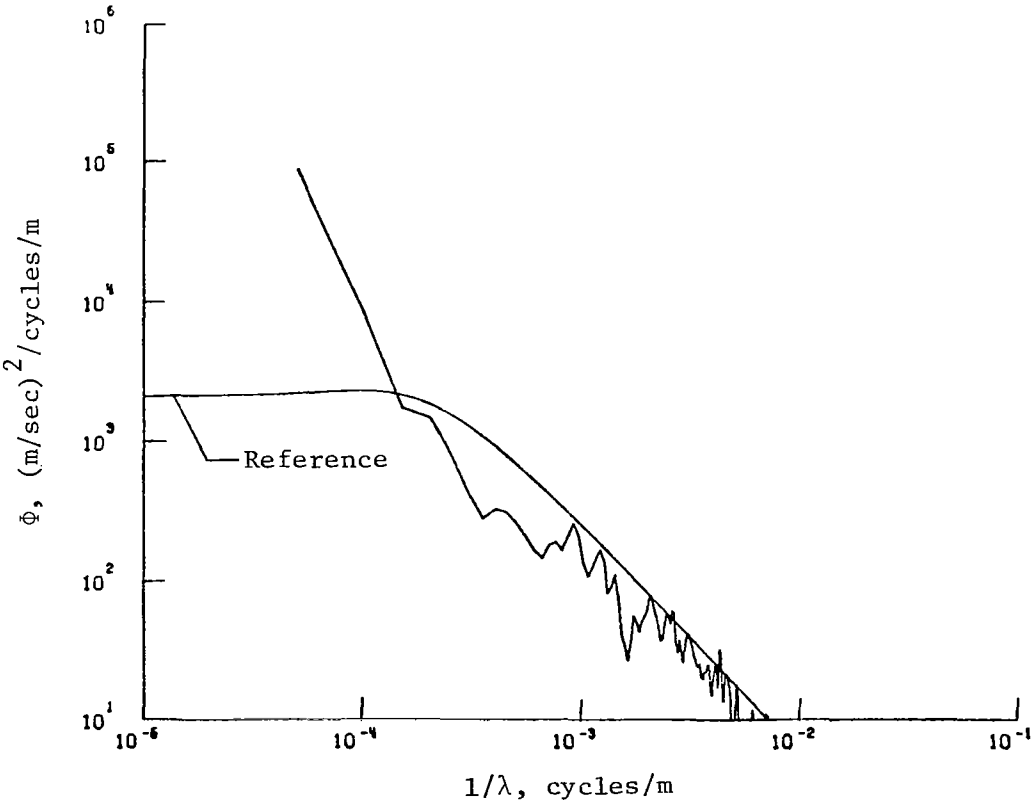

(b) Lateral component of gust velocity.

Figure 32.- Continued.

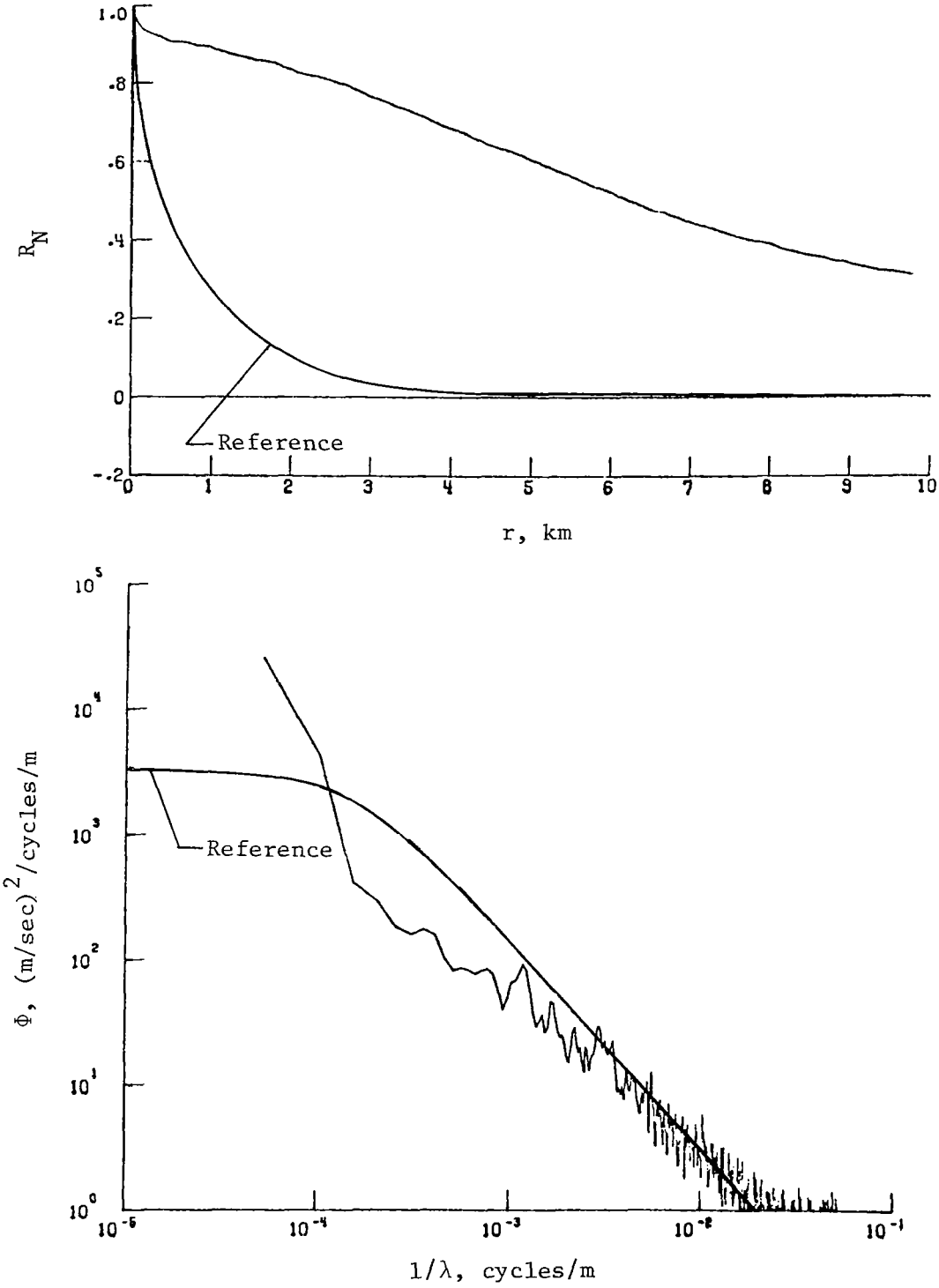

(c) Longitudinal component of gust velocity.

Figure 32.- Concluded.

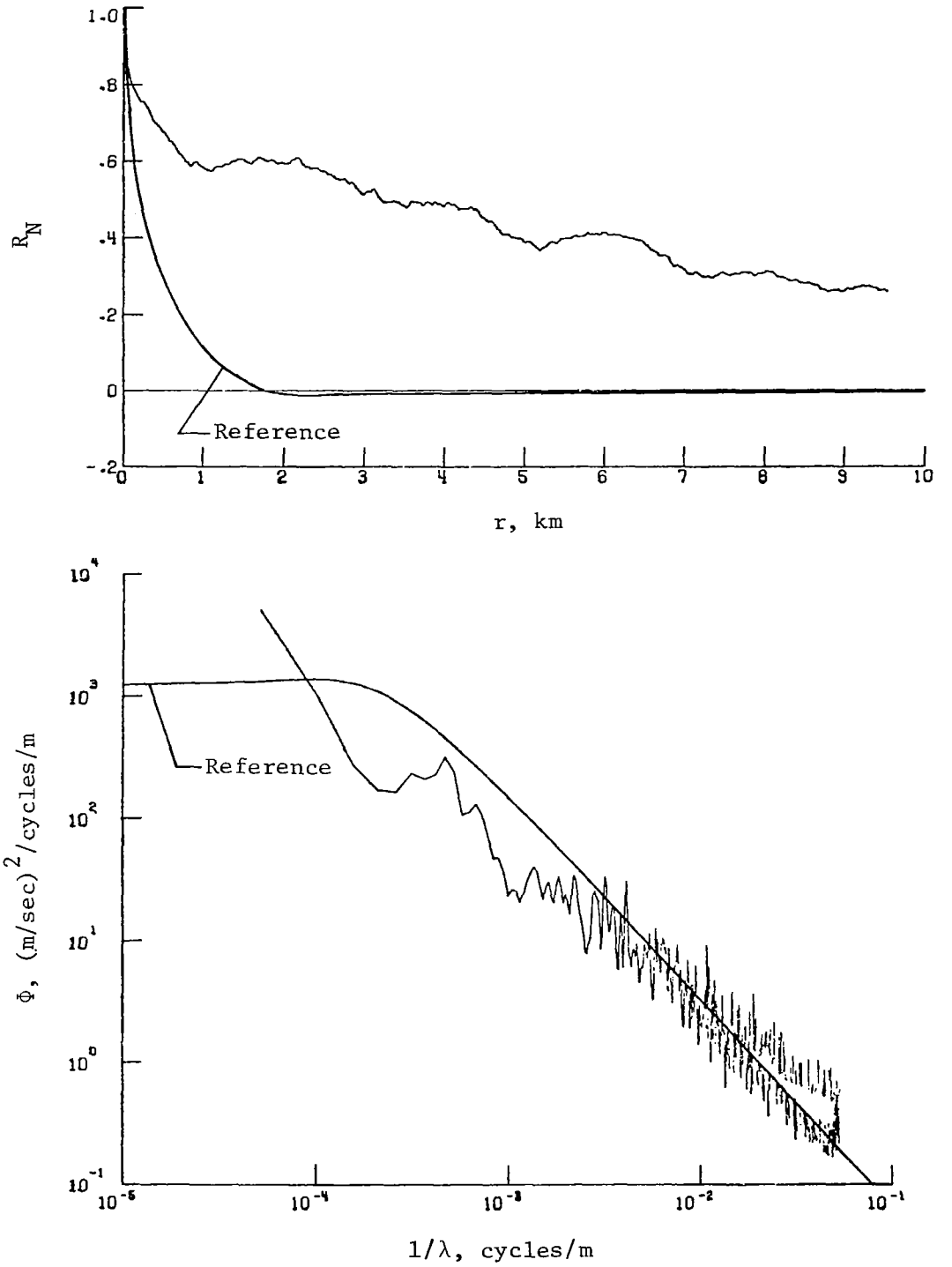

(a) Vertical component of gust velocity.

Figure 33.- Power spectra and autocorrelation functions for flight 38, run 7.

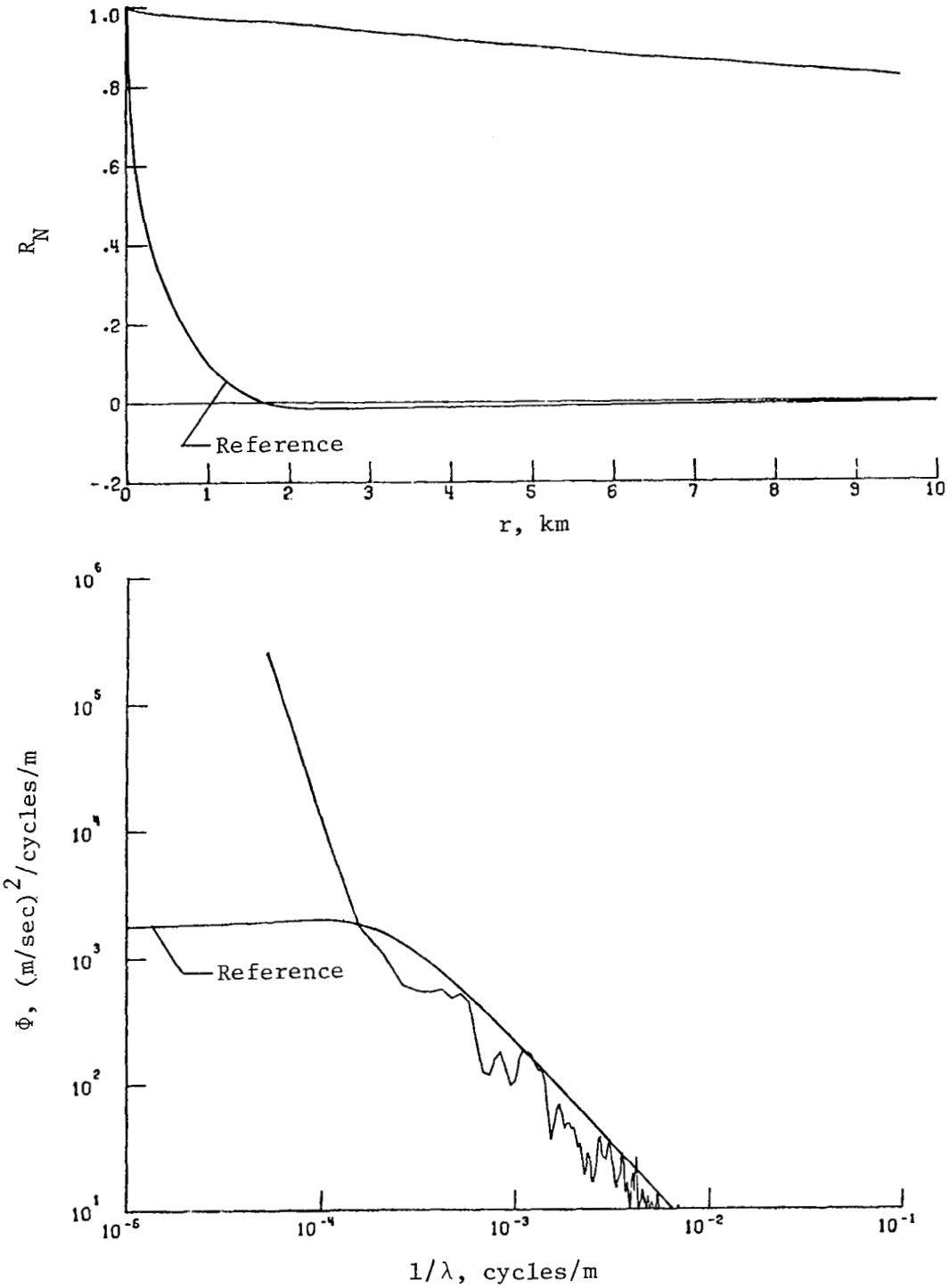

(b) Lateral component of gust velocity.

Figure 33.- Continued.

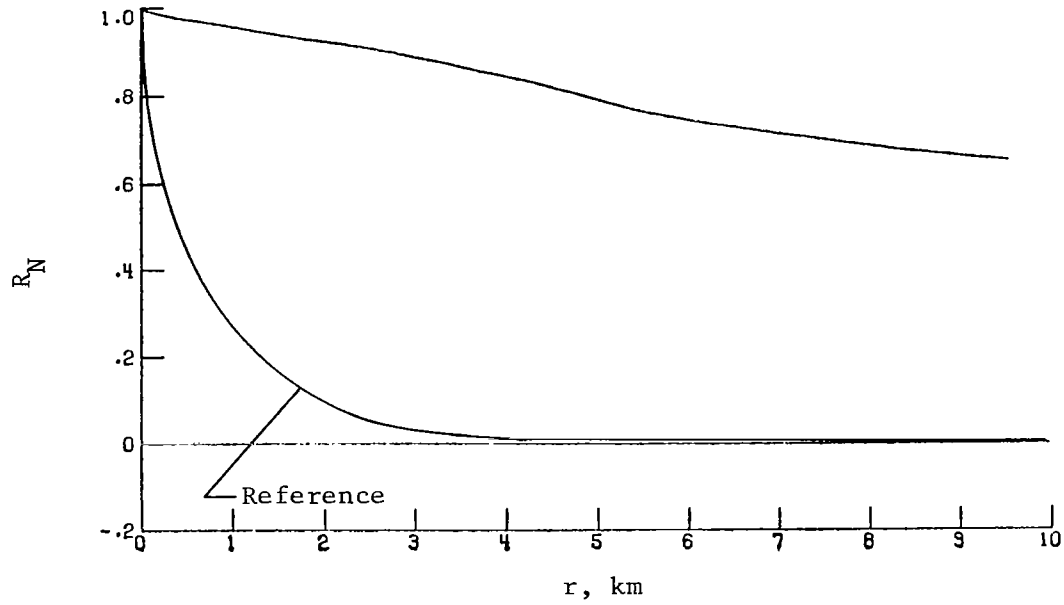

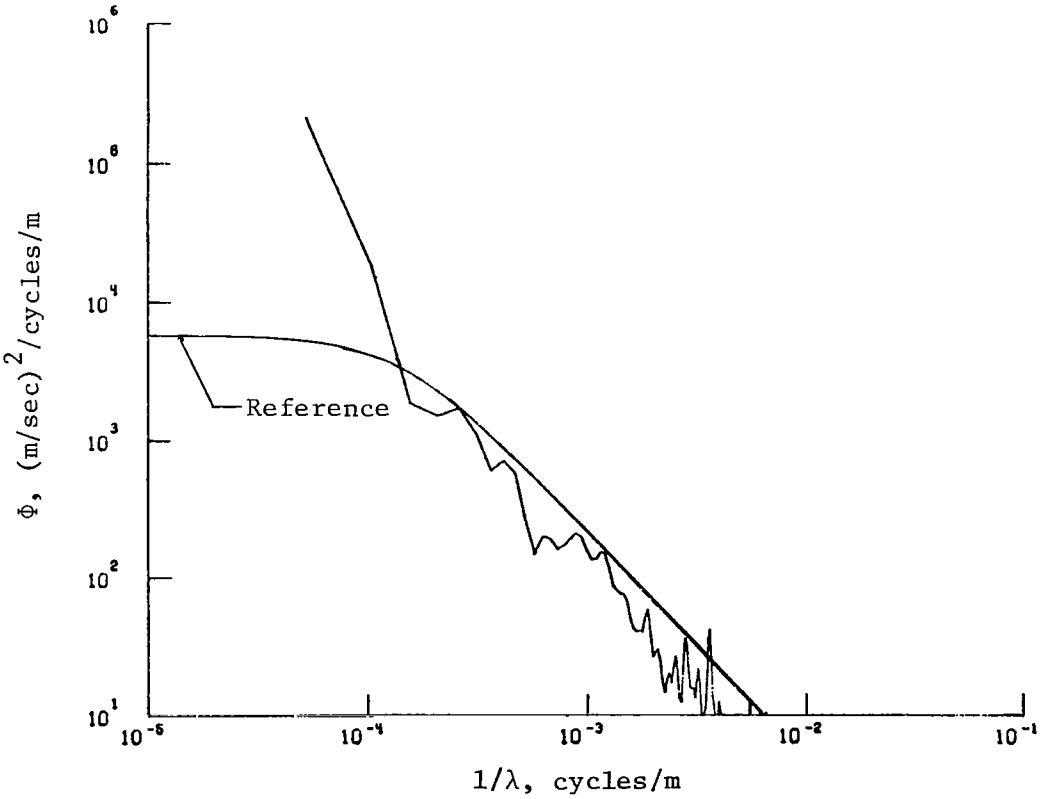

(c) Longitudinal component of gust velocity.

Figure 33.- Concluded.

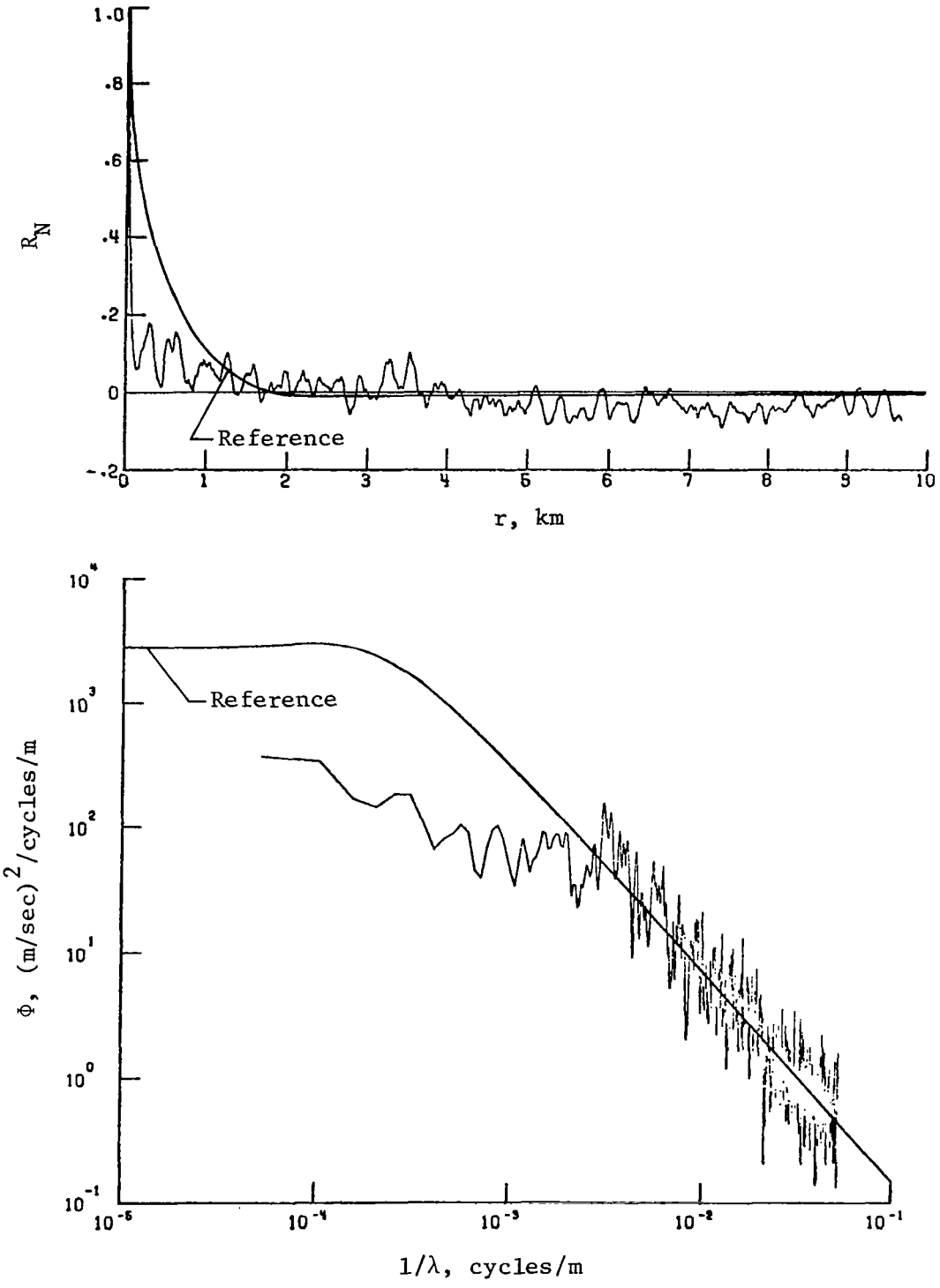

(a) Vertical component of gust velocity.

Figure 34.- Power spectra and autocorrelation functions for flight 41, run 8.

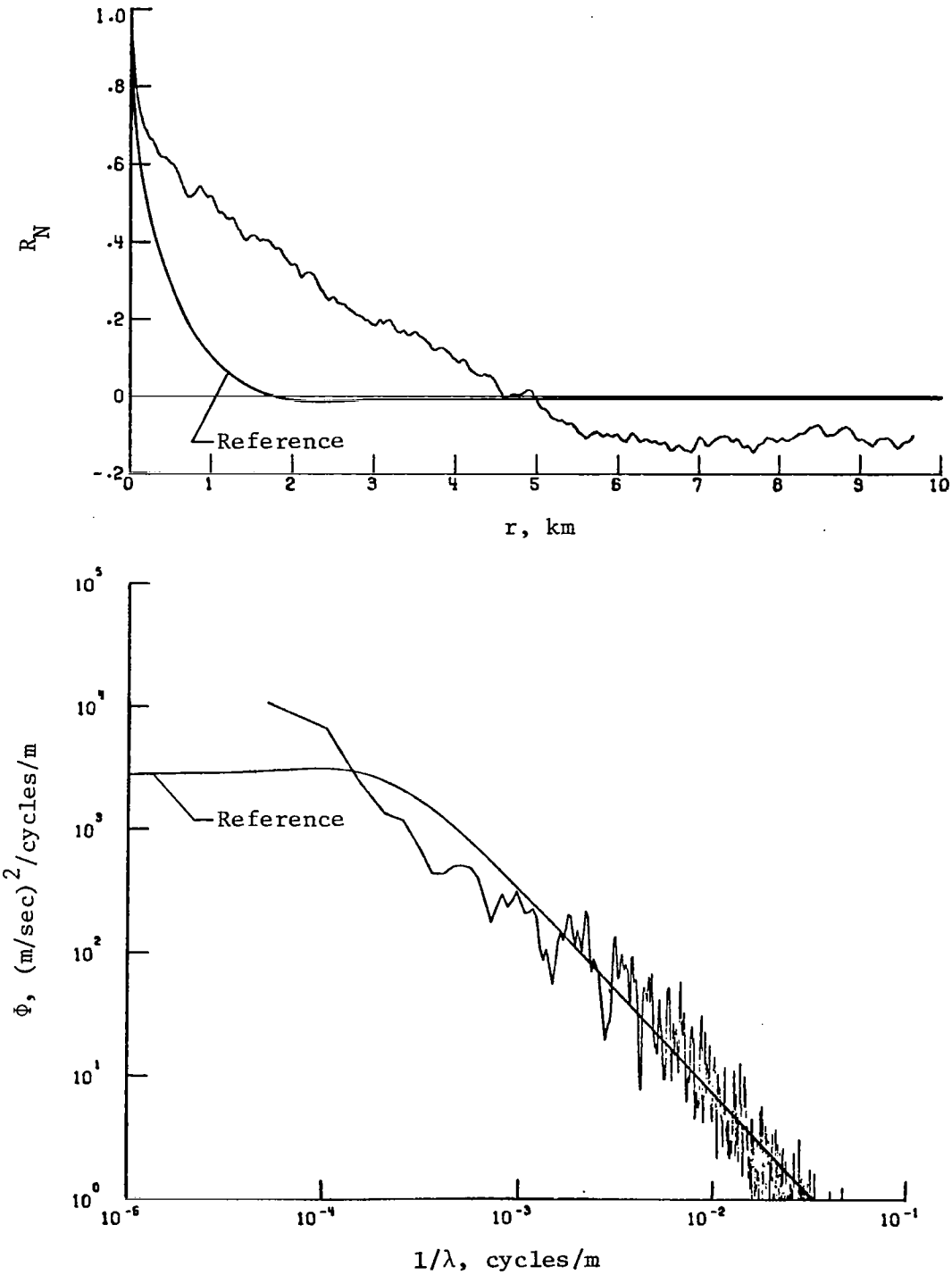

(b) Lateral component of gust velocity.

Figure 34.- Continued.

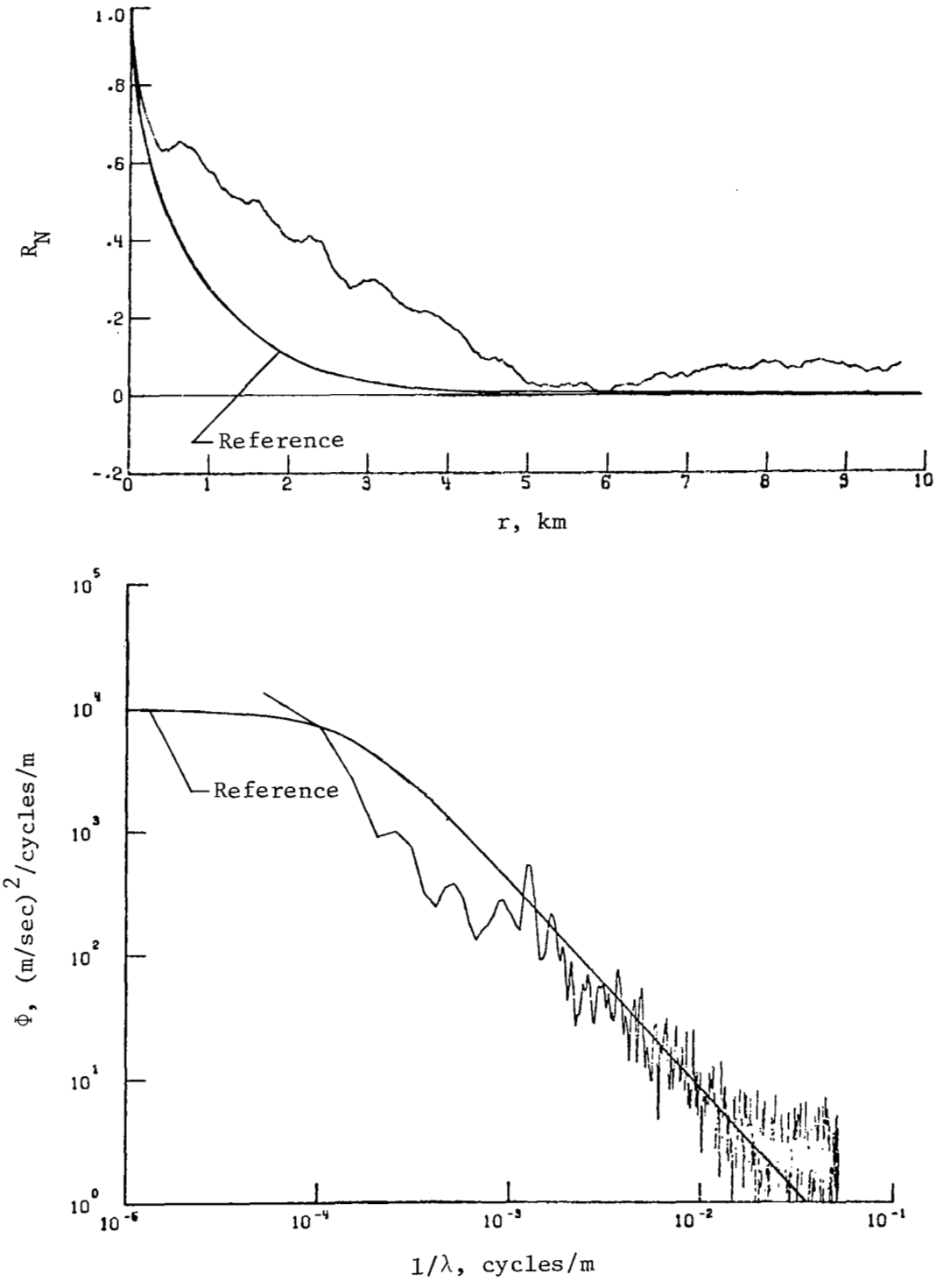

(c) Longitudinal component of gust velocity.

Figure 34.- Concluded.

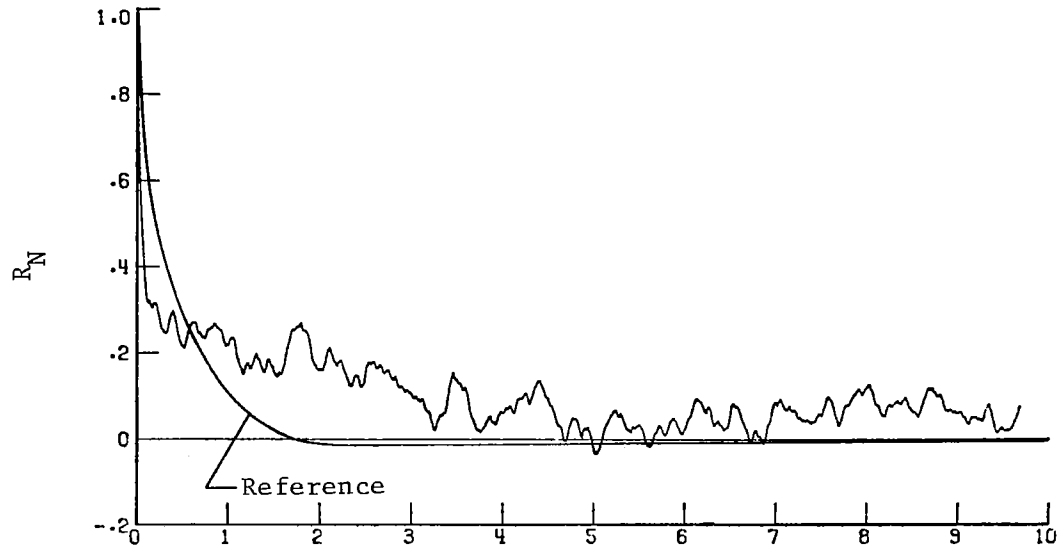

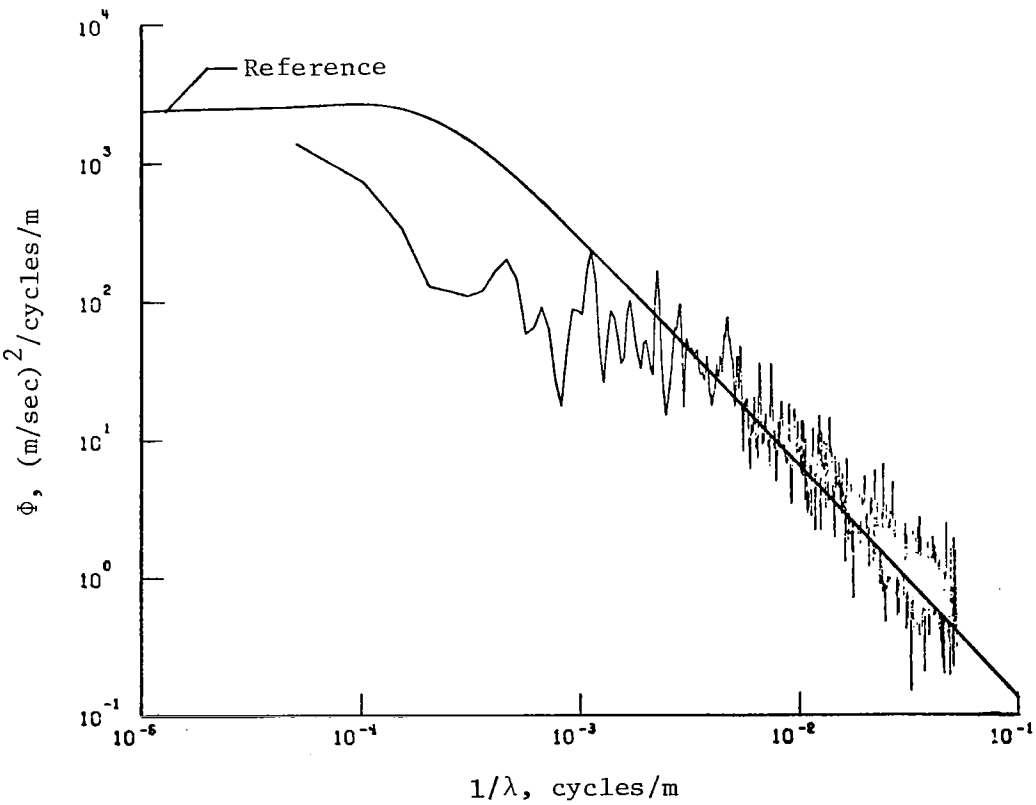

(a) Vertical component of gust velocity.

Figure 35.- Power spectra and autocorrelation functions for flight 41, run 10.

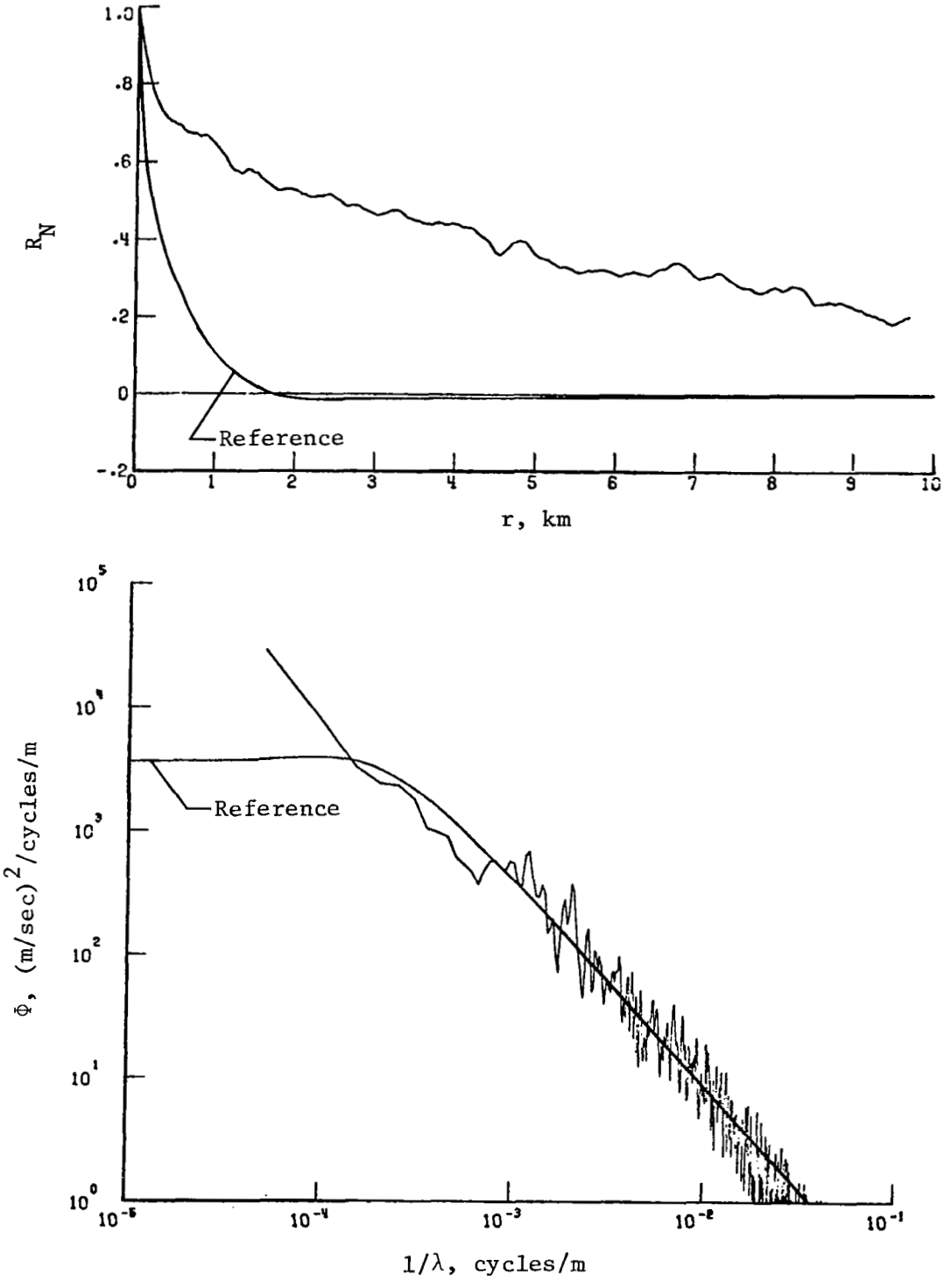

(b) Lateral component of gust velocity.

Figure 35.- Continued.

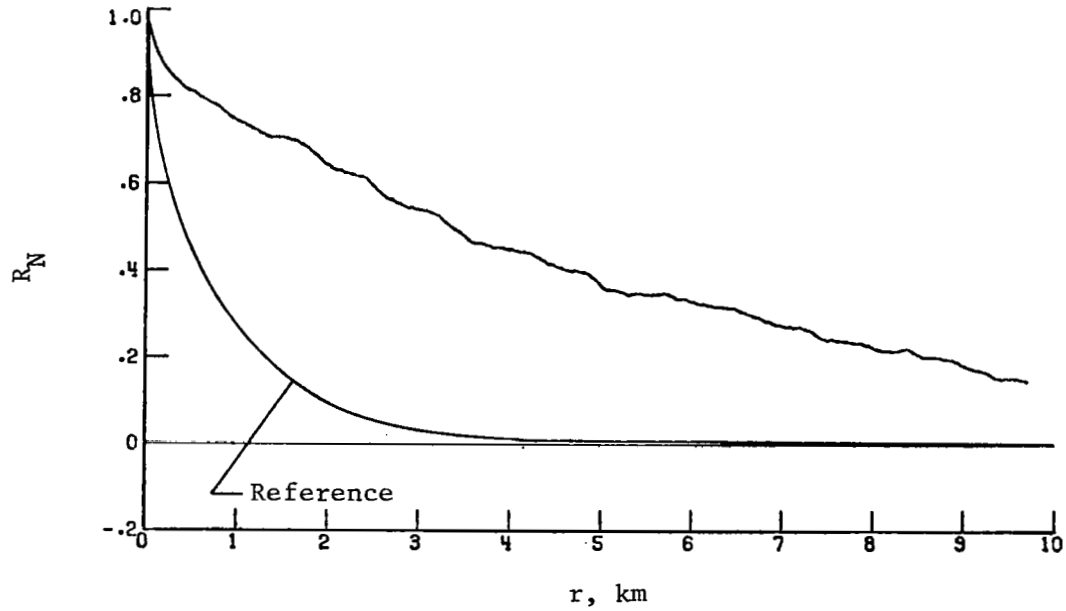

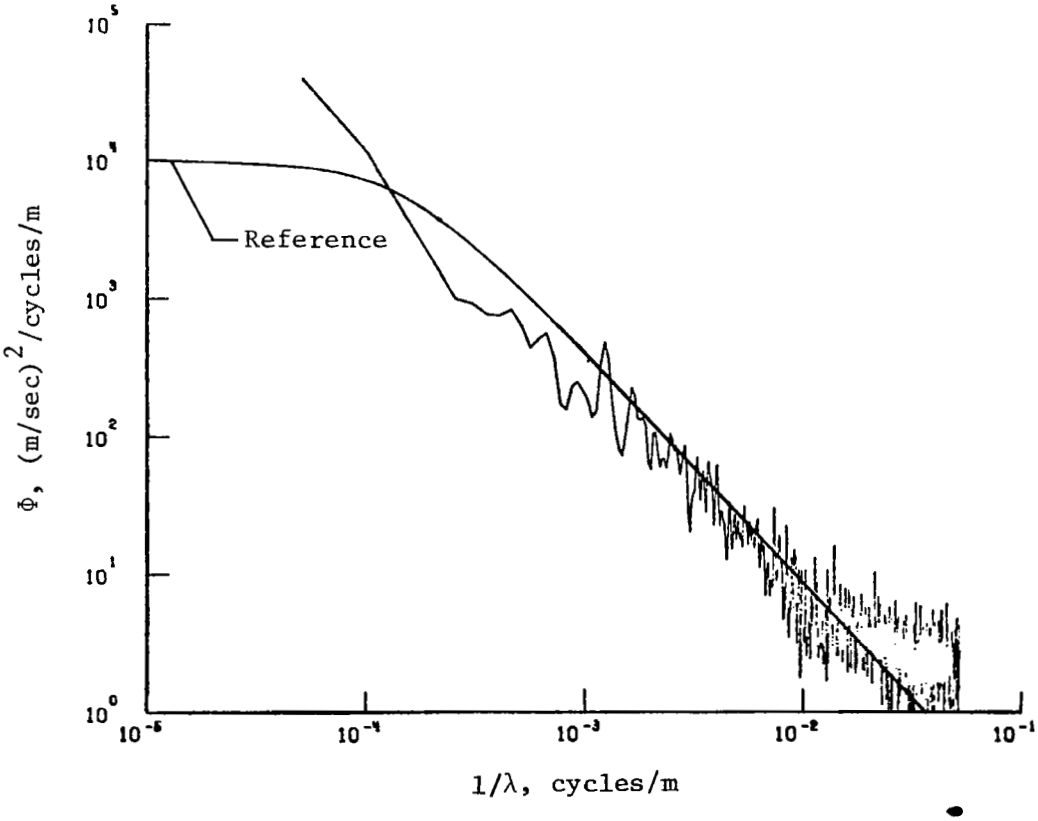

(c) Longitudinal component of gust velocity.

Figure 35.- Concluded.

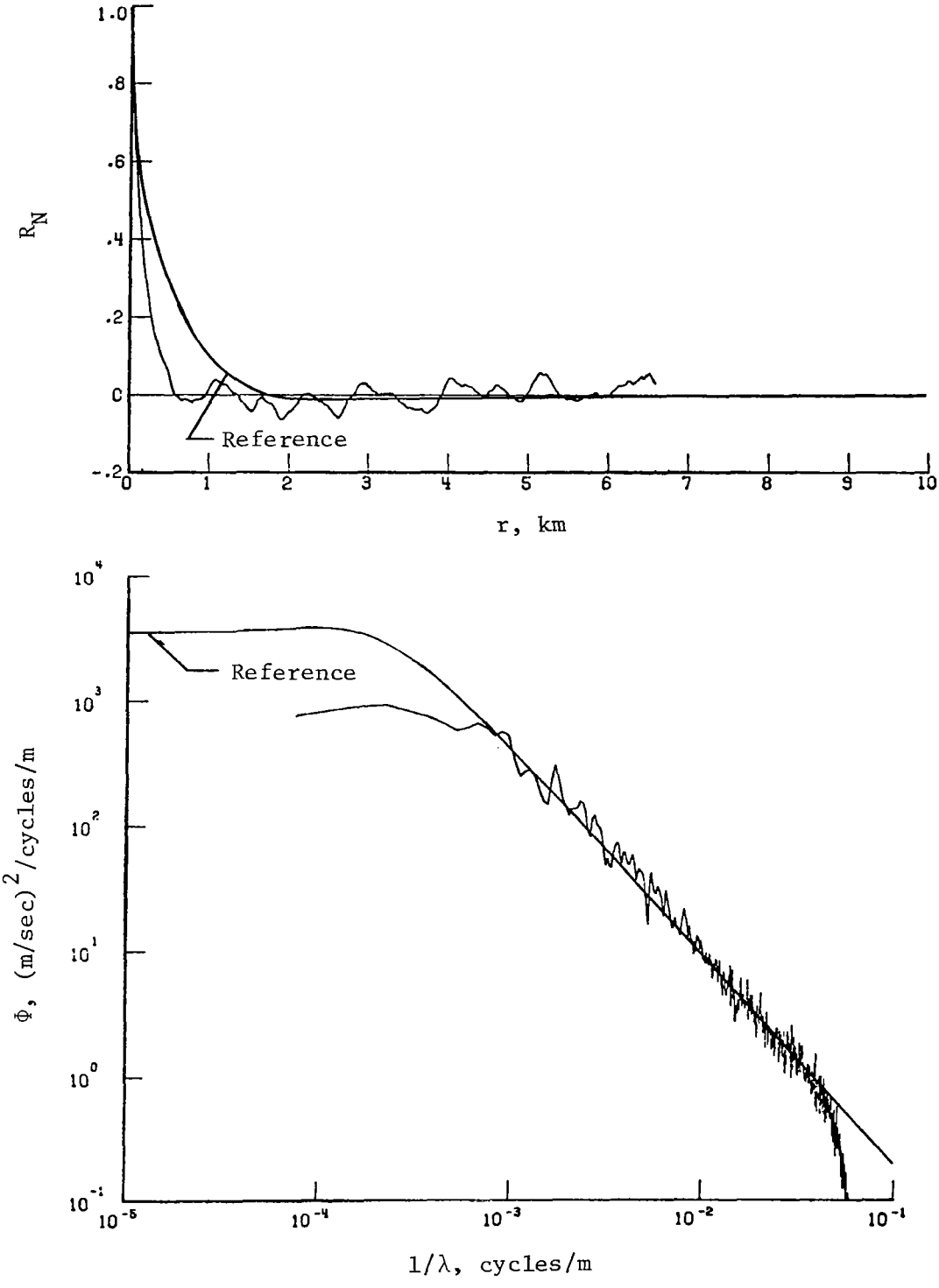

(a) Vertical component of gust velocity.

Figure 36.- Power spectra and autocorrelation functions for flight 8, run 2.

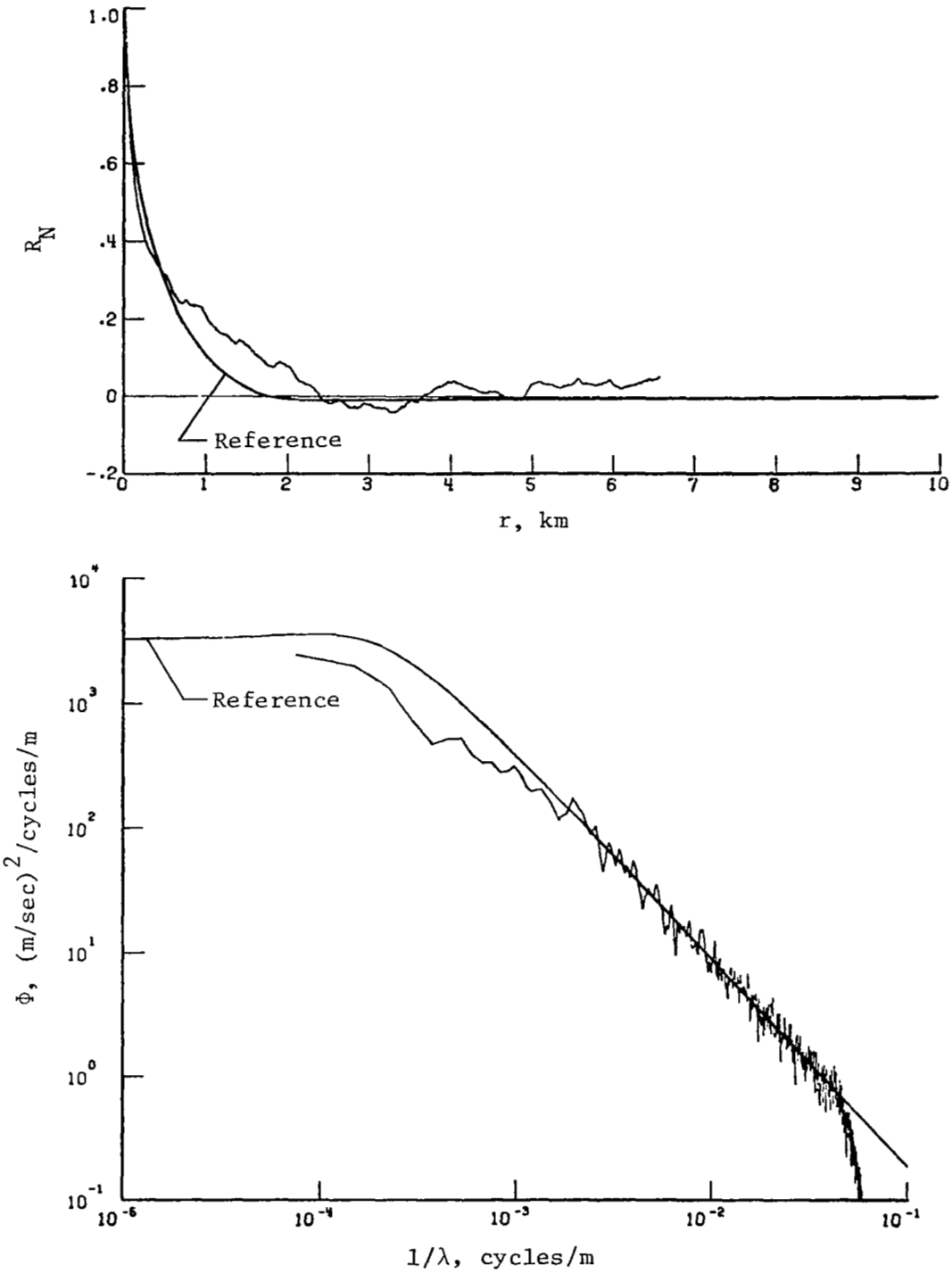

(b) Lateral component of gust velocity.

Figure 36.- Continued.

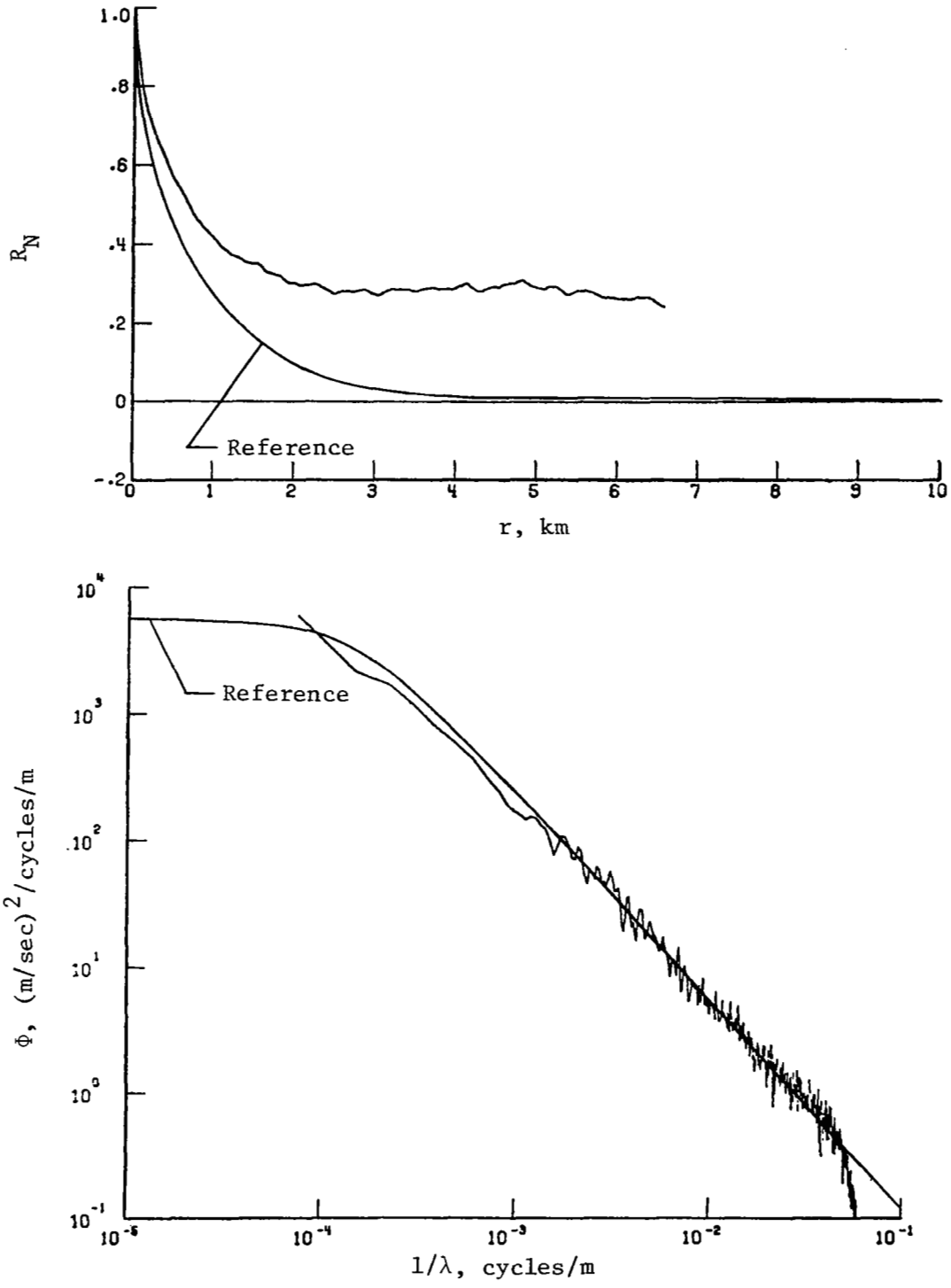

(c) Longitudinal component of gust velocity.

Figure 36.- Concluded.

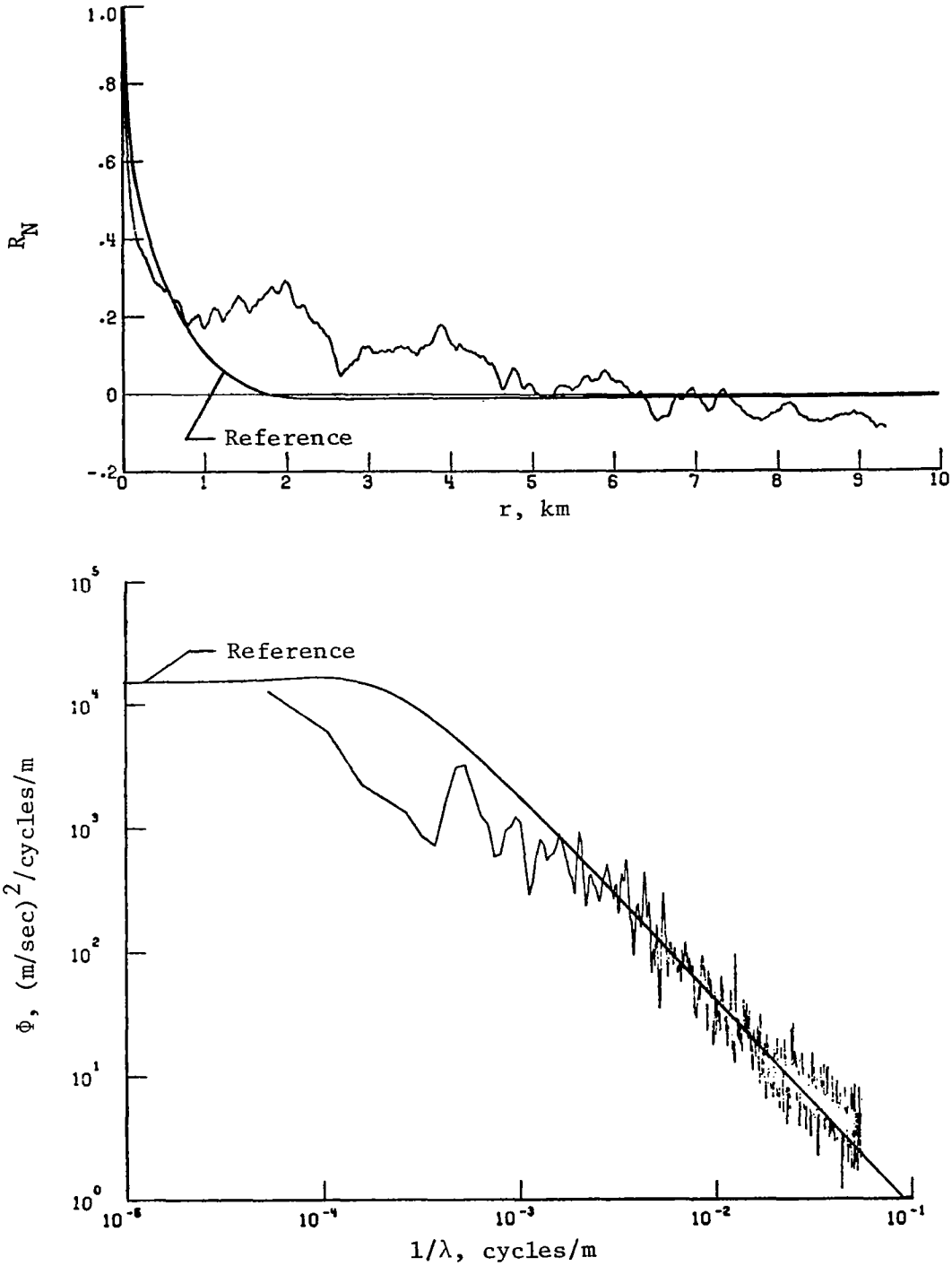

(a) Vertical component of gust velocity.

Figure 37.- Power spectra and autocorrelation functions for flight 32, run 2.

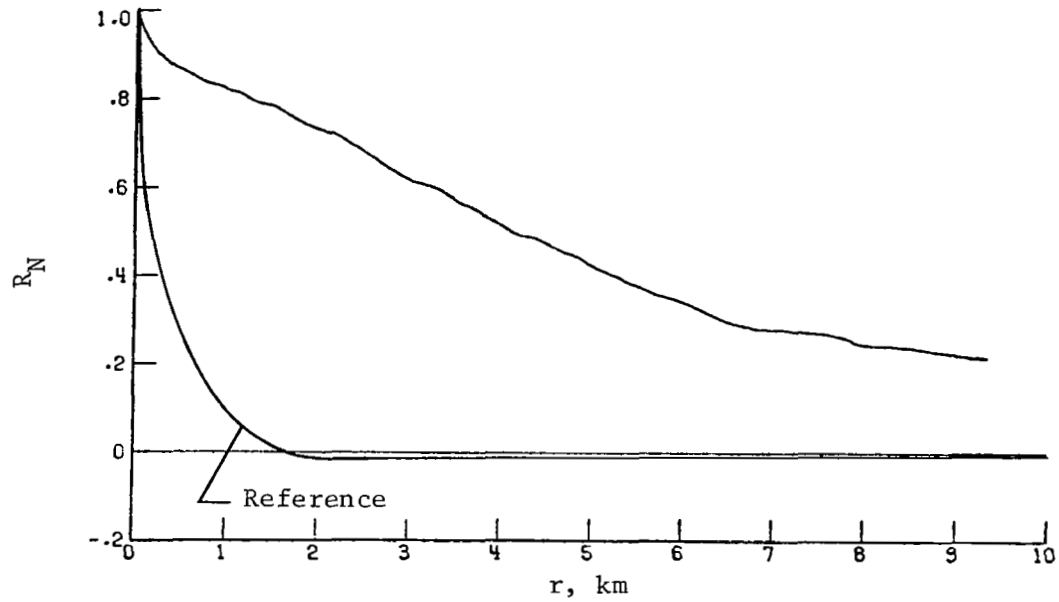

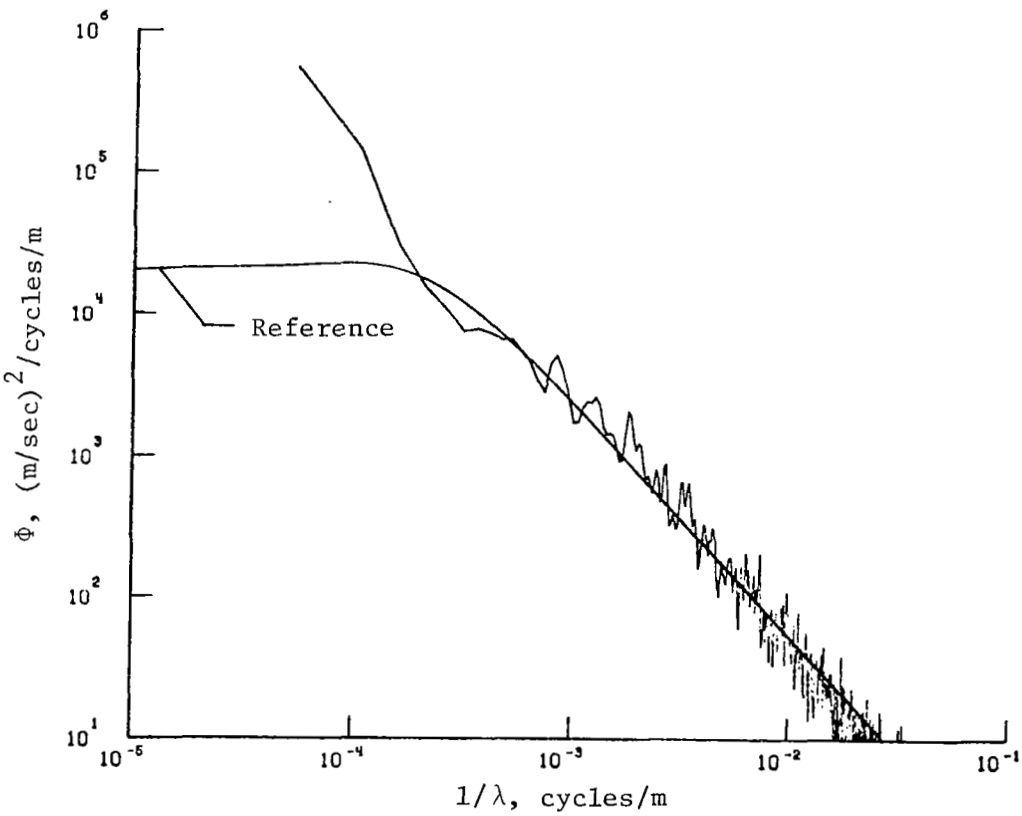

(b) Lateral component of gust velocity.

Figure 37.- Continued.

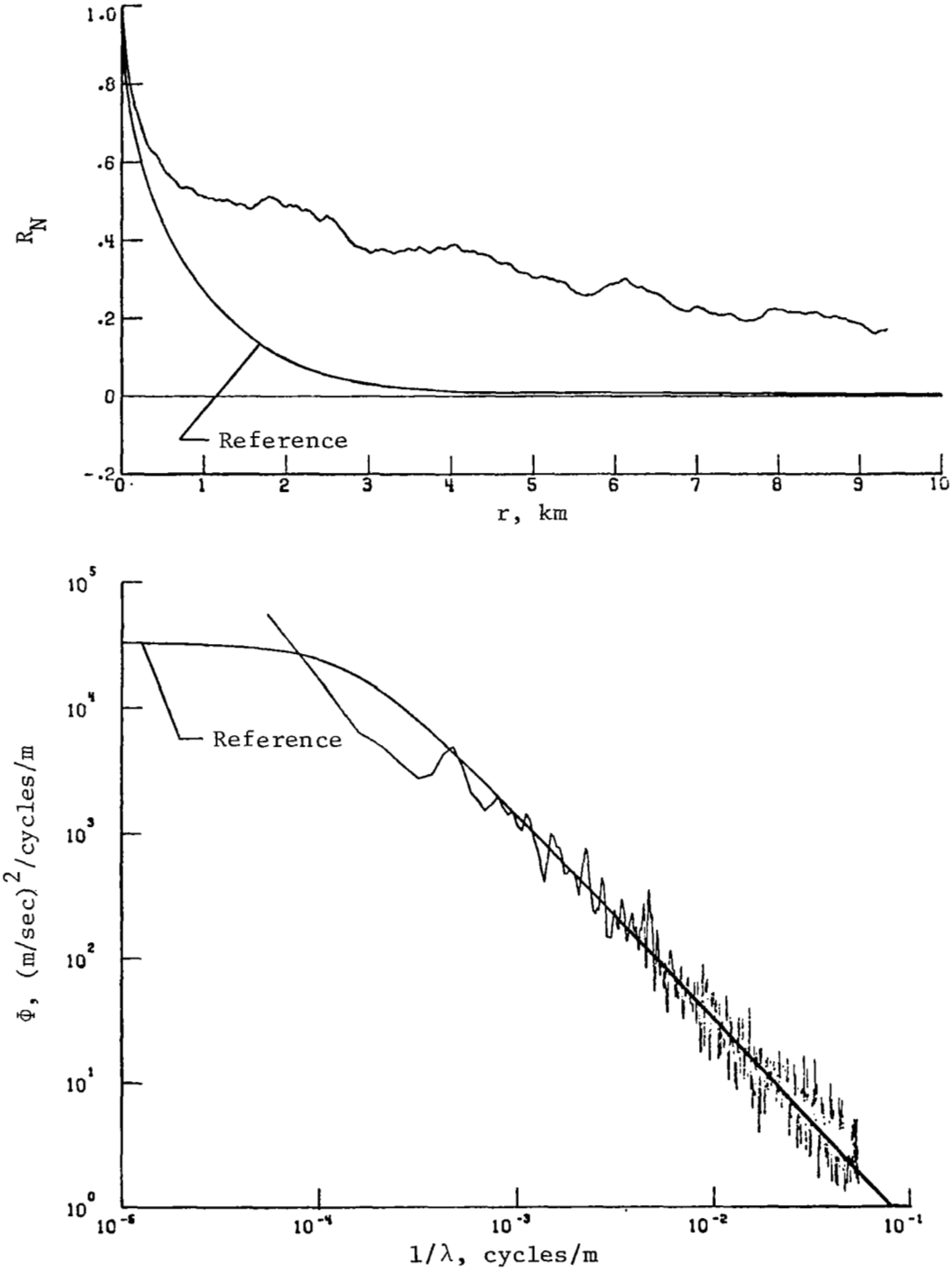

(c) Longitudinal component of gust velocity.

Figure 37.- Concluded.

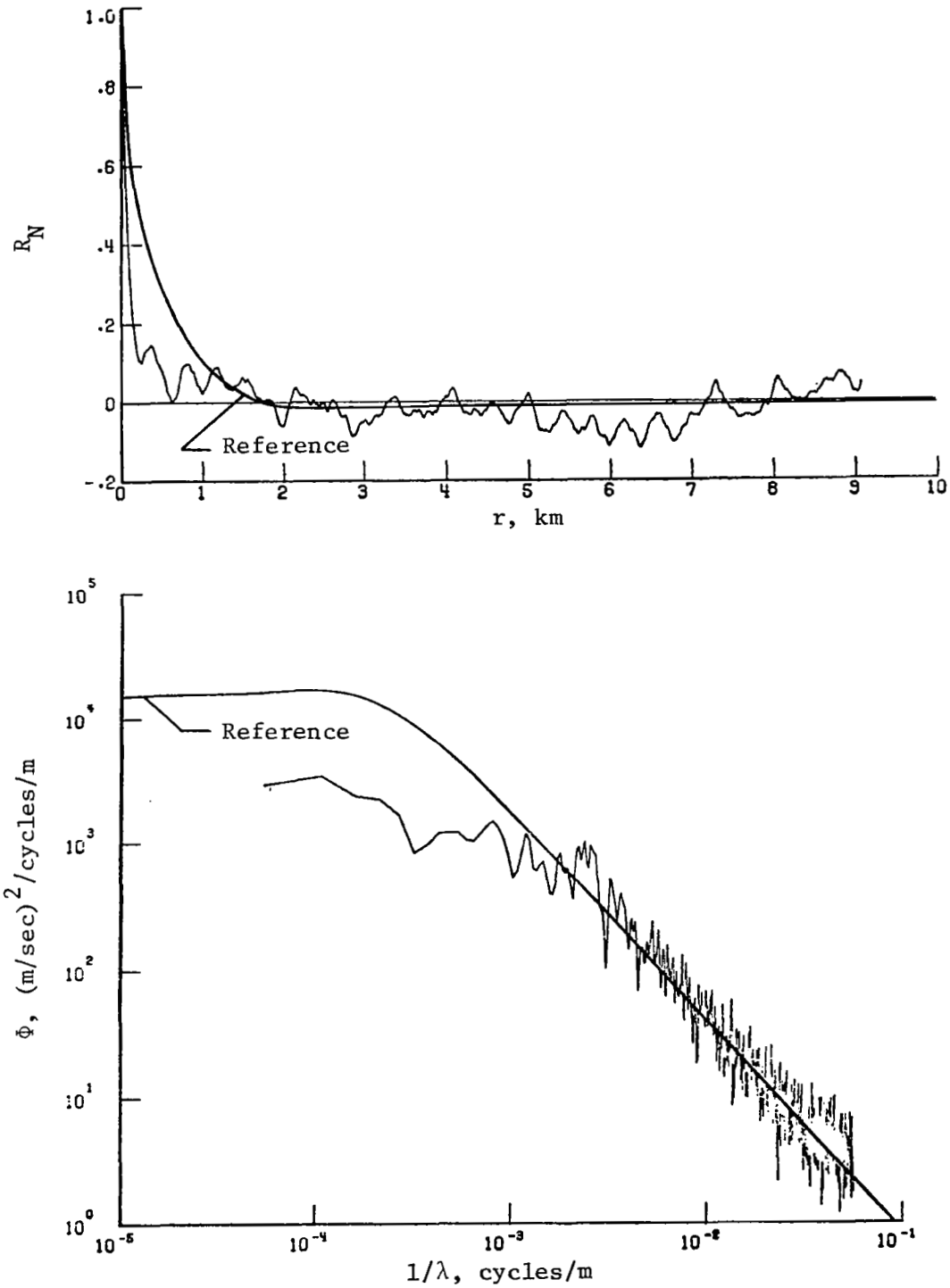

(a) Vertical component of gust velocity.

Figure 38.- Power spectra and autocorrelation functions for flight 32, run 3.

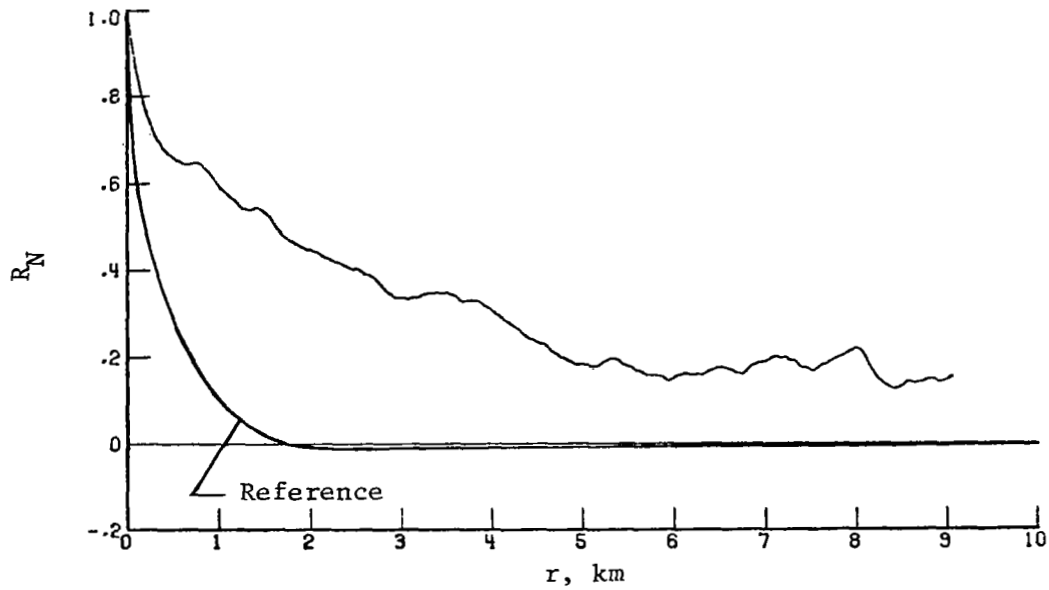

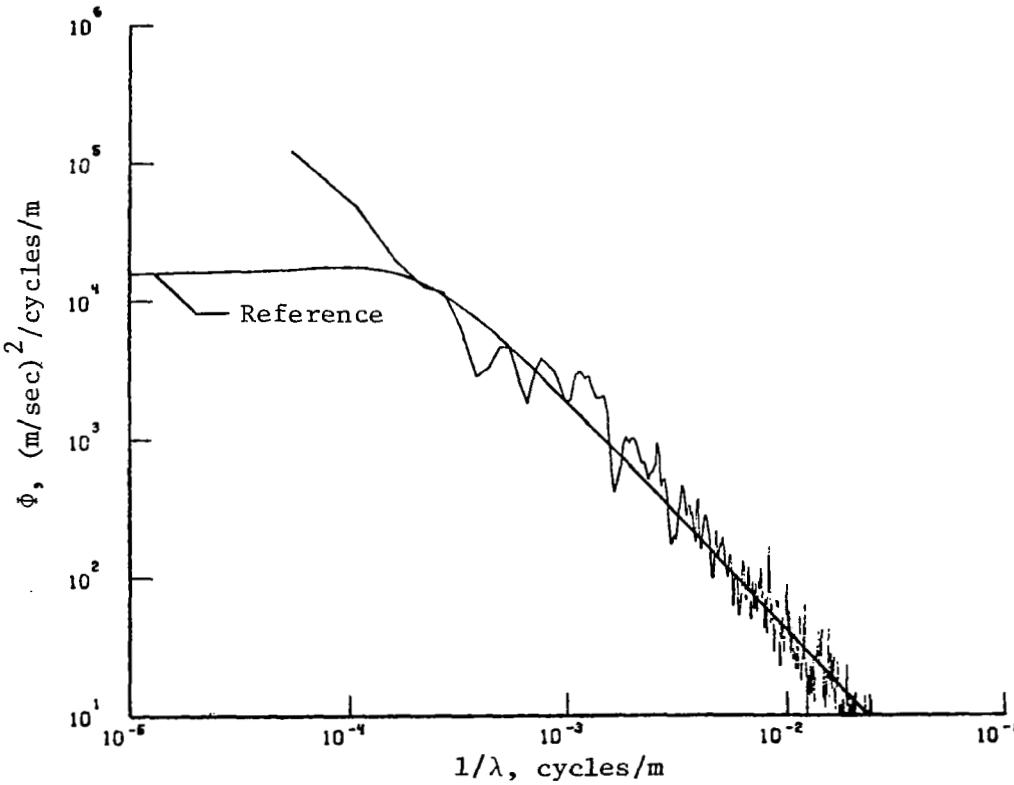

(b) Lateral component of gust velocity.

Figure 38.- Continued.

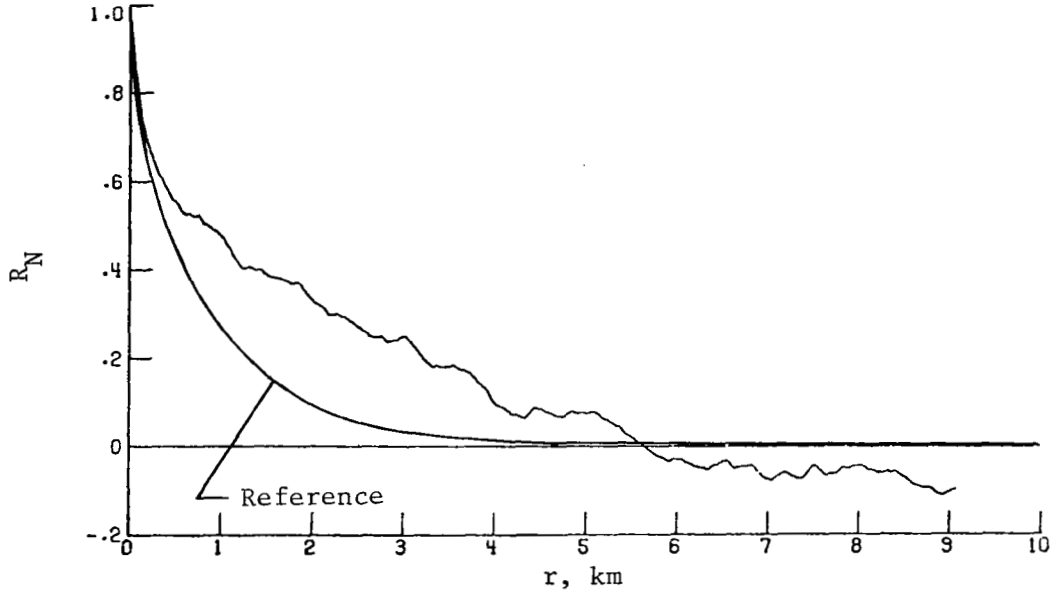

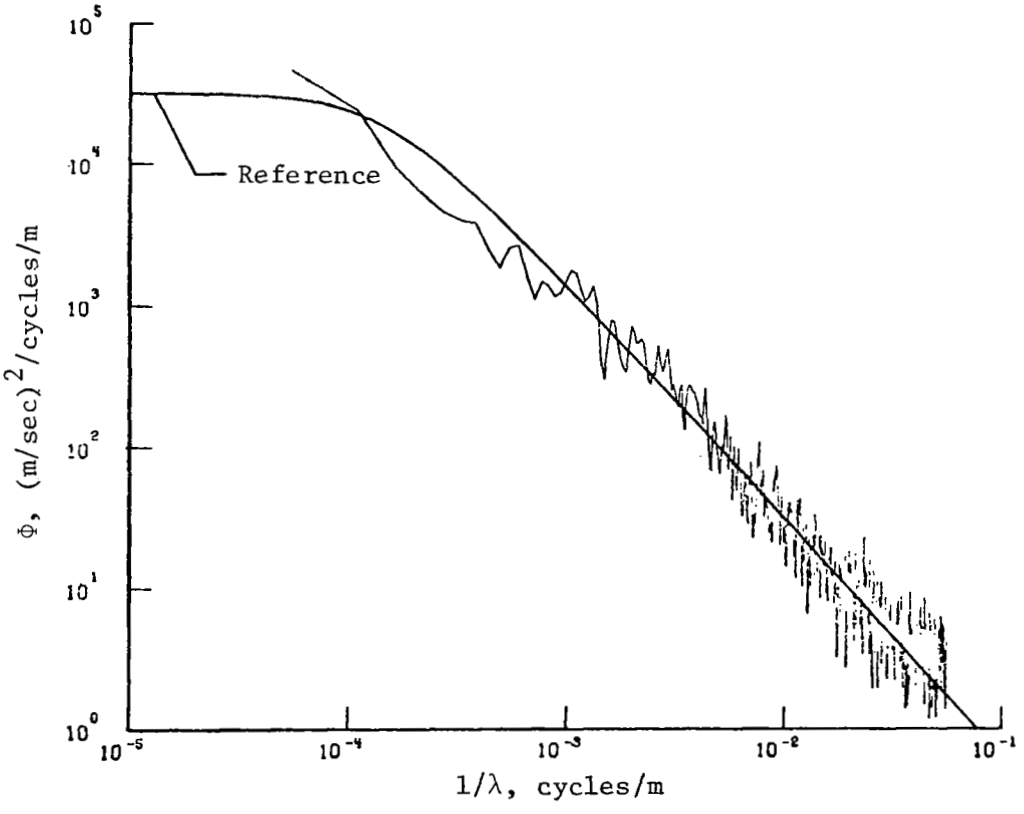

(c) Longitudinal component of gust velocity.

Figure 38.- Concluded.

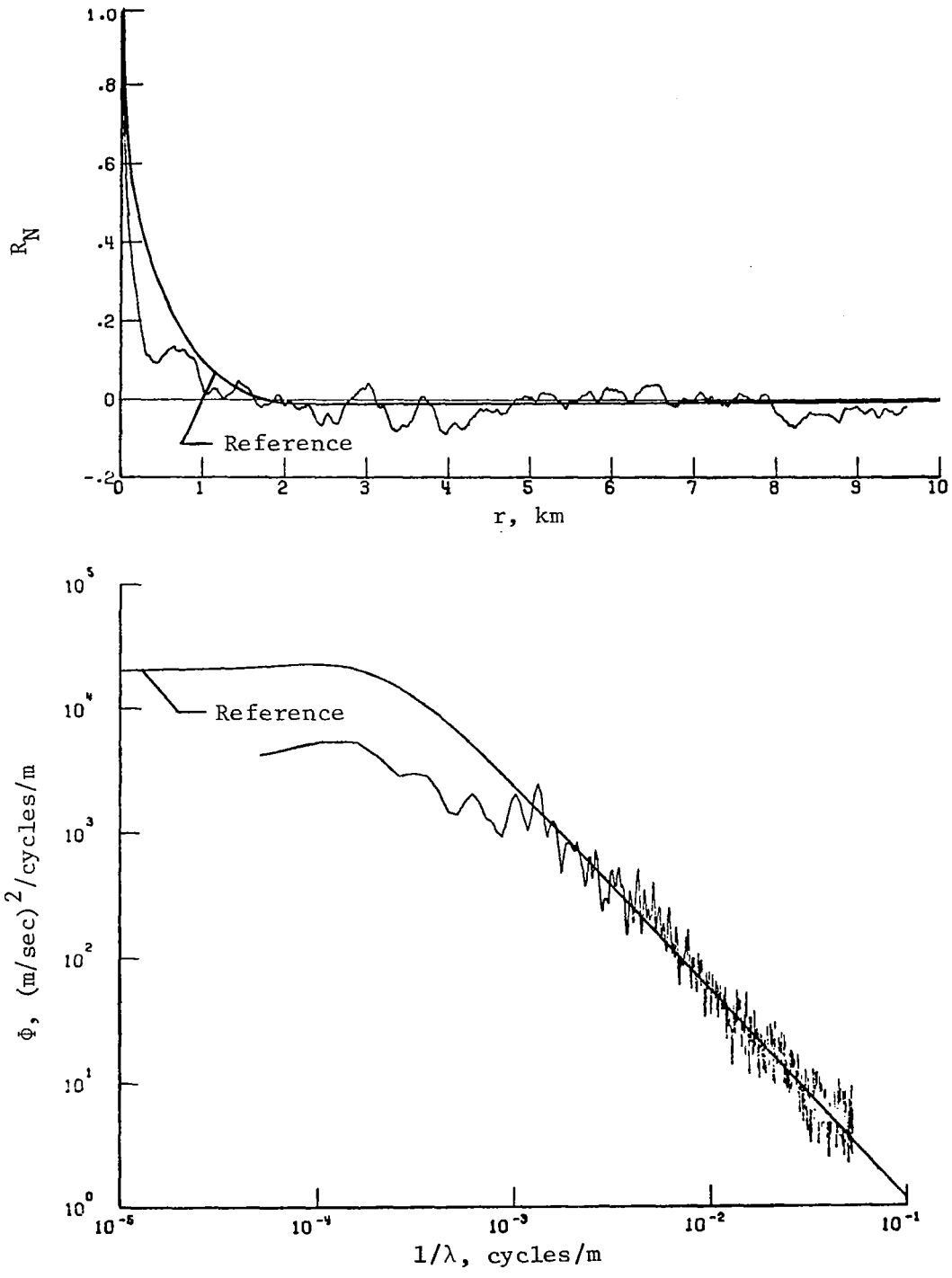

(a) Vertical component of gust velocity.

Figure 39.- Power spectra and autocorrelation functions for flight 32, run 4.

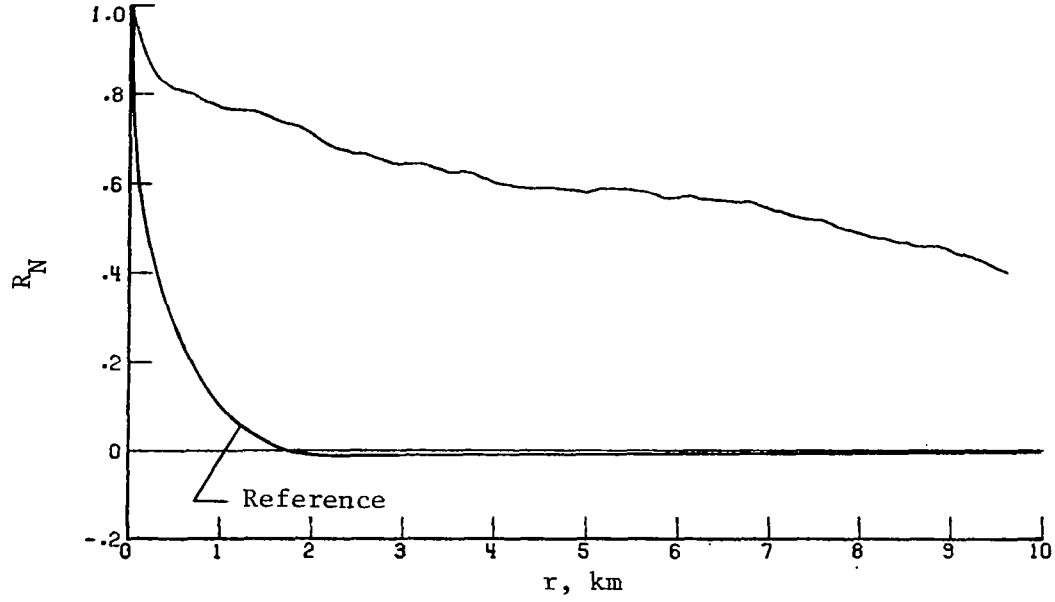

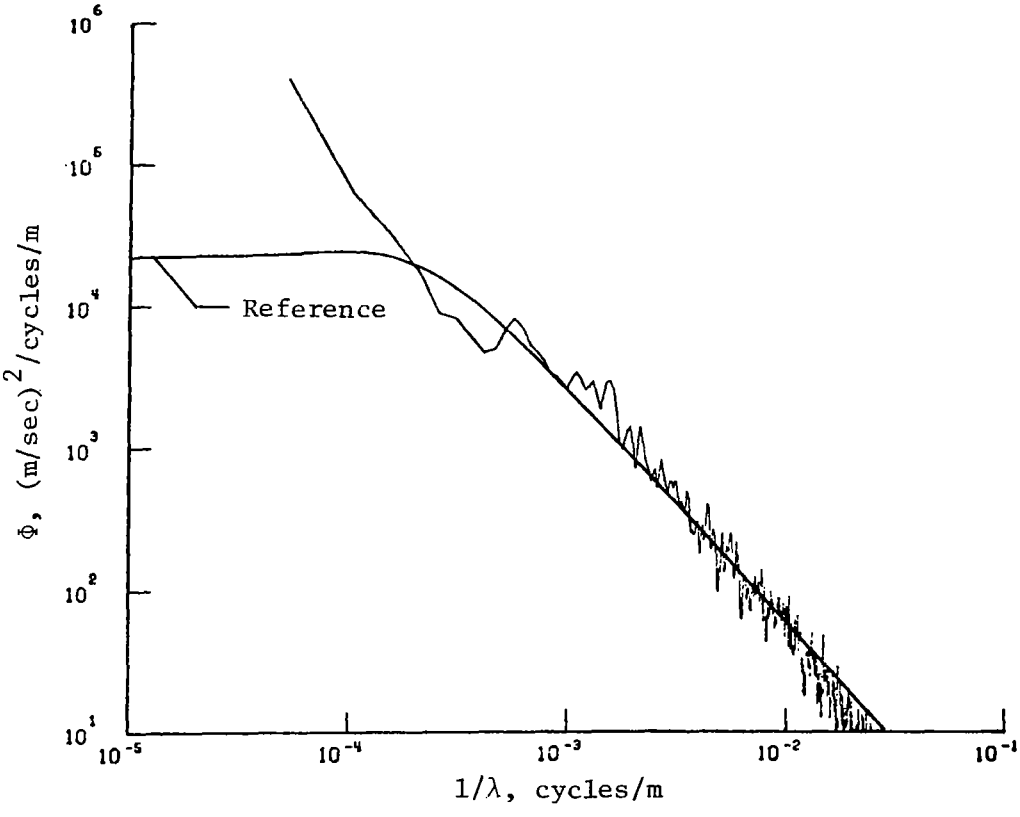

(b) Lateral component of gust velocity.

Figure 39.- Continued.

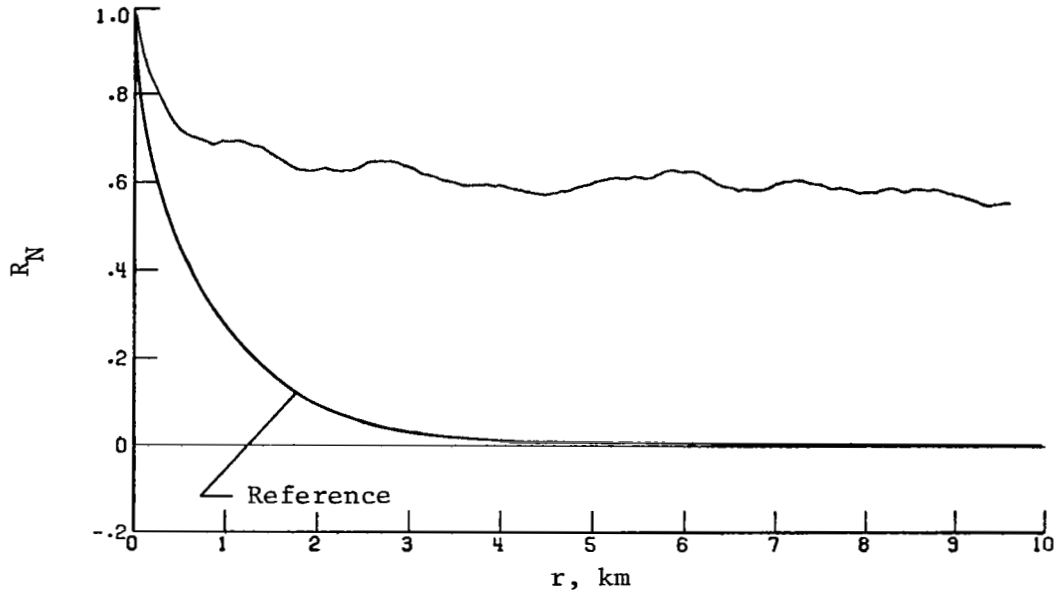

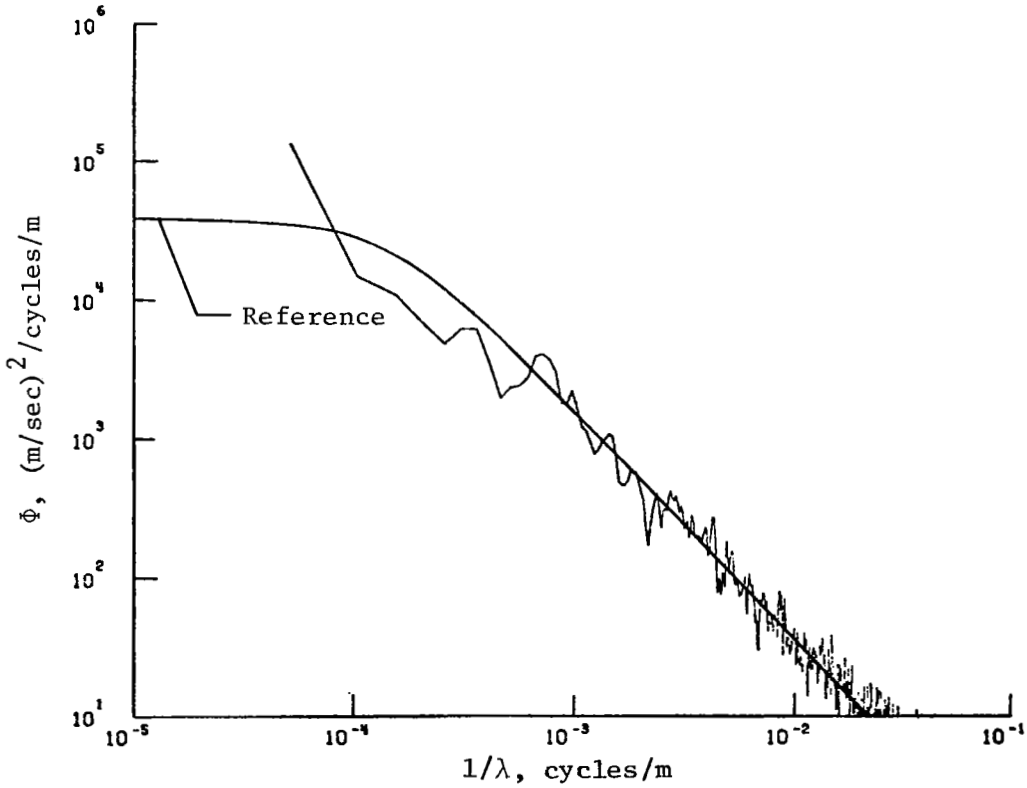

(c) Longitudinal component of gust velocity.

Figure 39.- Concluded.

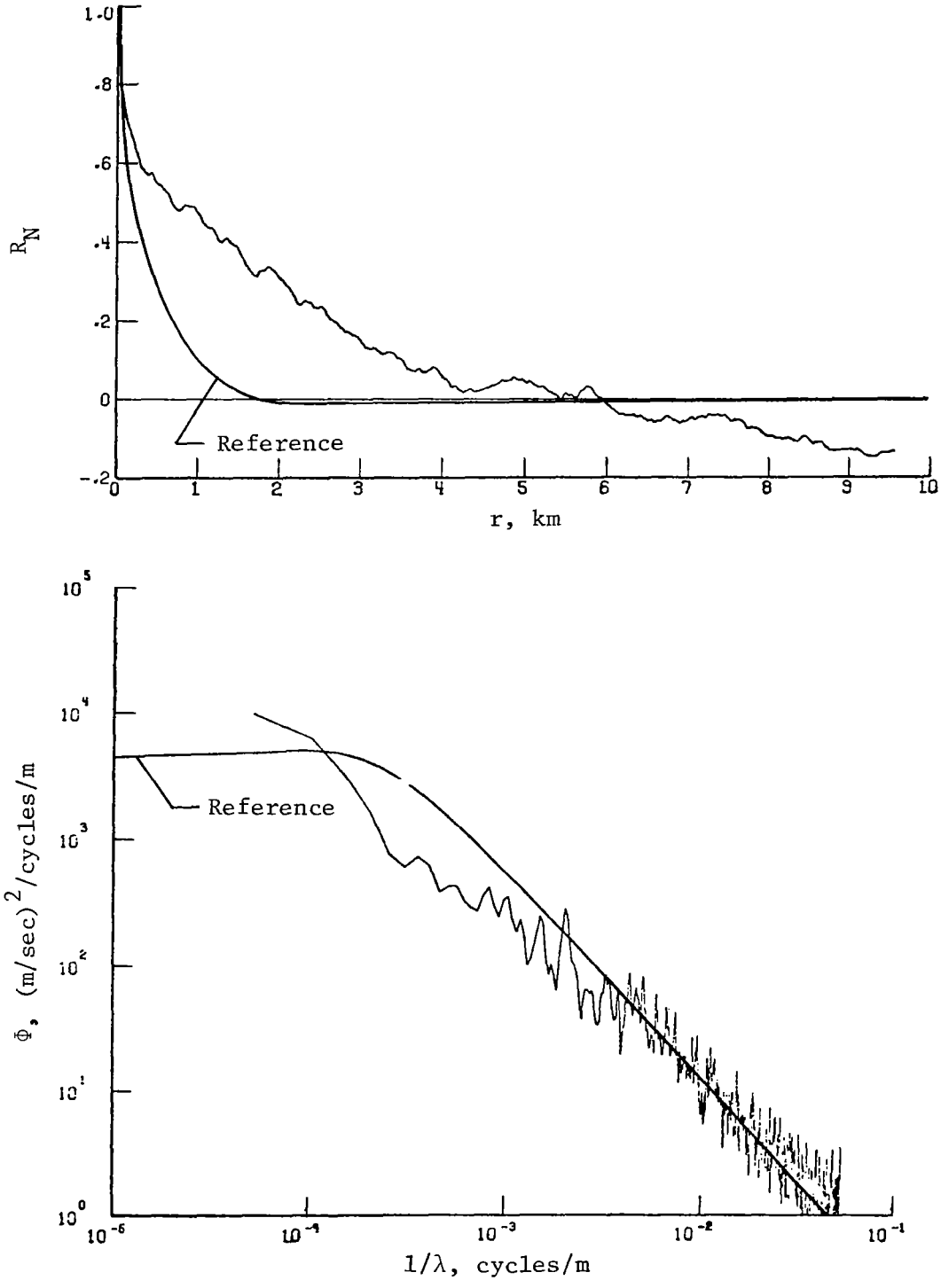

(a) Vertical component of gust velocity.

Figure 40.- Power spectra and autocorrelation functions for flight 32, run 7.

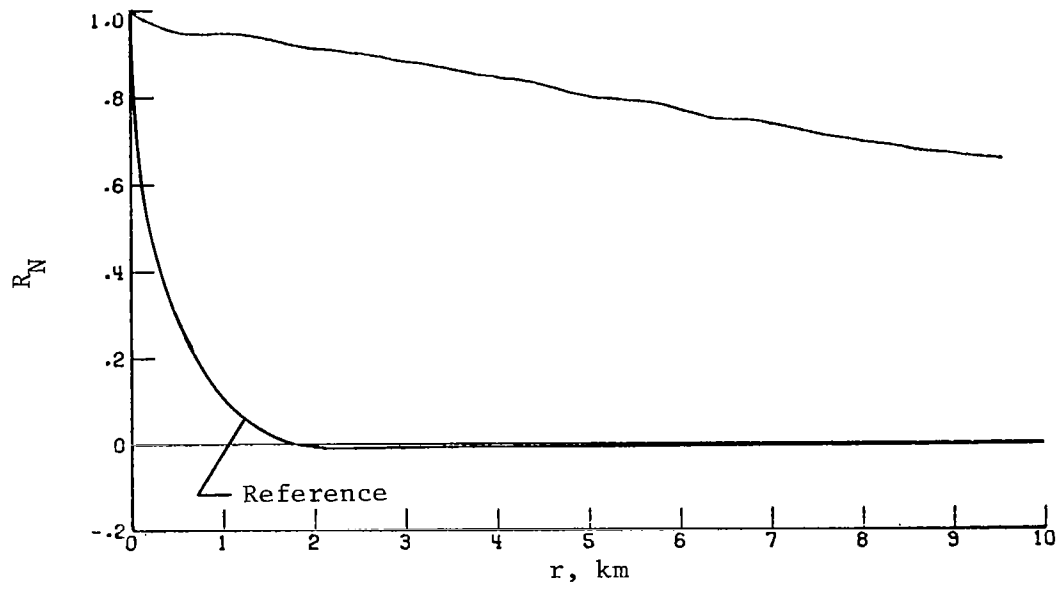

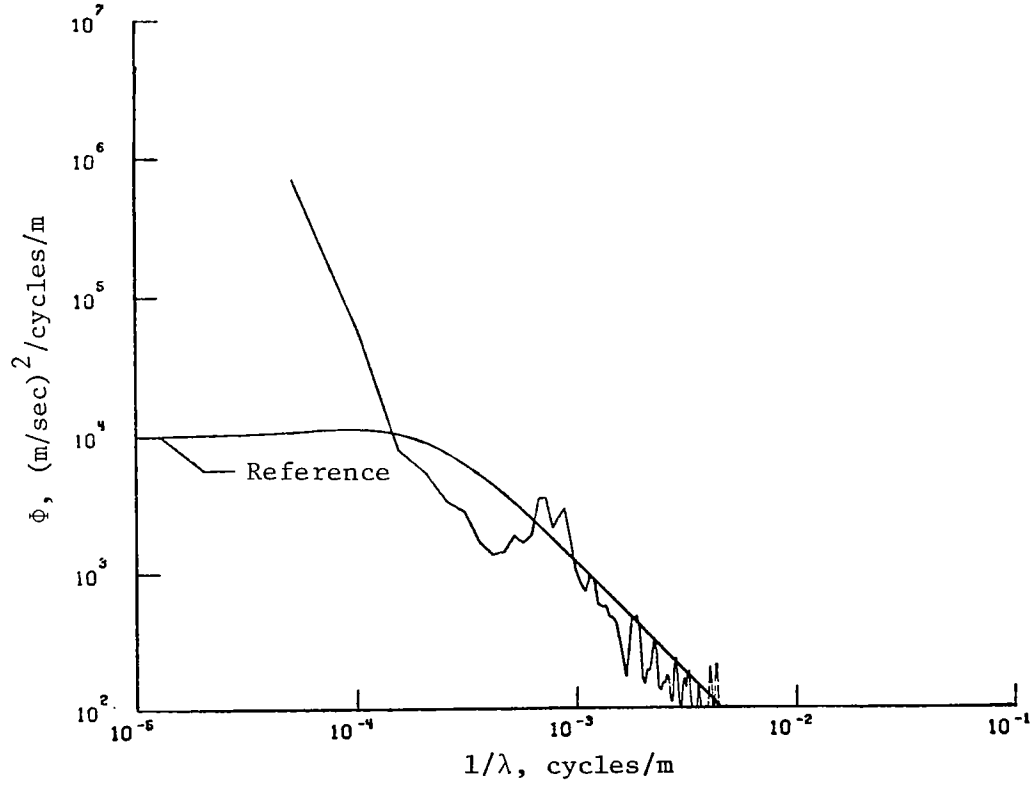

(b) Lateral component of gust velocity.

Figure 40.- Continued.

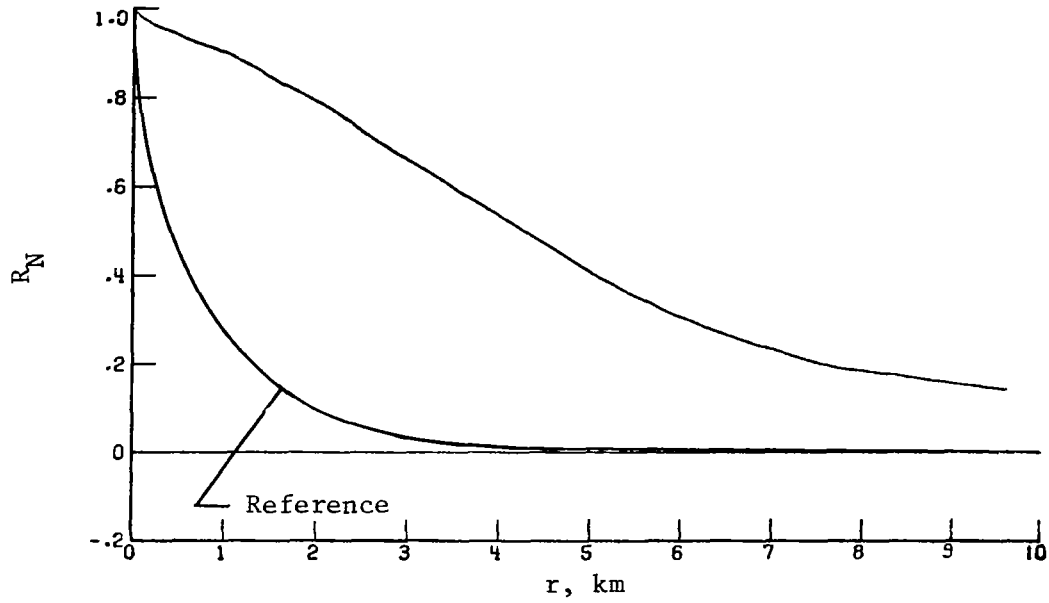

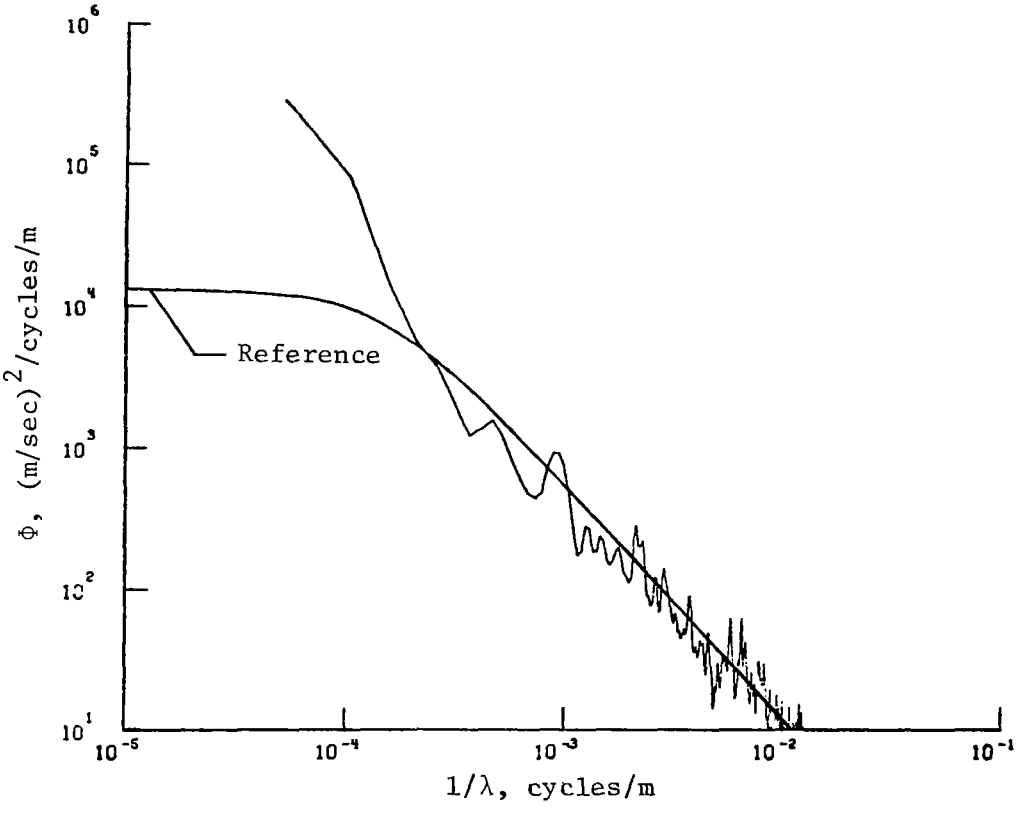

(c) Longitudinal component of gust velocity.

Figure 40.- Concluded.

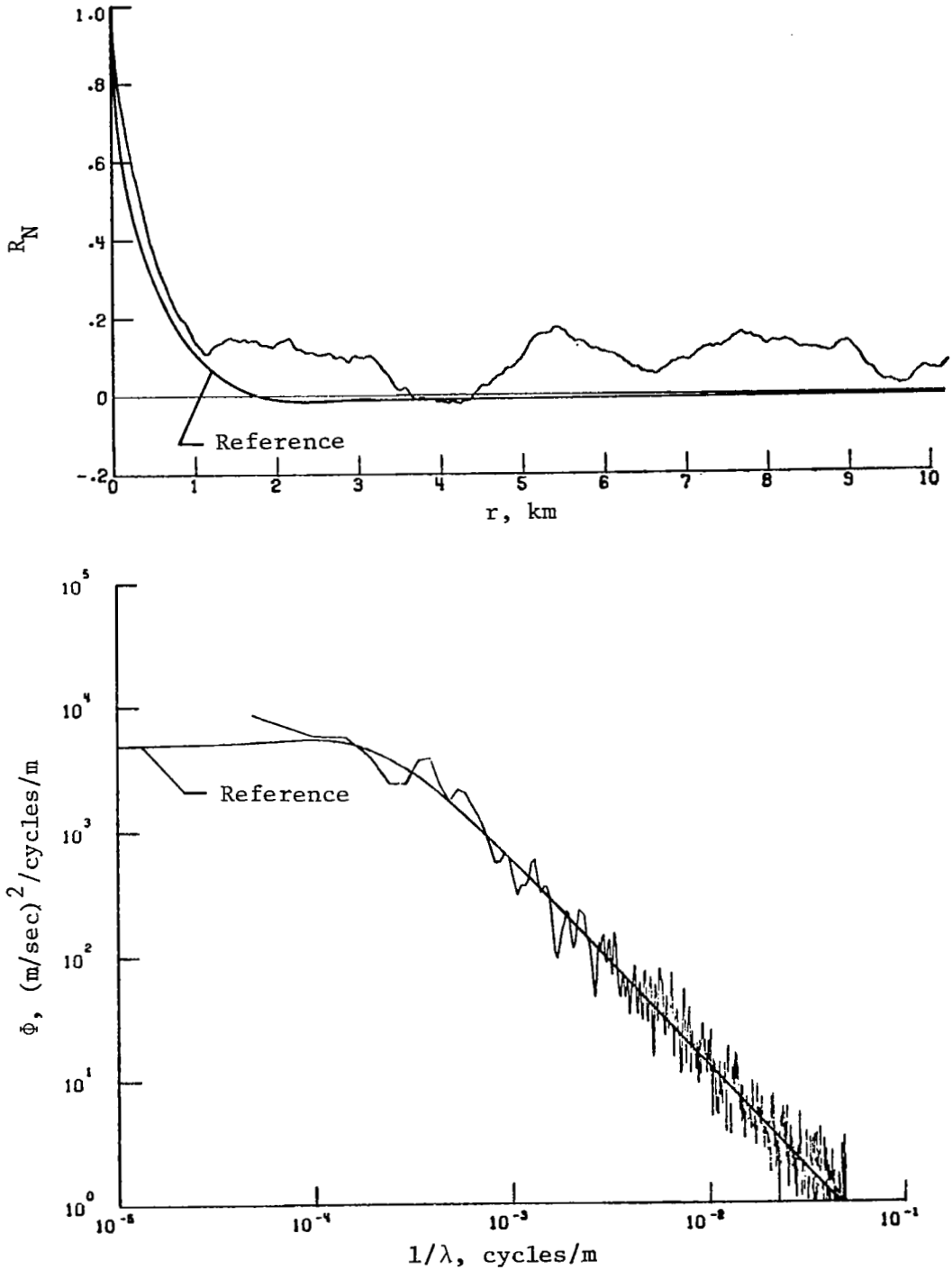

(a) Vertical component of gust velocity.

Figure 41.- Power spectra and autocorrelation functions for flight 42, run 2.

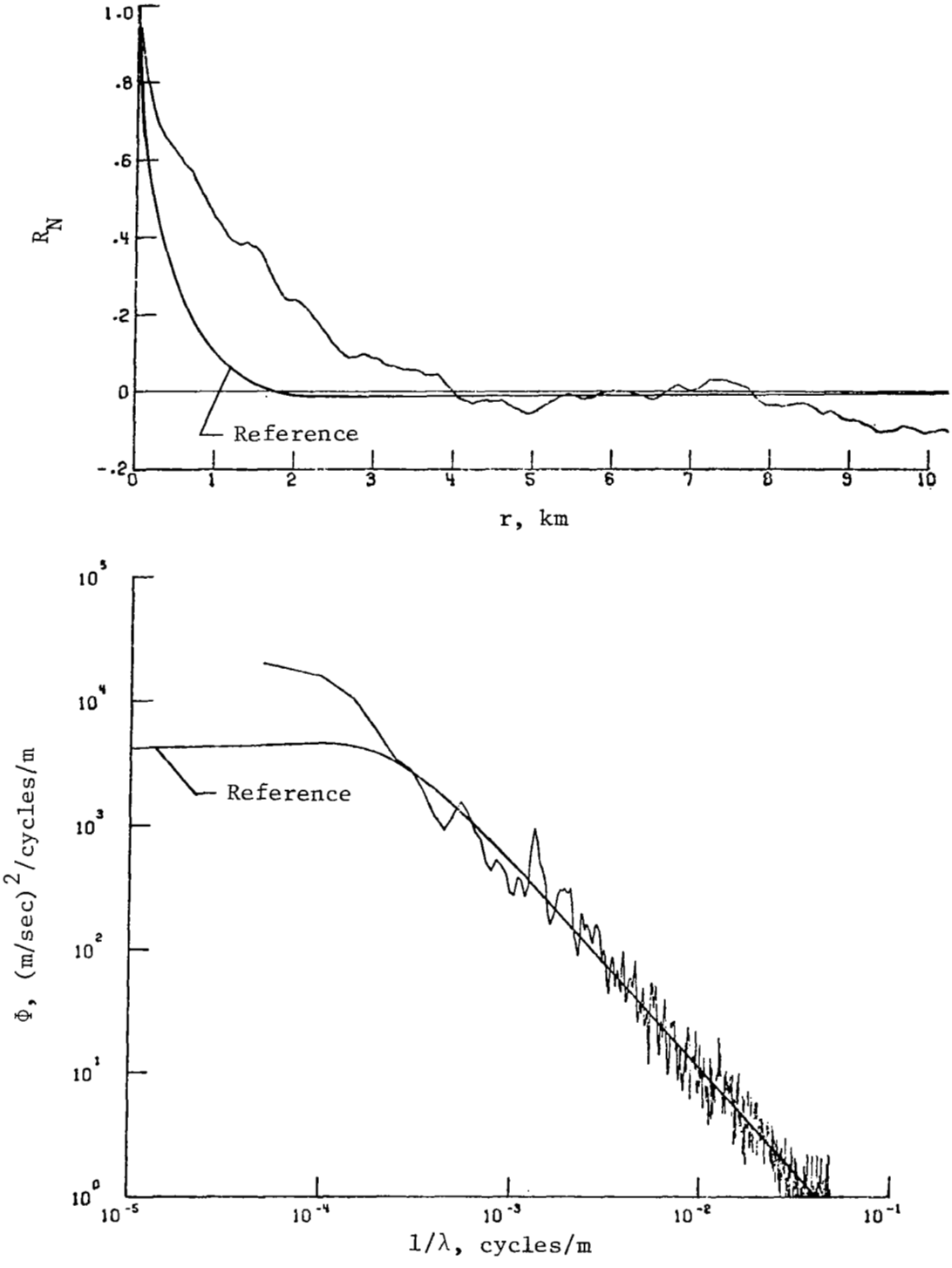

(b) Lateral component of gust velocity.

Figure 41.- Continued.

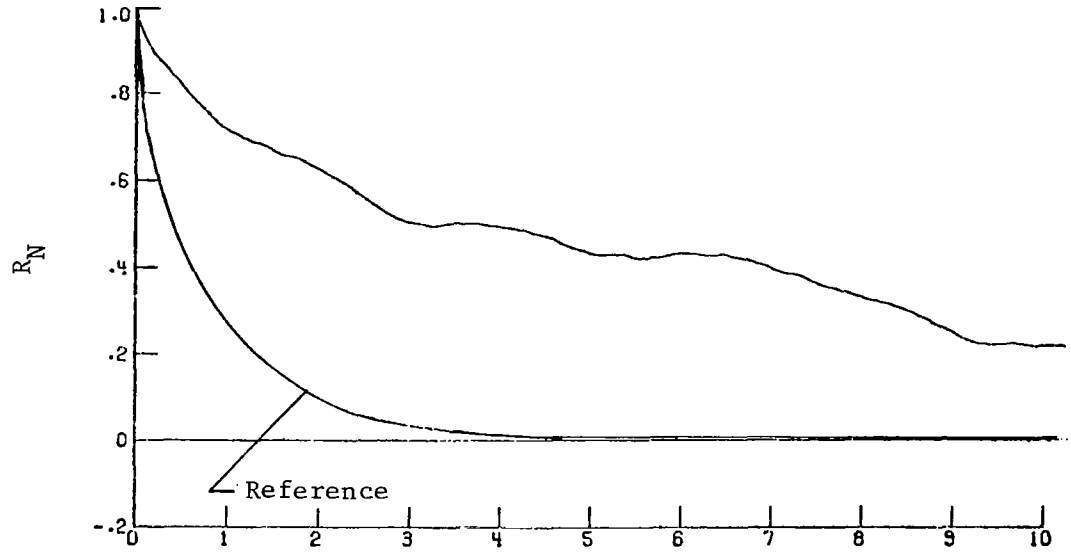

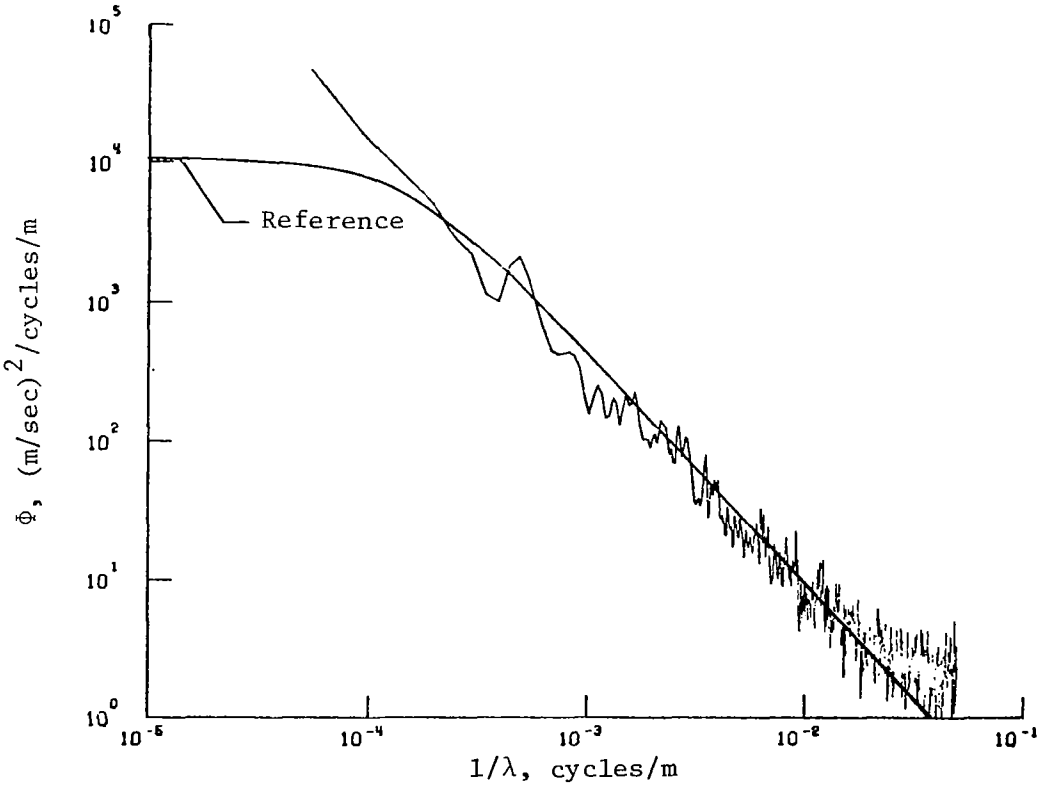

(c) Longitudinal component of gust velocity.

Figure 41.- Concluded.

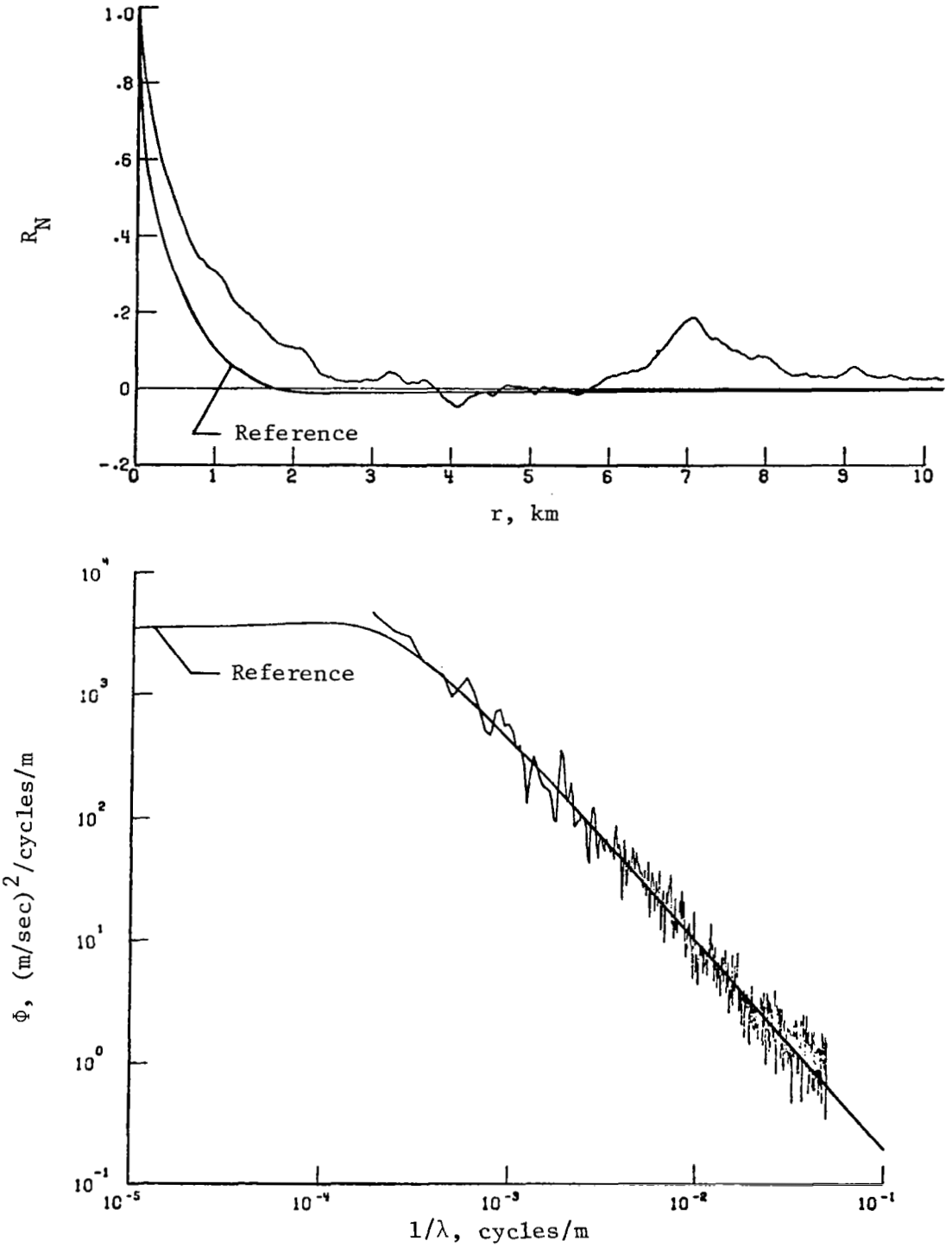

(a) Vertical component of gust velocity.

Figure 42.- Power spectra and autocorrelation functions for flight 42, run 3.

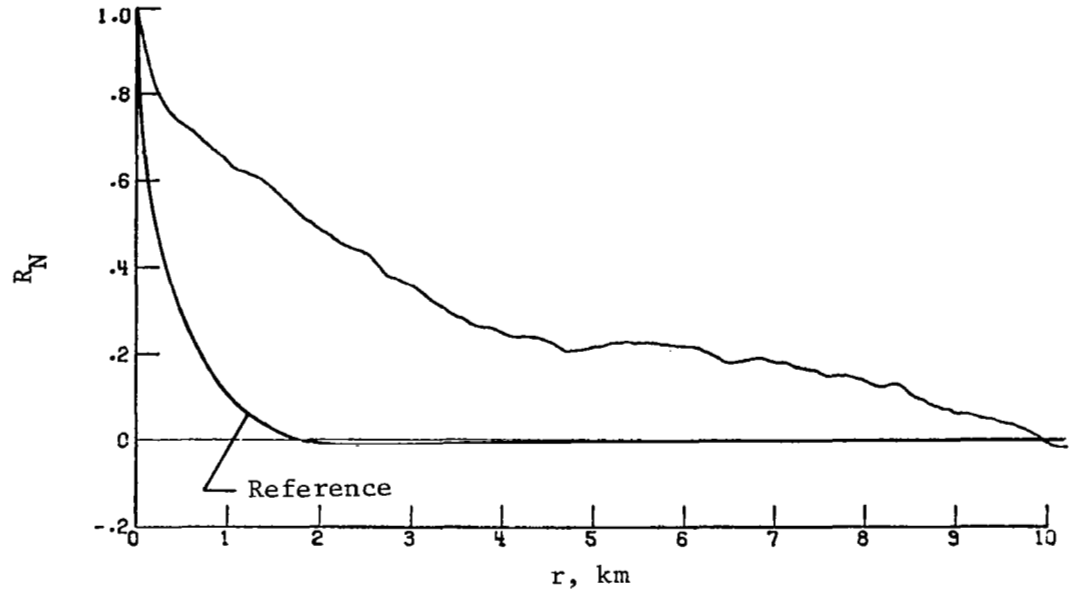

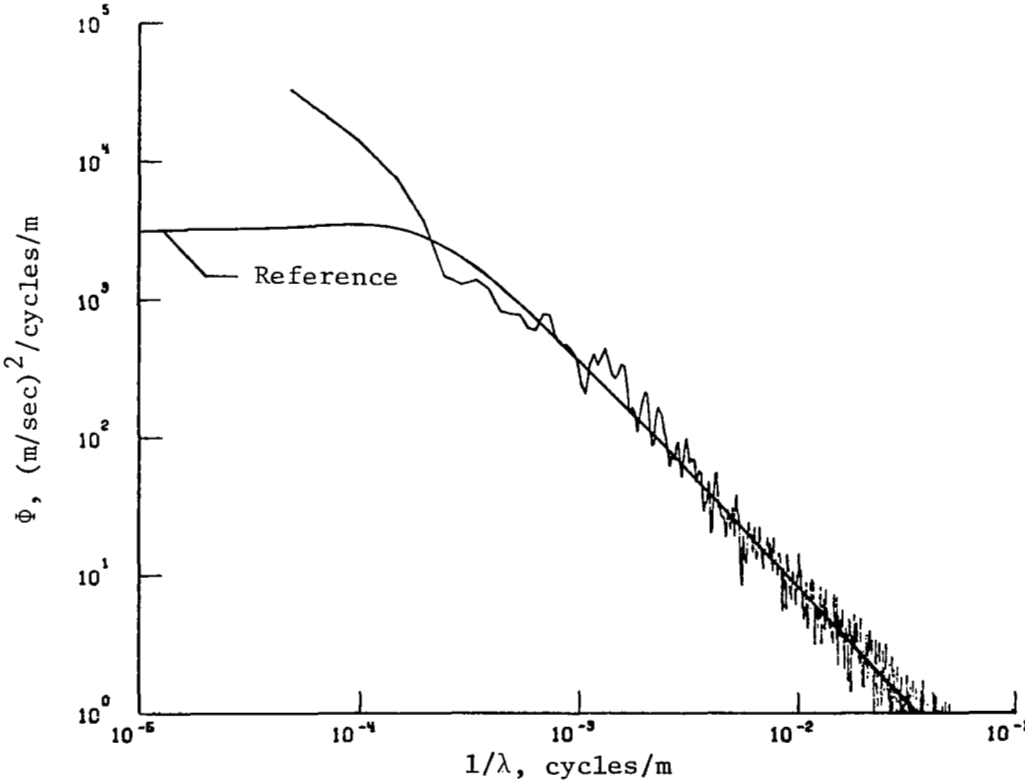

(b) Lateral component of gust velocity.

Figure 42.- Continued.

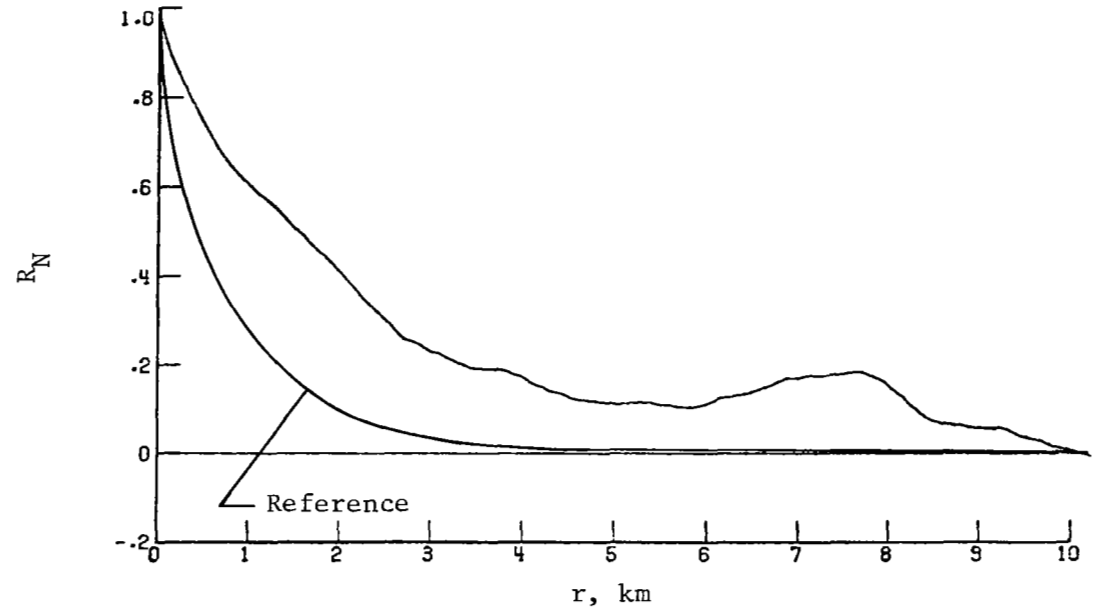

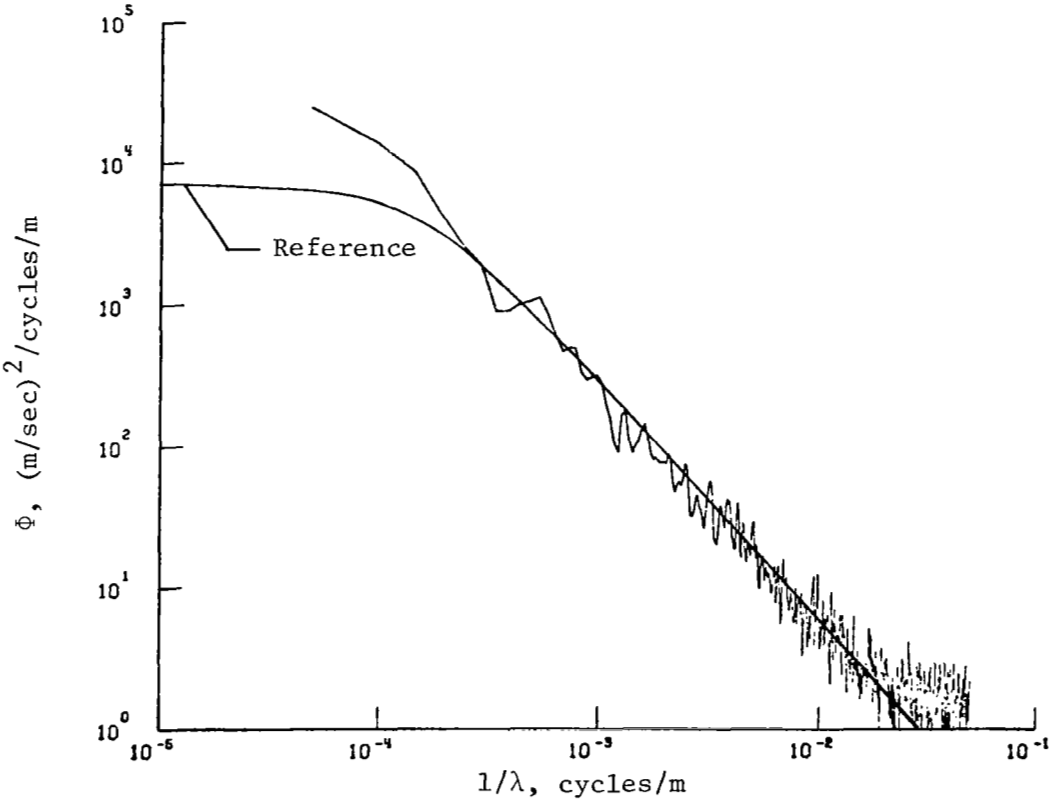

(c) Longitudinal component of gust velocity.

Figure 42.- Concluded.

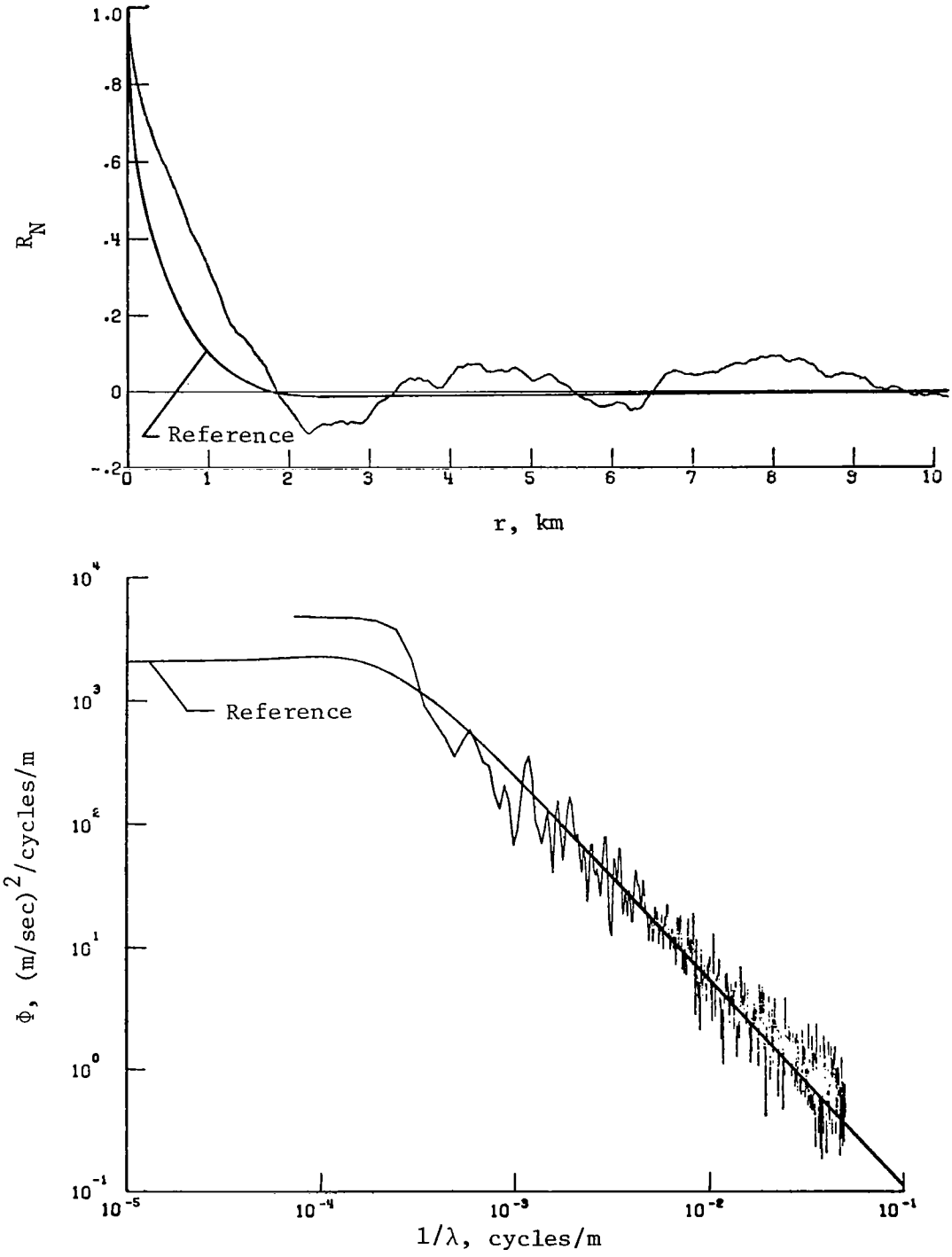

(a) Vertical component of gust velocity.

Figure 43.- Power spectra and autocorrelation functions for flight 42, run 4.

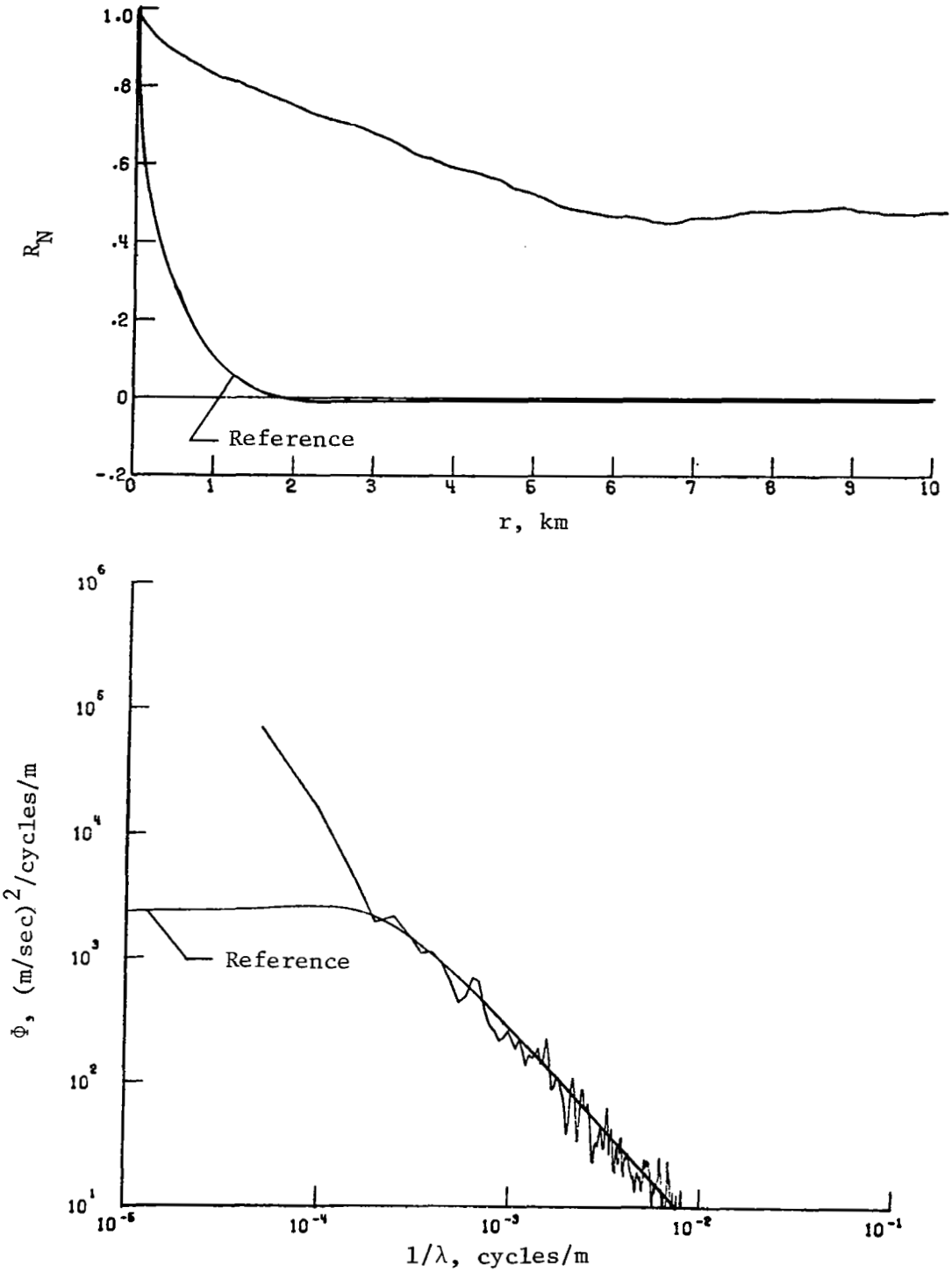

(b) Lateral component of gust velocity.

Figure 43.- Continued.

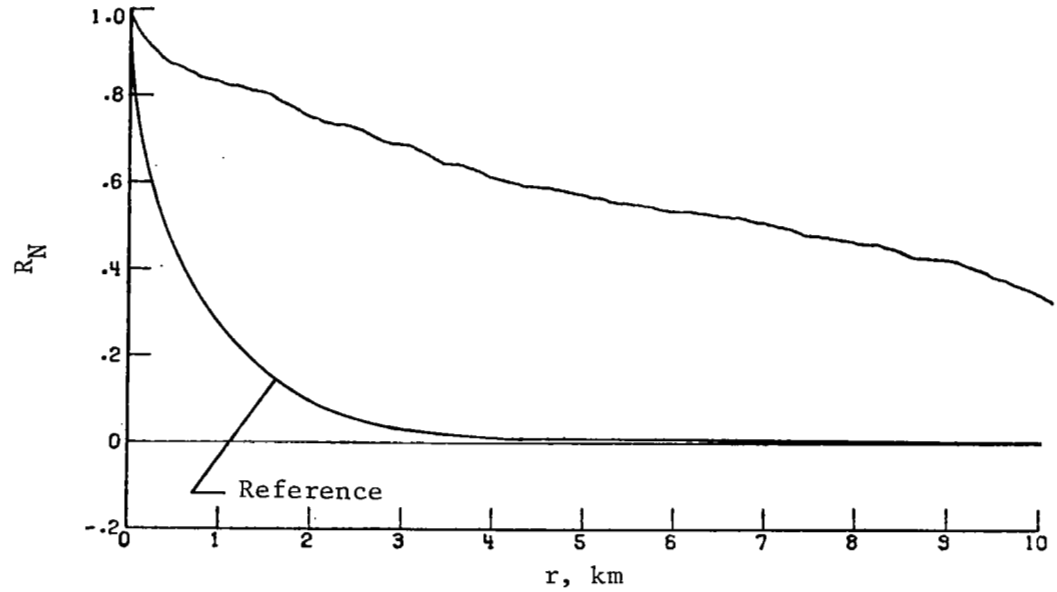

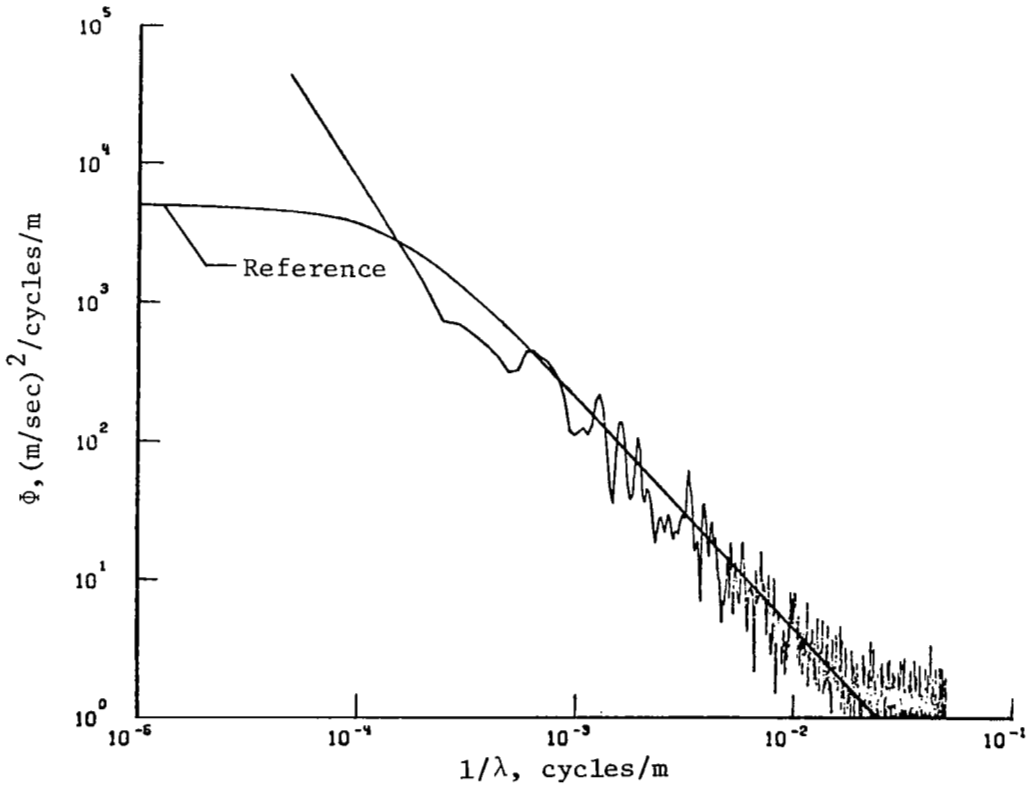

(c) Longitudinal component of gust velocity.

Figure 43.- Concluded.

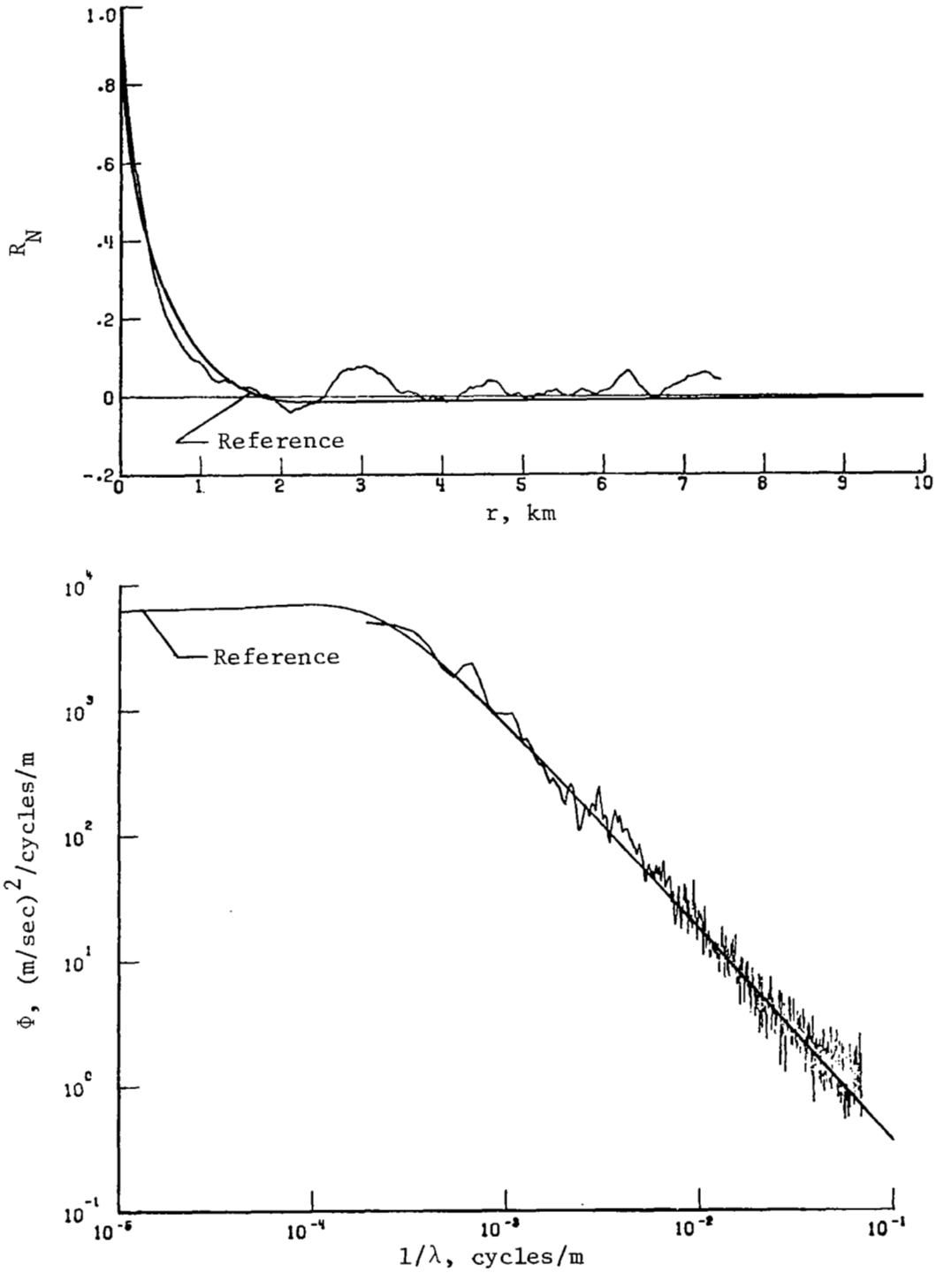

(a) Vertical component of gust velocity.

Figure 44.- Power spectra and autocorrelation functions for flight 42, run 6.

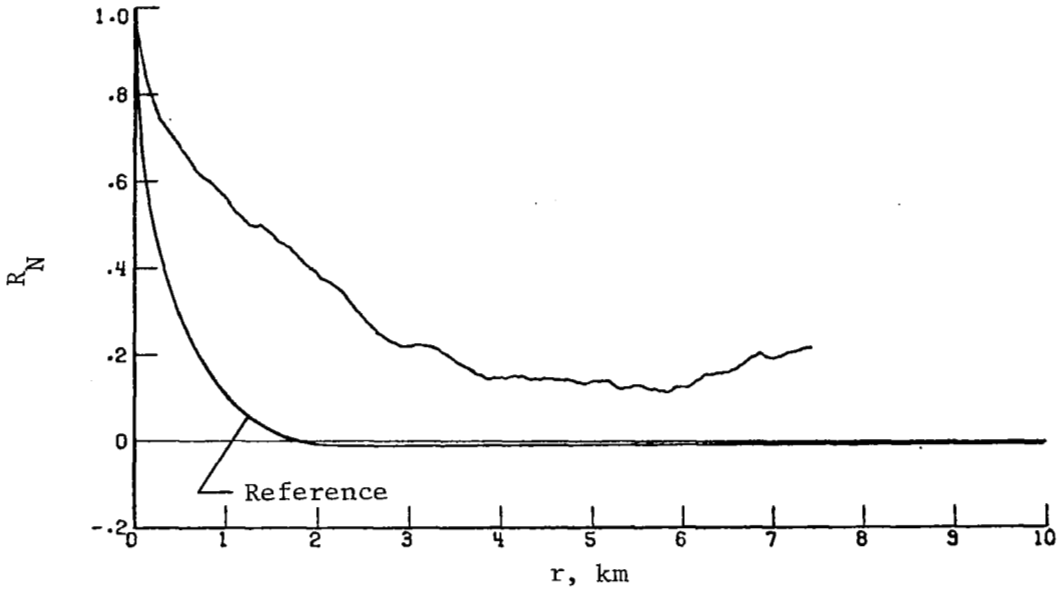

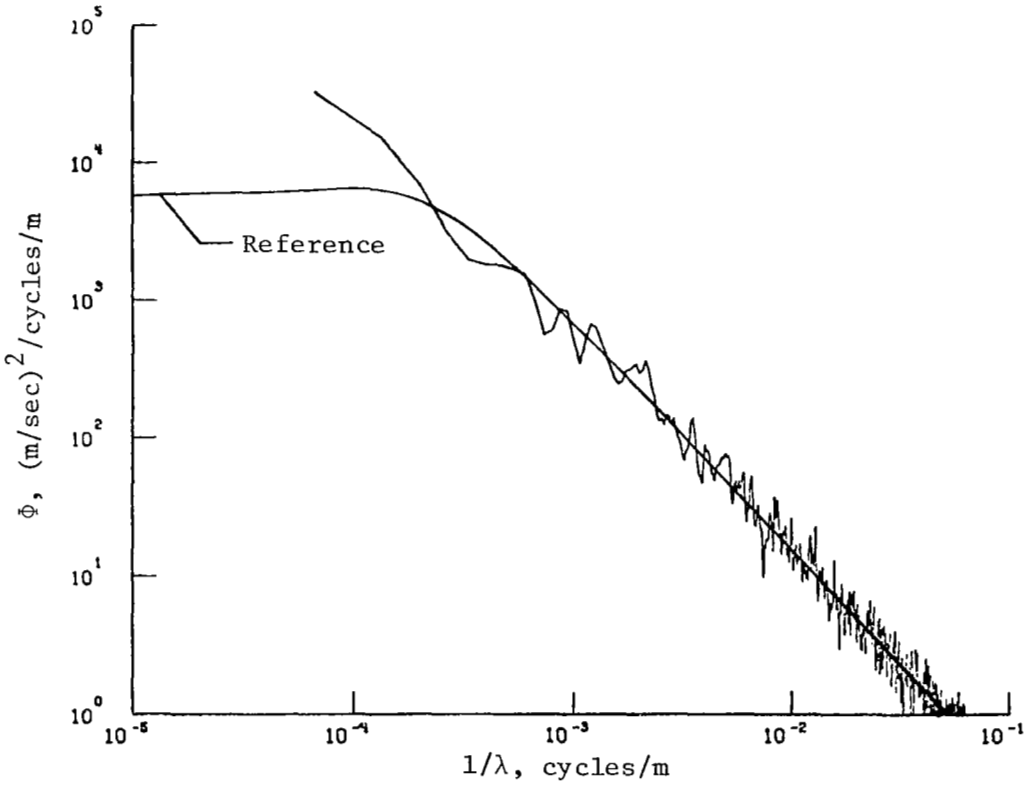

(b) Lateral component of gust velocity.

Figure 44.- Continued.

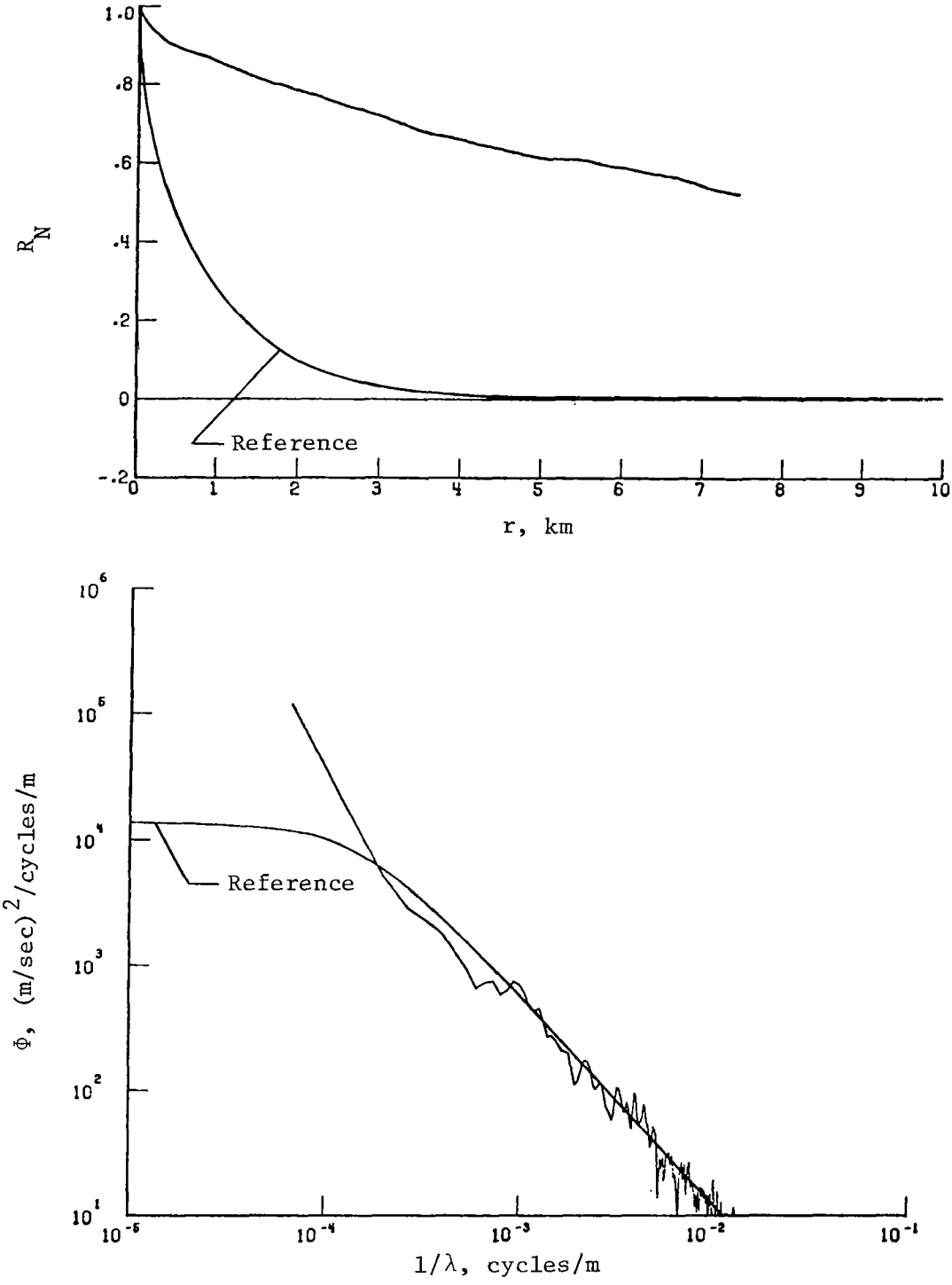

(c) Longitudinal component of gust velocity.

Figure 44.- Concluded.

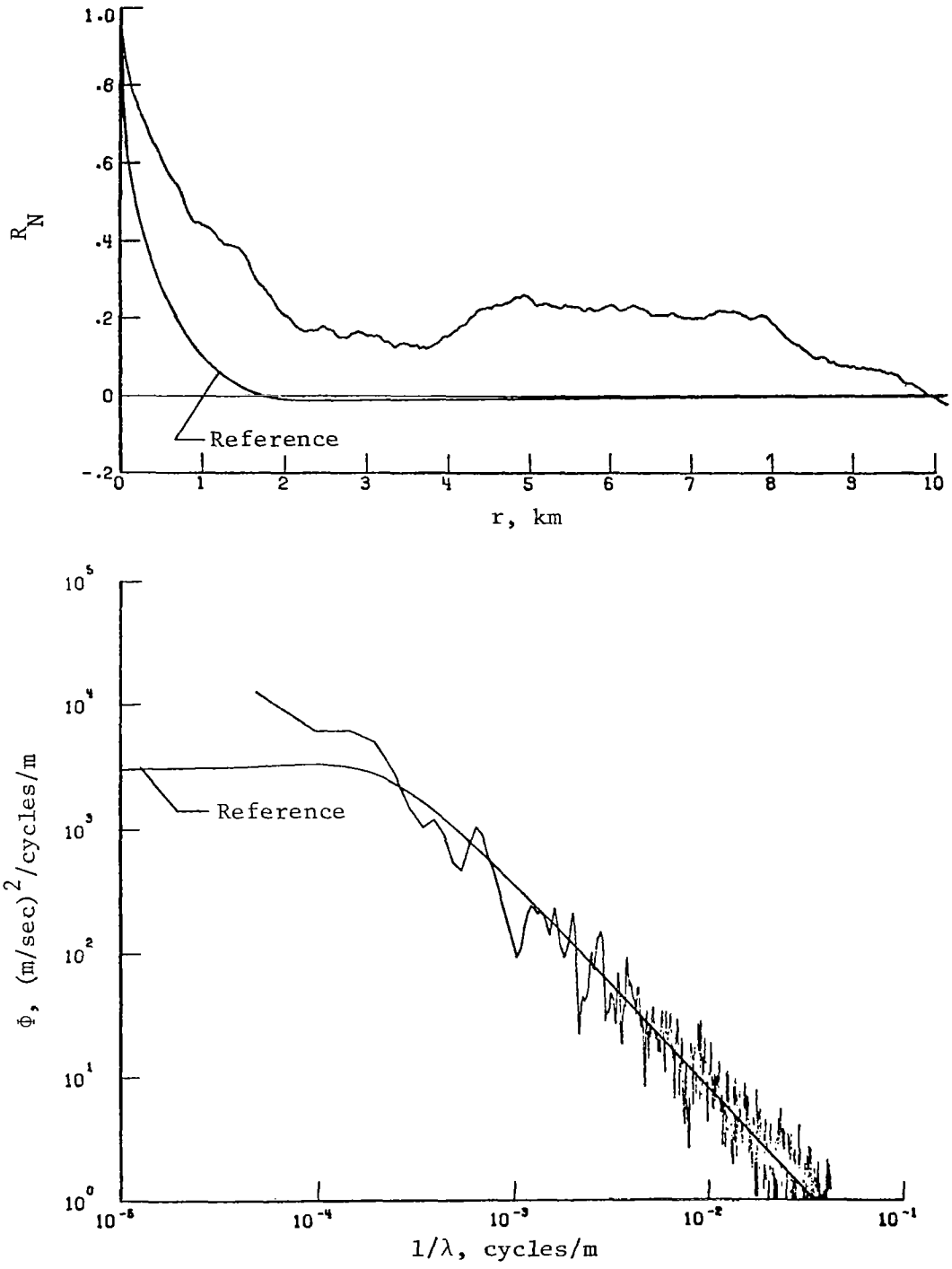

(a) Vertical component of gust velocity.

Figure 45.- Power spectra and autocorrelation functions for flight 42, run 8.

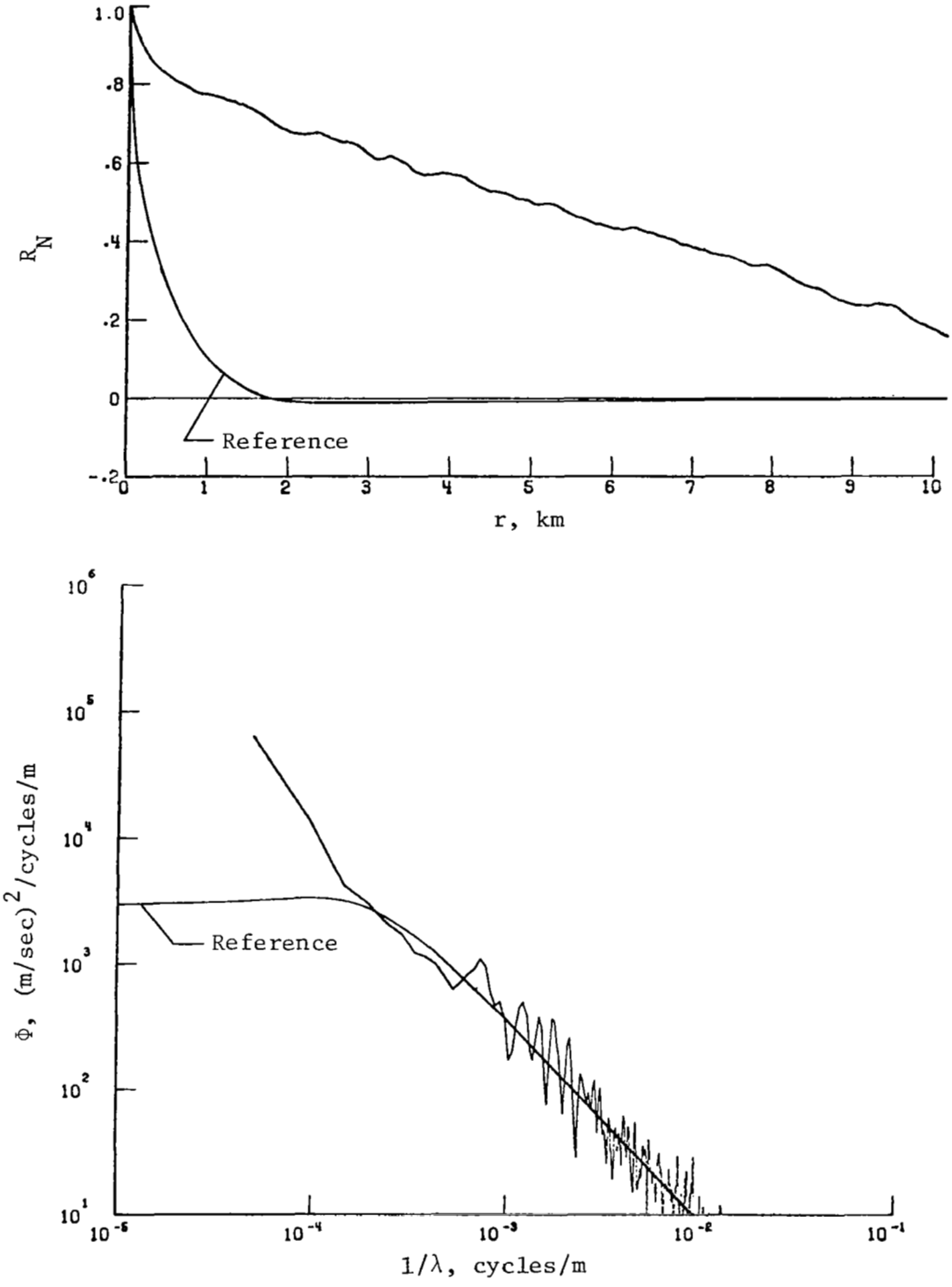

(b) Lateral component of gust velocity.

Figure 45.- Continued.

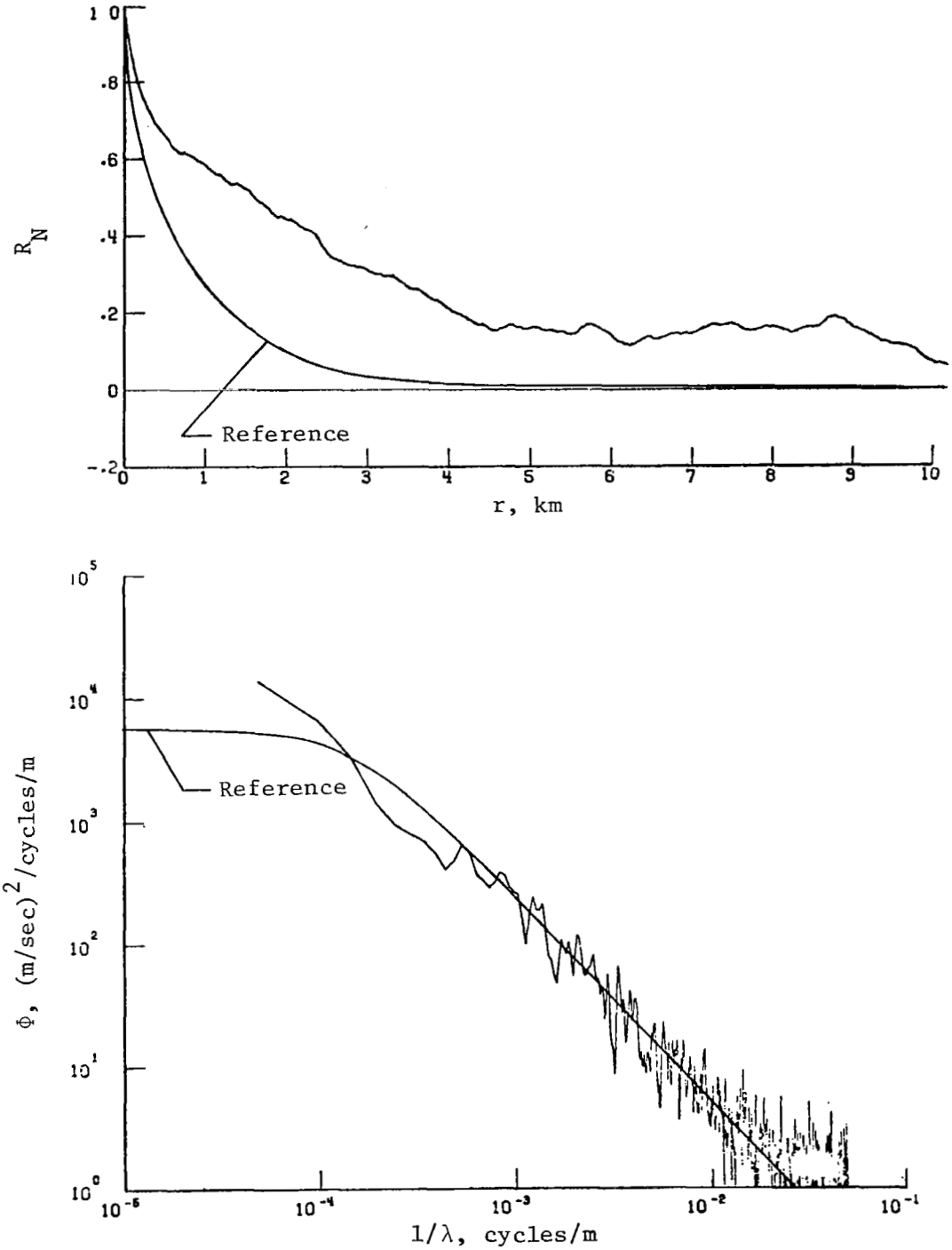

(c) Longitudinal component of gust velocity.

Figure 45.- Concluded.

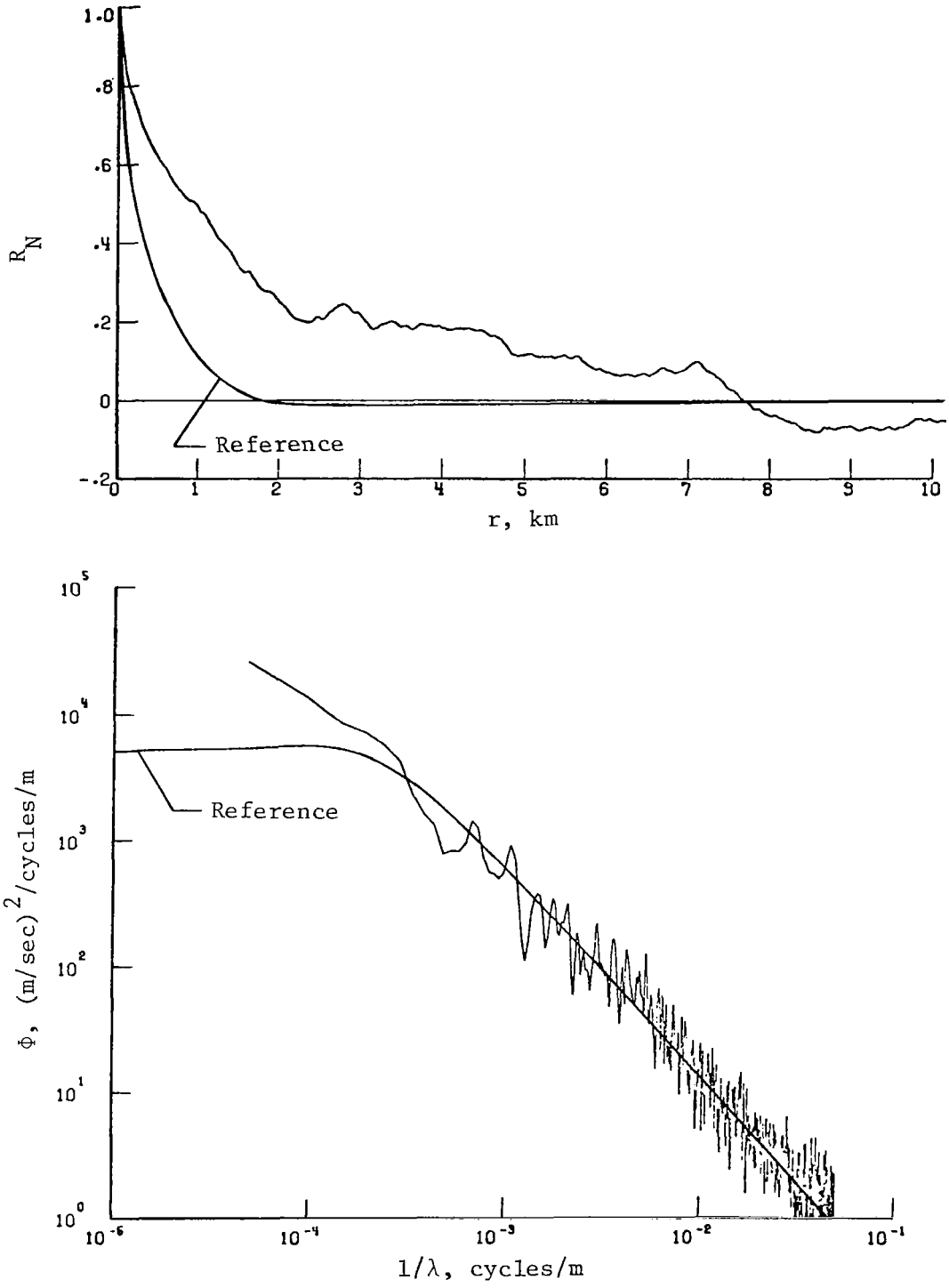

(a) Vertical component of gust velocity.

Figure 46.- Power spectra and autocorrelation functions for flight 42, run 9.

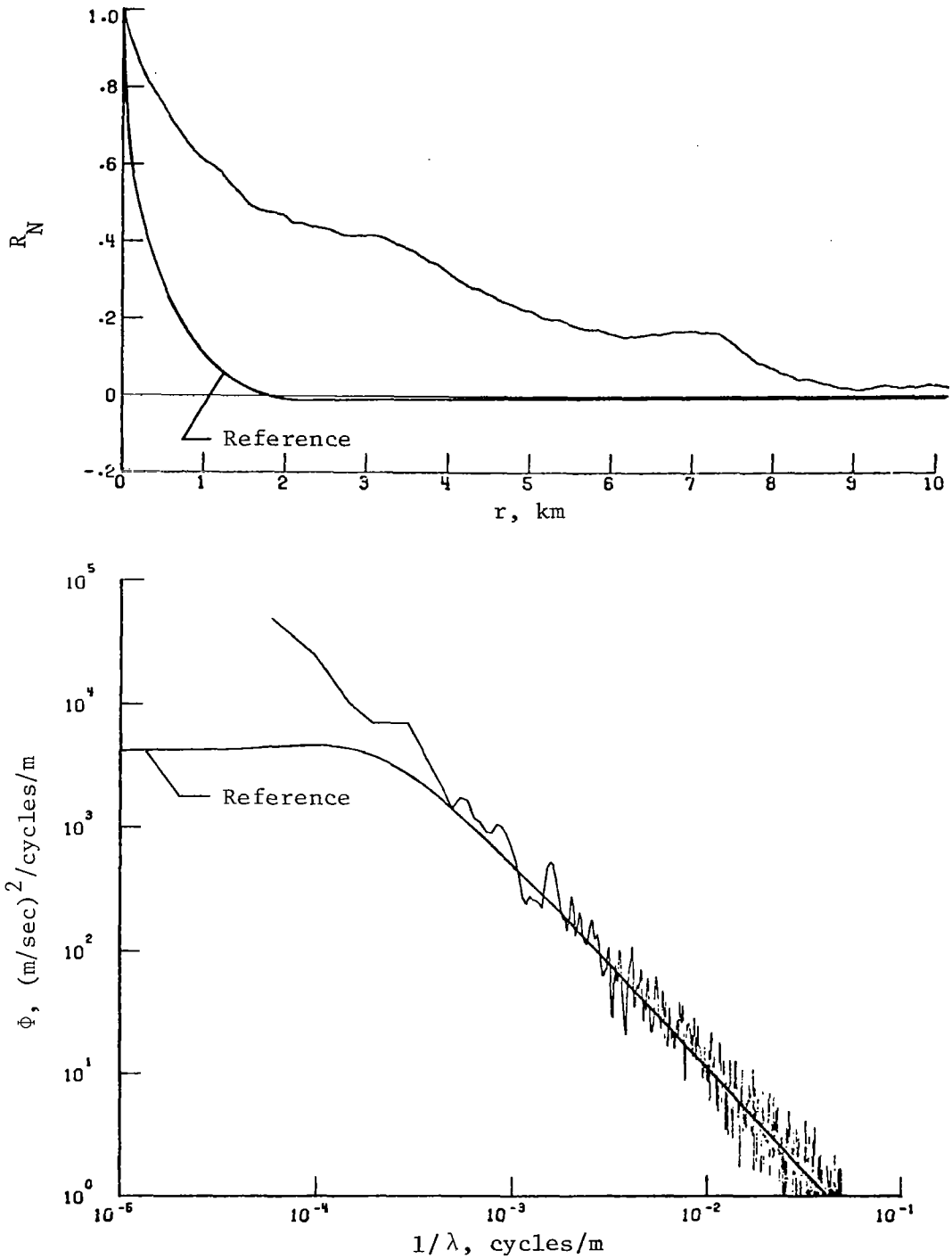

(b) Lateral component of gust velocity.

Figure 46.- Continued.

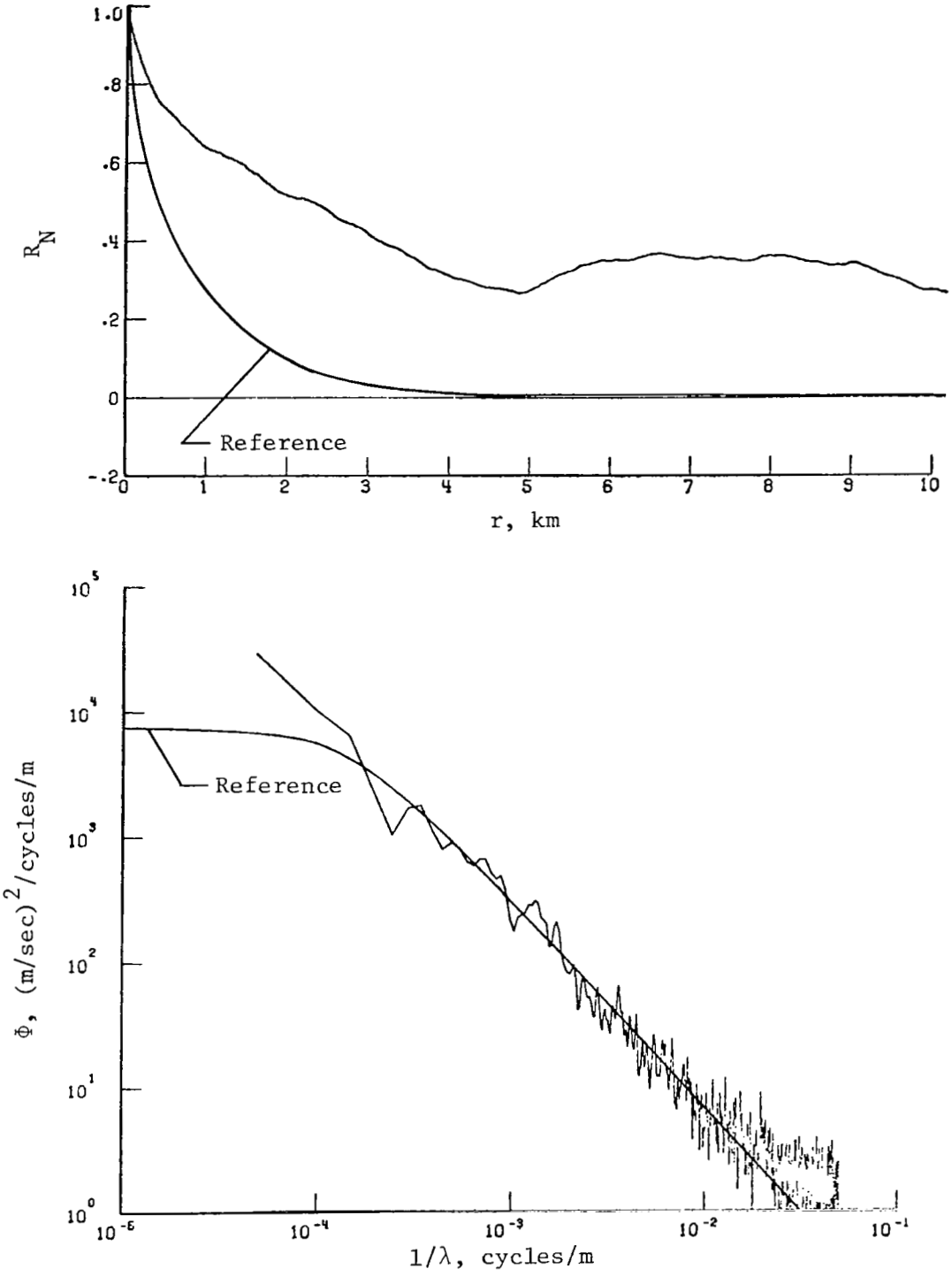

(c) Longitudinal component of gust velocity.

Figure 46.- Concluded.

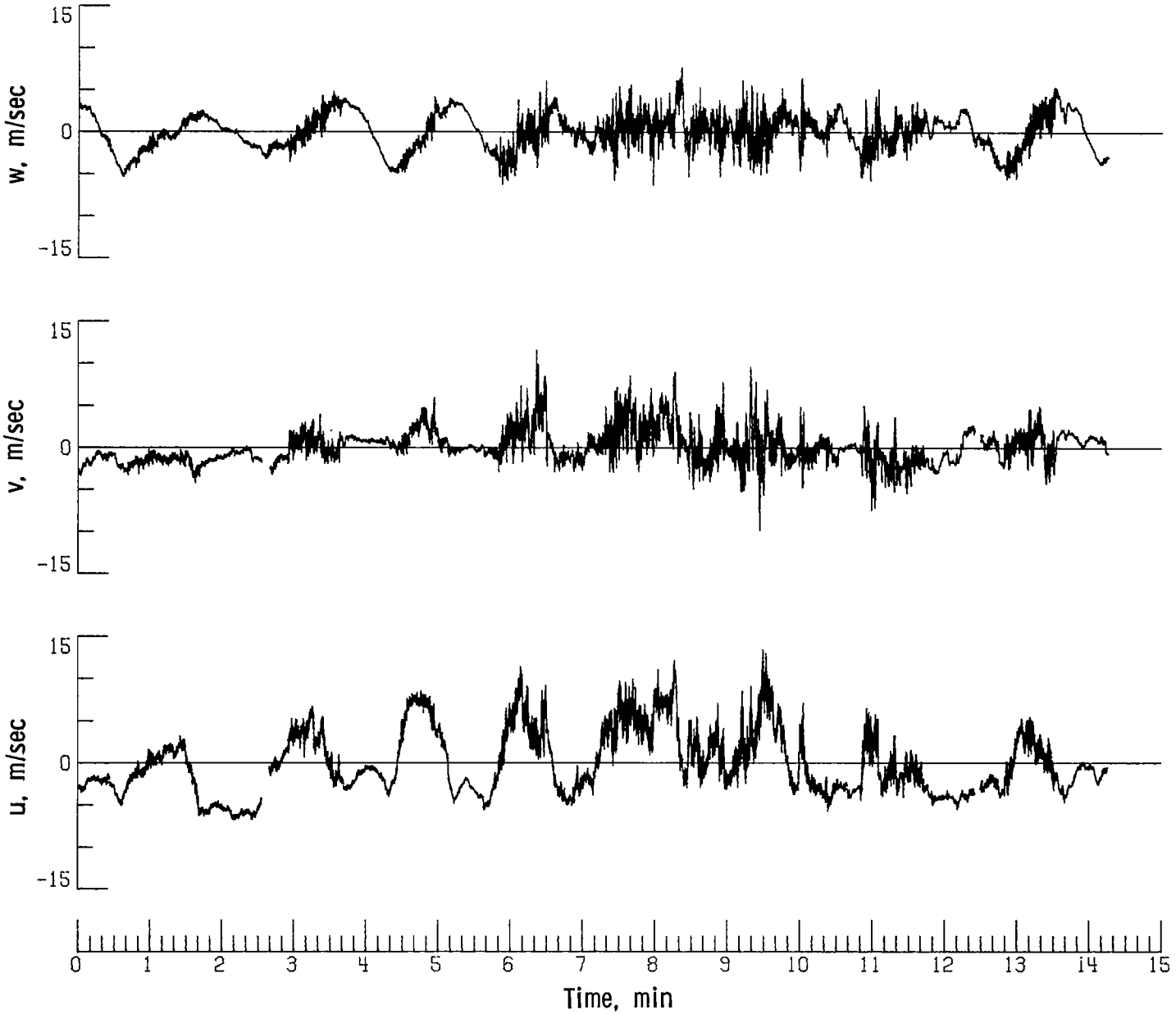

(a) Flight 20, run 1.

Figure 47.- Time histories of mountain waves at an altitude of 1924 m (6311 ft).

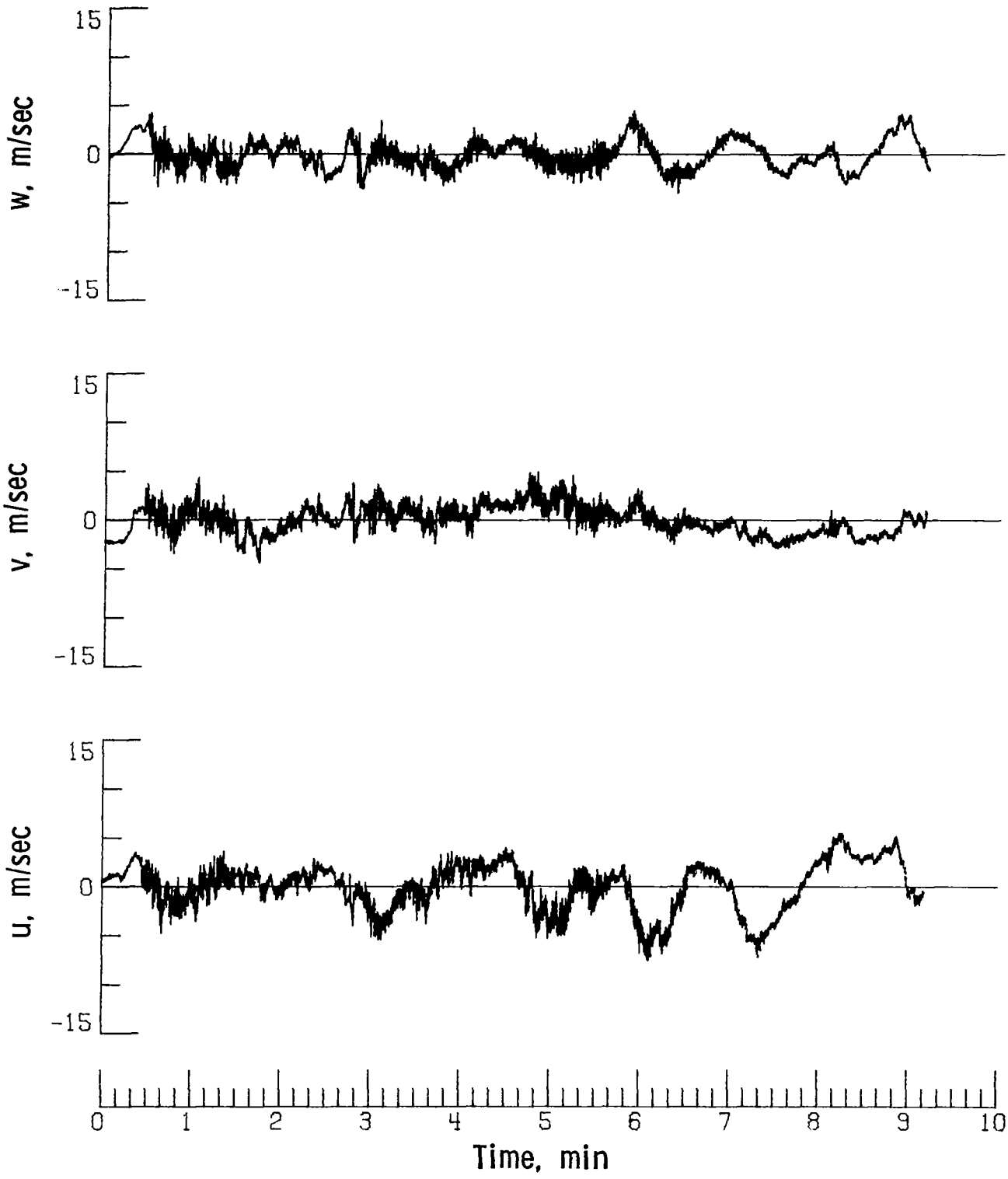

(b) Flight 20, run 2.

Figure 47.- Continued.

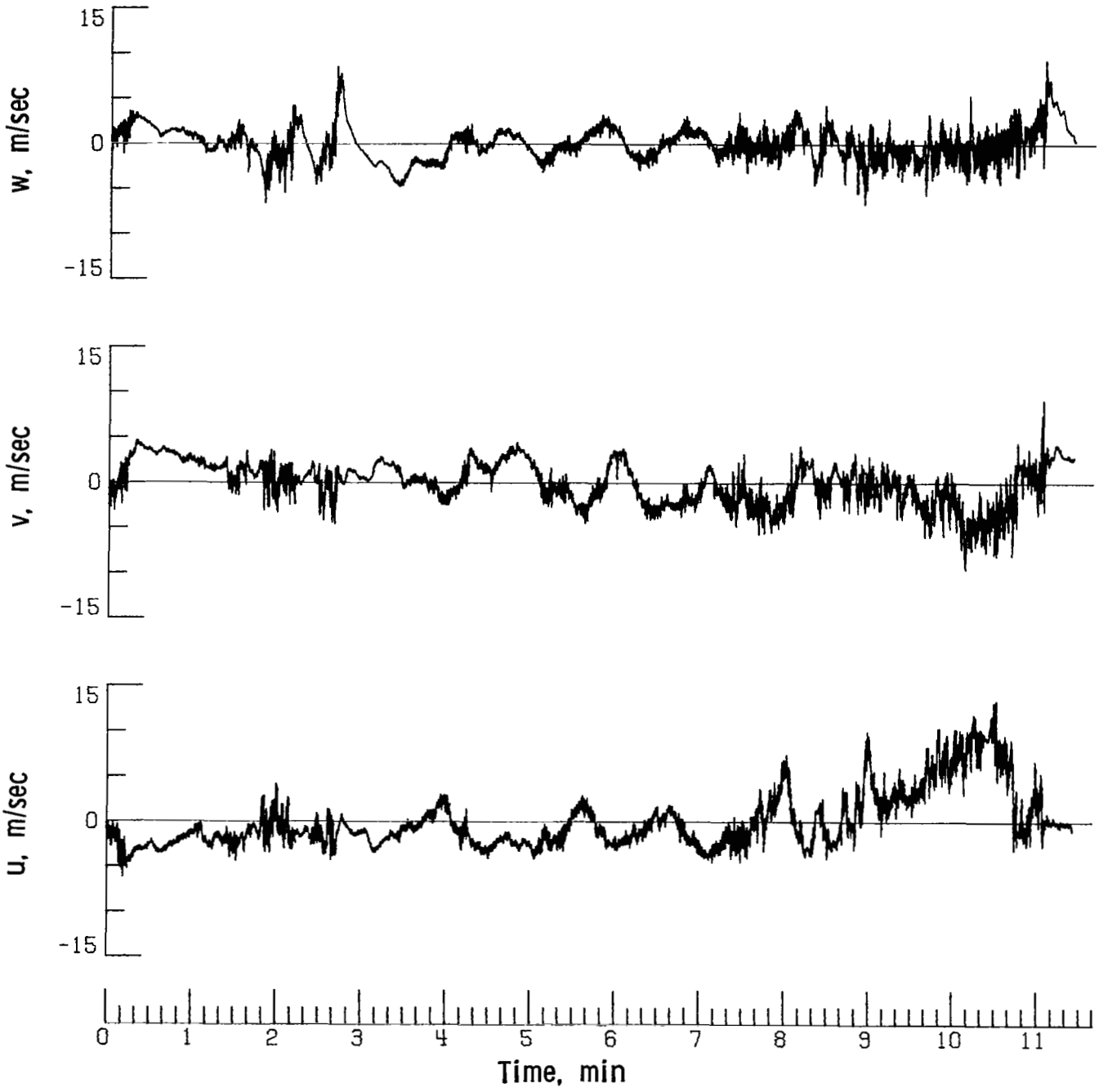

(c) Flight 20, run 3.

Figure 47.- Continued.

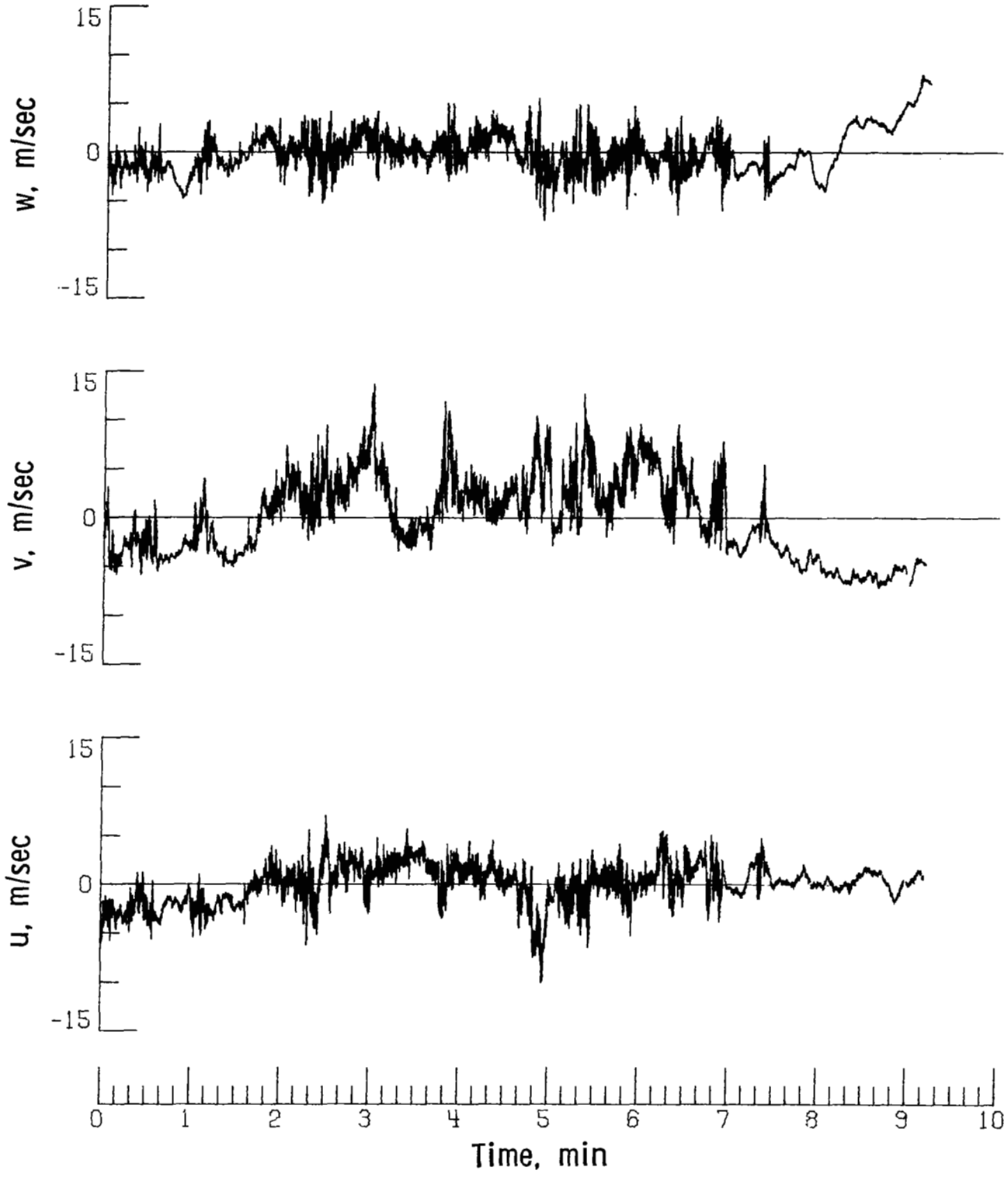

(d) Flight 20, run 4.

Figure 47.- Continued.

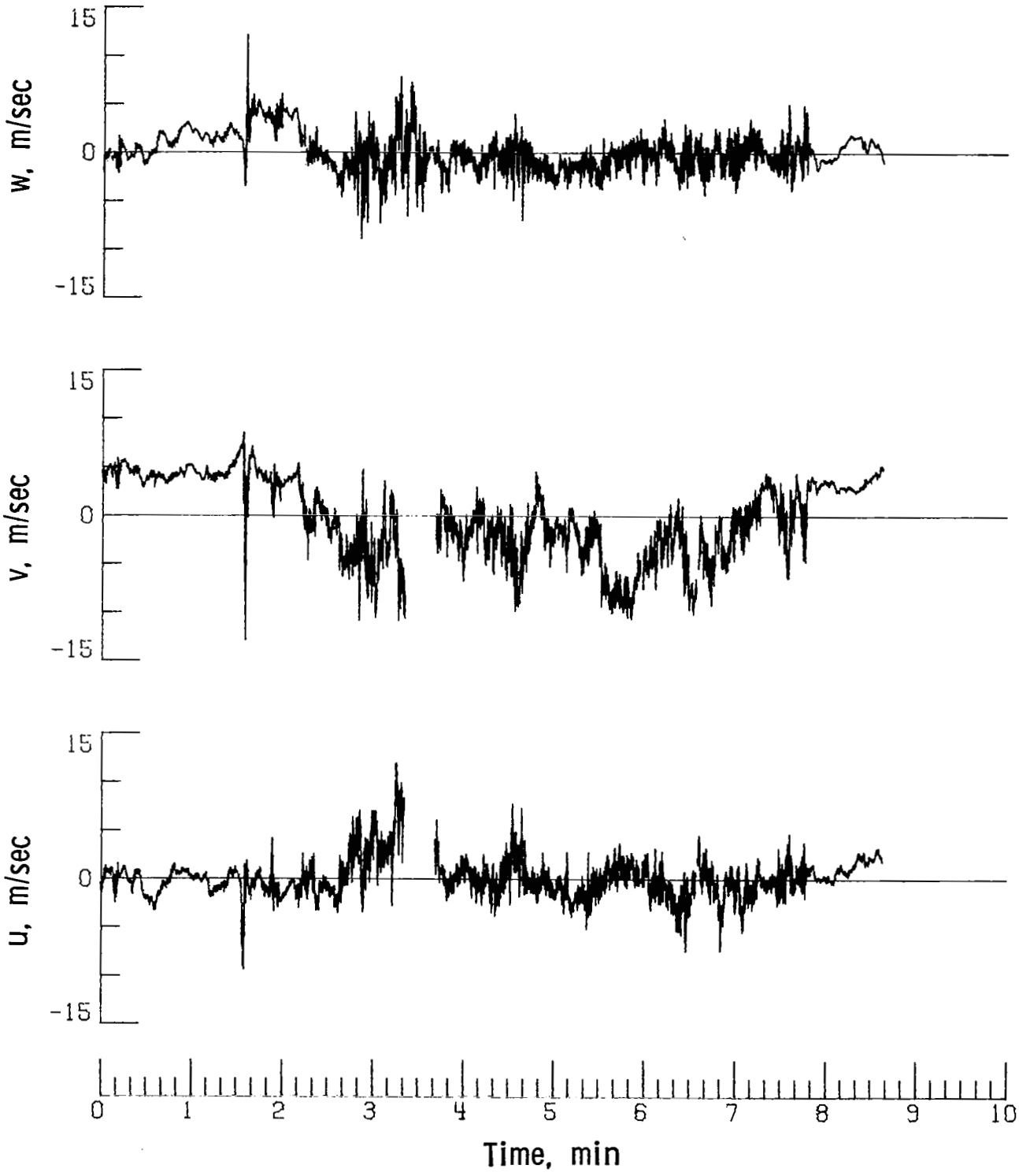

(e) Flight 20, run 5.

Figure 47.- Concluded.

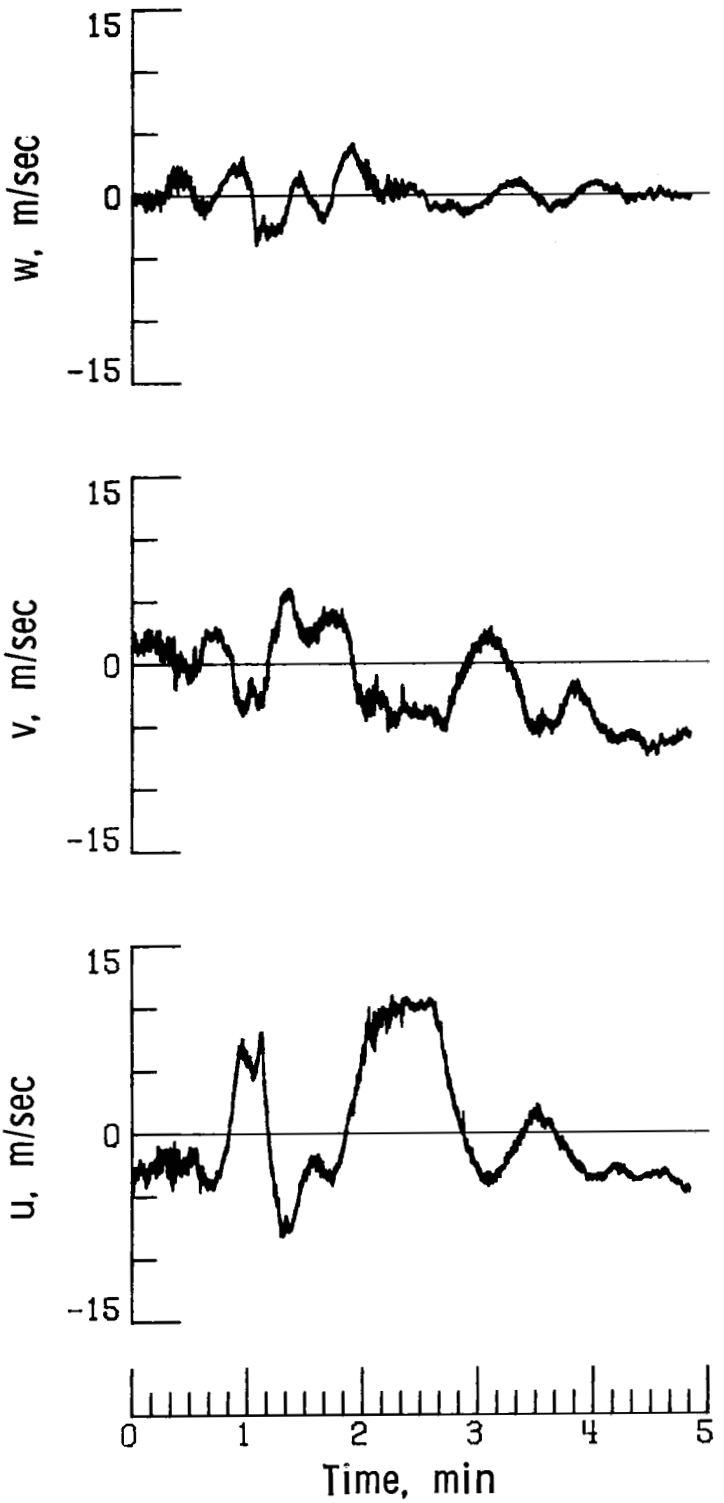

Figure 48.- Time histories of mountain waves at an altitude of about 14 000 m (≈46 000 ft). Flight 30, run 3.

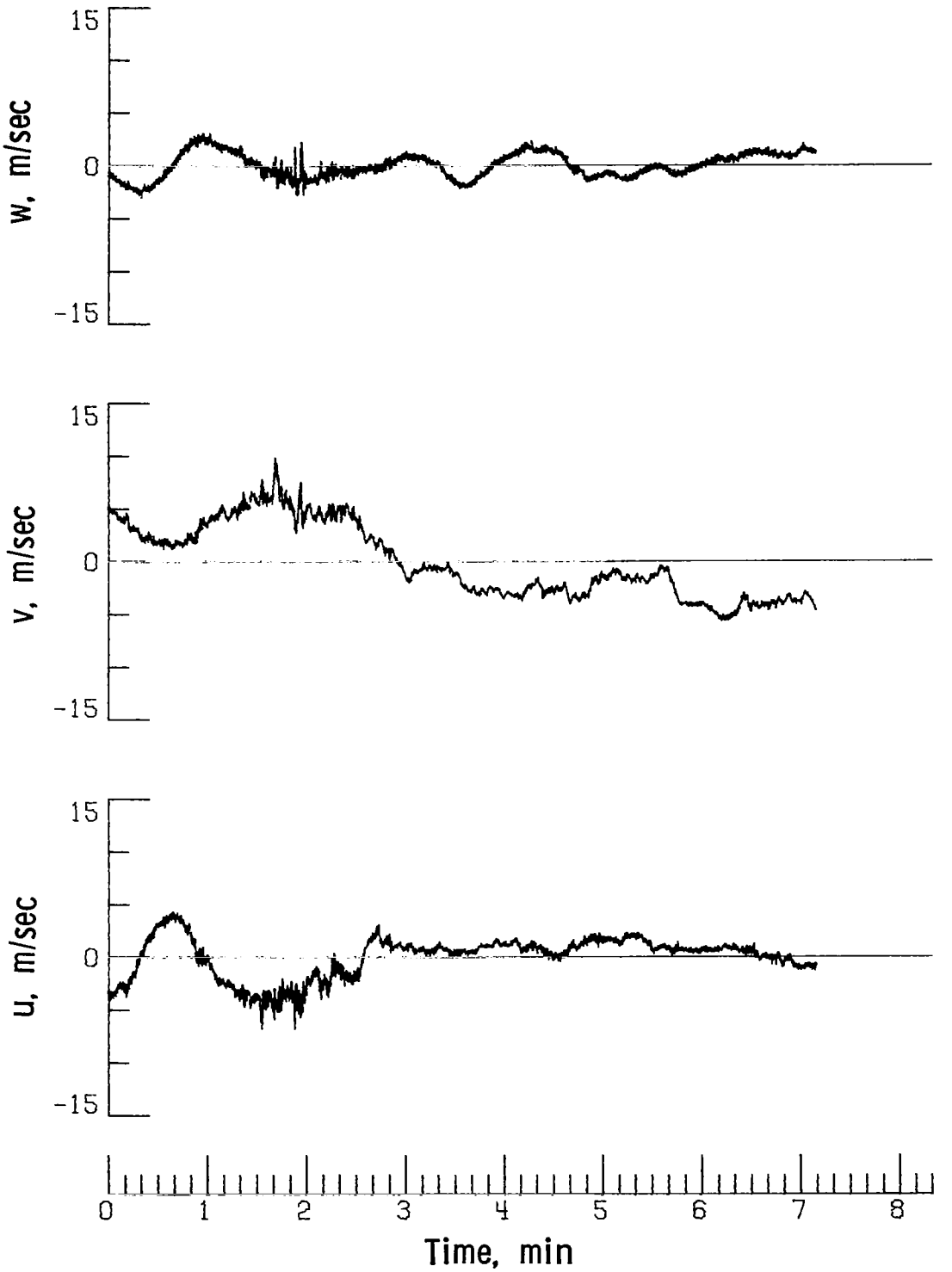

(a) Flight 38, run 3.

Figure 49.- Time histories of jet stream with long-wavelength effects at an altitude of about 10 700 m (≈35 000 ft).

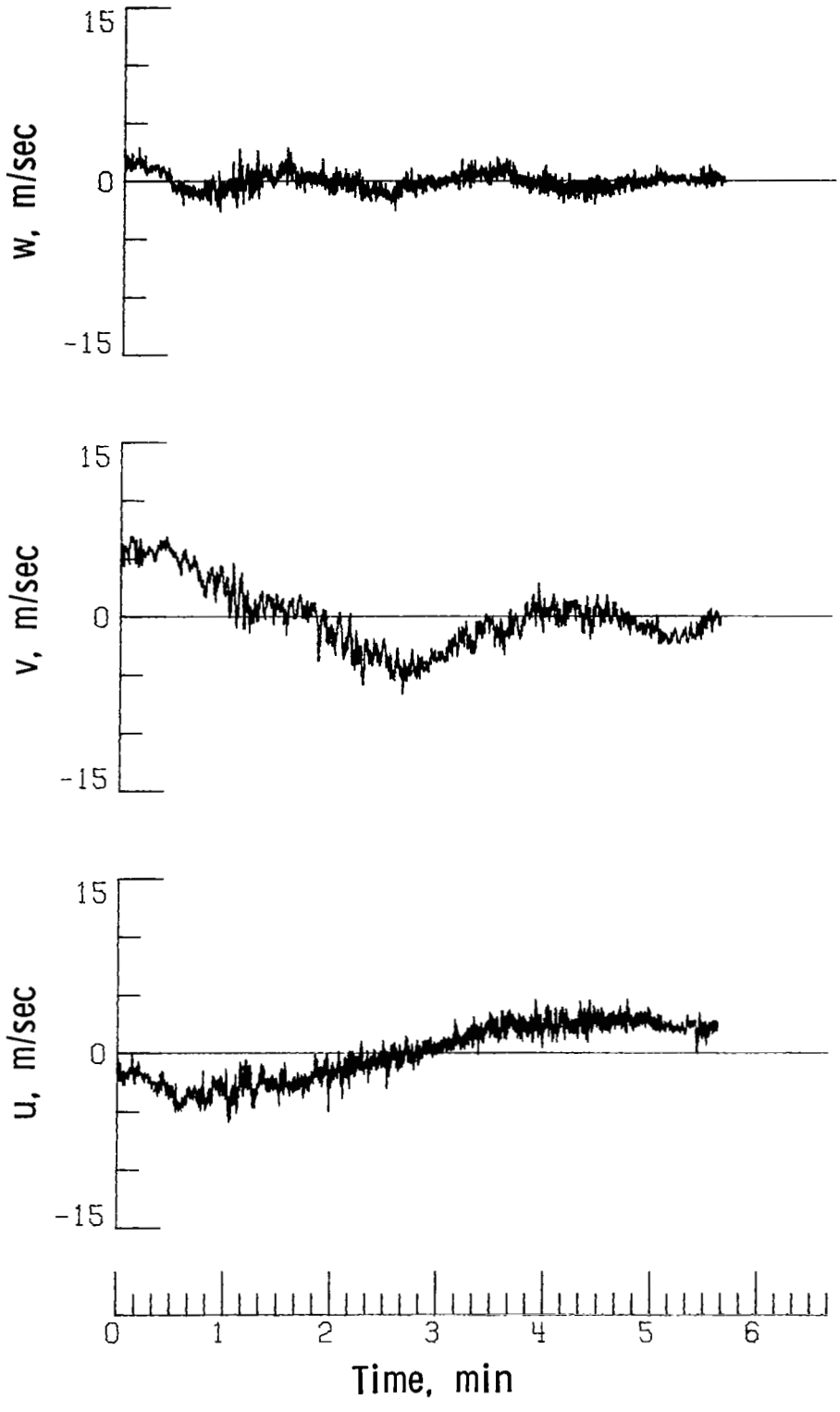

(b) Flight 38, run 5.

Figure 49.- Continued.

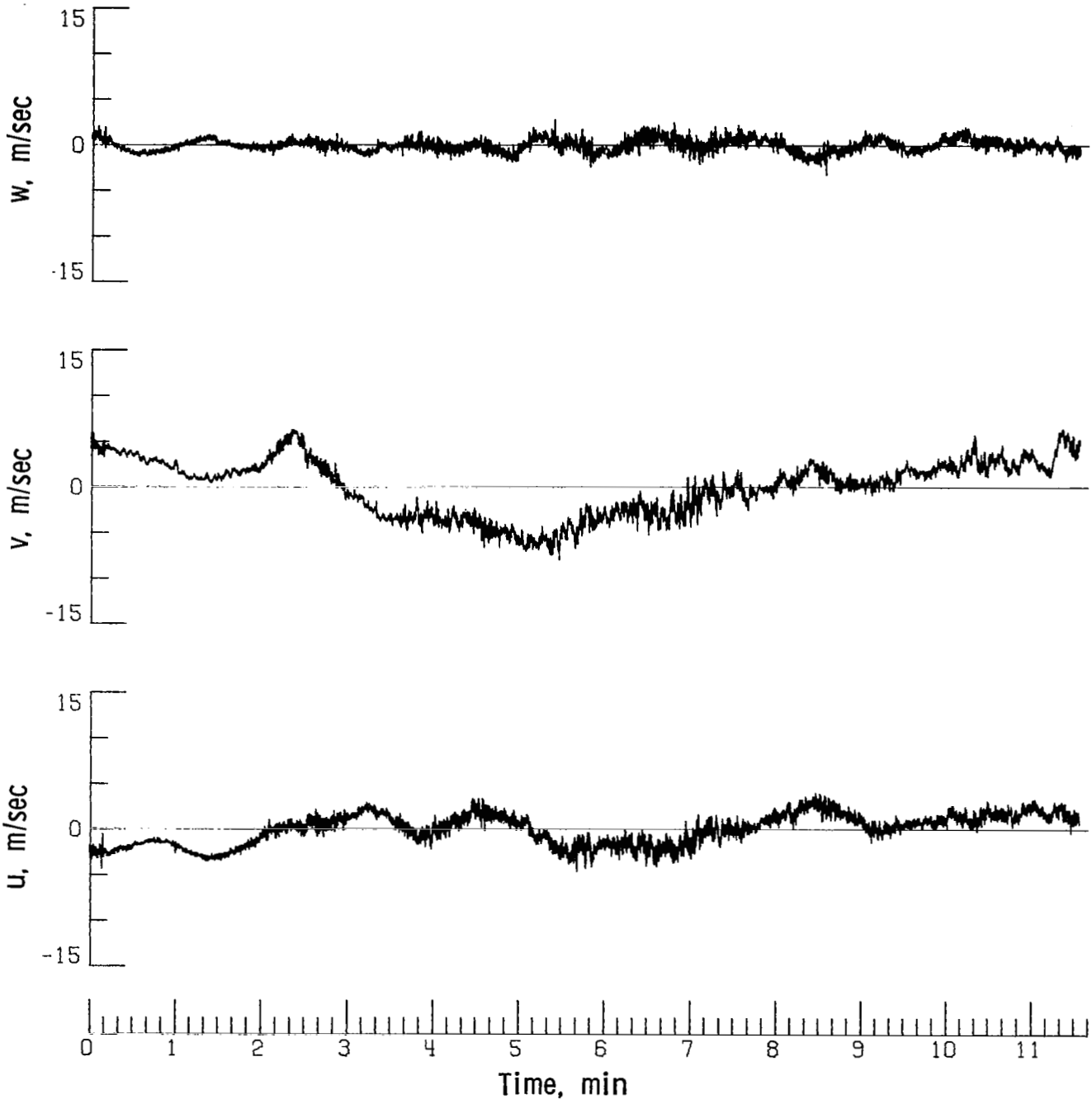

(c) Flight 38, run 6.

Figure 49.- Continued.

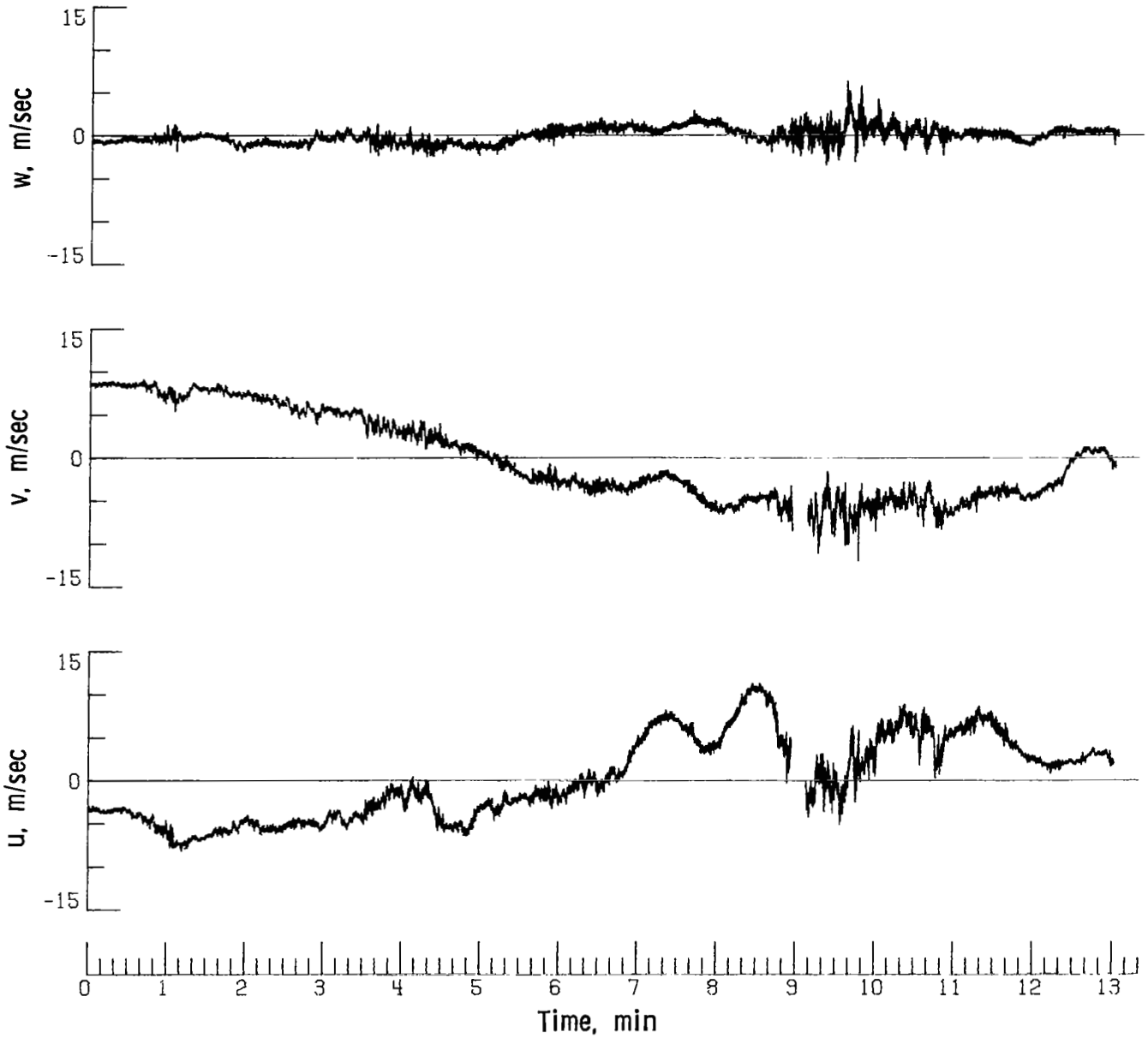

(d) Flight 38, run 7.

Figure 49.- Concluded.

1. Report No.	2. Government Accession No.	3. Recipient's Catalog No.
NASA TP-1979		

4. Title and Subtitle	5. Report Date
POWER SPECTRAL MEASUREMENTS OF CLEAR-AIR TURBULENCE TO LONG WAVELENGTHS FOR ALTITUDES UP TO 14 000 METERS	April 1982
	6. Performing Organization Code: 505-44-23-06
7. Author(s): Harold N. Murrow, William E. McCain, and Richard H. Rhyne	8. Performing Organization Report No.: L-14820
	10. Work Unit No.
9. Performing Organization Name and Address: NASA Langley Research Center, Hampton, VA 23665	11. Contract or Grant No.
	13. Type of Report and Period Covered: Technical Paper
12. Sponsoring Agency Name and Address: National Aeronautics and Space Administration, Washington, DC 20546	14. Sponsoring Agency Code

15. Supplementary Notes

16. Abstract

Measurements of three components of clear-air atmospheric turbulence have been made with an airplane incorporating a special instrumentation system to provide accurate data resolution to wavelengths of approximately 12 500 m (40 000 ft). Flight samplings covered an altitude range from approximately 500 to 14 000 m (1500 to 46 000 ft) in various meteorological conditions. This report presents individual autocorrelation functions and power spectra for the three turbulence components from 43 data runs taken primarily from mountain-wave and jet-stream encounters. The flight location (Eastern or Western United States), date, time, run length, intensity level (standard deviation), and values of statistical degrees of freedom for each run are provided in tabular form. The data presented in this report, along with detailed meteorological descriptions for each sampling flight presented in previously published reports, should provide adequate information for detailed meteorological correlations. Some time histories which contain predominant low-frequency wave motion are also presented.

17. Key Words (Suggested by Author(s))	18. Distribution Statement
Atmospheric turbulence Power spectra Autocorrelation functions	Unclassified - Unlimited Subject Category 47

19. Security Classif. (of this report)	20. Security Classif. (of this page)	21. No. of Pages	22. Price
Unclassified	Unclassified	161	A08

For sale by the National Technical Information Service, Springfield, Virginia 22161

NASA-Langley, 1982